TNFR SUPERFAMILY OLIGOMERIZATION AND SIGNALING

EDITED BY: Cristian Roberto Smulski, Marta Rizzi and Olivier Micheau
PUBLISHED IN: Frontiers in Cell and Developmental Biology

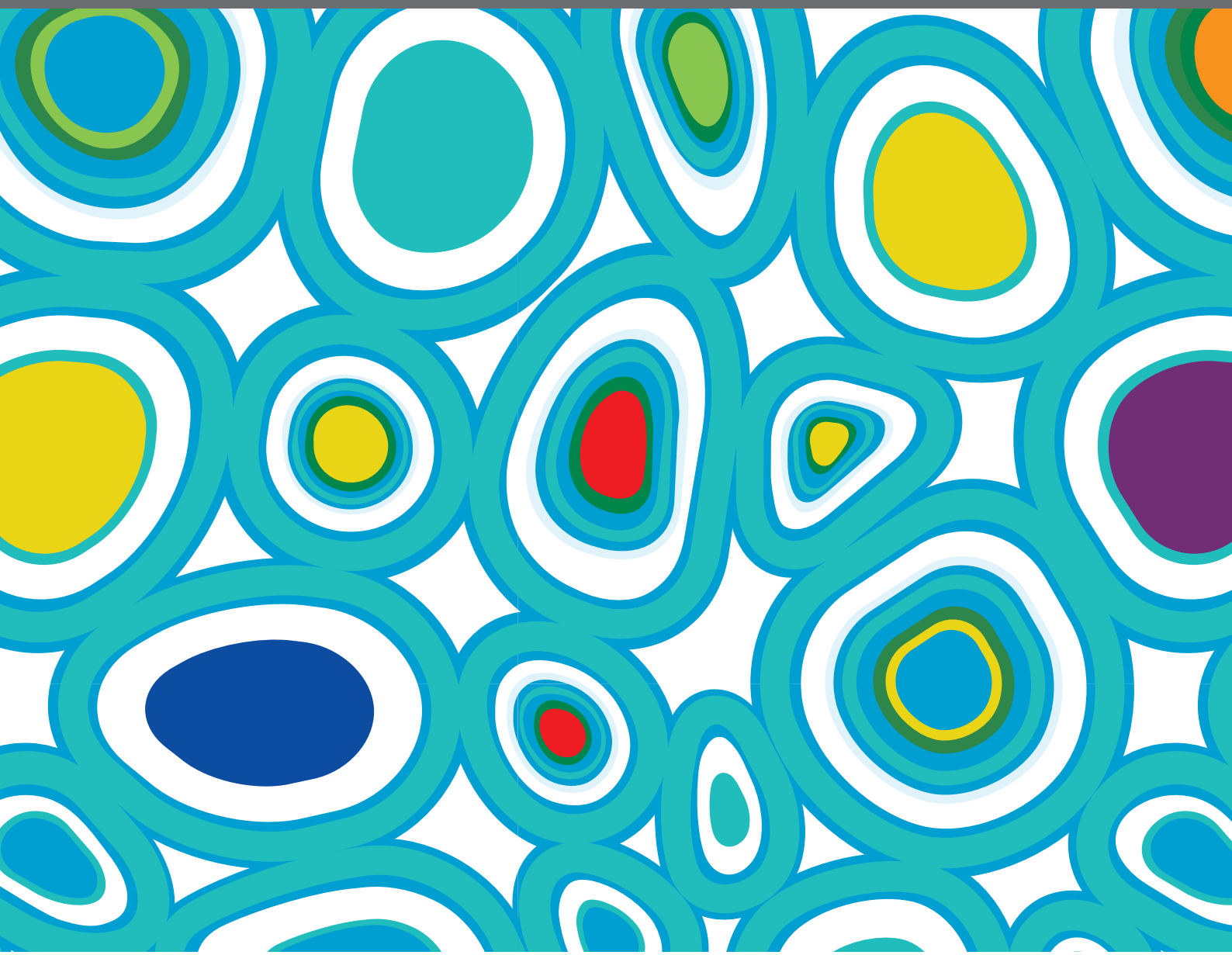

frontiers Research Topics

frontiers

ISSN 1664-8714
ISBN 978-2-88966-846-5
DOI 10.3389/978-2-88966-846-5

About Frontiers

Frontiers is more than just an open-access publisher of scholarly articles: it is a pioneering approach to the world of academia, radically improving the way scholarly research is managed. The grand vision of Frontiers is a world where all people have an equal opportunity to seek, share and generate knowledge. Frontiers provides immediate and permanent online open access to all its publications, but this alone is not enough to realize our grand goals.

Frontiers Journal Series

The Frontiers Journal Series is a multi-tier and interdisciplinary set of open-access, online journals, promising a paradigm shift from the current review, selection and dissemination processes in academic publishing. All Frontiers journals are driven by researchers for researchers; therefore, they constitute a service to the scholarly community. At the same time, the Frontiers Journal Series operates on a revolutionary invention, the tiered publishing system, initially addressing specific communities of scholars, and gradually climbing up to broader public understanding, thus serving the interests of the lay society, too.

Dedication to Quality

Each Frontiers article is a landmark of the highest quality, thanks to genuinely collaborative interactions between authors and review editors, who include some of the world's best academicians. Research must be certified by peers before entering a stream of knowledge that may eventually reach the public - and shape society; therefore, Frontiers only applies the most rigorous and unbiased reviews.
Frontiers revolutionizes research publishing by freely delivering the most outstanding research, evaluated with no bias from both the academic and social point of view. By applying the most advanced information technologies, Frontiers is catapulting scholarly publishing into a new generation.

What are Frontiers Research Topics?

Frontiers Research Topics are very popular trademarks of the Frontiers Journals Series: they are collections of at least ten articles, all centered on a particular subject. With their unique mix of varied contributions from Original Research to Review Articles, Frontiers Research Topics unify the most influential researchers, the latest key findings and historical advances in a hot research area! Find out more on how to host your own Frontiers Research Topic or contribute to one as an author by contacting the Frontiers Editorial Office: frontiersin.org/about/contact

TNFR SUPERFAMILY OLIGOMERIZATION AND SIGNALING

Topic Editors:
Cristian Roberto Smulski, Bariloche Atomic Centre (CNEA), Argentina
Marta Rizzi, University of Freiburg Medical Center, Germany
Olivier Micheau, Université de Bourgogne, France

Citation: Smulski, C. R., Rizzi, M., Micheau, O., eds. (2021). TNFR Superfamily Oligomerization and Signaling. Lausanne: Frontiers Media SA.
doi: 10.3389/978-2-88966-846-5

Table of Contents

frontiers in Cell and Developmental Biology

EDITORIAL
published: 20 April 2021
doi: 10.3389/fcell.2021.682472

Editorial: TNFR Superfamily Oligomerization and Signaling

Olivier Micheau[1,2]*, *Marta Rizzi*[3]* and *Cristian R. Smulski*[4]*

[1] INSERM, LNC, UMR 1231, Dijon, France, [2] Université de Bourgogne Franche-Comté, Dijon, France, [3] Department of Rheumatology and Clinical Immunology, Faculty of Medicine, University Medical Center Freiburg, University of Freiburg, Freiburg, Germany, [4] Medical Physics Department, Bariloche Atomic Centre Comisión Nacional de Energía Atómica (CNEA) and Consejo Nacional de Investigaciones Científicas y Técnicas (CONICET), San Carlos de Bariloche, Argentina

Keywords: TNF/TNFR superfamily, oligomerization, signaling, therapeutic targets, specific targeting

Editorial on the Research Topic

TNFR Superfamily Oligomerization and Signaling

INTRODUCTION

The TNF/TNFR superfamily comprises 19 ligands and 30 receptors, all representing therapeutically relevant targets in a wide range of human diseases (Micheau, 2017; Yi et al., 2018). TNF family ligands are type 2 membrane bound proteins with a common structural motif that mediates ligand trimerization: the TNF homology domain (Bodmer et al., 2002). Each trimer subunit binds to one TNF receptor (TNFR) subunit, inducing receptor oligomerization that represents the minimal active unit in most members of the family. The outcome of signaling following ligand binding results from the interplay of different factors: ligand architecture, assembly of receptor units in the appropriate location, posttranslational modifications and transmembrane helix associations. The "TNFR Superfamily Oligomerization and Signaling" Research Topic covers many of these features and provides new insights into complex regulatory mechanisms.

TNFR TARGETING AND SIGNALING MODULATION

TNF-TNFR1 constitutes one of the most studied ligand-receptor pairs of the family. Signaling outcome ranges from NF-kB and MAPK activation to apoptosis or necroptosis (Ting and Bertrand, 2016). To achieve this, a number of events, including phosphorylation and ubiquitination are triggered upon ligand binding. These events are tightly regulated by a plethora of molecules that dictates the signaling outcome. Disruption of these events can lead to severe inflammatory diseases as reviewed by Webster and Vucic Notably, TNF can bind to a second receptor of the family, TNFR2, whose immune function differs from TNFR1. Indeed, several TNF family ligands can bind to more than one receptor. Because of this, ligand-blocking therapies are likely to affect a handful set of ligand-receptor pairs with unwanted effects. To overcome this problem, selective targeting of TNFR1 and TNFR2 has been developed showing a great therapeutic potential in several diseases as reviewed by Fischer et al. In the context of selective targeting of TNFR1 and 2, Wei et al. proposed a model in which the engineered protein "Atsttrin" (a derivative of progranulin) promotes cartilage repair primarily through TNFR2-Akt pathway, despite being able to bind and signal through both receptors.

Another example of a ligand binding to several receptors is TRAIL. This ligand can bind to two decoy receptors (DcR1 and DcR2) and to two functional receptors (DR4 and DR5) (LeBlanc and Ashkenazi, 2003). Binding to DR4 and DR5 triggers apoptosis in cancer cells (French and Tschopp, 1999). However, resistance to TRAIL induced apoptosis has been described in several tumor cells (Deng and Shah, 2020). Setroikrom et al. have described a novel

OPEN ACCESS

Edited and reviewed by:
Ana Cuenda,
Consejo Superior de Investigaciones Científicas (CSIC), Spain

***Correspondence:**
Olivier Micheau
omicheau@u-bourgogne.fr
Marta Rizzi
marta.rizzi@uniklinik-freiburg.de
Cristian R. Smulski
cristian.smulski@gmail.com

Specialty section:
This article was submitted to Signaling, a section of the journal Frontiers in Cell and Developmental Biology

Received: *18 March 2021*
Accepted: *25 March 2021*
Published: *20 April 2021*

Citation:
Micheau O, Rizzi M and Smulski CR (2021) Editorial: TNFR Superfamily Oligomerization and Signaling. Front. Cell Dev. Biol. 9:682472. doi: 10.3389/fcell.2021.682472

mechanism of resistance in colon cancer cells through selective segregation of DR5 into extracellular vesicles (EVs). Indeed, membrane bound receptors through EVs may not only modulate signaling pathways associated with TNF/TNFR superfamily members, but are likely to mediate communication between cells in complex systems.

OLIGOMERIZATION OF LIGANDS AND RECEPTORS

Amongst the TNF family ligands, the B cell activating factor (BAFF) has a unique feature that allows assembly of 20 adjacent trimers in a virus-like capsid called BAFF 60-mer, resulting in stronger activation of its receptors, *in vitro* (Cachero et al., 2006; Vigolo et al., 2018). However, it is unclear which is the physiological form of soluble BAFF in humans. Eslami et al. investigated the presence of highly oligomeric forms of BAFF in different human fluids, and detected high molecular weight forms of BAFF only in cord blood. This BAFF displayed some but not all properties of BAFF 60-mer. Moreover, an activity that dissociates BAFF 60-mer into trimers was identified which could be related to the exclusive presence of BAFF 3-mer in adult human serum and cerebrospinal fluid.

Ligand-induced receptor oligomerization is a critical step for signal transduction. Noteworthy, not all receptors of the family respond similarly to soluble or membrane-bound ligands. This phenomenon seems to be related to the oligomeric threshold intrinsic to each signaling pathway. Kucka and Wajant have reviewed the most relevant aspects of receptor oligomerization for TNFRs signaling, including clustering of free and bound TNFRs, receptor oligomerization requirement for specific signaling pathways, and how this knowledge contributes for the rational design and development of TNFR agonists that target specific members of the family. Moreover, Levoin et al. have described, in a comprehensive manner, how CD95 sub-domains and their post-translational modifications contribute to receptor aggregation and cell signaling, upon binding to different ligand forms. One emerging property of TNFRs is the ability of their transmembrane domains to mediate ligand independent associations. In the current topic Zhao et al. have solved the trimeric structure of transmembrane domain of TNFR1. Comparison of this structure with that of Fas and DR5 revealed similarities such as trimerization, but also significant structural divergences, undserscoring the importance of a systematic investigation of other TNFR family members. In line with this conclusion, Sica and Smulski have analyzed and compared the assembly of the previously solved transmembrane regions of p75NTR, Fas, and DR5 using coarse grained molecular dynamic simulations. This tool has proven useful for unbiassed prediction of oligomerization levels, residues involved in interactions, and impact of disease-associated mutations in this region.

Overall, the current Research Topic has covered important landmarks of the macromolecular complexes and signaling pathways engaged by TNF/TNFR family members. Although other features must be understood for proper selective therapeutic intervention, including spatial localization and function of the receptors (Staniek et al., 2019), their post-translational modifications, that may directly affect their signal transduction capabilities (Wagner et al., 2007; Dufour et al., 2017), receptor shedding and decoy activities (Hoffmann et al., 2015; Laurent et al., 2015; Smulski et al., 2017b), and potential interactions between members of the family (Smulski et al., 2017a). Understanding the complex function and signaling interplay can be exploited to design effective treatments, as recently shown in experimental melanoma (Bertrand et al., 2017; Montfort et al., 2019). Inhibition of TNF-induced TNFR1 signaling is sufficient to overcome resistance to immune checkpoint inhibitors, restoring the anti-tumoral immune response. The ongoing clinical trials translating this finding are promising (Montfort et al., 2021), showing high response rates in advanced and/or metastatic melanoma patients. Finally, despite the fact that most family members have been known for more than two decades, including TNF and TNFR1, new therapeutic opportunities may emerge as a result of our better understanding of TNF/TNFR family members.

AUTHOR CONTRIBUTIONS

All authors listed have made a substantial, direct and intellectual contribution to the work, and approved it for publication.

FUNDING

OM was supported by grants from the ANR (Agence Nationale de la Recherche) program Investissements d'Avenir Labex LipSTIC (ANR-11-LABX-0021-01), project ISITE-BFC (contract ANR-15-IDEX-0003), the European commission H2020 Marie Skłodowska-Curie Actions (DISCOVER, 777995), the Conseil Regional de Bourgogne, COFECUB/CAMPUS FRANCE (Me 888-17), la Ligue Nationale Contre le Cancer, and the fondation ARC (Association pour la Recherche sur le cancer). MR was supported by a grant from the DFG (SFB1160, B02) and CS was supported by the National research council (CONICET) and by a grant from FONCYT (PICT-2018-01107).

ACKNOWLEDGMENTS

We would like to acknowledge the contribution of all the authors and reviewers of this topic, as well as of the members of the Frontiers in Cell and Developmental Biology Editorial Office.

REFERENCES

Bertrand, F., Montfort, A., Marcheteau, E., Imbert, C., Gilhodes, J., Filleron, T., et al. (2017). TNFα blockade overcomes resistance to anti-PD-1 in experimental melanoma. *Nat. Commun.* 8, 2256–2213. doi: 10.1038/s41467-017-02358-7

Bodmer, J.-L., Schneider, P., and Tschopp, J. (2002). The molecular architecture of the TNF superfamily. *Trends Biochem. Sci.* 27, 19–26. doi: 10.1016/S0968-0004(01)01995-8

Cachero, T. G., Schwartz, I. M., Qian, F., Day, E. S., Bossen, C., Ingold, K., et al. (2006). Formation of virus-like clusters is an intrinsic property of the tumor necrosis factor family member BAFF (B cell activating factor). *Biochemistry* 45, 2006–2013. doi: 10.1021/bi051685o

Deng, D., and Shah, K. (2020). TRAIL of hope meeting resistance in cancer. *Trends Cancer* 6, 989–1001. doi: 10.1016/j.trecan.2020.06.006

Dufour, F., Rattier, T., Shirley, S., Picarda, G., Constantinescu, A. A., Morlé, A., et al. (2017). N-glycosylation of mouse TRAIL-R and human TRAIL-R1 enhances TRAIL-induced death. *Cell Death Differ.* 24, 500–510. doi: 10.1038/cdd.2016.150

French, L. E., and Tschopp, J. (1999). The TRAIL to selective tumor death. *Nat. Med.* 5, 146–147. doi: 10.1038/5505

Hoffmann, F. S., Kuhn, P.-H., Laurent, S. A., Hauck, S. M., Berer, K., Wendlinger, S. A., et al. (2015). The immunoregulator soluble TACI is released by ADAM10 and reflects B cell activation in autoimmunity. *J. Immunol.* 194, 542–552. doi: 10.4049/jimmunol.1402070

Laurent, S. A., Hoffmann, F. S., Kuhn, P.-H., Cheng, Q., Chu, Y., Schmidt-Supprian, M., et al. (2015). γ-Secretase directly sheds the survival receptor BCMA from plasma cells. *Nat. Commun.* 6:7333. doi: 10.1038/ncomms8333

LeBlanc, H. N., and Ashkenazi, A. (2003). Apo2L/TRAIL and its death and decoy receptors. *Cell Death Differ.* 10, 66–75. doi: 10.1038/sj.cdd.4401187

Micheau, O. (2017). *TRAIL, Fas Ligand, TNF and TLR3 in Cancer*. Berlin: Springer. doi: 10.1007/978-3-319-56805-8

Montfort, A., Colacios, C., Levade, T., Andrieu-Abadie, N., Meyer, N., and Ségui, B. (2019). The TNF paradox in cancer progression and immunotherapy. *Front. Immunol.* 10:1818. doi: 10.3389/fimmu.2019.01818

Montfort, A., Filleron, T., Virazels, M., Dufau, C., Milhès, J., Pagès, C., et al. (2021). Combining nivolumab and ipilimumab with infliximab or certolizumab in patients with advanced melanoma: first results of a phase Ib clinical trial. *Clin. Cancer Res.* 27, 1037–1047. doi: 10.1158/1078-0432.CCR-20-3449

Smulski, C. R., Decossas, M., Chekkat, N., Beyrath, J., Willen, L., Guichard, G., et al. (2017a). Hetero-oligomerization between the TNF receptor superfamily members CD40, Fas and TRAILR2 modulate CD40 signalling. *Cell Death Dis.* 8, e2601–e2601. doi: 10.1038/cddis.2017.22

Smulski, C. R., Kury, P., Seidel, L. M., Staiger, H. S., Edinger, A. K., Willen, L., et al. (2017b). BAFF- and TACI-dependent processing of BAFFR by ADAM proteases regulates the survival of B cells. *Cell Rep.* 18, 2189–2202. doi: 10.1016/j.celrep.2017.02.005

Staniek, J., Lorenzetti, R., Heller, B., Janowska, I., Schneider, P., Unger, S., et al. (2019). TRAIL-R1 and TRAIL-R2 mediate TRAIL-dependent apoptosis in activated primary human B lymphocytes. *Front. Immunol.* 10, 471–413. doi: 10.3389/fimmu.2019.00951

Ting, A. T., and Bertrand, M. J. M. (2016). More to life than NF-κB in TNFR1 signaling. *Trends Immunol.* 37, 535–545. doi: 10.1016/j.it.2016.06.002

Vigolo, M., Chambers, M. G., Willen, L., Chevalley, D., Maskos, K., Lammens, A., et al. (2018). A loop region of BAFF controls B cell survival and regulates recognition by different inhibitors. *Nat. Commun.* 9:1199. doi: 10.1038/s41467-018-03323-8

Wagner, K. W., Punnoose, E. A., Januario, T., Lawrence, D. A., Pitti, R. M., Lancaster, K., et al. (2007). Death-receptor O-glycosylation controls tumor-cell sensitivity to the proapoptotic ligand Apo2L/TRAIL. *Nat. Med.* 13, 1070–1077. doi: 10.1038/nm1627

Yi, F., Frazzette, N., Cruz, A. C., Klebanoff, C. A., and Siegel, R. M. (2018). Beyond cell death: new functions for TNF family cytokines in autoimmunity and tumor immunotherapy. *Trends Mol. Med.* 24, 642–653. doi: 10.1016/j.molmed.2018.05.004

Conflict of Interest: The authors declare that the research was conducted in the absence of any commercial or financial relationships that could be construed as a potential conflict of interest.

frontiers in Cell and Developmental Biology

REVIEW
published: 05 May 2020
doi: 10.3389/fcell.2020.00314

CD95 Structure, Aggregation and Cell Signaling

Nicolas Levoin[1], Mickael Jean[2] and Patrick Legembre[3]**

[1] Bioprojet Biotech, Saint-Grégoire, France, [2] Univ Rennes, CNRS, ISCR-UMR 6226, Rennes, France, [3] INSERM U1262, CRIBL, Université de Limoges, Limoges, France

CD95 is a pre-ligand-associated transmembrane (TM) receptor. The interaction with its ligand CD95L brings to a next level its aggregation and triggers different signaling pathways, leading to cell motility, differentiation or cell death. This diversity of biological responses associated with a unique receptor devoid of enzymatic property raises the question of whether different ligands exist, or whether the fine-tuned control of CD95 aggregation and conformation, its distribution within certain plasma membrane sub-domains or the pattern of post-translational modifications account for this such broad-range of cell signaling. Herein, we review how the different domains of CD95 and their post-translational modifications or the different forms of CD95L can participate in the receptor aggregation and induction of cell signaling. Understanding how CD95 response goes from cell death to cell proliferation, differentiation and motility is a prerequisite to reveal novel therapeutic options to treat chronic inflammatory disorders and cancers.

Keywords: aggregation, apoptosis, Fas, inflammation, migration, stoichiometry

OPEN ACCESS

Edited by:
Olivier Micheau,
Université de Bourgogne, France

Reviewed by:
Inna N. Lavrik,
University Hospital Magdeburg, Germany
Fabien Picaud,
University of Franche-Comté, France
Ana Martin-Villalba,
German Cancer Research Center (DKFZ), Germany

****Correspondence:***
Nicolas Levoin
n.levoin@bioprojet.com
Patrick Legembre
patrick.legembre@inserm.fr;
plegembre@hotmail.com

Specialty section:
This article was submitted to Signaling, a section of the journal Frontiers in Cell and Developmental Biology

Received: *25 February 2020*
Accepted: *08 April 2020*
Published: *05 May 2020*

Citation:
Levoin N, Jean M and Legembre P (2020) CD95 Structure, Aggregation and Cell Signaling. Front. Cell Dev. Biol. 8:314. doi: 10.3389/fcell.2020.00314

INTRODUCTION

Many Tumor necrosis factor (TNF) receptor superfamily members display significant roles in the progression of human diseases, such as the death domain (DD)-containing receptors including CD95, TNF-related apoptosis-inducing ligand receptor (DR4 and DR5), TNFR1, DR3, DR6, nerve growth factor receptor (NGFR), and ectodysplasin receptor (EDAR, **Figure 1A**). These receptors are characterized by the presence of an intracellular DD, which is required for their apoptosis-inducing activity (Dostert et al., 2019). Several of them, including CD95 and TNFR1, are known to form multimers not only in the presence but also in the absence of their cognate trimeric ligands (Chan et al., 2000; Siegel et al., 2000), rendering complex to determine the nature and role of their aggregation in the cell signaling process. This review discusses how the CD95 stoichiometry is controlled by receptor-dependent and independent processes, and how stoichiometry can affect the implementation of apoptotic or non-apoptotic signals.

A UNIQUE CD95 RECEPTOR BUT AT LEAST TWO FORMS OF THE LIGAND

CD95

CD95 (also known as Fas, Apo-1, TNFRSF6) is a 319 amino acid type I transmembrane glycoprotein (Itoh et al., 1991; **Figure 1B**). In the presence of its ligand CD95L, the receptor interacts with

the adaptor protein Fas-associated protein with death domain (FADD) through homotypic DD-mediated interactions. FADD in turn recruits the protease caspase-8 and the long form of the regulator of apoptosis cellular FADD-like interleukin-1-β-converting enzyme-inhibitory protein ($cFLIP_L$) *via* death effector domain (DED) homotypic binding. Together, these proteins form a complex designated DISK for death-inducing signaling complex (Kischkel et al., 1995). The initial steps of CD95-DISK formation are quite well defined and some of them are shared with other death receptors of the TNFR superfamily.

Although initially described as a pure death receptor, CD95 undergoes a paradigm change, which might lead to a therapeutic revolution. Indeed, cumulative evidence support that CD95 is not only able to trigger a cell death signal but can also promote inflammation and normal and tumor cell growth and migration through the implementation of non-apoptotic cellular functions including PI3K, NFkB, and JNK MAPKs (Desbarats and Newell, 2000; Desbarats et al., 2003; Kleber et al., 2008; O' Reilly et al., 2009; Hoogwater et al., 2010; Tauzin et al., 2011; Gao et al., 2016; Poissonnier et al., 2016). Members of DISK including FADD and caspase-8 could also participate in the induction of these non-apoptotic cell signaling pathways (Barnhart et al., 2004; Kreuz et al., 2004). Notably, caspase-8 acts through its scaffolding function to drive cytokines production in various cancer cell lines upon CD95L stimulation (Henry and Martin, 2017). Production of pro-inflammatory chemokines in dying cells results in the recruitment of monocytes and neutrophils that engulf the dying cells expressing the "find me" signal (Cullen et al., 2013). How CD95L triggers these apoptotic and non-apoptotic signaling pathways and their respective biologic functions remain to be better understood.

CD95L

CD95 ligand also known as CD95L (FasL, TNFSF6 or CD178) is a type II transmembrane protein with a long cytoplasmic domain, a transmembrane (TM) domain, a stalk region, a TNF homology domain (THD) that mediates homotrimerization and a C-terminal region involved in CD95 binding (**Figure 1C**). The TM CD95L (membrane-CD95L or m-CD95L) can be cleaved in its stalk region by several matrix metalloproteases (MMPs) including MMP3, MMP7, MMP9, a disintegrin and metalloprotease-domain-containing protein (ADAM)-10 (Guegan and Legembre, 2018). The resulting soluble form of CD95L (s-CD95L) is a homotrimer (Tanaka et al., 1998) whose binding to CD95 fails to induce cell death (Suda et al., 1997; Schneider et al., 1998). Although the pathophysiological roles of s-CD95L remain to be elucidated, it accumulates in the bloodstream of patients suffering from a variety of diseases, including certain cancers such as NK cell lymphomas (Tanaka et al., 1996), ovarian cancers (De La Motte Rouge et al., 2019), and triple-negative breast cancer (TNBC) (Malleter et al., 2013). In TNBC women, high concentrations of s-CD95L are associated with the risk of relapse and metastatic dissemination (Malleter et al., 2013). s-CD95L levels are also elevated in inflammatory and autoimmune disorders such as systemic lupus erythematosus (SLE) (Tauzin et al., 2011; Poissonnier et al., 2016), rheumatoid arthritis (RA) (Hashimoto et al., 1998), and acute lung injury (ALI) (Herrero et al., 2011).

CD95 STRUCTURE

CD95 is detected homotrimerized independently of the presence of its ligand (Papoff et al., 1996; Siegel et al., 2000). Different domains in the death receptor seem to contribute to its aggregation, including the cytoplasmic DD (Ashkenazi and Dixit, 1998), TM and extracellular regions. Due to the TM nature, aggregation propensity and domain flexibility, the whole CD95 structure has not been solved yet. Nevertheless, 3D structures of some parts of the receptor have been deciphered by electron microscopy, X-ray crystallography or NMR spectroscopy (**Figure 2A**). Although CD95 structure has been extensively studied by these biophysical methods, the conformation of some important domains within the receptor, including a part of the pre-ligand assembly domain (PLAD) and the calcium-inducing domain (CID) (**Figures 1B**, **2A,B**) are absent from these pictures, precluding a comprehensive understanding of the CD95-mediated cell signaling.

Extracellular Region

The extracellular region of TNF receptors is characterized by the presence of cysteine-rich domains (CRDs), which contain six cysteine residues engaged in the formation of three disulfide bridges (Bodmer et al., 2002). The number of CRDs in a given receptor varies from one to four, and CD95 encompasses 3 CRDs (**Figures 1B**, **2C**; Bodmer et al., 2002). The repeated and regular arrangement of CRDs confers an elongated shape to the receptors. In the absence of stimulation, CD95 is found at the plasma membrane as monomers or homodimers and homotrimers associated through their respective extracellular N-terminal PLAD, encompassing the amino acid residues 17–82 (or amino acid residues 1–66 according to the mature protein) (Papoff et al., 1999; Siegel et al., 2000). Accordingly, the elimination of PLAD in DD-mutated CD95 constructs abrogates their dominant-negative inhibitory effect, while expression of PLAD alone exerts a dominant negative action on the CD95-mediated apoptotic signal (Papoff et al., 1999; Siegel et al., 2000). More precisely, the minimal domain required for CD95 homotypic interaction contains amino acids 59–82 (43–66 without the peptide signal) (Edmond et al., 2012).

The structure of CD95 extracellular domain (ECD) has been determined after complexation with a Fab fragment of agonistic (i.e., apoptotic) anti-CD95 antibodies, bound to the CRDs 1 and 2 (Chodorge et al., 2012). The CD95/Fab complex is monomeric (**Figure 2C**), and although the antibody is an agonist, it shares only a short region with the CD95/CD95L interface, mainly the arginine at position 102 (based on the human CD95 precursor sequence with 16 amino acids subtracted to obtain the position on the mature sequence corresponding to R86, see **Figure 1B**). CD95 ECD exhibits a linear organization and its putative orientation to the membrane is predicted based on the solved Holo trimeric

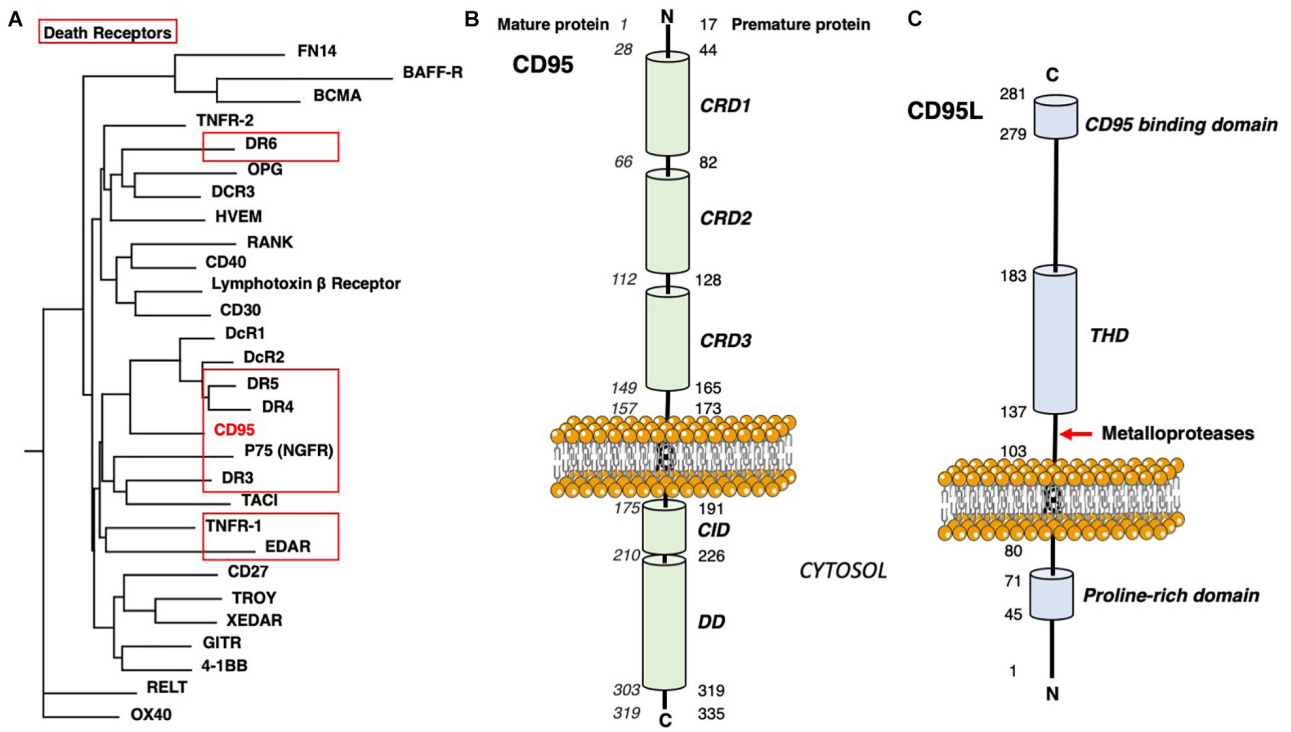

FIGURE 1 | CD95 domains. **(A)** Phylogenetic tree of human TNF receptors. DD-containing receptors are surrounded in red. Sequences were aligned with MAFFT 7 (Katoh and Standley, 2013) following L-INS-I strategy with BLOSUM 30 matrix, incorporating Mafft homologs and bootstrapping. MaxAlign option was used to increase the number of gap-free sites. The tree was built with Phylip 3.6 (Felsenstein, 1989) using a Neighbor-Joining method. **(B)** Main domains in the CD95 protein. **(C)** Main domains in the CD95L protein.

structure of other members of the TNFR family, including DcR3/CD95L (PDB:4MSV), DR5/TRAIL (1D0G), TNFR2/TNF (3ALQ), and DcR3/TL1A (3MI8). The PLAD residues consist of amino acids 17–82 (1–66 without the peptide signal) (Papoff et al., 1996; Siegel et al., 2000) and part of this region is missing from the X-ray data, i.e., amino acids arginine 17 (first amino acid following the peptide signal) to histidine 54 (**Figure 1B**). Also, the CD95 domains encompassing amino acid residues K148 to E156 and K164 to S170 are absent from X-ray and NMR analyses (**Figure 2A**). Threading approaches (Dunbrack, 2006) previously allowed us to build some plausible models of a completed ECD (including PLAD) in a trimeric organization (Levoin, 2017). However, in the present work focused on understanding of the trimeric assembly, we preferred not modeling a region whose structure is not strongly supported by experimental evidence. Therefore, to fill the two main gaps within the CD95 extracellular structure, we interrogated the PDB using PISA (Krissinel and Henrick, 2007) to find 3D homologs to the CD95 crystal structure (PDB : 3TJE). This method seems more appropriate than classical sequence-based screen, because sequence homology between DRs is rather low, and it is accepted that structure is more conserved than sequence (Murzin, 1998). Using this approach, we found that the structure of CD40 ECD (PDB : 3QD6) was close to that of CD95, with good geometric superposition and extended sequence solved (PISA Qscore = 0.55, with RMSD = 1.4 Å for 87 amino acids). Therefore, we completed the structure of CD95 protomer (residue N48 to E167, **Figure 2B**) using CD40 as a structural template. Afterward, each protomer served to assemble homotrimers through protein-protein docking, using SymmDock software (Schneidman-Duhovny et al., 2005b). We imposed a symmetric nature of the complex as a constraint, and the predicted four best solutions are presented **Figure 3**. These associations can be described as close Nt/remote Ct (model 1), close Nt/close Ct (model 2), remote Nt/close Ct (model 3), and remote Nt/remote Ct (model 4). The second solution is definitely the most compatible with biochemical data, because PLAD is known to be necessary and sufficient for receptor aggregation (Papoff et al., 1996; Siegel et al., 2000), and model 2 is the only one that orientates the amino terminal region in a way that can draw a large interface between PLADs. According to this computer-driven model, the interface between protomers occurred mostly between amino acid residues N48 to L52, K61 to P65 in CRD1, E114 to N118 in CRD2, R128 to V139 and C146 to E167 in CRD3. A noticeable structural feature of all trimer models is that protomers are tilted to the membrane, with an angle of about 45° for model 1 to 9° for model 2.

It is noteworthy that the homotypic PLAD affinity is rather low, almost in the mM range (Cao et al., 2011) suggesting that other domains in CD95 could exert a complementary role for the receptor homotrimerization, in agreement with the proposed trimeric model.

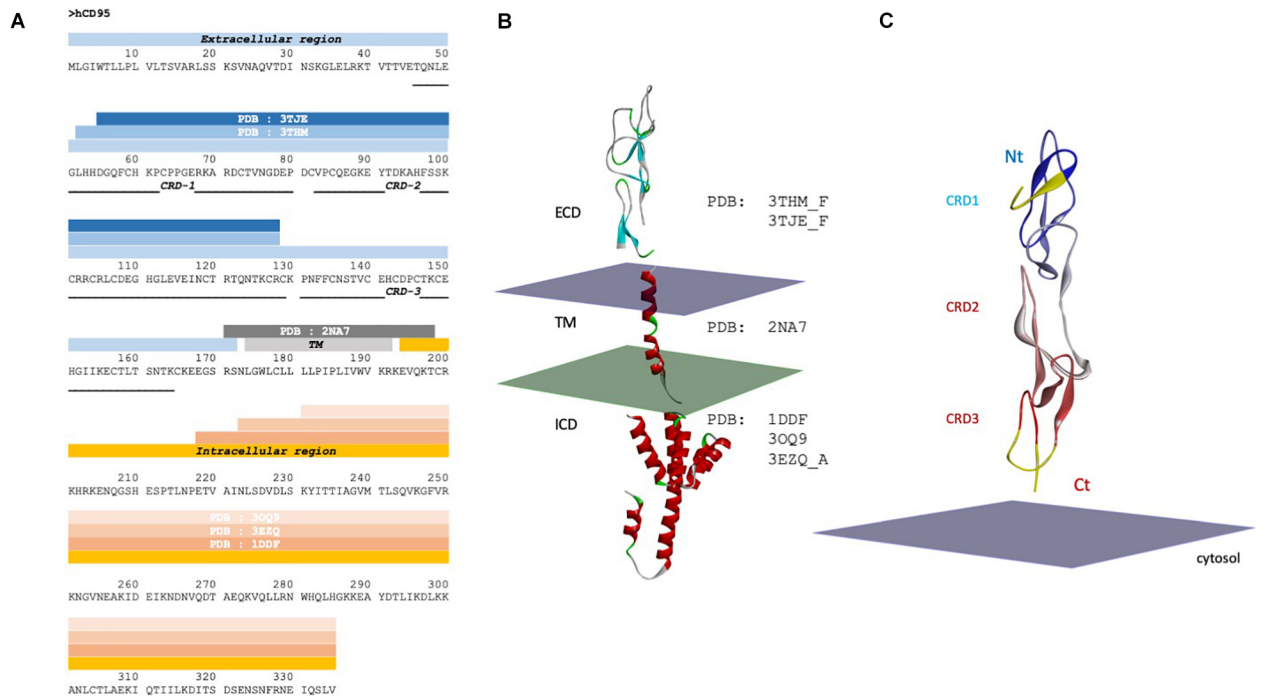

FIGURE 2 | CD95 sequence and structure. **(A)** Sequence of CD95 with solved 3D structures and corresponding PDB ID code. Blue, gray and orange strips represent the extracellular domain, the transmembrane domain and the intracellular region of CD95, respectively. CRD, cysteine rich domain; TM, transmembrane; ICD, intracellular domain; ECD, extracellular domain. **(B)** Domains of a monomeric CD95 whose structure has been experimentally solved. The plasma membrane is symbolized by two parallel planes, with the outer leaflet in purple and the cytosolic couleur in green. Note that the orientation toward membrane is a hypothesis. **(C)** Structure of the extracellular domain of CD95. Crystal structure of CD95 ECD domain (PDB:3TJE), colored according to the sequence order (blue to red, from Nt to Ct extremities). The yellow structure (amino acid residues N31 to D55) represents the gap in the crystal structure, which has been completed using CD40 homology. Nt: Amino-terminal region; Ct: COOH-terminal region.

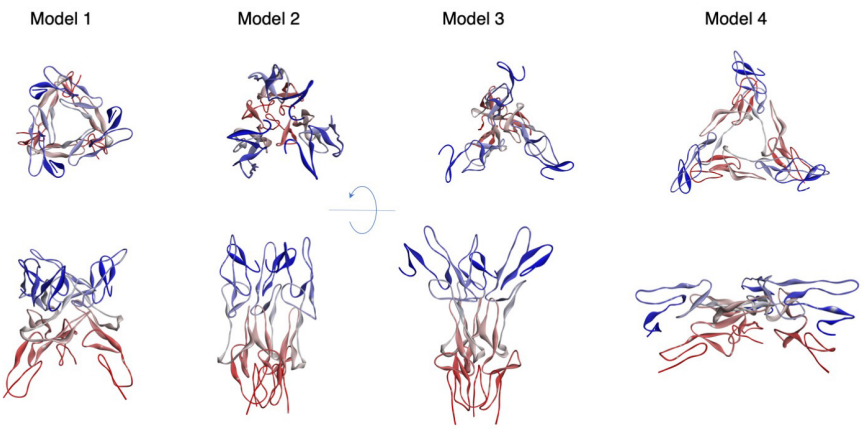

FIGURE 3 | Models of trimeric CD95 ECD. Four models of the trimeric Apo CD95 ECD are depicted according to their decreasing docking score from left to right. Trimers were obtained by protomer docking, performed with SymmDock (Schneidman-Duhovny et al., 2005a). Ct ends are depicted in red, while the CD95 Nt region is in blue.

Transmembrane Domain (TM)

Recent studies highlight that for several death receptors, the TM domain is involved in their aggregation. For example, DR5 TM helix promotes the assembly of high-order complexes responsible for cell death induction, independently of the ectodomain. Nuclear magnetic resonance (NMR) analysis of this TM region in bicelles shows different trimerization and dimerization interfaces responsible for a supramolecular dimer-trimer network (Pan et al., 2019). Surprisingly, elimination of the DR5 ECD triggers cell death in a TM-dependent and ligand (TRAIL)-independent

manner, suggesting that the extracellular region of DR5 exerts an inhibitory action on the receptor activation; TRAIL binding overcoming this auto-inhibitory process (Pan et al., 2019).

The CD95 TM domains have also been investigated by NMR in lipid/detergent bicelles (Fu et al., 2016) and these structures are found associated as stable trimers (**Figure 4A**). While the ends of the three helices display a certain flexibility, their core was more rigid (**Figure 4B**). The amino terminal portions of the helices (extracellular side) are closer and less flexible than their C-terminal counterparts (mean d1 = 9.7 ± 0.5 Å vs. d2 = 18.2 ± 2.6 Å, respectively, between L174 or V195 Cα of each protomer, for the 15 NMR structures). Unlike DR5, a proline motif is present in CD95 TM and in many members of the TNFR superfamily, including TNFR1, DR3, DR4, and CD40. This proline-rich sequence (P183 and P185 residues in the human sequence) within the CD95 TM helix favors packing of CD95 protomers through van der Waals interactions (Fu et al., 2016).

Transmembrane mutants affect the CD95L-mediated cell death program to a lesser extent than DD mutants (Fu et al., 2016). Indeed, co-expression of wild type and TM mutants does not disturb the formation of CD95 homotrimer in the absence of CD95L, indicating that the TM region of CD95 does not participate in its pre-ligand association (Fu et al., 2016). Nonetheless, CD95 TM domain probably stabilizes CD95 aggregation and/or conformation in the presence of CD95L because mutants within this domain impinge on the induction of apoptosis in cells exposed to CD95L (Fu et al., 2016).

Super-resolution microscopy data points out that monomers, dimers, and trimers of receptors co-exist on the plasma membrane before ligand binding, supporting that CD95 stoichiometry results from a dynamic equilibrium among oligomeric states (Fu et al., 2016), which could differ according to the expression level of the receptor itself and other factors that remain to be identified. Interestingly, somatic mutations exist in the human CD95 TM domain associated with malignancy, such as P183L associated with lymphoma or C178R mutation with squamous cell carcinoma (Tauzin et al., 2012) and these mutations abrogate the trimerization of TM domains in bicelles (Fu et al., 2016). Because TM mutants disrupting the CD95 homotrimerization impede the CD95L-induced apoptotic program, we can envision that this stoichiometry corresponds to its minimal arrangement required for induction of cell signaling.

Intracellular Domain (ICD)

Like other death receptors, CD95 does not possess any intrinsic enzymatic activity and thereby initiates signaling cascades by recruiting proteins through protein-protein interactions (PPIs) in a dynamic manner. Most of the intracellular domain (ICD) is constituted by a DD, a scaffolding unit recruiting FADD through homotypic interactions. FADD in turn is a hub that binds caspase-8 and c-FLIP (Ferrao and Wu, 2012), and this complex cooperatively activates the apoptotic program (Hughes et al., 2016).

The 3D structure of CD95 DD has been solved in complex with FADD by different teams (**Figures 5A,B**; Scott et al., 2009; Wang et al., 2010). Due to the different experimental conditions used in these studies, including low pH/high salt concentration vs. neutral pH and low salt concentration, and different methods (i.e., X-ray and NMR), the CD95 structures obtained are not completely superimposable (**Figure 5A**) and probably represent different conformational states of the domain. The X-ray structure of CD95 performed at pH 4 (Scott et al., 2009) reveals a dramatic shift in the carboxy-terminal region of the DD encompassing helices 5 and 6, resulting in the opening of the globular structure to render amino acids of the interface accessible to the FADD DD. This modification of the DD conformation was not detected in other X-ray studies of the CD95/FADD complex (Wang et al., 2010) or NMR analyses of CD95 alone (Huang et al., 1996) or combined with FADD (Esposito et al., 2010). Interestingly, mutations of residues within DD, which favor the opening of helix 6, enhance CD95-induced cell apoptosis, presumably because of an improved DISK formation. Unexpectedly, Driscoll's team showed that shifting pH from 6.2 to 4 causes the loss of CD95/FADD interaction (Esposito et al., 2010) weakening the conclusions drawn at low pH or suggesting that acidic conditions could affect the way CD95 implements cell signaling (Monet et al., 2016).

The first crystallized CD95-DD/FADD complex showed a tetrameric arrangement (4:4) mostly mediated by CD95 domains (**Figure 5C**; Scott et al., 2009). However, the predicted orientation toward the membrane renders this model hardly compatible with the full assembly of the receptors. Indeed, **Figure 5C**α illustrates that two chains of the tetramer are too far from the membrane. An alternative perpendicular orientation (**Figure 5C**β) seems also improbable for the same reason. Therefore, we suppose that this assembly results from crystal packing, and that a relevant biologic dimer is close to **Figure 5C**γ. The second crystal structure of CD95 DD showed an asymmetric oligomeric complex composed of 5 CD95 DDs and 5 FADDs (**Figure 5D**; Wang et al., 2010). This latter study revealed that half of the residues involved in CD95/CD95, CD95/FADD or FADD/FADD interfaces are positively or negatively charged, suggesting again a sensitivity to salts or pH for the formation of the aggregated complex and thereby signal induction. Although the structure of this complex matches with the data obtained using electron microscopy, it remains questionable because rebuilt from the supposed orientation shown in **Figure 5A**, the structure is asymmetric, and one DD penetrates the membrane (**Figure 5D**α). Optimization of the pentameric complex shows again a questionable asymmetry (**Figure 5D**β), even if the juxtamembrane region that we designated CID for Calcium-Inducing Domain (**Figure 1B**) is long and flexible enough to accommodate such a variability.

Calcium-inducing domain encompasses a 36 amino-acids sequence (amino acids K191 to D226), which is predicted to be disordered, explaining why it has never been solved by structural studies. Molecular modeling can, however, illuminate this structure at a single molecule level, showing that CID presented sparsely and transiently folded small α helix (Poissonnier et al., 2016). The role of this peptide in the DD conformation and orientation to the plasma membrane and thereby in the recruitment of FADD is difficult to predict.

While the DD (amino acid residues 210–303) is involved in cell death, the biological roles of the last 15 residues of

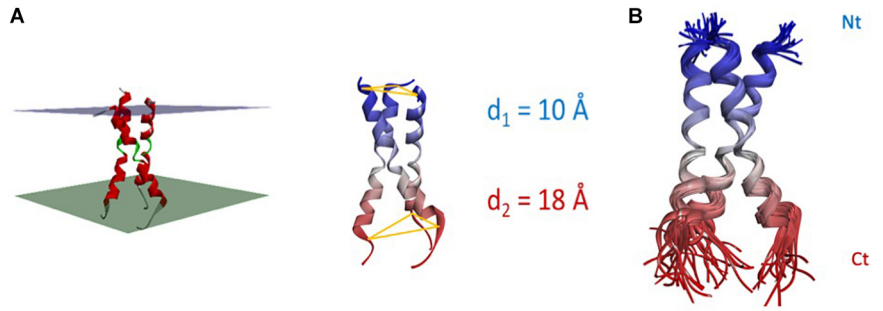

FIGURE 4 | Structure and flexibility of CD95 TM. **(A)** Left panel: NMR-based structure of the trimeric TM helices according to PDB: 2NA7. The helix bundle is virtually inserted in a membrane, whose thickness is a hypothesis. Right panel: the Nt interdistance is less wide than its Ct counterpart (d1 = 9.7 ± 0.5 Å vs. d2 = 18.2 ± 2.6 Å between L174 or V195 Cα, for the 15 NMR structures). **(B)** Superposition of the 15 NMR structures, showing that the core of the bundle is quite rigid, while both ends are more flexible.

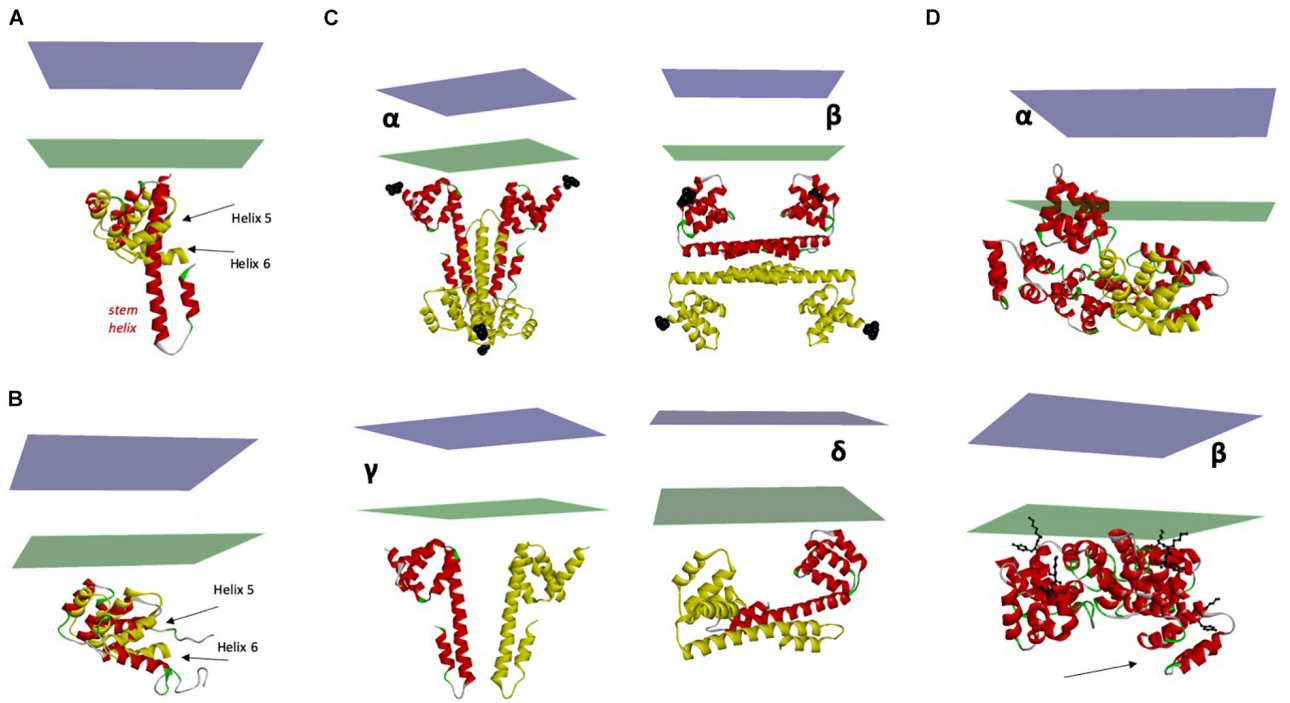

FIGURE 5 | Structure and flexibility of CD95 ICD. **(A)** Superimposition of the two crystal structures of CD95 death domain (PDB:3EZQ in red and PDB:3OQ9 in yellow). In addition to the displacement of its juxtamembrane region, note the transformation of the α helices 5 and 6 within the death domain into a long stem helix. **(B)** Superimposition of Holo and Apo structures of the CD95 death domain (PDB:3OQ9 in yellow and PDB:1DDF in red). Note that there is still a conformational rearrangement of helices 5 and 6, but with a limited amplitude. **(C)** Different X-ray structures of ICD and their orientation toward the plasma membrane. Panels α to δ: proposed orientations of the tetrameric crystal structure of CD95:FADD complex (only CD95 is depicted). The N-terminal region of the death domain starting at N223 is the closest residue to TM and is labeled with black spheres. Chains in red seem correctly oriented regarding the plasma membrane, but the orientation of chains in yellow renders the position of the tetramer improbable. Panels γ to δ: only the closest dimers to the membrane are considered. Drawing in γ represents the most probable orientation toward the membrane. **(D)** Orientation of the pentameric CD95-DD, taking as reference the protomer showed in **Figure 2B**. Note that using this model, one DD is inserted into the plasma membrane. β. Optimized orientation of the pentameric CD95-DD regarding the position of the amino terminal residues K231 and Y232 (black balls and sticks) to the plasma membrane. Note the asymmetry of the structure, particularly for chain **(A)** (arrow).

CD95 (amino acids 303–319) remain largely unknown. The protein tyrosine phosphatase FAP-1 (Sato et al., 1995) or Dlg1 (Gagnoux-Palacios et al., 2018) can interact with this carboxy-terminal region and inhibit cell death, through unknown molecular mechanisms.

In conclusion, 3D structures of CD95 combined with biochemical and cellular data suggest the existence of different conformations for CD95-DD but their roles in the recruitment of FADD or other partners and the implementation of cell signaling remain to be understood.

Reconstitution of a Whole CD95 ECD/TM Structure

Apo CD95

Superposition of the trimeric model 2 shown in **Figure 3** to the experimental TM bundle showed a near perfect alignment (**Figure 6A**). The only 3 residues lacking in the ECD (i.e., E_{168}GS) near the outer leaflet of the plasma membrane could form a short loop with a flexible glycine. This loop can easily fill the gap between ECD and TM, supporting our trimeric model 2. Indeed, the estimated distance between α carbon of each protomer of CD95 ECD at position E167 corresponds to 51 Å for model 1, 18 Å for model 2, 14 Å for model 3, and 64 Å for model 4, while trimeric NMR-based TM showed an average distance of 21 Å between α carbon at position R171 (Fu et al., 2016).

Holo CD95

The structure of the CD95L complexed with the decoy receptor DcR3 in a trimeric complex has been solved (Liu et al., 2016). Based on structural similarities, we superimposed our previously rebuilt CD95 ECD to DcR3 receptor, resulting in a trimeric CD95L/CD95 complex (**Figure 6B**). The homotrimeric Apo CD95 structure exhibits a packed conformation (**Figure 6A**), so a large opening of this quaternary structure is necessary to allow the insertion of the CD95L homotrimer (**Figure 6B**). In this Holo conformation, the structural organization of the CD95L/CD95 trimer reveals that the missing three amino acids of CD95 ECD cannot fill anymore the gap between ECD and TM, with a distance between α carbon of each ECD CD95 at position E167 of 39 Å (**Figure 6B**). This observation raises two hypotheses: either the distance of the TM bundle changes between Apo and Holo CD95 trimers, or CD95 CRD3 is very flexible and naturally pivots under CD95L to cover partially its bottom side, probably around the hinge formed by N132 (**Figure 6C**). The second scenario seems the most plausible, because, first, TM domain has to be trimeric to implement the apoptotic signaling pathway in the presence of CD95L (Fu et al., 2016), and second, the lack of electron density in the crystal structure of CD95 CRD3 suggests a flexible domain. Moreover, the slope of the CD95 ECD protomers inside the trimer is reminiscent of an inverted iris-like mechanism observed for certain channels and transporters (Yoder et al., 2018; McCarthy et al., 2019), in which the inducer engenders a small conformation change, echoed into a huge amplitude modification at the opposite end of the structure. Marchesi et al. (2018) recently theorized the mechanical lever effect of the iris-like motion, and concluded that this mechanism reduces by 3 the force required to open channels. If this iris-like mechanism permits an amplification of motion from ECD to TM in response to small extracellular ligands (i.e., cyclic nucleotide and ATP), an inverted physical principle might here switch an important extracellular movement (i.e., insertion of a large ligand) into a minimal TM perturbation. Based on this mechanism, the trimeric TM would not need to dissociate when CD95 ECD widely opens to accept the homotrimeric CD95L. Moreover, a small motion in the juxtamembrane hinge region (for example, E_{168}GS) should counterbalance the large shift of the PLAD domain (**Figure 6C**). In agreement with a movement of the CD95 juxtamembrane domain, we estimated in our model a distance of 7 Å between the CD95 residue S137 and its partner on CD95L (P206), which was shown critical for the interaction (Schneider et al., 1997). Because this distance is too important for an implication of P206 in CD95/CD95L interaction, the receptor requires to approach the ligand, either through CRD3 flexibility or by a rotation/rocking of the receptor protomer following the iris-like hypothesis. These conformational rearrangements will require further investigations using normal mode analysis (Wako and Endo, 2017) and molecular dynamics (Arroyo-Manez et al., 2011; Wang et al., 2018).

EXTERNAL FACTORS MEDIATED STOICHIOMETRY

CD95 Post-translational Modifications (PTMs)

CD95 can be glycosylated and different reports indicate that sialylation of asparagines 118 and 136 (corresponding to N102 and N120 in the human mature CD95 protein), improves the induction of the cell death program (Peter et al., 1995; Keppler et al., 1999). However, more recent data challenged the involvement of these glycosylations in the induction of cell death (Shatnyeva et al., 2011). Because the elimination of these glycosylations do not affect the stability or the plasma membrane expression of CD95 (Shatnyeva et al., 2011), it could be interesting in the future to explore the effect of these PTMs on the induction of the CD95-mediated non-apoptotic signaling pathways.

Several other PTMs affect the extent of oligomerization of CD95 prior to or following its interaction with CD95L. These include S-palmitoylation of the juxtamembrane cysteine at position 199 (Chakrabandhu et al., 2007; Feig et al., 2007) and S-nitrosylations on both C199 and C304 (Leon-Bollotte et al., 2011). S-glutathionylation of CD95 at cysteine 294 (mouse amino acid sequence) promotes its aggregation and subsequent caspase activation and apoptosis (Anathy et al., 2009). Glutaredoxins (Grxs) reverse this process. Therefore, reactive oxygen species (ROS) can enhance CD95-mediated caspase-8 activation, which in turn cleaves and inactivates Grx1, generating a positive feedback loop sealing the cell fate. Also, CD95 S-glutathionylation promotes its distribution into lipid rafts and its avidity for CD95L (Anathy et al., 2009). These results highlight that CD95 aggregation and signaling can be modulated by a redox-based mechanism.

Phosphorylation of CD95 on different serine/threonine and tyrosine (Y232 and Y291) within its intracellular region can modulate its signaling pathways (Chakrabandhu and Hueber, 2016). The replacement of Y291 by phenylalanine prevents recruitment of the AP-2 adaptor complex and the subsequent clathrin-mediated CD95 internalization but does not affect FADD binding and cell death induction (Lee et al., 2006). Interestingly, although this Y291 mutation inhibits the induction

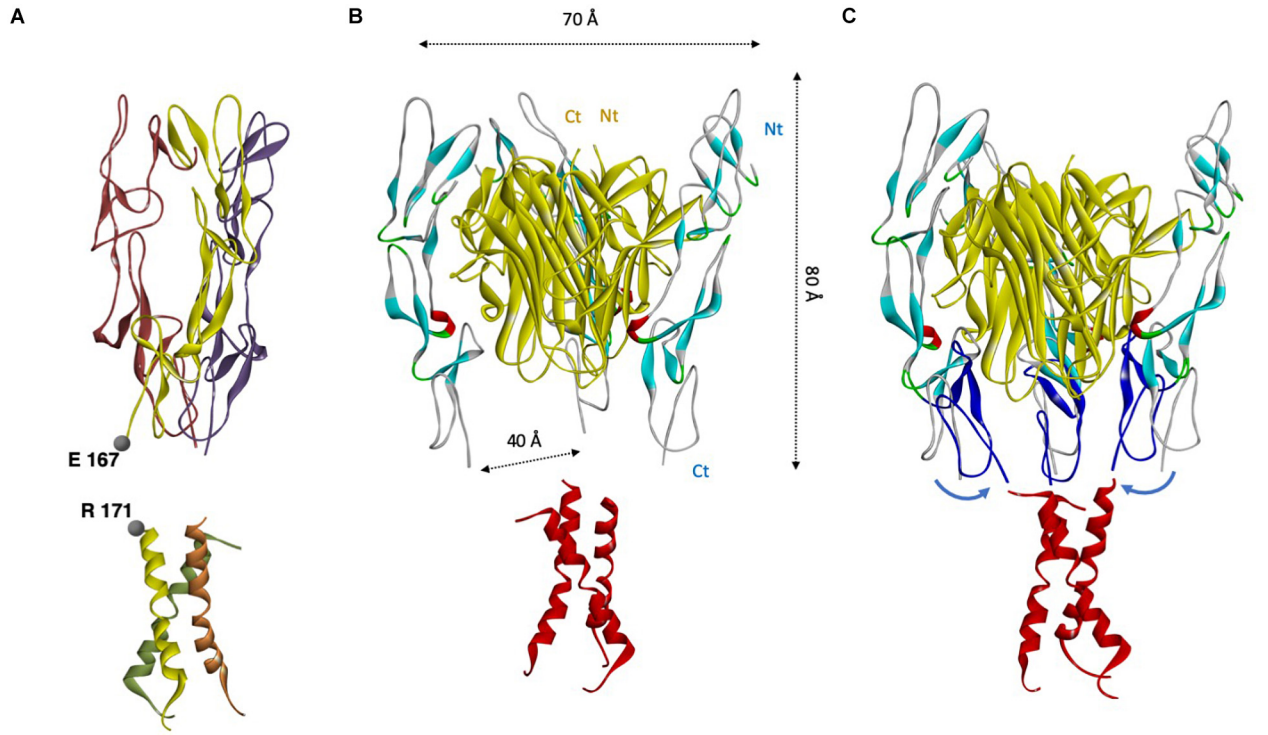

FIGURE 6 | CD95/CD95L complex and its association to the homotrimeric CD95 TM. **(A)** Manual alignment of trimeric Apo CD95 ECD model and experimental trimeric TM. Only residues E_{168}GS are missing, and ECD E167 and TM R171 appeared close. **(B)** CD95-ECD was rebuilt using CD40 structure as a template. Next, this protomer was geometrically superimposed to the DcR3 homotrimer structure interacting with homotrimeric CD95L (yellow) with Maestro, Schrödinger Inc. (optimization of the α carbons superposition, with a final RMSD of 7.5 Å between DcR3 and CD95). CD95 TM is depicted in red. **(C)** Unlike the Apo CD95-ECD, the Holo Ct ends of CD95-ECD are too remote (each Ct end is distant from 40 Å) to be connected to the Nt ends of CD95-TM (in red) by the only 3 missing amino acids. The most probable rearrangement following ligand binding is a rotation/rocking of the whole CRD3 depicted in navy blue around N132 (the resulting modeled position is in navy blue ribbons, marked by blue arrows).

of the apoptotic signaling pathway (Lee et al., 2006), it fails to alter the induction of non-apoptotic signals such as NF-KB and MAPK (Lee et al., 2006) suggesting that similarly to TNF-R1 signaling (Micheau and Tschopp, 2003), apoptotic and non-apoptotic machinery are assembled within different sub-cellular localizations.

In addition to receptor tyrosine kinases (RTKs) described below (see paragraph III-2), src-family kinases (SFKs) can phosphorylate tyrosines in CD95 leading to the inhibition of the apoptotic program and these phosphorylation marks might serve as poor prognostic markers in several types of cancer, including breast, ovarian, and colon cancers (Chakrabandhu et al., 2016). Of note, this Y291 phosphorylation can also recruit some phosphatases including SHP-1 and SHP-2 and SH2-containing inositol phosphatase (SHIP), whose activities counteract the granulocyte–macrophage colony-stimulating factor (GM-CSF)-mediated pro-survival signal in neutrophils (Daigle et al., 2002). In conclusion, phosphorylation of Y291 within DD of CD95 might participate in the inhibition of the CD95-mediated apoptotic pathway and at least in certain cells including neutrophils, might terminate the cytokine-mediated pro-survival signaling pathways rendering difficult to predict the role of this PTM in the cell fate.

CD95 ECD Partners

The tyrosine-protein kinase c-Met, also known as hepatocyte growth factor receptor (HGFR), can be associated with CD95, *via* a YLGA amino-acids sequence located in the N-terminal region of the c-Met α-chain (Wang et al., 2002), and CD95L also bears a ^{244}YLGA^{247} sequence. Nonetheless, the observed competition between c-Met and CD95L for CD95 interaction raises some questions because the YLGA-containing c-Met sequence (i) competes with CD95L for CD95 binding, despite the fact that the CD95/CD95L interface involves amino acid residues different from the CD95L YLGA sequence (Schneider et al., 1997) and (ii) seems to disrupt CD95 oligomerization even if the CD95/CD95 aggregation requires CRD1 (PLAD) and TM domains different from the CRD2 and CRD3 regions involved in CD95/CD95L interface. Therefore, it remains to better understand how c-Met and CD95 interact to elucidate how this receptor affects the CD95 signaling pathway.

Of note, an additional RTK, namely epidermal growth factor receptor (EGFR) has been linked to the modulation of the CD95-mediated signaling pathway. Accordingly, Haussinger's team reported that the hydrophobic bile salts can trigger cell death in hepatocytes through activation of EGFR, which induces CD95 tyrosine phosphorylation and implementation of cell death

(Reinehr et al., 2003a,b). By contrast, other groups established that the EGFR-induced MAPK pathway counteracts CD95-mediated apoptosis in hepatocyte cells exposed to bile salts (Qiao et al., 2001) and this RTK also inhibits the CD95-mediated apoptotic signaling pathway in glioma cells (Steinbach et al., 2002) rendering difficult to conclude on the role of EGFR in the modulation of the CD95-mediated cell death program. On the other hand, the presence of EGFR exerts a pivotal role in the induction of the CD95-mediated non-apoptotic signaling pathways. In the presence of CD95L, CD95 recruits EGFR to implement the PI3K signaling pathway in TNBC cells (Malleter et al., 2013) or the MAPK pathway (i.e., extracellular signal-regulated kinase) in hepatic stellate cells (HSCs) (Reinehr et al., 2008) and thereby promotes cell migration or proliferation, respectively.

Interestingly, a recent study highlighted the role of CD95 in sensing the cell survival of epithelial cells and thereby the maintain of tissue integrity (Gagnoux-Palacios et al., 2018). In adherens junction, the proximity of E-cadherin and α-catenin to CD95 favors the recruitment of Dlg1 to the C-terminal region of CD95 (Gagnoux-Palacios et al., 2018). Dlg1impinges on the DISK formation in cells exposed to m-CD95L and the loss of adherens junction will favor the release of this anti-apoptotic factor to promote cell death, a mechanism that could prevent metastatic dissemination of pre-tumor cells. Another method for adhesion molecules to control cell death has been also established for ICAM-2 (Perez et al., 2002). ICAM-2 over-expression or its interaction with leukocyte function-antigen-1 (LFA-1) induces ezrin phosphorylation by src tyrosine kinase and PI3K/AKT activation (Perez et al., 2002), which in turn impairs the induction of the CD95-mediated apoptotic program in leukocytes. This study points out that the PI3K activation by adhesion molecules can protect cells from apoptotic signal induced by death receptors.

Ion-Driven CD95 Stoichiometry

As aforementioned, upon addition of CD95L, CD95 undergoes conformational modification of its DD, inducing a shift of helix 6 and fusion with helix 5, promoting both oligomerization of the receptor and recruitment of the adaptor protein FADD (Scott et al., 2009). However, the idea of an elongated C-terminal α-helix favoring the *cis*-dimerization of CD95-DD in the acidic conditions (pH 4) was challenged by Driscoll and colleagues (Esposito et al., 2010) who did not observe the fusion of the last two helices at a more neutral pH (pH 6.2). These findings raise the question of whether a local decrease in intracellular pH might affect the CD95 conformation by promoting the opening of the CD95-DD and eventually by contributing to the formation of a complex that elicits a sequence of events distinct from what occurs at physiologic pH. Accordingly, we recently observed that CD95 activates the Na^+/H^+ exchanger 1 (NHE1) in the presence of s-CD95L (Monet et al., 2016). NHE1 catalyzes an electroneutral exchange of extracellular Na^+ for intracellular H^+, and its activity is necessary for cell migration (Putney et al., 2002; Frantz et al., 2007). While the presence of s-CD95L activates NHE1, no such modulation is observed in cells stimulated with a cytotoxic, multi-aggregated CD95L, suggesting that an acidic pH may surround the intracellular region of CD95 in cells stimulated with cytotoxic CD95L as compared to that in cells exposed to s-CD95L (Monet et al., 2016). This observation might explain how a drop of pH close to CD95 could promote a receptor conformation recruiting FADD and thereby, unleash the apoptotic signaling pathway.

By contrast, NHE1 activation by CD95 (Monet et al., 2016) alkalinizes the intracellular region and could prevent modification of DD helix 5 and 6 fusion (Scott et al., 2009). Of note, acidification can affect the protein conformation through the modulation of histidines as demonstrated for the phosphoinositide binding of cofilin, which is pH-dependent and decreases at high pH (Frantz et al., 2008). Interestingly, the intracellular region of CD95 encompasses four histidines and two of them (H282 and H285, i.e., H266 and H269 in the mature protein) are localized upstream helix 5 (Tauzin et al., 2012).

Lipid-Driven CD95 Stoichiometry

CD95 aggregation relies on the plasma membrane composition in lipids. Indeed, CD95 aggregation is slower in 1,2-dipalmitoyl-sn-glycero-3-phosphocholine (DPPC) than in 1,2-dioleoyl-sn-glycero-3-phosphocholine (DOPC), thereby the apoptotic program is faster in the latter lipid environment (Gulculer Balta et al., 2019). CD95 engagement triggers the accumulation of ceramide in a caspase-8-dependent manner, which in turn contributes to its aggregation and thereby favors the induction of cell death (Grassme et al., 2003). The initial stage of the CD95 response could be described as a two-step process, first requiring a certain degree of CD95 aggregation to secondarily promoting a caspase-8-driven intracellular signaling pathway that results in the aggregation and distribution of unstimulated CD95 into lipid rafts (Siegmund et al., 2017) which seems to favor the apoptotic response (Gajate et al., 2004). S-palmitoylation of CD95 (Chakrabandhu et al., 2007; Feig et al., 2007) appears to promote CD95 redistribution into lipid rafts (Muppidi and Siegel, 2004; Chakrabandhu et al., 2007).

Ligand-Mediated CD95 Stoichiometry

Two Ligands

Contrary to its receptor, CD95L is a type II transmembrane protein whose N-term extremity is in the cytoplasm (**Figure 1C**). The membrane-bound native CD95L (m-CD95L) can be processed by several proteases, including MMP3, MMP7, MMP9, and ADAM-10 (Tauzin et al., 2012), to release a soluble form of the ligand (s-CD95L) (**Figure 1C**). m-CD95L is responsible for the DISK assembly, whereas s-CD95L can trigger the formation of a different complex designated MISC (Malleter et al., 2013; Poissonnier et al., 2016). While most of the studies on s-CD95L report that this ligand possesses an homotrimeric stoichiometry, its membrane-bound counterpart shows a higher degree of aggregation such as large synapse of CD95L are observed between CD95L-expressing T-cells or NK cells and their cellular targets. Human CD95L self-association domain spans between amino acid residues 137–183 (Voss et al., 2008) and the last three amino acids are important for CD95 interaction (**Figure 1C**; Orlinick et al., 1997).

CD95L ectodomain contains three putative sites for N-linked glycosylation (N184, N250, and N260) and a lack of glycosylation alters the expression level of this ligand, probably by acting on its stability and/or intracellular trafficking (Schneider et al., 1997; Voss et al., 2008). Although CD95L/CD95 structure and surface plasmon resonance analyses reveal that CD95L glycosylation is not interfering with CD95 binding, the glycosylated ligand triggers a stronger cell death signal as compared to its sugar-free counterpart (Liu et al., 2016). While this difference of function has been associated with the fact that CD95L glycosylation might reduce the magnitude of its aggregation level (Liu et al., 2016), other studies showed no effect on the induction of cell death signal (Orlinick et al., 1997; Schneider et al., 1997; Voss et al., 2008), rendering difficult to conclude on the exact biological role played by the N-glycosylation of CD95L. Although O-glycosylation for DR5 (Wagner et al., 2007) and N-glycosylation for DR4 do not alter the intensity of their interaction with TRAIL (Dufour et al., 2017), these PTMs enhance the apoptotic signal through molecular mechanisms that remain to be elucidated (Micheau, 2018). A possible explanation could come from galectins, which are small proteins capable to bind to the β-galactoside sugars present in the extracellular region of TNF receptors family members. Of note, different galectins can bind and aggregate DR4, DR5, and CD95 and thereby, stimulate or inhibit cell death (Micheau, 2018) suggesting the subtle role played by glycosylation in the implementation of cell signaling by death receptors.

CD95 Ligands and Aggregation

The role of CD95L in the extend of CD95 aggregation is not clearly understood. Although most studies report that the metalloprotease-cleaved CD95L engenders homotrimer unable to induce cell death (Tanaka et al., 1996, 1998; Tauzin et al., 2011; Suda et al., 1997; Schneider et al., 1998) but instead triggers pro-inflammatory signaling pathways, in certain pathologies, a soluble CD95L is accumulated and reaches an aggregation level of CD95 allowing the implementation of the cell death program (Bajou et al., 2008; Herrero et al., 2011). Moreover, although the homotrimeric s-CD95L does not induce cell death, a recombinant and hexameric form does (Holler et al., 2003), supporting that the extent to which CD95L is multimerized is a pivotal step in determining whether non-apoptotic signaling or cell death is induced. Notably, some pathophysiological conditions could favor s-CD95L oligomerization, thereby promoting its cytotoxic activity. CD95L in the bronchoalveolar lavage (BAL) fluid of patients suffering from acute respiratory distress syndrome (ARDS) undergoes oxidation at methionines 224 and 225, promoting its aggregation and thereby rendering it cytotoxic (Herrero et al., 2011). In addition, in ARDS BAL fluid, another methionine oxidation occurs at position 121 within CD95 and prevents its cleavage by MMP7 which can explain why this cytotoxic ligand retains its stalk region (Herrero et al., 2011). Nonetheless, whether this corresponds to an alternatively cleaved form of s-CD95L with higher-level stoichiometry or a full-length exosome-bound m-CD95L remains to be elucidated.

The stoichiometry of CD95L can also be increased by external elements including fibronectin in the extracellular matrix (Aoki et al., 2001), rendering the inactive molecule apoptotic and raising the question of which domain within the soluble ligand interacts with fibronectin.

The different responses obtained with soluble and membrane-bound CD95L are a common feature among the TNF superfamily. For instance, while soluble TNF binds efficiently both TNFR1 and TNFR2, it stimulates TNFR1 signaling and induces cell death, but fails to trigger any response with TNFR2 (Grell et al., 1995). More importantly, the artificial oligomerization of soluble ligands restores the implementation of a classical response (Wajant, 2015) indicating that the ligand stoichiometry modulates the cell signaling in this superfamily. However, the difference between soluble and membrane-bound ligand signaling can be not so tremendous that what is observed for TNR2 or CD95. For instance, membrane TWEAK (TNF-like weak inducer of apoptosis) induces both alternative and classical NFκB pathways while soluble TWEAK only triggers the classical NFκB pathway (Wajant, 2015).

Agonistic Antibodies

An interesting study using a set of agonistic anti-CD95 antibodies revealed an inverse correlation between antibody affinity and cell death (Chodorge et al., 2012). A structure–function analysis disclosed that dissociation rate (Koff) of anti-CD95 antibodies is crucial for receptor activation because beyond affinity, dissociation of one antibody arm allows antibodies to bring together more CD95 monomers, forming a receptor cluster required to trigger cell death (Chodorge et al., 2012). These observations strengthen that the level of CD95 aggregation is important to induce the cell death process. However, the role of aggregation in the induction of non-apoptotic signaling pathways has not been investigated in this study and could be interesting to address.

DISCUSSION

Unsurprisingly, initial therapeutic solutions involving CD95 focused on the apoptotic pathway. Most of research efforts have dealt on deciphering the molecular basis of apoptosis induction by CD95 and considering the biological functions of CD95 in light of this role. Although non-apoptotic functions of CD95 (Alderson et al., 1993) have been reported soon after CD95 cloning (Itoh et al., 1991; Alderson et al., 1993), these have been largely neglected over the years. As a consequence, no CD95 agonists have become a standard of care in inflammatory disorders or cancers. It is now clear that CD95 can contribute to multiple biological functions, including inflammation and tumorigenesis through the induction of non-apoptotic signaling pathways. Accordingly, a CD95 decoy receptor blocking both the apoptotic and non-apoptotic signaling pathways, Asunercept (APG101), has nevertheless entered clinical trials for glioma and myelodysplastic syndrome (Wick et al., 2014; Boch et al., 2018).

Overall, the evidence that homotrimeric ligand can activate certain receptor-associated signaling pathways favors the concept

of a two-step model of TNFRSF activation. In a first step, there is ligand induced formation of homotrimeric TNFSF/TNFRSF complex, triggering some signaling pathways (mainly non-apoptotic signaling pathways). In a second step, there is multimerization of the homotrimeric complex through different mechanisms including oligomerization, transactivation, plasma membrane or microdomain redistribution/exclusion inducing different signaling pathways. Each of these steps constitute possible targets for therapeutic agents and should be scrutinized in future studies.

AUTHOR CONTRIBUTIONS

NL and PL designed the experiments (computer modeling) and wrote the manuscript. MJ wrote the manuscript.

FUNDING

This work was supported by the INCa PLBIO, Ligue Contre le Cancer, Fondation ARC, Fondation de France (Price Jean Valade), and ANR PRICE.

REFERENCES

Alderson, M. R., Armitage, R. J., Maraskovsky, E., Tough, T. W., Roux, E., Schooley, K., et al. (1993). Fas transduces activation signals in normal human T lymphocytes. *J. Exp. Med.* 178, 2231–2235. doi: 10.1084/jem.178.6.2231

Anathy, V., Aesif, S. W., Guala, A. S., Havermans, M., Reynaert, N. L., Ho, Y. S., et al. (2009). Redox amplification of apoptosis by caspase-dependent cleavage of glutaredoxin 1 and S-glutathionylation of Fas. *J. Cell Biol.* 184, 241–252. doi: 10.1083/jcb.200807019

Aoki, K., Kurooka, M., Chen, J. J., Petryniak, J., Nabel, E. G., and Nabel, G. J. (2001). Extracellular matrix interacts with soluble CD95L: retention and enhancement of cytotoxicity. *Nat. Immunol.* 2, 333–337. doi: 10.1038/86336

Arroyo-Manez, P., Bikiel, D. E., Boechi, L., Capece, L., Di Lella, S., Estrin, D. A., et al. (2011). Protein dynamics and ligand migration interplay as studied by computer simulation. *Biochim. Biophys. Acta* 1814, 1054–1064. doi: 10.1016/j.bbapap.2010.08.005

Ashkenazi, A., and Dixit, V. M. (1998). Death receptors: signaling and modulation. *Science* 281, 1305–1308. doi: 10.1126/science.281.5381.1305

Bajou, K., Peng, H., Laug, W. E., Maillard, C., Noel, A., Foidart, J. M., et al. (2008). Plasminogen activator inhibitor-1 protects endothelial cells from FasL-mediated apoptosis. *Cancer Cell* 14, 324–334. doi: 10.1016/j.ccr.2008.08.012

Barnhart, B. C., Legembre, P., Pietras, E., Bubici, C., Franzoso, G., and Peter, M. E. (2004). CD95 ligand induces motility and invasiveness of apoptosis-resistant tumor cells. *EMBO J.* 23, 3175–3185. doi: 10.1038/sj.emboj.7600325

Boch, T., Luft, T., Metzgeroth, G., Mossner, M., Jann, J. C., Nowak, D., et al. (2018). Safety and efficacy of the CD95-ligand inhibitor asunercept in transfusion-dependent patients with low and intermediate risk MDS. *Leuk. Res.* 68, 62–69. doi: 10.1016/j.leukres.2018.03.007

Bodmer, J. L., Schneider, P., and Tschopp, J. (2002). The molecular architecture of the TNF superfamily. *Trends Biochem. Sci.* 27, 19–26. doi: 10.1016/s0968-0004(01)01995-8

Cao, J., Meng, F., Gao, X., Dong, H., and Yao, W. (2011). Expression and purification of a natural N-terminal pre-ligand assembly domain of tumor necrosis factor receptor 1 (TNFR1 PLAD) and preliminary activity determination. *Protein J.* 30, 281–289. doi: 10.1007/s10930-011-9330-4

Chakrabandhu, K., Herincs, Z., Huault, S., Dost, B., Peng, L., Conchonaud, F., et al. (2007). Palmitoylation is required for efficient Fas cell death signaling. *EMBO J.* 26, 209–220. doi: 10.1038/sj.emboj.7601456

Chakrabandhu, K., Huault, S., Durivault, J., Lang, K., Ta Ngoc, L., Bole, A., et al. (2016). An evolution-guided analysis reveals a multi-signaling regulation of fas by tyrosine phosphorylation and its implication in human cancers. *PLoS Biol.* 14:e1002401. doi: 10.1371/journal.pbio.1002401

Chakrabandhu, K., and Hueber, A. O. (2016). Fas versatile signaling and beyond: pivotal role of tyrosine phosphorylation in context-dependent signaling and diseases. *Front. Immunol.* 7:429. doi: 10.3389/fimmu.2016.00429

Chan, F. K., Chun, H. J., Zheng, L., Siegel, R. M., Bui, K. L., and Lenardo, M. J. (2000). A domain in TNF receptors that mediates ligand-independent receptor assembly and signaling. *Science* 288, 2351–2354. doi: 10.1126/science.288.5475.2351

Chodorge, M., Zuger, S., Stirnimann, C., Briand, C., Jermutus, L., Grutter, M. G., et al. (2012). A series of Fas receptor agonist antibodies that demonstrate an inverse correlation between affinity and potency. *Cell Death Differ.* 19, 1187–1195. doi: 10.1038/cdd.2011.208

Cullen, S. P., Henry, C. M., Kearney, C. J., Logue, S. E., Feoktistova, M., Tynan, G. A., et al. (2013). Fas/CD95-induced chemokines can serve as "find-me" signals for apoptotic cells. *Mol. Cell* 49, 1034–1048. doi: 10.1016/j.molcel.2013.01.025

Daigle, I., Yousefi, S., Colonna, M., Green, D. R., and Simon, H. U. (2002). Death receptors bind SHP-1 and block cytokine-induced anti-apoptotic signaling in neutrophils. *Nat. Med.* 8, 61–67. doi: 10.1038/nm0102-61

De La Motte Rouge, T., Corne, J., Cauchois, A., Le Boulch, M., Poupon, C., Henno, S., et al. (2019). Serum CD95L level correlates with tumor immune infiltration and is a positive prognostic marker for advanced high-grade serous ovarian cancer. *Mol. Cancer Res.* 17, 2537–2548. doi: 10.1158/1541-7786.MCR-19-0449

Desbarats, J., Birge, R. B., Mimouni-Rongy, M., Weinstein, D. E., Palerme, J. S., and Newell, M. K. (2003). Fas engagement induces neurite growth through ERK activation and p35 upregulation. *Nat. Cell Biol.* 5, 118–125. doi: 10.1038/ncb916

Desbarats, J., and Newell, M. K. (2000). Fas engagement accelerates liver regeneration after partial hepatectomy. *Nat. Med.* 6, 920–923. doi: 10.1038/78688

Dostert, C., Grusdat, M., Letellier, E., and Brenner, D. (2019). The TNF family of ligands and receptors: communication modules in the immune system and beyond. *Physiol. Rev.* 99, 115–160. doi: 10.1152/physrev.00045.2017

Dufour, F., Rattier, T., Shirley, S., Picarda, G., Constantinescu, A. A., Morle, A., et al. (2017). N-glycosylation of mouse TRAIL-R and human TRAIL-R1 enhances TRAIL-induced death. *Cell Death Differ.* 24, 500–510. doi: 10.1038/cdd.2016.150

Dunbrack, R. L. Jr. (2006). Sequence comparison and protein structure prediction. *Curr. Opin. Struct. Biol.* 16, 374–384. doi: 10.1016/j.sbi.2006.05.006

Edmond, V., Ghali, B., Penna, A., Taupin, J. L., Daburon, S., Moreau, J. F., et al. (2012). precise mapping of the CD95 pre-ligand assembly domain. *PLoS One* 7:e46236. doi: 10.1371/journal.pone.0046236

Esposito, D., Sankar, A., Morgner, N., Robinson, C. V., Rittinger, K., and Driscoll, P. C. (2010). Solution NMR investigation of the CD95/FADD homotypic death domain complex suggests lack of engagement of the CD95 C terminus. *Structure* 18, 1378–1390. doi: 10.1016/j.str.2010.08.006

Feig, C., Tchikov, V., Schutze, S., and Peter, M. E. (2007). Palmitoylation of CD95 facilitates formation of SDS-stable receptor aggregates that initiate apoptosis signaling. *EMBO J.* 26, 221–231. doi: 10.1038/sj.emboj.7601460

Felsenstein, J. (1989). Mathematics vs. Evolution: mathematical evolutionary theory. *Science* 246, 941–942. doi: 10.1126/science.246.4932.941

Ferrao, R., and Wu, H. (2012). Helical assembly in the death domain (DD) superfamily. *Curr. Opin. Struct. Biol.* 22, 241–247. doi: 10.1016/j.sbi.2012.02.006

Frantz, C., Barreiro, G., Dominguez, L., Chen, X., Eddy, R., Condeelis, J., et al. (2008). Cofilin is a pH sensor for actin free barbed end formation: role of phosphoinositide binding. *J. Cell Biol.* 183, 865–879. doi: 10.1083/jcb.200804161

Frantz, C., Karydis, A., Nalbant, P., Hahn, K. M., and Barber, D. L. (2007). Positive feedback between Cdc42 activity and H+ efflux by the Na-H exchanger NHE1 for polarity of migrating cells. *J. Cell Biol.* 179, 403–410. doi: 10.1083/jcb.200704169

Fu, Q., Fu, T. M., Cruz, A. C., Sengupta, P., Thomas, S. K., Wang, S., et al. (2016). Structural basis and functional role of intramembrane trimerization of the Fas/CD95 death receptor. *Mol. Cell* 61, 602–613. doi: 10.1016/j.molcel.2016.01.009

Gagnoux-Palacios, L., Awina, H., Audebert, S., Rossin, A., Mondin, M., Borgese, F., et al. (2018). Cell polarity and adherens junction formation inhibit epithelial Fas cell death receptor signaling. *J. Cell Biol.* 217, 3839–3852. doi: 10.1083/jcb.201805071

Gajate, C., Del Canto-Janez, E., Acuna, A. U., Amat-Guerri, F., Geijo, E., Santos-Beneit, A. M., et al. (2004). Intracellular triggering of Fas aggregation and recruitment of apoptotic molecules into Fas-enriched rafts in selective tumor cell apoptosis. *J. Exp. Med.* 200, 353–365. doi: 10.1084/jem.20040213

Gao, L., Gulculer, G. S., Golbach, L., Block, H., Zarbock, A., and Martin-Villalba, A. (2016). Endothelial cell-derived CD95 ligand serves as a chemokine in induction of neutrophil slow rolling and adhesion. *eLife* 5:e18542. doi: 10.7554/eLife.18542

Grassme, H., Cremesti, A., Kolesnick, R., and Gulbins, E. (2003). Ceramide-mediated clustering is required for CD95-DISC formation. *Oncogene* 22, 5457–5470. doi: 10.1038/sj.onc.1206540

Grell, M., Douni, E., Wajant, H., Lohden, M., Clauss, M., Maxeiner, B., et al. (1995). The transmembrane form of tumor necrosis factor is the prime activating ligand of the 80 kDa tumor necrosis factor receptor. *Cell* 83, 793–802. doi: 10.1016/0092-8674(95)90192-2

Guegan, J. P., and Legembre, P. (2018). Nonapoptotic functions of Fas/CD95 in the immune response. *FEBS J.* 285, 809–827. doi: 10.1111/febs.14292

Gulculer Balta, G. S., Monzel, C., Kleber, S., Beaudouin, J., Balta, E., Kaindl, T., et al. (2019). 3D Cellular architecture modulates tyrosine kinase activity, thereby switching CD95-mediated apoptosis to survival. *Cell Rep.* 29, 2295–2306.e6. doi: 10.1016/j.celrep.2019.10.054

Hashimoto, H., Tanaka, M., Suda, T., Tomita, T., Hayashida, K., Takeuchi, E., et al. (1998). Soluble Fas ligand in the joints of patients with rheumatoid arthritis and osteoarthritis. *Arthritis Rheum.* 41, 657–662. doi: 10.1002/1529-0131(199804)41:4<657::aid-art12>3.0.co;2-n

Henry, C. M., and Martin, S. J. (2017). Caspase-8 acts in a non-enzymatic role as a scaffold for assembly of a pro-inflammatory "FADDosome" complex upon TRAIL stimulation. *Mol. Cell* 65, 715–729.e5. doi: 10.1016/j.molcel.2017.01.022

Herrero, R., Kajikawa, O., Matute-Bello, G., Wang, Y., Hagimoto, N., Mongovin, S., et al. (2011). The biological activity of FasL in human and mouse lungs is determined by the structure of its stalk region. *J. Clin. Invest.* 121, 1174–1190. doi: 10.1172/JCI43004

Holler, N., Tardivel, A., Kovacsovics-Bankowski, M., Hertig, S., Gaide, O., Martinon, F., et al. (2003). Two adjacent trimeric Fas ligands are required for Fas signaling and formation of a death-inducing signaling complex. *Mol. Cell Biol.* 23, 1428–1440. doi: 10.1128/mcb.23.4.1428-1440.2003

Hoogwater, F. J., Nijkamp, M. W., Smakman, N., Steller, E. J., Emmink, B. L., Westendorp, B. F., et al. (2010). Oncogenic K-Ras turns death receptors into metastasis-promoting receptors in human and mouse colorectal cancer cells. *Gastroenterology* 138, 2357–2367. doi: 10.1053/j.gastro.2010.02.046

Huang, B., Eberstadt, M., Olejniczak, E. T., Meadows, R. P., and Fesik, S. W. (1996). NMR structure and mutagenesis of the Fas (APO-1/CD95) death domain. *Nature* 384, 638–641. doi: 10.1038/384638a0

Hughes, M. A., Powley, I. R., Jukes-Jones, R., Horn, S., Feoktistova, M., Fairall, L., et al. (2016). Co-operative and hierarchical binding of c-FLIP and caspase-8: a unified model defines how c-FLIP isoforms differentially control cell fate. *Mol. Cell* 61, 834–849. doi: 10.1016/j.molcel.2016.02.023

Itoh, N., Yonehara, S., Ishii, A., Yonehara, M., Mizushima, S.-I., Sameshima, M., et al. (1991). The polypeptide encoded by the cDNA for human cell surface antigen Fas can mediate apoptosis. *Cell* 66, 233–243. doi: 10.1016/0092-8674(91)90614-5

Katoh, K., and Standley, D. M. (2013). MAFFT multiple sequence alignment software version 7: improvements in performance and usability. *Mol. Biol. Evol.* 30, 772–780. doi: 10.1093/molbev/mst010

Keppler, O. T., Peter, M. E., Hinderlich, S., Moldenhauer, G., Stehling, P., Schmitz, I., et al. (1999). Differential sialylation of cell surface glycoconjugates in a human B lymphoma cell line regulates susceptibility for CD95 (APO-1/Fas)-mediated apoptosis and for infection by a lymphotropic virus. *Glycobiology* 9, 557–569. doi: 10.1093/glycob/9.6.557

Kischkel, F. C., Hellbardt, S., Behrmann, I., Germer, M., Pawlita, M., Krammer, P. H., et al. (1995). Cytotoxicity-dependent APO-1 (Fas/CD95)-associated proteins form a death-inducing signaling complex (DISC) with the receptor. *EMBO J.* 14, 5579–5588. doi: 10.1002/j.1460-2075.1995.tb00245.x

Kleber, S., Sancho-Martinez, I., Wiestler, B., Beisel, A., Gieffers, C., Hill, O., et al. (2008). Yes and PI3K bind CD95 to signal invasion of glioblastoma. *Cancer Cell* 13, 235–248. doi: 10.1016/j.ccr.2008.02.003

Kreuz, S., Siegmund, D., Rumpf, J. J., Samel, D., Leverkus, M., Janssen, O., et al. (2004). NFkappaB activation by Fas is mediated through FADD, caspase-8, and RIP and is inhibited by FLIP. *J. Cell Biol.* 166, 369–380. doi: 10.1083/jcb.200401036

Krissinel, E., and Henrick, K. (2007). Inference of macromolecular assemblies from crystalline state. *J. Mol. Biol.* 372, 774–797. doi: 10.1016/j.jmb.2007.05.022

Lee, K. H., Feig, C., Tchikov, V., Schickel, R., Hallas, C., Schutze, S., et al. (2006). The role of receptor internalization in CD95 signaling. *EMBO J.* 25, 1009–1023. doi: 10.1038/sj.emboj.7601016

Leon-Bollotte, L., Subramaniam, S., Cauvard, O., Plenchette-Colas, S., Paul, C., Godard, C., et al. (2011). S-nitrosylation of the death receptor fas promotes fas ligand-mediated apoptosis in cancer cells. *Gastroenterology* 140, 2009–2018. doi: 10.1053/j.gastro.2011.02.053

Levoin, N. (2017). Sketching of CD95 oligomers by in silico investigations. *Methods Mol. Biol.* 1557, 153–171. doi: 10.1007/978-1-4939-6780-3_15

Liu, W., Ramagopal, U., Cheng, H., Bonanno, J. B., Toro, R., Bhosle, R., et al. (2016). Crystal structure of the complex of human FasL and its decoy receptor DcR3. *Structure* 24, 2016–2023. doi: 10.1016/j.str.2016.09.009

Malleter, M., Tauzin, S., Bessede, A., Castellano, R., Goubard, A., Godey, F., et al. (2013). CD95L cell surface cleavage triggers a prometastatic signaling pathway in triple-negative breast cancer. *Cancer Res.* 73, 6711–6721. doi: 10.1158/0008-5472.CAN-13-1794

Marchesi, A., Gao, X., Adaixo, R., Rheinberger, J., Stahlberg, H., Nimigean, C., et al. (2018). An iris diaphragm mechanism to gate a cyclic nucleotide-gated ion channel. *Nat. Commun.* 9:3978. doi: 10.1038/s41467-018-06414-8

McCarthy, A. E., Yoshioka, C., and Mansoor, S. E. (2019). Full-length P2X7 structures reveal how palmitoylation prevents channel desensitization. *Cell* 179, 659–670.e13. doi: 10.1016/j.cell.2019.09.017

Micheau, O. (2018). Regulation of TNF-related apoptosis-inducing ligand signaling by glycosylation. *Int. J. Mol. Sci.* 19:E715. doi: 10.3390/ijms19030715

Micheau, O., and Tschopp, J. (2003). Induction of TNF receptor I-mediated apoptosis via two sequential signaling complexes. *Cell* 114, 181–190. doi: 10.1016/s0092-8674(03)00521-x

Monet, M., Poet, M., Tauzin, S., Fouque, A., Cophignon, A., Lagadic-Gossmann, D., et al. (2016). The cleaved FAS ligand activates the Na(+)/H(+) exchanger NHE1 through Akt/ROCK1 to stimulate cell motility. *Sci. Rep.* 6:28008. doi: 10.1038/srep28008

Muppidi, J. R., and Siegel, R. M. (2004). Ligand-independent redistribution of Fas (CD95) into lipid rafts mediates clonotypic T cell death. *Nat. Immunol.* 5, 182–189. doi: 10.1038/ni1024

Murzin, A. G. (1998). How far divergent evolution goes in proteins. *Curr. Opin. Struct. Biol.* 8, 380–387. doi: 10.1016/s0959-440x(98)80073-0

O' Reilly, L. A., Tai, L., Lee, L., Kruse, E. A., Grabow, S., Fairlie, W. D., et al. (2009). Membrane-bound Fas ligand only is essential for Fas-induced apoptosis. *Nature* 461, 659–663. doi: 10.1038/nature08402

Orlinick, J. R., Elkon, K. B., and Chao, M. V. (1997). Separate domains of the human fas ligand dictate self-association and receptor binding. *J. Biol. Chem.* 272, 32221–32229. doi: 10.1074/jbc.272.51.32221

Pan, L., Fu, T. M., Zhao, W., Zhao, L., Chen, W., Qiu, C., et al. (2019). Higher-order clustering of the transmembrane anchor of DR5 drives signaling. *Cell* 176, 1477–1489.e14. doi: 10.1016/j.cell.2019.02.001

Papoff, G., Cascino, I., Eramo, A., Starace, G., Lynch, D. H., and Ruberti, G. (1996). An N-terminal domain shared by Fas/Apo-1 (CD95) soluble variants prevents cell death in vitro. *J. Immunol.* 156, 4622–4630.

Papoff, G., Hausler, P., Eramo, A., Pagano, M. G., Di Leve, G., Signore, A., et al. (1999). Identification and characterization of a ligand-independent oligomerization domain in the extracellular region of the CD95 death receptor. *J. Biol. Chem.* 274, 38241–38250. doi: 10.1074/jbc.274.53.38241

Perez, O. D., Kinoshita, S., Hitoshi, Y., Payan, D. G., Kitamura, T., Nolan, G. P., et al. (2002). Activation of the PKB/AKT pathway by ICAM-2. *Immunity* 16, 51–65. doi: 10.1016/s1074-7613(02)00266-2

Peter, M. E., Hellbardt, S., Schwartz-Albiez, R., Westendorp, M. O., Walczak, H., Moldenhauer, G., et al. (1995). Cell surface sialylation plays a role in modulating sensitivity towards APO-1-mediated apoptotic cell death. *Cell Death Differ.* 2, 163–171.

Poissonnier, A., Sanseau, D., Le Gallo, M., Malleter, M., Levoin, N., Viel, R., et al. (2016). CD95-mediated calcium signaling promotes T helper 17 trafficking to inflamed organs in lupus-prone mice. *Immunity* 45, 209–223. doi: 10.1016/j.immuni.2016.06.028

Putney, L. K., Denker, S. P., and Barber, D. L. (2002). The changing face of the Na+/H+ exchanger, NHE1: structure, regulation, and cellular actions. *Annu. Rev. Pharmacol. Toxicol.* 42, 527–552. doi: 10.1146/annurev.pharmtox.42.092001.143801

Qiao, L., Studer, E., Leach, K., Mckinstry, R., Gupta, S., Decker, R., et al. (2001). Deoxycholic acid (DCA) causes ligand-independent activation of epidermal growth factor receptor (EGFR) and FAS receptor in primary hepatocytes: inhibition of EGFR/mitogen-activated protein kinase-signaling module enhances DCA-induced apoptosis. *Mol. Biol. Cell.* 12, 2629–2645. doi: 10.1091/mbc.12.9.2629

Reinehr, R., Graf, D., and Haussinger, D. (2003a). Bile salt-induced hepatocyte apoptosis involves epidermal growth factor receptor-dependent CD95 tyrosine phosphorylation. *Gastroenterology* 125, 839–853. doi: 10.1016/s0016-5085(03)01055-2

Reinehr, R., Schliess, F., and Haussinger, D. (2003b). Hyperosmolarity and CD95L trigger CD95/EGF receptor association and tyrosine phosphorylation of CD95 as prerequisites for CD95 membrane trafficking and DISC formation. *FASEB J.* 17, 731–733. doi: 10.1096/fj.02-0915fje

Reinehr, R., Sommerfeld, A., and Haussinger, D. (2008). CD95 ligand is a proliferative and antiapoptotic signal in quiescent hepatic stellate cells. *Gastroenterology* 134, 1494–1506. doi: 10.1053/j.gastro.2008.02.021

Sato, T., Irie, S., Kitada, S., and Reed, J. C. (1995). FAP-1: a protein tyrosine phosphatase that associates with Fas. *Science* 268, 411–415. doi: 10.1126/science.7536343

Schneider, P., Bodmer, J. L., Holler, N., Mattmann, C., Scuderi, P., Terskikh, A., et al. (1997). Characterization of Fas (Apo-1, CD95)-Fas ligand interaction. *J. Biol. Chem.* 272, 18827–18833. doi: 10.1074/jbc.272.30.18827

Schneider, P., Holler, N., Bodmer, J. L., Hahne, M., Frei, K., Fontana, A., et al. (1998). Conversion of membrane-bound Fas(CD95) ligand to its soluble form is associated with downregulation of its proapoptotic activity and loss of liver toxicity. *J. Exp. Med.* 187, 1205–1213. doi: 10.1084/jem.187.8.1205

Schneidman-Duhovny, D., Inbar, Y., Nussinov, R., and Wolfson, H. J. (2005a). Geometry-based flexible and symmetric protein docking. *Proteins* 60, 224–231. doi: 10.1002/prot.20562

Schneidman-Duhovny, D., Inbar, Y., Nussinov, R., and Wolfson, H. J. (2005b). PatchDock and SymmDock: servers for rigid and symmetric docking. *Nucleic Acids Res.* 33, W363–W367.

Scott, F. L., Stec, B., Pop, C., Dobaczewska, M. K., Lee, J. J., Monosov, E., et al. (2009). The Fas-FADD death domain complex structure unravels signalling by receptor clustering. *Nature* 457, 1019–1022. doi: 10.1038/nature07606

Shatnyeva, O. M., Kubarenko, A. V., Weber, C. E., Pappa, A., Schwartz-Albiez, R., Weber, A. N., et al. (2011). Modulation of the CD95-induced apoptosis: the role of CD95 N-glycosylation. *PLoS One* 6:e19927. doi: 10.1371/journal.pone.0019927

Siegel, R. M., Frederiksen, J. K., Zacharias, D. A., Chan, F. K., Johnson, M., Lynch, D., et al. (2000). Fas preassociation required for apoptosis signaling and dominant inhibition by pathogenic mutations. *Science* 288, 2354–2357. doi: 10.1126/science.288.5475.2354

Siegmund, D., Lang, I., and Wajant, H. (2017). Cell death-independent activities of the death receptors CD95, TRAILR1, and TRAILR2. *FEBS J.* 284, 1131–1159. doi: 10.1111/febs.13968

Steinbach, J. P., Supra, P., Huang, H. J., Cavenee, W. K., and Weller, M. (2002). CD95-mediated apoptosis of human glioma cells: modulation by epidermal growth factor receptor activity. *Brain Pathol.* 12, 12–20. doi: 10.1111/j.1750-3639.2002.tb00418.x

Suda, T., Hashimoto, H., Tanaka, M., Ochi, T., and Nagata, S. (1997). Membrane Fas ligand kills human peripheral blood T lymphocytes, and soluble Fas ligand blocks the killing. *J. Exp. Med.* 186, 2045–2050. doi: 10.1084/jem.186.12.2045

Tanaka, M., Itai, T., Adachi, M., and Nagata, S. (1998). Downregulation of Fas ligand by shedding. *Nat. Med.* 4, 31–36. doi: 10.1038/nm0198-031

Tanaka, M., Suda, T., Haze, K., Nakamura, N., Sato, K., Kimura, F., et al. (1996). Fas ligand in human serum. *Nat. Med.* 2, 317–322.

Tauzin, S., Chaigne-Delalande, B., Selva, E., Khadra, N., Daburon, S., Contin-Bordes, C., et al. (2011). The naturally processed CD95L elicits a c-yes/calcium/PI3K-driven cell migration pathway. *PLoS Biol.* 9:e1001090. doi: 10.1371/journal.pbio.1001090

Tauzin, S., Debure, L., Moreau, J. F., and Legembre, P. (2012). CD95-mediated cell signaling in cancer: mutations and post-translational modulations. *Cell. Mol. Life Sci.* 69, 1261–1277. doi: 10.1007/s00018-011-0866-4

Voss, M., Lettau, M., Paulsen, M., and Janssen, O. (2008). Posttranslational regulation of Fas ligand function. *Cell Commun. Signal.* 6:11. doi: 10.1186/1478-811X-6-11

Wagner, K. W., Punnoose, E. A., Januario, T., Lawrence, D. A., Pitti, R. M., Lancaster, K., et al. (2007). Death-receptor O-glycosylation controls tumor-cell sensitivity to the proapoptotic ligand Apo2L/TRAIL. *Nat. Med.* 13, 1070–1077. doi: 10.1038/nm1627

Wajant, H. (2015). Principles of antibody-mediated TNF receptor activation. *Cell Death Differ.* 22, 1727–1741. doi: 10.1038/cdd.2015.109

Wako, H., and Endo, S. (2017). Normal mode analysis as a method to derive protein dynamics information from the protein data bank. *Biophys. Rev.* 9, 877–893. doi: 10.1007/s12551-017-0330-2

Wang, L., Yang, J. K., Kabaleeswaran, V., Rice, A. J., Cruz, A. C., Park, A. Y., et al. (2010). The Fas-FADD death domain complex structure reveals the basis of DISC assembly and disease mutations. *Nat. Struct. Mol. Biol.* 17, 1324–1329. doi: 10.1038/nsmb.1920

Wang, X., Defrances, M. C., Dai, Y., Pediaditakis, P., Johnson, C., Bell, A., et al. (2002). A mechanism of cell survival: sequestration of Fas by the HGF receptor Met. *Mol. Cell* 9, 411–421.

Wang, Y., Bugge, K., Kragelund, B. B., and Lindorff-Larsen, K. (2018). Role of protein dynamics in transmembrane receptor signalling. *Curr. Opin. Struct. Biol.* 48, 74–82. doi: 10.1016/j.sbi.2017.10.017

Wick, W., Fricke, H., Junge, K., Kobyakov, G., Martens, T., Heese, O., et al. (2014). A phase II, randomized, study of weekly APG101+reirradiation versus reirradiation in progressive glioblastoma. *Clin. Cancer Res.* 20, 6304–6313. doi: 10.1158/1078-0432.CCR-14-0951-T

Yoder, N., Yoshioka, C., and Gouaux, E. (2018). Gating mechanisms of acid-sensing ion channels. *Nature* 555, 397–401. doi: 10.1038/nature25782

Conflict of Interest: The authors declare that the research was conducted in the absence of any commercial or financial relationships that could be construed as a potential conflict of interest.

The handling Editor declared a past co-authorship with one of the authors PL.

frontiers in Cell and Developmental Biology

ORIGINAL RESEARCH
published: 19 May 2020
doi: 10.3389/fcell.2020.00318

Death Receptor 5 Displayed on Extracellular Vesicles Decreases TRAIL Sensitivity of Colon Cancer Cells

*Rita Setroikromo†, Baojie Zhang†, Carlos R. Reis, Rima H. Mistry and Wim J. Quax**

Department of Chemical and Pharmaceutical Biology, Groningen Research Institute of Pharmacy, University of Groningen, Groningen, Netherlands

Tumor necrosis factor–related apoptosis inducing ligand (TRAIL) is considered to be a promising antitumor drug because of its selective proapoptotic properties on tumor cells. However, the clinical application of TRAIL is until now limited because of the resistance of several cancer cells, which can occur at various levels in the TRAIL signaling pathway. The role of decoy receptors that can side-track TRAIL, thereby preventing the formation of an activated death receptor, has been extensively studied. In this study, we have focused on extracellular vesicles (EVs) that are known to play a role in cell-to-cell communication and that can be released by donor cells into the medium transferring their components to recipient cells. TRAIL-induced apoptotic signaling is triggered upon the binding of two death receptors, DR4 and DR5. Here, we found that DR5 but not DR4 is present in the conditioned medium (CM)–derived from various cancer cells. Moreover, we observed that DR5 was exposed on EVs and can act as "decoy receptor" for binding to TRAIL. This results in a strongly reduced number of apoptotic cells upon treatment with DR5-specific TRAIL variant DHER in CM. This reduction happened with EVs containing either the long or short isoform of DR5. Taken together, we demonstrated that colon rectal tumor cells can secrete DR5-coated EVs, and this can cause TRAIL resistance. This is to our knowledge a novel finding and provides new insights into understanding TRAIL sensitivity.

Keywords: extracellular vesicles, DR5, TRAIL, apoptosis, conditioned medium, receptor–ligand trafficking

OPEN ACCESS

Edited by:
Olivier Micheau, Université de Bourgogne, France

Reviewed by:
Marine Eduard Gasparian, Institute of Bioorganic Chemistry (RAS), Russia
Ladislav Andera, Institute of Molecular Genetics (ASCR), Czechia

***Correspondence:**
Wim J. Quax
w.j.quax@rug.nl

† These authors have contributed equally to this work

Specialty section:
This article was submitted to Signaling, a section of the journal Frontiers in Cell and Developmental Biology

Received: *24 January 2020*
Accepted: *09 April 2020*
Published: *19 May 2020*

Citation:
Setroikromo R, Zhang B, Reis CR, Mistry RH and Quax WJ (2020) Death Receptor 5 Displayed on Extracellular Vesicles Decreases TRAIL Sensitivity of Colon Cancer Cells. Front. Cell Dev. Biol. 8:318. doi: 10.3389/fcell.2020.00318

INTRODUCTION

The secretion of extracellular vesicles (EVs) is an evolutionally conserved process spanning from bacteria to humans and plants (Rivera et al., 2010; Van Niel et al., 2018; Cui et al., 2019). The significance of EVs on the one hand relates to their capacity to eliminate unwanted components from the cell and on the other hand to their capability to communicate with other cells by exchanging components–from DNA to protein–and thereby influencing the signal transduction pathways of target cells (Colombo et al., 2014; Yáñez-Mó et al., 2015). They are highly heterogeneous and can be broadly divided into two main categories based on their biogenesis and characterizations (Colombo et al., 2014; Van Niel et al., 2018). The term *exosomes* (30–100 nm) was first used to describe the EVs released by reticulocytes during differentiation

(Johnstone et al., 1987). It originates from inward budding of endosome membrane creating the so-called cargo-containing intraluminal vesicle (ILV) inside the early endosome. These early endosomes can either be directed to the lysosomes or fused together and mature to the late multivesicular endosomes (MVEs). MVEs when fused with cell membrane can release their cargo-containing ILV in the extracellular space, and these small vesicles are called exosomes (McGough and Vincent, 2016). The other group of EVs is named microvesicles (50–1,000 nm, up to 10 μm), which are directly formed after budding or fission of plasma membrane in response to diverse cell stimulation; this includes the apoptotic bodies. Owing to their varied compositions, increasing evidence shows that EVs act as signaling vesicles not only in normal cell homeostasis but also in many pathological conditions (Cocucci et al., 2009).

Cancer is a diverse group of diseases caused by proliferating cells traditionally treated with chemotherapy and/or radiotherapy. These, however, also give harmful side effects to healthy cells. More preferred therapeutics are being developed in such a way that they selectively target cancer cells and treatment with tumor necrosis factor–related apoptosis inducing ligand (TRAIL) is considered to be promising because of its naturally proapoptotic properties specifically directed to cancer cells (Wong et al., 2019). Binding of TRAIL to two death receptors (DR4 and DR5) triggers the recruitment of Fas-associated death domain and subsequent pro–caspase-8. This complex, also known as death-inducing signaling complex (DISC), will initiate downstream caspase-dependent apoptotic signaling and eventually leads to cell death (Nagata, 1997). Although cancer cells are more prone to TRAIL-induced cell death than normal cells, this signaling pathway can be interrupted by many other factors that lead to resistance in several cancer cells. For instance, three decoy receptors (DcR1, DcR2, and OPG) can also bind to TRAIL and thereby decrease the availability of free TRAIL for the binding to the death receptors, leading to inhibition of apoptosis (Mahalingam et al., 2009). Despite the importance of this classical ligand–receptor binding to induce apoptosis, ligand-induced receptor internalization, and/or intercellular receptor trafficking are also important for adequate transduction of the apoptosis signaling. Likewise, nuclear localization of DR5 by importin β1 decreases TRAIL-induced cell death in human tumor cells (Kojima et al., 2011). The presence of death receptors in autophagosomes rather than plasma prevents TRAIL-induced apoptosis in breast cancer cells (Di et al., 2013). In addition, the surface levels of DR4 are controlled by MARCH-8–mediated ubiquitination, which results in differential endosomal trafficking of surface DR4 and DR5, and thereby regulates the resistance to TRAIL (Van De Kooij et al., 2013). Given the evidences that degradation and secretion of death receptors are important for the extent of the apoptosis signaling, we want to know if death receptors are secreted and expressed on the surface of EVs.

In this study, we demonstrate that DR5 molecules are on the surface of EVs, and these can compete with the DR5 on target cells for TRAIL binding, leading to a decrease of the apoptosis signaling. These findings contribute a new insight into mechanisms of TRAIL resistance.

MATERIALS AND METHODS

Cell Lines and Culture Conditions

Human colorectal carcinoma cell lines (Colo205, HCT 116, and DLD-1), human Burkitt lymphoma B cell line (BJAB), and the Chinese hamster ovary cell line (CHO) were cultured in RPMI1640 medium supplemented with 10% fetal bovine serum, 100 U/mL penicillin, and 100 μg/mL streptomycin in a humidified incubator at 37°C with 5% CO_2. All materials mentioned above were purchased from Thermo Fisher Scientific (Waltham, MA, United States). BJAB cell lines, the wild-type cells BJAB (BJAB WT), BJAB overexpressing DR5 (BJAB DR5), and a deficient DR5 short isoform (BJAB DR5s DEF) were kindly provided by Dr. Andrew Thornburn (University of Colorado Health Sciences Centre, Aurora, CO, United States). CHO cell lines, the wild-type cells (CHO WT), a mutant overexpressing DR5 long isoform (CHO TV1), and a mutant overexpressing DR5 short isoform (CHO TV2) were provided by Organon (Oss, Netherlands).

Reagents

Soluble (aa 114–281) wild-type TRAIL (TRAIL WT), DR4-specific TRAIL variant (4C7), and DR5-specific TRAIL variant (DHER) were constructed and produced as previously described (Van Der Sloot et al., 2006; Reis et al., 2010).

Collecting Conditioned Medium and Isolation of EVs

Cells were cultured at the concentration of 150,000 cells/mL in exosome-free medium for 48 h in humidified incubator at 37°C with 5% carbon dioxide. Medium was collected and spun down at 250 *g* for 10 min to discard the floating cells. This supernatant is from now on called conditioned medium (CM). EVs were isolated by differential centrifugation strategy: first, sedimentation of CM at 3,000 *g* for 15 min; second, sedimentation of the supernatant at 17,000 *g* for 20 min; and finally with ultracentrifugation at 30,000 *g* for 3 h. From the last run, the pellet was used as EVs and resuspended in phosphate-buffered saline (PBS) and stored at −80°C.

Cell Viability Assay

Cell viability assays were conducted using MTS assay. Cells were seeded in triplicate in 96-well plates at the density of 10,000 cells/mL in medium and incubated in a humidified incubator at 37°C with 5% CO_2. The following day, cells were treated with TRAIL WT or variants for 24 h, and assayed for viability with MTS reagent according to the manufacturer's instruction (Promega, Madison, WI, United States). The cell viability was determined by measuring the absorbance at 490 nm using a microplate reader (Thermo Labsystems, Helsinki, Finland).

Western Blot

Cells were harvested and lysed with RIPA buffer supplemented with EDTA-free proteinase inhibitor cocktail (Roche, Basel, Switzerland). Samples were loaded on precast 4 to 12% sodium dodecyl sulfate–polyacrylamide gel electrophoresis gels (Thermo

Fisher Scientific) and transferred onto 0.45 μm nitrocellulose membrane. Next, the membranes were blocked for 1 h at room temperature in 5% non-fat milk and probed overnight at 4°C. The following primary antibodies were used: DR5 (Sigma, Zwijndrecht, Netherlands), DR4 (Imgenix, Cambridge, United Kingdom), histone H2A (Abcam, Cambridge, United Kingdom), and CD63 (Pharmingen, San Diego, CA, United States). After incubating with secondary antibodies, membranes were detected using Pierce ECL kit (Thermo Fisher Scientific).

Apoptotic Assay

Apoptosis induction was measured using annexin V–fluorescein isothiocyanate (FITC) staining and quantified by flow cytometry. Cells were seeded in six-well plates overnight prior to the treatment. The next day, cells were treated with TRAIL variant for 24 h. After treatment, cells were collected, washed with PBS twice, and incubated for 20 min with annexin V–FITC solution on ice. The cells were analyzed using a FACS Calibur flow cytometer (BD Biosciences, Franklin Lakes, NJ, United States).

Detection of DRs on EVs by Transmission Electron Microscopy

The isolated EV suspension was incubated with DR5 antibody (ENZO life sciences, Bruxelles, Belgium) and placed as a drop gently on formvar/carbon-coated nickel grid for 60 min. The grids were washed three times with 0.1% exosome-free bovine serum albumin PBS solution and incubated for 10 min in 2% paraformaldehyde. The grids were washed three times with PBS and incubated for 40 min with secondary antibody conjugated with 10-nm gold particles. The grids were washed 3 times with PBS and post fixated with 2.5% glutaraldehyde for 10 min and 2% uranyl acetate for 15 min. The excess liquid was gently removed from the grids and dried before analyzing under transmission electron microscope.

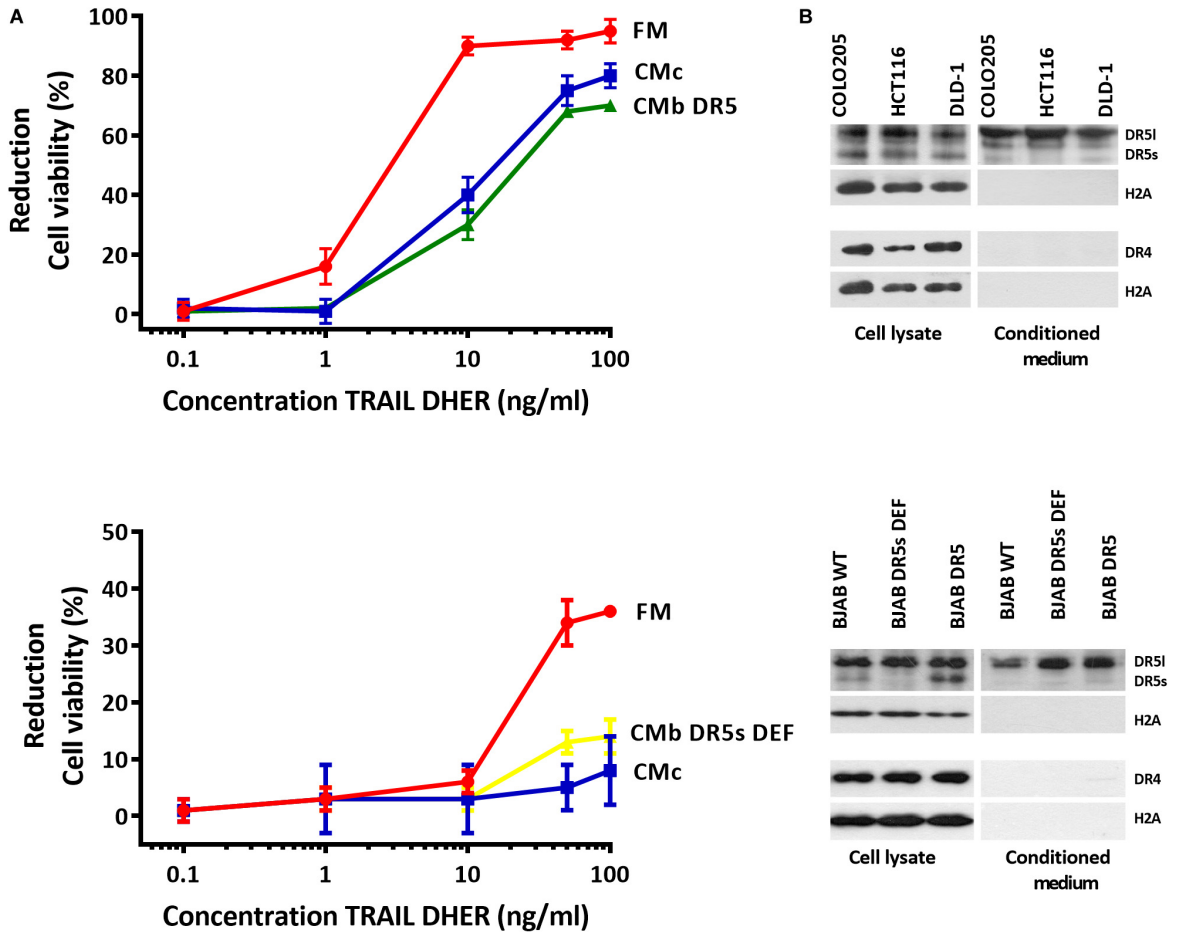

FIGURE 1 | Conditioned medium inhibits DR5-mediated apoptosis in Colo205 cells. Colo205 (**A**, upper) and BJAB cells (**A**, below) were treated with TRAIL DHER variant for 24 h in the presence of fresh medium (FM) or conditioned medium derived from either Colo205 (CMc), BJAB expressing both DR5 isotypes (CMb DR5), or BJAB cells deficient for DR5 short isoform (CMb DR5s DEF) cells. Conditioned medium was collected after cultivation of cells at a density of 150,000 cells/mL for 48 h. Cell death was measured by MTS assay. Data expressed as the mean ± SD of triplicate samples. Similar results were obtained in three independent experiments. **(B)** Total cell extract and conditioned medium (CM) of three colon carcinoma cell lines (upper) and Burkitt lymphoma cell lines (below) were analyzed for DR4, DR5, and H2A expression with Western blot. The absence of H2A in CM indicates no contamination of cellular nucleosome proteins. Similar results were obtained in three independent experiments.

Data Analysis

Data are presented as mean ± SD from triplicates in one experiment, and experiments were repeated three times. *P* values were analyzed by two-way analysis of variance in Tukey multiple comparisons with GraphPad Prism version 7.0 (San Diego, CA, United States). $^{**}p \leq 0.01$, $^{***}\ p \leq 0.001$, and $^{****}p \leq 0.0001$. Data from apoptosis assays were analyzed by FlowJo V10 (BD Biosciences).

RESULTS

Conditioned Medium Inhibits DR5-Mediated Cell Death in Cancer Cells

Most cancer cells release EVs, and the mode of action of those organelles depends on their cargo proteins (Raposo et al., 1996; Denzer et al., 2000; Rivoltini et al., 2016). We hypothesize that secreted death receptors displayed via the EVs can act as decoy receptors and therefore reduce the apoptosis signaling. We cultivated Colo205 and BJAB cells at the concentration of 150,000 cells/mL in exosome-free medium for 48 h, and the medium was collected and used as CM. Colo205 and BJAB cells were treated for 24 h with DR5 TRAIL variant (DHER) in fresh medium or CM derived either from Colo205 (CMc) or BJAB (CMb). We examined the cell viability of Colo205 and BJAB cells with MTS assay. We also used in this experiment BJAB mutants that expressed respectively only the DR5 long isoform (CMb DR5s DEF) or both isoforms (CMb DR5). We observed in both TRAIL-treated cells incubated in fresh medium considerable higher percentages of cell death than in cells grown in CM. This protection was observed for CM derived from Colo205 as from BJAB cells. The protective effect of CM was dose dependent and most prominent at 10 ng/mL DHER for Colo205 and for BJAB DR5 cells at 50 ng/mL (**Figure 1A**). This indicates that the CM contains factors that are able to inhibit DR5-mediated cell death signaling. Interestingly, Western blot analysis of the CM from three different colon carcinoma cells (Colo2015, HCT116, and DLD-1) and BJAB mutants revealed that only DR5 was secreted in significant levels in CM, and DR4 levels were almost negligible (**Figure 1B**). Next, the long DR5 isoform seems to be sufficient for this protective effect as cells expressing only the long isoform (BJAB DR5s DEF) were also able to reduce the cell death. The absence of H2A in the supernatant confirms the purity of the sample preparation and absence of cellular nucleosome proteins in the CM.

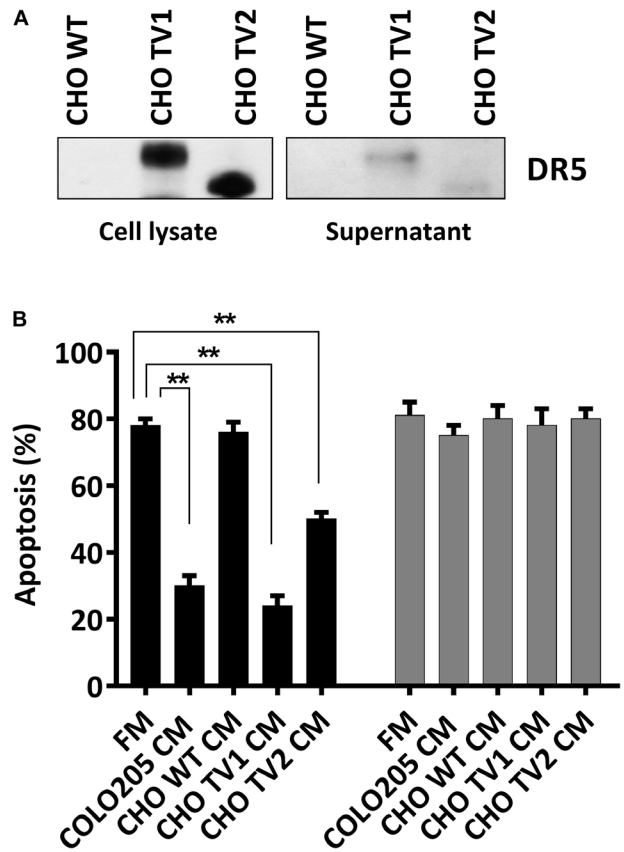

FIGURE 2 | Long and short isoforms of DR5 in conditioned medium protect against DR5-mediated apoptosis. **(A)** Western blot analysis of the expression of DR5 long and short isoforms of CHO wild-type (WT), CHOTV1, and CHO TV2 mutants in total cell lysate or in conditioned medium (CM). **(B)** Colo205 cells were treated with 10 ng/mL DHER (black) or 4C7 (gray) TRAIL variants for 24 h in the presence of fresh medium or conditioned medium derivate from either Colo205, CHO TV1, or CHO TV2 cells. Apoptosis was measured by annexin V staining. Data expressed as the mean ± SD of triplicate samples. Similar results were obtained in three independent experiments.

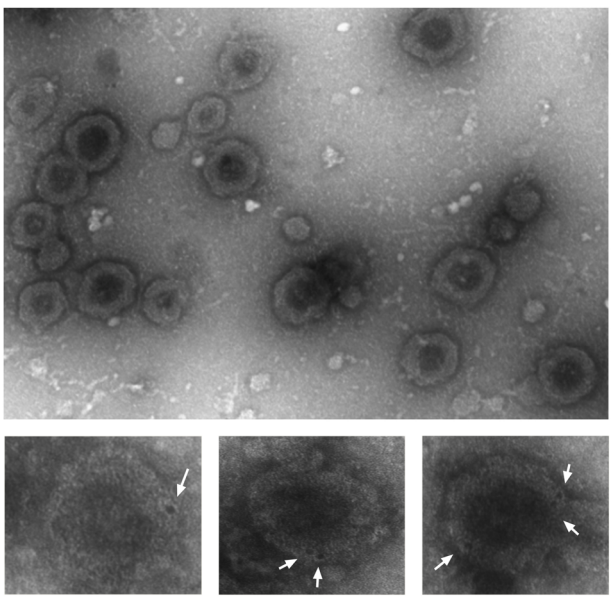

FIGURE 3 | Colo205 conditioned medium contains DR5-coated extracellular vesicles. Negative staining of EVs isolated from conditioned medium (upper picture). Bottom pictures are the zoom pictures of single EV stained with gold-labeled DR5 antibody (white arrows) and detected by transmission electron microscope. Scale bar is 500 nm. The experiment was repeated three times, and several EVs were analyzed.

Both Long and Short Isoforms of DR5 in CM Contribute to TRAIL Resistance

We have concluded that CM can prevent DR5-mediated cell death. To explore which isoforms of DR5 contribute to this resistance phenomenon, we used CHO cells expressing either the human long, or the short DR5 isoforms. Immunostaining with DR5 antibodies confirmed the expression of the different DR5 isotypes in total cell lysates of CHO mutants (CHO-TV1 and CHO-TV2), and both isotypes were secreted into the CM (**Figure 2A**). Treatment of Colo205 cells with 10 ng/mL TRAIL DHER variant in CM derived from Colo205, CHO-TV1, or CHO-TV2 cells resulted in significant inhibition of apoptosis compared to fresh medium or CM derived from CHO wild-type cells (CHO-WT CM), which lack both DR5 isoforms. This protective effect was specifically related to DR5, as no protection was observed with the 4C7 variant, which can induce apoptosis only via DR4 receptor (**Figure 2B**). The protective effect of CHO-TV1–derived CM versus CHO-WT–derived CM was at the same magnitude as COLO205-derived CM versus fresh medium. The short isoform (CHO-TV2) showed a slightly lower protective effect. We were not able to quantify the precise concentration of DR5 in the CMs, and therefore we only can conclude that both long and short isoforms of DR5 contribute to TRAIL-resistance mechanism of Colo205 cells.

DR5 Is Expressed at the Surface of EVs

To investigate whether DR5 was secreted out of the cells as soluble receptors or packed into vesicles, we fractionated the CM by differential centrifugation strategy and analyzed it with transmission electron microscope. The smallest vesicles ranging from 30 to 300 nm were sedimented by ultracentrifugation at 100,000 *g*. Bigger particles were first removed stepwise at lower speeds to avoid artificial small vesicles formation (Livshits et al., 2016). After negative staining various exosome-like vesicles, characteristics such as donut-like structures with different sizes, and shapes were observed (**Figure 3**, upper picture). Next, we asked whether secreted EVs are coated with DR5. Immunostaining with gold-labeled DR5 antibody showed

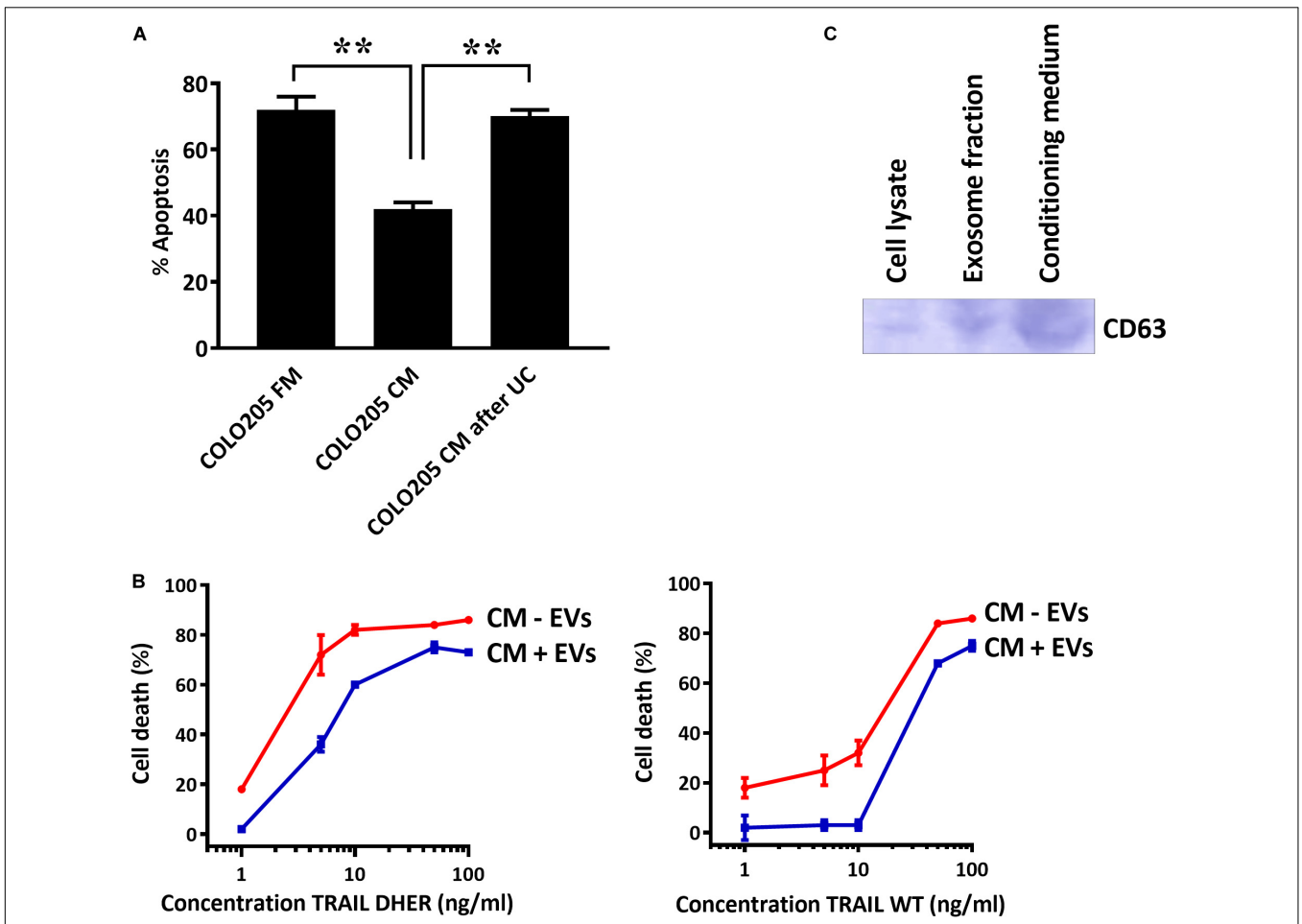

FIGURE 4 | DR5-coated EVs inhibit TRAIL-induced apoptosis. **(A)** Colo205 cells treated with TRAIL DHER in fresh medium (FM), conditioned medium (CM), or conditioned medium after ultracentrifuging (UC) and apoptotic cells were determined by annexin V staining. **(B)** Colo205 cells were cultured in CM containing either EVs (CM + EV) or depleted of EVs (CM - EV) and followed by the treatment with TRAIL DHER or TRAIL wild type (WT). Cell death was measured by MTS assay. **(C)** Western blot of CD63. Data expressed as the mean ± SD of triplicate samples. Similar results were obtained in three independent experiments.

DR5 at the surface of the EVs, visible as dark spots at the surface of the EV (**Figure 3**, bottom pictures).

Depletion of EVs in CM Restores the TRAIL DHER Sensitivity of Colo205 Cells

To confirm that the secreted EVs coated DR5 are responsible for the protection against cell death, we depleted EVs from CM and treated the cells with TRAIL DHER. Removing EVs from CM by sedimentation nullified completely the protective effect of CM upon TRAIL DHER treatment in Colo205 (**Figure 4A**). This protective effect was again observed when purified EVs were supplemented to fresh medium in Colo205 cells treated with TRAIL DHER or TRAIL wild type (**Figure 4B**). CD63 was used as positive control for the isolation of EVs (**Figure 4C**).

DISCUSSION

In the present study, we showed EVs coated with DR5 receptors can reduce the TRAIL-mediated apoptosis in cancer cells. This inhibition of the EVs was specific when apoptosis is triggered by DR5. TRAIL 4C7 variant, which triggers apoptosis via DR4, was not inhibited by CM. Both long and short isoforms of DR5 contribute to the inhibition of TRAIL-mediated apoptosis. This is the first report demonstrating the expression of DR5 on the surface of EVs, providing a new insight into the TRAIL-resistance phenomenon.

The endocytosis of TRAIL-DR complex and its importance on triggering the apoptosis signaling have been studied extensively. However, there are conflicting reports as to whether internalization of TRAIL-DR complex results either in inhibiting or enhancing the apoptotic signals depending on the cell types (Austin et al., 2006; Kohlhaas et al., 2007; Reis et al., 2017). One study showed that DR-mediated caspase activation rapidly disrupts clathrin-mediated endocytosis (CME), which in turn enhanced the apoptotic signals downstream of the DISC complexs (Austin et al., 2006). Recently, another study unraveled the molecular mechanism of CME-dependent endocytosis of death receptors. They showed that endocytosis of TRAIL-DR complex requires dynamin-1 protein, which is activated by ryanodine receptor-mediated Ca^{2+} release in response to caspase-8 activation. However, this selective regulation of TRAIL-DR endocytosis suppresses TRAIL-mediated apoptosis (Reis et al., 2017).

Internalized receptor complexes in the endocytic pathway can undergo different routes: receptors can be processed and recycled back to the surface or enter the degradation machinery. Ubiquitination of ligand–receptor complexes plays an important role in the endosomal sorting mechanism into MVE to direct the cargo toward the degradation machinery and in this way determine the fate of the protein. A study reported that the membrane-associated RING-CH ubiquitin ligase 8 (March-8) regulates the cell surface expression of DR4 and targets DR4 to the lysosomal degradation machinery (Van De Kooij et al., 2013). Interesting in their study was that March-8 had noticeable less preference for targeting DR5. Lys-273 at the cytoplasmic tail of DR4 is an important ubiquitin acceptor sites for March-8, and DR5 has no Lys-273 residue or homolog at membrane-proximal locations. Therefore, inefficient targeting of DR5 to lysosomes may be the reason that DR5 is preferentially displayed at EVs. Apart from internalization of receptors, receptors can also be released in the medium by exocytosis. This involves the release of small vesicle-like structure, which carries biomolecules such as plasma membrane receptors and other proteins into the extracellular space. The effect of the secreted DR-coated EVs on the apoptosis signaling has hardly been studied and may explain the variation in TRAIL response of cancer cells. Proteomic database search in Vesiclepedia[1] revealed that DR5 is present in exosomes of several cancer cells from brain, colorectal, kidney, glioblastoma, ovarian, prostate, lung, leukemia, and melanoma cancer. However, no functional biological data exist on the influence of DRs on EVs on TRAIL sensitivity. Despite the interesting findings of differential endocytosis and ubiquitination of DRs, more research should be done to understand the mechanism of intracellular receptors trafficking. Together with the new insight in TRAIL-resistance mechanism by DR5-coated EVs, TRAIL treatment in combination with inhibitors preventing secretion of EVs could be a promising combination strategy to treat TRAIL-resistant cancer cells.

In summary, we have uncovered the role of DR5-coated EVs in the resistance of cancer cells for TRAIL treatment. Secreted DR5-coated EVs inhibit TRAIL sensitivity of colon cancer cells. This protective effect was specific for DR5, as DR4 was absent in CM.

DATA AVAILABILITY STATEMENT

All datasets generated for this study are included in the article/supplementary material.

AUTHOR CONTRIBUTIONS

WQ is the principal investigation. CR initiated the concept of the manuscript. CR, RS, and BZ designed the experiments. CR, RS, BZ, and RM performed the experiments and analyzed the data. The manuscript was written by RS and BZ and was carefully revised by WQ.

FUNDING

This research was partly funded by The Dutch Technology Foundation (STW; grant 11056) and European Fund for Regional Development (KOP/EFRO; grants 068 and 073). BZ has received a Ph.D. scholarship from China Scholarship Council.

ACKNOWLEDGMENTS

The authors thank the department UMCG Microscopy and Imaging Centre for help with electron microscopy.

[1] http://microvesicles.org

REFERENCES

Van Niel, G., D'Angelo, G., and Raposo, G. (2018). Shedding light on the cell biology of extracellular vesicles. *Nature Reviews Molecular Cell Biology* 19, 213–228. doi: 10.1038/nrm.2017.125

Rivera, J., Cordero, R. J., Nakouzi, A. S., Frases, S., Nicola, A., and Casadevall, A. (2010). Bacillus anthracis produces membrane-derived vesicles containing biologically active toxins. *Proc. Natl. Acad. Sci. U. S. A.* 107, 19002–19007. doi: 10.1073/pnas.1008843107

Cui, Y., Gao, J., He, Y., and Jiang, L. (2019). Plant extracellular vesicles. *Protoplasma* 257, 3–12. doi: 10.1007/s00709-019-01435-6

Yáñez-Mó, M., Siljander, P. R., Andreu, Z., Zavec, A. B., Borràs, F. E., Buzas, E. I., et al. (2015). Biological properties of extracellular vesicles and their physiological functions. *Journal of Extracellular Vesicles* 4, 27066. doi: 10.3402/jev.v4.27066

Colombo, M., Raposo, G., and Théry, C. (2014). Biogenesis, Secretion, and Intercellular Interactions of Exosomes and Other Extracellular Vesicles. *Annu. Rev. Cell Dev. Biol.* 30, 255–289. doi: 10.1146/annurev-cellbio-101512-122326

Johnstone, R. M., Adam, M., Hammond, J. R., Orr, L., and Turbide, C. (1987). Vesicle formation during reticulocyte maturation. Association of plasma membrane activities with released vesicles (exosomes). *J. Biol. Chem.* 262, 9412–9420.

McGough, I. J., and Vincent, J. P. (2016). Exosomes in developmental signalling. *Dev.* 143, 2482–2493. doi: 10.1242/dev.126516

Cocucci, E., Racchetti, G., and Meldolesi, J. (2009). Shedding microvesicles: artefacts no more. *Trends in Cell Biology* 19, 43–51. doi: 10.1016/j.tcb.2008.11.003

Wong, S. H. M., Kong, W. Y., Fang, C. M., Loh, H. S., Chuah, L. H., Abdullah, S., et al. (2019). The TRAIL to cancer therapy: Hindrances and potential solutions. *Critical Reviews in Oncology/Hematology* 143, 81–94. doi: 10.1016/j.critrevonc.2019.08.008

Nagata, S. (1997). Apoptosis by death factor. *Cell* 88, 355–365. doi: 10.1016/S0092-8674(00)81874-7

Mahalingam, D., Szegezdi, E., Keane, M., Jong, S., and de & Samali, A. (2009). TRAIL receptor signalling and modulation: Are we on the right TRAIL? *Cancer Treatment Reviews* 35, 280–288. doi: 10.1016/j.ctrv.2008.11.006

Kojima, Y., Nakayama, M., Nishina, T., Nakano, H., Koyanagi, M., Takeda, K., et al. (2011). Importin β1 protein-mediated nuclear localization of Death Receptor 5 (DR5) limits DR5/Tumor Necrosis Factor (TNF)-related apoptosis-inducing ligand (TRAIL)-induced cell death of human tumor cells. *J. Biol. Chem.* 286, 43383–43393. doi: 10.1074/jbc.M111.309377

Di, X., Zhang, G., Zhang, Y., Takeda, K., Rivera Rosado, L. A., Zhang, B., et al. (2013). Accumulation of autophagosomes in breast cancer cells induces TRAIL resistance through downregulation of surface expression of death receptors 4 and 5. *Oncotarget* 4, 1349–1364. doi: 10.18632/oncotarget.1174

Van De Kooij, B., Verbrugge, I., de Vries, E., Gijsen, M., Montserrat, V., Maas, C., et al. (2013). Ubiquitination by the membrane-associated RING-CH-8 (MARCH-8) ligase controls steady-state cell surface expression of tumor necrosis factor-related apoptosis inducing ligand (TRAIL) receptor 1. *J. Biol. Chem.* 288, 6617–6628. doi: 10.1074/jbc.M112.448209

Reis, C. R., van der Sloot, A. M., Natoni, A., Szegezdi, E., Setroikromo, R., Meijer, M., et al. (2010). Rapid and efficient cancer cell killing mediated by high-affinity death receptor homotrimerizing TRAIL variants. *Cell Death Dis.* 1, e83. doi: 10.1038/cddis.2010.61

Van Der Sloot, A. M., Tur, V., Szegezdi, E., Mullally, M. M., Cool, R. H., Samali, A., et al. (2006). Designed tumor necrosis factor-related apoptosis-inducing ligand variants initiating apoptosis exclusively via the DR5 receptor. *Proc. Natl. Acad. Sci. U. S. A.* 103, 8634–8639. doi: 10.1073/pnas.0510187103

Raposo, G., Nijman, H. W., Stoorvogel, W., Liejendekker, R., Harding, C. V., Melief, C. J., et al. (1996). B lymphocytes secrete antigen-presenting vesicles. *J. Exp. Med.* 183, 1161–1172. doi: 10.1084/jem.183.3.1161

Denzer, K., Kleijmeer, M. J., Heijnen, H. F. G., Stoorvogel, W., and Geuze, H. J. (2000). Exosome: From internal vesicle of the multivesicular body to intercellular signaling device. *J. Cell Sci.* 113(Pt 19), 3365–3374.

Rivoltini, L., Chiodoni, C., Squarcina, P., Tortoreto, M., Villa, A., Vergani, B., et al. (2016). TNF-related apoptosis-inducing ligand (trail)-armed exosomes deliver proapoptotic signals to tumor site. *Clin. Cancer Res.* 22, 3499–3512. doi: 10.1158/1078-0432.CCR-15-2170

Livshits, M. A., Khomyakova, E., Evtushenko, E. G., Lazarev, V. N., Kulemin, N. A., Semina, S. E., et al. (2016). Isolation of exosomes by differential centrifugation: Theoretical analysis of a commonly used protocol. *Scientific Reports* 5, 7319. doi: 10.1038/srep17319

Austin, C. D., Lawrence, D. A., Peden, A. A., Varfolomeev, E. E., Totpal, K., De Mazière, A. M., et al. (2006). Death-receptor activation halts clathrin-dependent endocytosis. *Proc. Natl. Acad. Sci. U. S. A.* 103, 10283–10288. doi: 10.1073/pnas.0604044103

Kohlhaas, S. L., Craxton, A., Sun, X.-M., Pinkoski, M. J., and Cohen, G. M. (2007). Receptor-mediated endocytosis is not required for TRAIL-induced apoptosis. *J. Biol. Chem.* 282, 12831–12841. doi: 10.1074/jbc.M700438200

Reis, C. R., Chen, P. H., Bendris, N., and Schmid, S. L. (2017). TRAIL-death receptor endocytosis and apoptosis are selectively regulated by dynamin-1 activation. *Proc. Natl. Acad. Sci. U. S. A.* 114, 504–509. doi: 10.1073/pnas.1615072114

Conflict of Interest: The authors declare that the research was conducted in the absence of any commercial or financial relationships that could be construed as a potential conflict of interest.

frontiers in Cell and Developmental Biology

REVIEW
published: 21 May 2020
doi: 10.3389/fcell.2020.00365

The Balance of TNF Mediated Pathways Regulates Inflammatory Cell Death Signaling in Healthy and Diseased Tissues

Joshua D. Webster and Domagoj Vucic**

Departments of Pathology and Early Discovery Biochemistry, Genentech, South San Francisco, CA, United States

Tumor necrosis factor alpha (TNF; TNFα) is a critical regulator of immune responses in healthy organisms and in disease. TNF is involved in the development and proper functioning of the immune system by mediating cell survival and cell death inducing signaling. TNF stimulated signaling pathways are tightly regulated by a series of phosphorylation and ubiquitination events, which enable timely association of TNF receptors-associated intracellular signaling complexes. Disruption of these signaling events can disturb the balance and the composition of signaling complexes, potentially resulting in severe inflammatory diseases.

Keywords: TNF, RIP1 (RIPK1), RIP3 kinase, NEMO, necroptois, apoptosis, RIPK1 inhibitors

OPEN ACCESS

Edited by:
Cristian Roberto Smulski, Bariloche Atomic Centre (CNEA), Argentina

Reviewed by:
Fuminori Tokunaga, Osaka City University, Japan
James M. Murphy, Walter and Eliza Hall Institute of Medical Research, Australia

****Correspondence:***
Joshua D. Webster
webster.joshua@gene.com
Domagoj Vucic
domagoj@gene.com;
vucic.domagoj@gene.com

Specialty section:
This article was submitted to Signaling, a section of the journal Frontiers in Cell and Developmental Biology

Received: *18 March 2020*
Accepted: *23 April 2020*
Published: *21 May 2020*

Citation:
Webster JD and Vucic D (2020) The Balance of TNF Mediated Pathways Regulates Inflammatory Cell Death Signaling in Healthy and Diseased Tissues. Front. Cell Dev. Biol. 8:365. doi: 10.3389/fcell.2020.00365

STRUCTURE OF TNF AND TNF RECEPTORS

TNF is a type II transmembrane protein that is expressed at the plasma membrane as a trimer (Vassalli, 1992). Cleavage by tumor necrosis factor converting enzyme (TACE) can generate a soluble ligand that propagates signaling by binding to two receptors – TNFR1 (CD120a) and TNFR2 (CD120b) (Black et al., 1997; Moss et al., 1997). TNFR1 associates strongly with both membrane-bound and soluble TNF, while TNFR2 has much higher binding affinity for membrane-bound TNF (Grell et al., 1995). The extracellular region of both receptors has four homologous cysteine-rich domains (CRDs) but their intracellular regions are structurally different. The intracellular portion of TNFR1 possesses a protein-binding region called a death domain (DD), which allows homo- and hetero-typic interactions with other DD-containing proteins. TNFR2, on the other hand, has a TNF Receptor Associated Factor (TRAF) binding site that interacts with the TRAF family of signaling adaptors (Grell et al., 1995; Reddy et al., 2000). The distinct expression profiles and stark difference in the intracellular regions of the TNF receptors greatly influence their physiological roles and cellular activity. Through engaging DD adaptors, broadly expressed TNFR1 can activate proliferative nuclear factor-kappa B (NF-κB) and mitogen-activated protein kinase (MAPK) signaling as well as cell death (Wallach et al., 1999; Sessler et al., 2013). On the other hand, TNFR2 is mostly expressed in immune and endothelial tissues. In addition, since it lacks a DD, TNFR2 cannot stimulate cell death, but uses TRAF recruitment to trigger NF-κB and MAPK activation (Wallach et al., 1999; Sessler et al., 2013). Due to its wide spectrum of cellular activities and ubiquitous expression, TNFR1 plays a prevailing role in TNF signaling and will be more extensively covered in this article.

ACTIVATION OF NF-κB AND MAPK SIGNALING BY TNF

Binding of TNF to TNFR1 triggers receptor trimerization and leads to the assembly of the TNFR1-associated signaling complex (complex I) (**Figure 1**). Within complex I, the adaptor proteins receptor interacting protein 1 (RIP1; RIPK1) and TNF receptor associated death domain (TRADD) are recruited to TNFR1 through their respective death domains (Micheau and Tschopp, 2003). TRADD then recruits adaptor proteins TRAF2 and TRAF5, which enables the engagement of the E3 ligases cellular inhibitors of apoptosis 1 and 2 (c-IAP1, c-IAP2) and subsequent ubiquitination of various components of complex I (Bertrand et al., 2008; Mahoney et al., 2008; Varfolomeev et al., 2008; Dynek et al., 2010). c-IAP1/2 promote self-ubiquitination and ubiquitination of RIP1 with K63-, K48-, and K11-linked chains, which are critical for TNFR1 complex I signaling (Bertrand et al., 2008; Mahoney et al., 2008; Varfolomeev et al., 2008; Dynek et al., 2010). K63-linked polyubiquitin chains conjugated onto c-IAP1/2 allow the recruitment of the linear ubiquitin chain assembly complex (LUBAC), which generates linear ubiquitin chains on several molecules including RIP1, TNFR1, LUBAC itself, and NF-κB essential modulator (NEMO) (Haas et al., 2009; Tokunaga et al., 2009; Ikeda et al., 2011; Tokunaga et al., 2011; Varfolomeev and Vucic, 2016). The LUBAC complex consists of adaptor proteins SHANK-associated RH-domain interactor (SHARPIN) and heme-oxidized IRP2 ubiquitin ligase 1 (HOIL-1L), and the E3 enzyme HOIL-1L-interacting protein (HOIP) (Tokunaga and Iwai, 2012). LUBAC produces linear or M1-linked ubiquitin chains by catalyzing a head-to-tail ubiquitination where a peptide bond between the N-terminal methionine of ubiquitin and the C-terminal glycine of the next ubiquitin is generated (Kirisako et al., 2006; Tokunaga et al., 2009). The diverse ensemble of polyubiquitin chains assembled during TNF-induced activation of NF-κB and MAPK includes, but is not limited to, K11, K48, K63, and linear chains (Dynek et al., 2010; Gerlach et al., 2011). This set of polyubiquitin chains provides a docking platform for the recruitment and retention of the signaling kinase complexes consisting of kinases IKKα and IKKβ (inhibitor of kappa B kinase 1 and 2) and the adaptor NEMO (IKKγ; IKK complex), and transforming growth factor beta-activated kinase 1 (TAK1) along with its partners, the K63-linked ubiquitin binding proteins TAK1-binding proteins 2 and 3 (TAB2/3) (**Figure 1**; Shim et al., 2005; Haas et al., 2009). The recruitment of kinase complexes leads to the activation of NF-κB and MAPK signaling and subsequent gene activation and expression of pro-inflammatory cytokines, such as interleukin 6 and 8 (IL-6, IL-8), and pro-survival proteins like c-IAP2 and the caspase-8 inhibitor cellular FLICE inhibitory protein (cFLIP) (Scheidereit, 2006).

The specific polyubiquitination pattern on RIP1 that keeps it in complex I for proper downstream activation of NF-κB and MAPKs is fine-tuned by the activation of E3 ligases, such as c-IAP1/2 (Bertrand et al., 2008; Mahoney et al., 2008; Varfolomeev et al., 2008; Silke and Vucic, 2014). The combined deletion of c-IAP1 and c-IAP2 in mice results in embryonic lethality and severe liver and intestinal damage in the adulthood, which can be rescued by TNFR1 knock-out or by TNF blockade, further emphasizing the functional and genetic relationship between these E3 ligases and TNF signaling (Moulin et al., 2012; Zhang J. et al., 2019). However, these complexes are also governed through negative regulation by deubiquitinases (DUBs). TNF stimulation also leads to transcriptional upregulation of deubiquitinases tumor necrosis factor alpha-induced protein 3 (TNFAIP3 or A20) and OTU domain DUB 7B (also known as Cezanne) whose DUB activity can dampen NF-κB signaling (Wertz et al., 2004; Enesa et al., 2008). A20 is an ubiquitin chain-binding enzyme that removes K63-linked ubiquitin chains from RIP1 to reduce NF-κB activation. Binding of linear ubiquitin chains via its zinc finger 7 motif is critical for A20's recruitment to TNFR1 complex and suppression of inflammatory signaling (Tokunaga et al., 2012; Martens A. et al., 2020; Razani et al., 2020). Consequently, deletion of *A20* results in enhanced RIP1 ubiquitination and inflammation (Wertz et al., 2004; Zhou et al., 2016a). Cylindromatosis (CYLD) is another DUB whose recruitment to complex I can dampen NF-κB activation by hydrolyzing the K63-linked and linear polyubiquitin chains from the complex I components (Brummelkamp et al., 2003; Kovalenko et al., 2003; Trompouki et al., 2003). CYLD is recruited to the TNFR1 complex via the adaptor protein SPATA2, which binds the PUB (peptide:N-glycanase/UBA/X-containing protein) domain of HOIP through its PIM (PUB-interaction motif) (Elliott et al., 2016; Kupka et al., 2016; Schlicher et al., 2016; Wagner et al., 2016; Wei et al., 2017). Consequently, the absence of SPATA2, just like CYLD loss, enhances TNF stimulated NF-κB activation and dampens cell death (Elliott et al., 2016; Kupka et al., 2016; Schlicher et al., 2016; Wagner et al., 2016; Wei et al., 2017). Unlike these DUBs, which do not have a strict ubiquitin chain specificity, OTULIN (OTU deubiquitinase with linear specificity, also known as FAM105B or Gumby) binds the PUB domain of HOIP and selectively removes linear ubiquitin chains on LUBAC components thereby keeping uncontrolled TNF-associated inflammation in check (Fiil et al., 2013; Keusekotten et al., 2013; Elliott et al., 2014; Damgaard et al., 2016; Zhou et al., 2016b). Thus, a tightly controlled balance of E3 ligases and DUBs in the assembly and disassembly of diverse polyubiquitin chains on RIP1 and other signaling components is clearly needed for the appropriate level of signaling by complex I and corresponding gene activation.

Cell Death Induction by TNF

Dynamic changes of post-translational modifications of RIP1 and other components of TNFR1-associated signaling complexes can trigger a switch from inflammatory gene signaling to cell death via apoptosis or necroptosis (**Figure 2**). RIP1-dependent and RIP1-independent apoptotic signaling complexes can form in response to inhibited or altered NF-κB signaling (e.g., IKKβ or TAK1 inhibitors, genetic deletion of NF-κB) or the presence of transcriptional or translational inhibitors like actinomycin D or cycloheximide, respectively (Rubin et al., 1988; Micheau and Tschopp, 2003; Shan et al., 2018). A cytosolic complex II centered

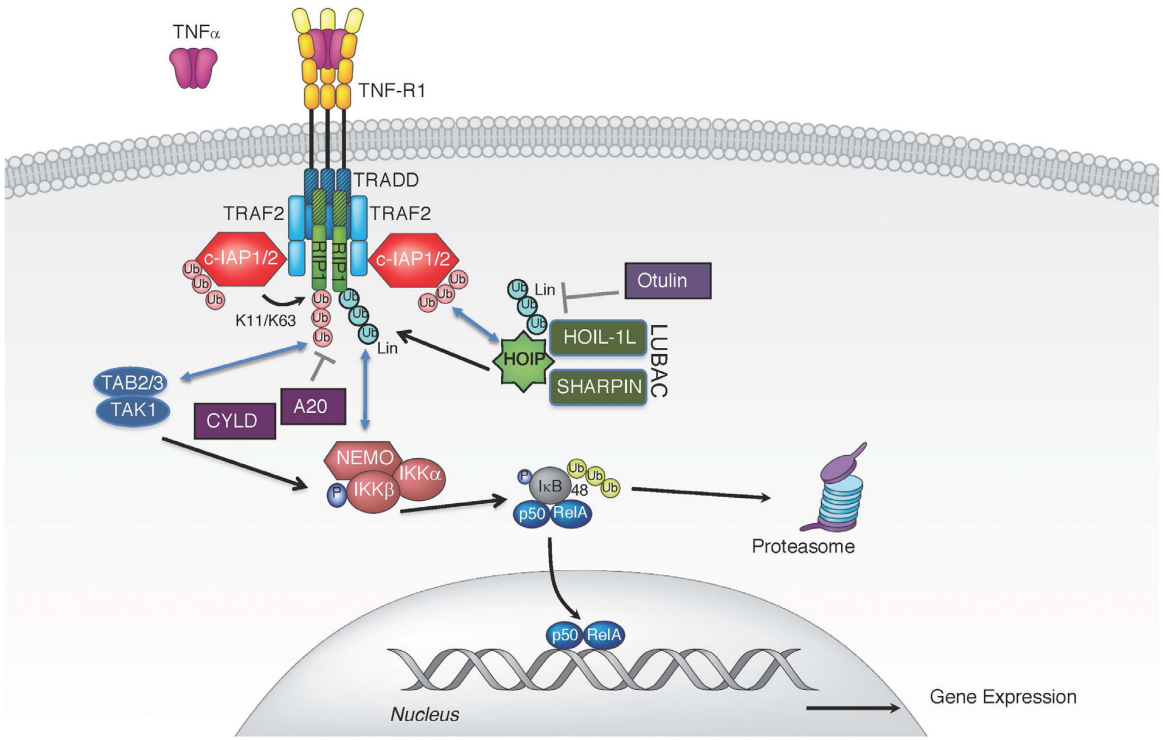

FIGURE 1 | TNF induced canonical NF-κB pathway. TNF stimulation triggers the recruitment of TRADD, TRAF2, RIP1, and c-IAP1/2 to TNFR1. E3 ligases c-IAP1/2 polyubiquitinate themselves and RIP1 with K11 and K63 ubiquitin linkages, creating a platform for further recruitment of LUBAC. LUBAC mediates linear polyubiquitin, resulting in gene expression via the IKK complex. Several DUBs have been implicated in the regulation of TNFR1-associated complex I by removing linear (CYLD and OTULIN) or K63-linked polyubiquitin chains (A20 and CYLD).

on TRADD recruits Fas-associated death domain (FADD) to activate caspase-8 and cause apoptotic cell death (Van Antwerp et al., 1996; Micheau and Tschopp, 2003; Wang et al., 2008). For RIP1-dependent apoptotic complex II, distinct ubiquitin modifications play a critical regulatory role in dictating the fate of cells. When E3 ligases c-IAP1/2 and LUBAC are degraded or absent, unmodified RIP1 dissociates from receptor-associated signaling complex I and associates with FADD through binding of their DDs (Micheau and Tschopp, 2003; Bertrand et al., 2008; Wang et al., 2008). FADD recruits pro-caspase 8 and/or its catalytically inactive homolog FLIP to form the death platform complex II using death effector domain (DED) interactions (Majkut et al., 2014). RIP1 dependent apoptosis can be further modulated by additional signaling proteins and E3 ligases (NEK1, APC11, LRKK2, and Cbl) that regulate the transition of RIP1 from complex I to complex II (Amin et al., 2018). Thus, the ubiquitination status of RIP1 determines the switch of RIP1 between pro-survival gene activation and cell death.

If caspase-8 is insufficiently activated or inhibited in complex II, RIP1 can autophosphorylate at S166 and bind RIP3 using their RIP homology interaction motifs (RHIM) leading to the formation of the necrosome (Sun et al., 2002; He et al., 2009; Wu et al., 2014; Laurien et al., 2020). Unlike complex I, where RIP1 kinase activity is dispensable, TNF stimulated necrosome formation is dependent on RIP1 kinase activity (Cho et al., 2009; He et al., 2009; Laurien et al., 2020). Within the necrosome, RIP3 undergoes auto-phosphorylation at S227 in human, and T231 and S232 in mouse RIP3 that is crucial for the execution of necroptotic cell death (Cho et al., 2009; He et al., 2009; Chen et al., 2013). Accordingly, genetic inactivation or chemical inhibition of their kinase functions blocks RIP1/3 dependent necroptotic cell death (Degterev et al., 2008; He et al., 2009; Newton et al., 2014). RIP3 phosphorylates necroptosis mediator mixed lineage kinase domain-like (MLKL) at residues T357 and S358 in human, and S345, S347, and T349 in mouse MLKL within its carboxy-terminal pseudokinase domain to execute necroptosis (Sun et al., 2012; Chen et al., 2013; Murphy et al., 2013; Khan et al., 2014; Wang et al., 2014; Rodriguez et al., 2016). How MLKL facilitates cell death is not entirely clear, but it does involve the disruption of cell membrane integrity. RIP3-phosphorylated MLKL undergoes a conformational change that exposes the N-terminal domain of MLKL, promoting its oligomerization and translocation to the membranes (Murphy et al., 2013; Dondelinger et al., 2014; Wang et al., 2014). Membrane associated MLKL may interfere directly with cell integrity by oligomeric insertion into the membrane thus causing membrane disruption/permeabilization/perturbation (Cai et al., 2014; Dondelinger et al., 2014; Hildebrand et al., 2014; Su et al., 2014; Wang et al., 2014). The pore-forming capacity of necroptosis results in a strong pro-inflammatory signal, a feature that places this cell death pathway at the core of many inflammatory and tissue-damage related diseases. However, RIP1

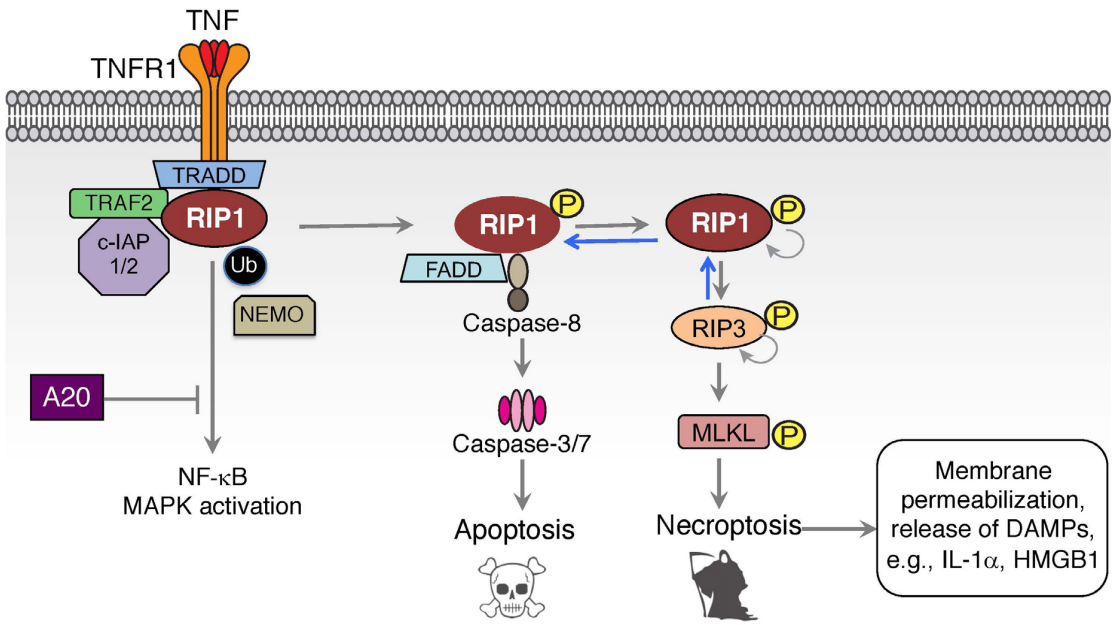

FIGURE 2 | TNF induced cell death signaling. Inhibition of NF-κB and MAPK signaling can divert TNF-mediated signaling to the formation of an intracellular complex II centered on FADD and caspase-8 in a RIP1-dependent apoptotic cell death. This cell death pathway can be augmented by A20 or by the absence of the E3 ligases c-IAP1/2 or LUBAC, thereby eliminating the ubiquitination of complex I components and promoting the switch to complex II. Activation of RIP1-dependent cell death under caspase-8 inhibited or deficient conditions can lead to a necroptotic form of cell death that is mediated by kinase activity of RIP1 and RIP3, and results in the activation of MLKL and membrane permeabilization.

autophosphorylation can result in RIP1-dependent apoptosis as well, and a number of *in vivo* inflammatory animal models involve a mixture of RIP1-dependent apoptosis and necroptosis as we will describe later in this article (Patel et al., 2020; Webster et al., 2020).

DISRUPTION IN TNF SIGNALING UBIQUITINATION MACHINERY IN PATIENTS WITH IMMUNODEFICIENCY AND AUTOINFLAMMATION

While TNF's importance in driving inflammatory diseases is well-established, the recent identification of patients with defects in TNF signaling components have shown the importance of tightly regulating this pathway and the potential consequences of its dysregulation (Manthiram et al., 2017; Oda and Kastner, 2017; **Figure 3**). *In vitro* and *in vivo* studies have suggested the critical role ubiquitin plays in TNF signaling, both in enabling signal complex formation and in protein degradation. For example, chronic proliferative dermatitis (*cpdm*) mice were originally characterized as a strain of C57BL/KaLawRij mice that developed eosinophilic dermatitis with epidermal hyperplasia, multi-systemic inflammation, and defects in lymphoid development (HogenEsch et al., 1993, 1999; Gijbels et al., 1996). Subsequent studies demonstrated that this phenotype was due to a spontaneous mutation in the *Sharpin* gene that resulted in diminished expression of SHARPIN and the other LUBAC components HOIP and HOIL-1L (Seymour et al., 2007; Gerlach et al., 2011; Tokunaga et al., 2011). Studies in these mice suggested that LUBAC mediated linear ubiquitination plays an important role in modulating inflammatory and cell death signaling downstream of TNFR1. However, the clinical validation of these observations has been more recently evident through the identification of patients with mutations in the genes encoding LUBAC components HOIP and HOIL-1L, and in mutations in the genes encoding the deubiquitinases OTULIN and A20.

Mutations in *HOIL-1L* were originally reported in 2012, in two families with immunodeficiency, as characterized by recurrent pyogenic infections, multi-systemic inflammation, and amylopectinosis (Boisson et al., 2012). The single described patient in the first family had a homozygous deletion of 2 nucleotides resulting in a premature stop codon. Patients in a second family had partial deletions of one allele and a nonsense point mutation in the second allele; suggesting an autosomal recessive mode of inheritance in both families. These *HOIL-1L* mutations caused an approximately 50% decrease in SHARPIN expression and near complete loss of HOIP expression. Loss of LUBAC expression resulted in impaired NF-κB activity in response to interleukin-1 beta (IL-1β) and, to a lesser extent, TNF in the patients' fibroblasts. Similarly, the patients' B cell responses to Toll-like receptor (TLR) 7 and 8 agonists, IL-1β, and CD40-ligand (CD40L) were also impaired. Interestingly, LUBAC deficiency had an opposing effect in monocytes. Specifically, monocytes had approximately four-fold increased IL-6 production following IL-1β stimulation and enhanced responses to TLR1 and 2 agonists (Boisson et al., 2012). While the

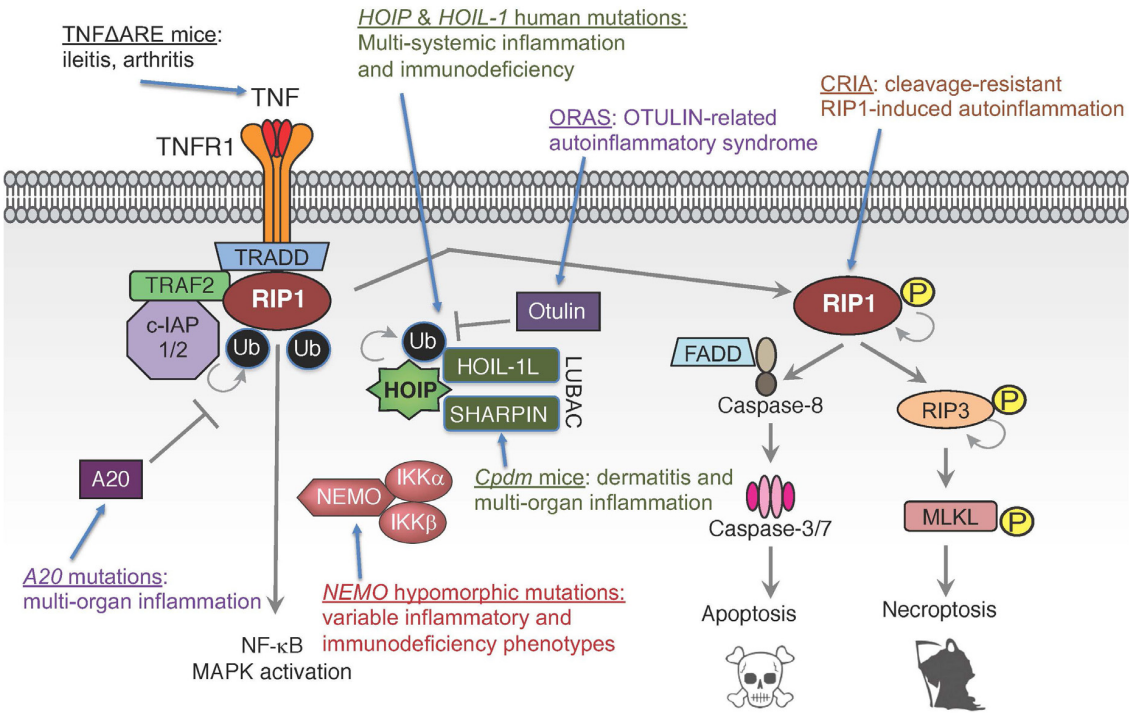

FIGURE 3 | Human mutations and genetic models in TNF signaling pathways. Mutations in multiple components of TNF signaling leading to functional dysregulation of E3 ligase complex LUBAC, deubiquitinases A20 and OTULIN, ubiquitin-binding protein NEMO, ligand TNF or pro-death kinase RIP1 can cause inflammatory diseases and/or immunodeficiency.

patients described above presented with immune dysregulation, other *HOIL-1L* mutant patients present with primary myopathy and less frequent to no evidence of immune dysfunction (Nilsson et al., 2013; Wang et al., 2013). These patients presented with muscle weakness in adolescence that progresses over time, and a subset of patients develop dilated cardiomyopathy (Nilsson et al., 2013; Wang et al., 2013). Histologically, myofibers contain periodic acid-Schiff positive, amylase-resistant inclusions characteristic of polyglucosan (Nilsson et al., 2013). The reason that some patients with *HOIL-1L* mutations present for myopathy while others present for immunodeficiency is not fully understood, but the phenotype might be influenced by the location of the mutation in the gene (Nilsson et al., 2013).

An autosomal recessive missense mutation in *HOIP* has also been identified in one patient. This mutation resulted in a loss of HOIP protein and reduced levels of SHARPIN and HOIL-1L, resulting in LUBAC deficiency (Boisson et al., 2015). A second patient was identified with compound heterozygous *HOIP* polymorphisms. These polymorphisms caused alternative RNA splicing that resulted in truncated HOIP protein and LUBAC destabilization (Oda et al., 2019). Clinical and biochemical phenotypes in *HOIP* mutant patients mirrored patients with *HOIL-1L* mutations. Specifically, patients with mutations or polymorphisms in *HOIP* presented with multi-systemic inflammation and immunodeficiency characterized by recurrent infections, chronic diarrhea, and antibody deficiency (Boisson et al., 2015; Oda et al., 2019). Patients' fibroblasts had blunted NF-κB responses to IL-1β and TNF, and their B cells had reduced response to CD40L (Boisson et al., 2015). Additionally, similar to HOIL-1L deficient patients, monocytes derived from these patients had increased response to IL-1β, resulting in elevated IL-6 and IL-1β production (Boisson et al., 2015).

Characterization of these patients confirms the critical role of LUBAC-mediated linear ubiquitination in NF-κB driven immune responses of fibroblasts and lymphocytes, and demonstrates that loss of this signaling has significant consequences including immunodeficiency and subsequent recurrent infections. However, the paradoxical increase in proinflammatory signaling in monocytes, which likely accounts for the concurrent multi-systemic inflammation, suggests that the role of LUBAC is dependent on cellular context and tight regulation of this pathway is critical to modulate inflammatory responses.

Deubiquitinases are critical to counter-regulate ubiquitin ligase activities. Just as c-IAP1/2 and LUBAC play fundamental roles in establishing signaling complexes downstream of the TNF receptor, deubiquitinases like OTULIN, CYLD, and A20 play equally important roles in modulating these complexes. Patients with reduced OTULIN expression due to autosomal recessive mutations develop fevers, dermatitis, and panniculitis (Damgaard et al., 2016, 2019; Zhou et al., 2016b; Nabavi et al., 2019). Comparable phenotypes are observed in patients with autosomal dominant mutations in the gene encoding A20, *TNFAIP3*. Specifically, these patients present with early

onset systemic inflammation including arthritis, ophthalmitis, and oral and genital ulcers (Zhou et al., 2016a). Initial characterization of cells from affected patients revealed that TNF stimulated peripheral blood mononuclear cells (PBMCs) and fibroblasts from *OTULIN* and *TNFAIP3* mutant patients have increased NF-κB activity compared to controls and increased p38 phosphorylation in fibroblasts, which is associated with increased ubiquitination (Zhou et al., 2016a,b). These changes were correlated with increased serum cytokines in *TNFAIP3* mutant patients (Zhou et al., 2016a), and increased LPS-induced production of interferon-gamma, IL-1β, IL-6, IL-12, and IL-18 in whole blood samples of OTULIN deficient patients (Zhou et al., 2016b). Fibroblasts from a subsequently identified patient with a unique homozygous *OTULIN* mutation had reduced NFκB and p38 activity in response to TNF (Damgaard et al., 2019). The differences between these patients and their responses to TNF is unclear, since mutations characterized in both studies reportedly resulted in decreased OTULIN activity (Zhou et al., 2016b; Damgaard et al., 2019; Nabavi et al., 2019). Interestingly, although the later study found that OTULIN deficient fibroblasts were hypo-responsive to TNF and *shOTULIN* THP-1 cells were hyper-responsive to TNF, both cell types had increased susceptibility to cell death induced by the combination of TNF and cyclohexamide (Damgaard et al., 2019), suggesting that cell death is a common end product of dysregulation of this pathway. The clinical data and cellular characterization of HOIP, HOIL-1L, OTULIN, and A20 deficient patients highlight the essential role of ubiquitination in modulating TNF signaling. On the surface, the data suggest that too little ubiquitination (e.g., HOIP or HOIL-1L deficiency) results in dampening of the immune response, and persistent ubiquitination (e.g., OTULIN or A20 deficiency) causes autoinflammation. However, there are added complexities to this perspective, as noted in the increased IL-1β response in HOIP and HOIL-1L deficient monocytes.

Aside from autoinflammation, *A20* mutations also occur in approximately 12% of B cell lymphomas, with the highest incidence in mucosa-associated lymphoid tissue (MALT) lymphoma (Kato et al., 2009). Reconstitution of an A20 deficient lymphoma cell line with wild-type A20 resulted in decreased proliferation, increased apoptosis, and decreased NF-κB signaling. Similarly, A20 expressing cells transplanted into immunodeficient mice failed to develop tumors, as opposed to mock transfected cells, which developed tumors (Kato et al., 2009). Therefore, A20 does not only regulate NF-κB signaling in the context of normal immune responses, but it also appears to act as a tumor suppressor, regulating NF-κB signaling in the context of tumorigenesis.

MUTATIONS IN ADAPTORS OF TNF SIGNALING AND IMMUNE DYSFUNCTION

Disease-associated mutations have also been identified in genes that encode target proteins of ubiquitination including *RIP1* and *NEMO*. Patients with autosomal recessive RIP1 deficiency are immunodeficient, as characterized by lymphopenia and recurrent infections, and develop inflammatory enterocolitis that resembles inflammatory bowel disease (IBD) (Cuchet-Lourenco et al., 2018; Abed et al., 2019; Uchiyama et al., 2019). Similar to patients with HOIP and HOIL-1L deficiencies, their fibroblasts had reduced MAPK and NF-κB signaling in response to TNF and polyinosinic:polycytidylic [poly(I:C)] (Cuchet-Lourenco et al., 2018). This was coupled with increased fibroblast death that appeared to be driven by necroptosis, as indicated by RIP3 and MLKL phosphorylation (Cuchet-Lourenco et al., 2018). However, while *ex vivo* stimulation of patients' monocytes with LPS produced less IL-6, TNF, and IL-12 in response to LPS, they had increased IL-1β production (Cuchet-Lourenco et al., 2018), suggesting increased inflammasome activation. In addition to mutations that result in RIP1 deficiency, mutations in the caspase-8 cleavage site of RIP1 (D324) have also been identified in patients with periodic fevers and lymphadenopathy (Lalaoui et al., 2020; Tao et al., 2020). Peripheral blood mononuclear cells from these patients had enhanced susceptibility to both apoptotic and necroptotic stimuli, and increased pro-inflammatory cytokine production including IL-6, TNF, interferon-gamma, and IL-10 (Lalaoui et al., 2020; Tao et al., 2020). Together, these results highlight and validate RIP1's unique physiological role in TNF signaling, as a mediator of pro-inflammatory signaling and as a regulator of cell death.

Mutations in *IKBKG*, the gene that encodes NEMO, are associated with both incontinentia pigmenti (Smahi et al., 2000) and X-linked recessive ectodermal dysplasia with immunodeficiency (Zonana et al., 2000; Doffinger et al., 2001). X-linked recessive ectodermal dysplasia with immunodeficiency is associated with hypomorphic mutations and the clinical phenotype is highly variable and may include recurrent infections, hyper-IgM levels, ectodermal dysplasia including coning teeth and hypodontia, inability to sweat, lymphedema, and osteopetrosis. This diverse presentation is due to both the variety of mutations that occur in these patients, but also the diversity of receptors associated with NF-κB signaling including ectodysplasin-A receptor, TNFR1, CD40, and receptor activator of NF-κB (RANK) (Zonana et al., 2000; Doffinger et al., 2001; Miot et al., 2017). While immunodeficiency due to both inadequate NF-κB mediated innate responses and CD40 signal in B cells is a primary medical concern in these patients, hematopoietic stem cell transplantation does not alleviate all of the associated disease. For instance, many patients have persistent colitis, even post-transplantation, which suggests epithelial specific defects are also important in the clinical phenotype (Miot et al., 2017).

DECIPHERING TNF SIGNALING REGULATION THROUGH GENETIC MOUSE MODELS

Identification and characterization of patients with monogenic defects in TNF signaling components has provided critical insights into the significance of these proteins in regulating inflammatory signaling, and provides clinical context as to

how dysfunction in this pathway can manifest in disease. While these clinical data are invaluable, there are experimental limits to what can be studied in patients and patient-derived samples. Therefore, spontaneous and genetically engineered mouse models have proven valuable tools to further interrogate TNF signaling pathways, to model diseases where these pathways likely play a role, and to identify how these pathways can be modulated when they go awry. A clear example of the value of these mouse models is the coincidental reporting of cleavage resistant *RIP1* mutations in patients with periodic fevers and the description of knock-in mice with complementary mutations (Newton et al., 2019; Zhang X. et al., 2019; Lalaoui et al., 2020; Tao et al., 2020). Genetic experiments in these mouse models demonstrated that observed clinical phenotypes were likely driven, at least in part, by TNFR1 and RIP1 kinase dependent apoptosis, but also highlight the complex role RIP1 plays in control both inflammatory and cell death pathways (Newton et al., 2019; Zhang X. et al., 2019; Lalaoui et al., 2020).

SHARPIN-deficient *cpdm* mice were the first LUBAC deficient mice characterized. SHARPIN deficiency results in reduced, but not eliminated, LUBAC activity and therefore is best characterized as a hypomorphic mouse (Seymour et al., 2007; Gerlach et al., 2011; Tokunaga et al., 2011). The most prominent phenotype in *cpdm* mice is eosinophilic dermatitis (HogenEsch et al., 1993) that begins around 1 week of age and progresses to severe disease by 6 weeks of age (Gijbels et al., 1996). Inflammatory infiltrates are also present in the joints, liver, and lung (Zhang et al., 2009) of these mice. Additionally, these mice develop eosinophilic esophagitis (Chien et al., 2015) and have hypoplastic lymphoid tissues (HogenEsch et al., 1999). While systemic immune infiltrates are partially dependent on lymphocytes, dermatitis in these mice is lymphocyte independent, indicating that this is an auto-inflammatory rather than autoimmune process (Potter et al., 2014). Loss of TNF or TNFR1 protects *cpdm* mice from both dermatitis and systemic inflammation, suggesting TNF signaling is the primary driver of inflammation (Gerlach et al., 2011; Kumari et al., 2014; Rickard et al., 2014). RIP1 kinase inhibition is also protective against dermatitis and reduces systemic inflammation in *cpdm* mice (Berger et al., 2014; Patel et al., 2020; Webster et al., 2020). *Cpdm* mice that express catalytically inactive $RIP1^{K45A}$ do not develop dermatitis or systemic inflammation (Berger et al., 2014), and treatment with a RIP1 inhibitor, even starting at 6 weeks of age when there is disease induction, provides significant amelioration of the dermatitis and reduces immune infiltrates in the liver (Webster et al., 2020). Interestingly, while RIP3 loss delays the development of dermatitis in SHARPIN deficient mice (Kumari et al., 2014; Rickard et al., 2014), MLKL loss does not affect the development of dermatitis (Rickard et al., 2014). Consistent with this data, caspase-3 is robustly activated in the epidermis of SHARPIN deficient mice (Liang et al., 2011; Kumari et al., 2014; Rickard et al., 2014; Webster et al., 2020), while phosphorylated RIP3 positive cells were rarely detected in the dermis (Webster et al., 2020). Furthermore, the loss of 1 *caspase-8* allele in addition to RIP3 deficiency prevented the development of inflammatory lesions in most *cpdm* mice (Rickard et al., 2014). Together, this suggests that while RIP1 kinase activity drives the inflammation in *cpdm* mice, RIP1 is only partially signaling through RIP3 and the inflammation is primarily driven by apoptosis rather than necroptosis. Therefore, in some contexts, especially when epithelial barriers are disrupted, excessive apoptosis can be pro-inflammatory. Loss of caspase-1 also prevents the development of inflammatory lesions in c*pdm* mice. This protection is thought to be due to SHARPIN's role in regulating caspase-1 activity in a LUBAC independent manner (Nastase et al., 2016).

Aside from the inflammatory lesions in the skin, joints and visceral organs, *cpdm* mice also have defective lymphoid development that includes altered splenic architecture and absence of Peyer's patches (HogenEsch et al., 1999). Loss of TNF or TNFR1 does not restore the splenic architecture in *cpdm* mice (Gerlach et al., 2011; Kumari et al., 2014), but this is suspected to be partially due to the intrinsic defects in lymphoid development in the absence of TNFR1 signaling (Kumari et al., 2014). Similarly, caspase-1 deficient *cpdm* mice do not develop normal lymphoid architecture (Nastase et al., 2016). However, Peyer's patches were restored in $Rip3^{-/-}Casp8^{\pm}$ *cpdm* mice (Rickard et al., 2014). The role of RIP1 kinase activity in the lymphoid phenotype of *cpdm* mice is not well characterized as evaluations of lymphoid tissues in *cpdm* with catalytically inactive $RIP1^{K45A}$ have not been reported (Berger et al., 2014). While treatment with a RIP1 inhibitor after the onset of dermatitis did not restore the lymphoid architecture, this might be due to the late timing of the intervention and it is possible that germline loss of RIP1 kinase activity may restore the lymphoid architecture (Webster et al., 2020).

In contrast to the hypomorphic phenotype of *cpdm* mice, *Hoip* and *Hoil-1l* knock-out mice die around embryonic day 10.5 due to increased endothelial cell death and vascular collapse, most notably in the yolk sac (Peltzer et al., 2014; Peltzer et al., 2018). The timing of this is notable because this is also the stage when *Caspase-8* knock-out mice die due to RIP3 dependent necroptosis (Varfolomeev et al., 1998; Kaiser et al., 2011). While loss of caspase-8 and RIP3, loss of RIP1 catalytic activity due to the expression of catalytically inactive $RIP1^{K45A}$, or loss of TNF signaling can extend survival to later embryonic stages in HOIL-1L deficient mice, only the combined loss of RIP1, RIP3, and caspase-8 is protective, which suggests cell death is a primary driver of embryonic lethality in these mice (Peltzer et al., 2018). Epidermal specific deletion of *Hoip* and *Hoil-1l* results in dermatitis in the perinatal period and death by post-partum day 6. Similar lesions are observed following inducible deletion of *Hoip* in adult mice (Taraborrelli et al., 2018). Dermatitis in epithelial-specific knock-out mice indicates that the inflammation is driven by an epithelial autonomous process, rather than being initiated by aberrant immune cell signaling. Similar to SHARPIN deficient mice, increased cell death, as evidenced by increased cleaved caspase-3 immunolabeling and terminal deoxynucleotidyl transferase dUTP nick end labeling (TUNEL), was observed in the epidermis of these mice. In germline epidermal specific *Hoip* and *Hoil-1l* knock-out mice, cell death is apparent at embryonic day 18.5 and precedes inflammatory cell infiltration into the dermis, suggesting that cell death

is a cause rather than a consequence of inflammation. The significance of cell death in driving dermatitis is further supported by the fact that loss of caspase-8 and either MLKL or RIP3 is protective in these mice (Taraborrelli et al., 2018). Interestingly, while dermatitis appears to be solely driven by TNFR1 signaling in SHARPIN deficient mice, loss of TNFR1 only delays the onset of dermatitis to approximately 70 days, which appears to be due to concurrent signaling through other death receptors including TNF-related apoptosis inducing ligand (TRAIL) receptor and CD95. Additionally, in contrast to SHARPIN deficient mice, loss of RIP1 kinase activity through the expression of catalytically inactive $RIP1^{D138N}$ does not show dramatic protection in these mice. However, the combination of small molecule RIP1 kinase inhibition and loss of TNFR1 expression provides more efficient protection in *Hoil-1l* knock-out mice, suggesting that RIP1 inhibition can provide a benefit independent of TNFR1 in some circumstances (Taraborrelli et al., 2018).

Both the similarities and differences between SHARPIN deficient mice that have hypomorphic LUBAC function and epidermal specific *Hoip* and *Hoil-1L* knock-out mice provide key insights into this pathway and its role in disease. Firstly, disruption in TNF stimulated linear ubiquitination can result in severe dermatitis. Cell death, predominantly apoptosis, is a key driver of inflammation in the skin of these mice, and inhibition of cell death can rescue the inflammation. This suggests that modulation of cell death pathways should be further considered for inflammatory skin diseases. Secondly, RIP1 inhibition was more effective when LUBAC activity was reduced rather than when it was eliminated (Berger et al., 2014; Taraborrelli et al., 2018). However, there was a benefit to RIP1 inhibition in addition to TNFR1 loss in the HOIP and HOIL-1L deficient mice (Taraborrelli et al., 2018), suggesting that the efficacy of RIP1 inhibition as a single agent might be context and disease specific. Additionally, the synergistic role of TNFR1 loss and RIP1 inhibition suggests that RIP1 inhibition is not just another means to disrupt the TNF signaling pathway, but scenarios where anti-TNFs and RIP1 inhibitors could be used in combination should be explored further.

Inducible inactivation of OTULIN's DUB function in adult mice results in extensive hepatocyte and intestinal crypt cell death, and inflammation, primarily driven by myeloid cells, in the heart and liver (Heger et al., 2018). Similarly, co-deletion of *Birc2* and *Birc3*, which encode c-IAP1 and c-IAP2, respectively, in adult mice results in extensive hepatocyte death and crypt degeneration with intestinal villous atrophy and secondary inflammation (Zhang J. et al., 2019). In both OTULIN and c-IAP1/2 deficient mice, cell death in the liver and intestines was associated with extensive cleaved caspase-3 immunolabeling, suggesting a predominance of apoptosis (Heger et al., 2018; Zhang J. et al., 2019). While loss of RIP3 alone does not prevent lesions in either mouse, loss of caspase-8 and RIP3 rescued both the cell death and, to a significant degree, the associated inflammation. Since caspase-8 loss is embryonic lethal due to RIP3 mediated necroptosis, it is impossible to determine the independent contribution of apoptosis. However, the lack of protection with RIP3 loss alone and the extensive cleaved caspase-3 labeling suggests that apoptosis is the primary driver of the pro-inflammatory phenotype in these mice. In line with these observations in systemic, inducible *Otulin* or *Birc2/3* knock-out mice, hepatocyte specific deletion of *Otulin* results in hepatocyte apoptosis with resultant compensatory hyperplasia and inflammation that can progress to hepatocellular carcinoma (Damgaard et al., 2020; Verboom et al., 2020). Increased cell death and steatosis is evident in these mice by postnatal day 9. Interestingly, steatosis and increased liver enzymes were also identified in an OTULIN deficient patient (Damgaard et al., 2020). This hepatic injury can be alleviated by the loss of RIP1 kinase activity due to expression of the $RIP1^{D138N}$ kinase dead protein, and more completely rescued by hepatocyte-specific *Fadd* deletion, indicating that the injury is driven by apoptosis signaling (Verboom et al., 2020), although loss of TNFR1 is not sufficient to protect against liver pathology in these mice (Damgaard et al., 2020). mTOR signaling is also increased in livers with hepatocyte-specific OTULIN deficiency. While treatment with the mTOR inhibitor rapamycin reduced the proliferative lesions and fibrosis in these mice, it did not reduce serum alanine aminotransferase (ALT) or aspartate aminotransferase (AST) levels, which suggests that while mTOR may be important for the proliferative response, it might not be the driver of the initial hepatocyte injury (Damgaard et al., 2020).

In contrast to germline loss of other components of the ubiquitin machinery, including LUBAC, OTULIN, and c-IAP1/2, that result in embryonic lethality, A20 deficient mice survive to birth, but subsequently develop multi-systemic inflammation that includes dermatitis, hepatitis, nephritis, enteritis, and arthritis (Lee et al., 2000). Inflammation in these mice appears to be lymphocyte independent because there was no protection when A20 deficient mice were crossed to *Rag1* knock-out mice (Lee et al., 2000). Consistent with their development of multi-systemic inflammation, *A20* knock-out mice have increased susceptibility to LPS and TNF, and this is associated with persistent NF-κB signaling in mouse embryonic fibroblasts (MEFs) (Lee et al., 2000). Loss of RIP3 or RIP1 kinase activity due the D138A kinase dead mutation significantly prolongs the survival of A20 deficient mice; however, a similar benefit is not observed in *Mlkl* knock-out mice (Onizawa et al., 2015; Newton et al., 2016). The difference in protection between RIP3 and MLKL deficient mice highlights the potential for necroptotic-independent functions of RIP3, which are not fully characterized.

DYSREGULATION OF TNF SIGNALING IN INTESTINAL INFLAMMATION AND ARTHRITIS

The role of TNF in inflammatory bowel disease and rheumatoid arthritis has been well established both in mouse models and in clinical practice (Williams et al., 1992; Elliott et al., 1993; Targan et al., 1997; Kontoyiannis et al., 1999). Constitutive

TNF over-expression in the TNFΔARE mice, which have increased *Tnf* mRNA production and stability, develop Crohn's-like ileitis that can progress to transmural and granulomatous inflammation and arthritis (Kontoyiannis et al., 1999). Ileitis even develops when TNF over-expression is restricted to intestinal enterocytes, although the disease onset and progression is delayed compared to mice with systemic TNF over-expression (Roulis et al., 2011; Bamias et al., 2013a). However, while TNF signaling in enterocytes causes apoptosis, it is not sufficient to cause ileitis, indicating the importance of paracrine signaling in other stromal and immune cells, rather than just enterocyte-restricted autocrine signaling (Roulis et al., 2011). Considering the permissive effects of TNF and the complexity of inflammatory bowel disease, it should not be surprising that disease progression requires an interplay of the epithelial, stromal, and hematopoietic compartments. Arthritis in TNFΔARE mice is characterized by synovial hyperplasia and myeloid infiltrates that progresses to cartilage and bone erosion and fibrosis, resulting in pannus (Kontoyiannis et al., 1999). Similarly, bone phenotype spontaneous mutation 1 (BPSM1) mice that have increased TNF expression due to a spontaneous insertion of a small interspersed element (SINE) in the 3' untranslated region of *Tnf*, develop severe, progressive arthritis and valvular endocarditis with aortic aneurysm (Lacey et al., 2015). Development of arthritis requires local TNF production, as evidenced by the lack of joint changes in TNFΔARE mice with intestinal-specific TNF hyper-secretion (Bamias et al., 2013b). In BPSM1 mice, bone marrow transplantation of wild-type or BPSM1 cells and genetic crosses with $Tnfr1^{-/-}$ mice suggest that while myeloid cells are necessary for TNF production in this model, TNFR1 signaling on non-hematopoietic cells, presumable synoviocytes, is required for the development of arthritis (Lacey et al., 2015). TNF blockade is also protective in collagen-induced and anti-collagen antibody-induced arthritis models (Williams et al., 1992; Patel et al., 2020), and this is consistent with the clinical benefit of TNF blockade in rheumatoid arthritis patients. While RIP1 inhibition provided a similar benefit in anti-collagen antibody-induced arthritis model, there was no synergistic benefit in combining TNF and RIP1 inhibition (Patel et al., 2020). This is in contrast to the added protective benefit of combinatorial blockade in the development of dermatitis in LUBAC deficient mice (Taraborrelli et al., 2018). Therefore, the benefit of combination therapies is likely to be context specific and requires further exploration.

Patients with hypomorphic *NEMO* mutations frequently develop colitis. The fact that this colitis is not responsive to hematopoietic stem cell transplantation suggests that NEMO deficiency has cell autonomous effects in intestinal enterocytes (Miot et al., 2017). This has been studied in mice by using a Cre recombinase driven by the *villin* promoter to specifically delete *Nemo* from intestinal epithelial cells. Enterocyte-specific NEMO loss results in severe colitis, particularly in the proximal colon, and small intestinal crypt cell death with Paneth cell loss (Nenci et al., 2007; Vlantis et al., 2016). While TNFR1 loss and germ-free conditions protect against colitis, increased cell death in the small intestine remains (Vlantis et al., 2016). Similar to *SHARPIN*-mutant mice, RIP3 loss affords inconsistent and incomplete protection in NEMO deficient mice, while inactivation of RIP1 kinase activity via $RIP1^{D138N}$ or RIP3 and FADD combined ablation provide complete protection (Vlantis et al., 2016). Pharmacologic RIP1 inhibition is similarly fully protective in these mice (Patel et al., 2020). Again, this suggests that RIP1 mediated apoptosis can drive both extensive tissue damage and inflammation in the context of dysfunctional TNF signaling.

While TNF signaling is biased toward cell death pathways in NEMO deficient mice, presumably in part due to a lack of NF-κB signaling, enterocytes with overactive NF-κB signaling are also sensitive to TNF-induced cell death. $IKK\beta\ (EE)^{IEC}$ mice have constitutive NF-κB signaling in intestinal epithelial cells (Guma et al., 2011). These mice have increased sensitivity to LPS due to MAPK mediated TNF production (Guma et al., 2011). TNF stimulation in enteroids from these mice causes intestinal epithelial cell apoptosis, as noted by increased cleaved caspase-3 and caspase-8. Genetic loss of RIP1 catalytic activity through expression of $RIP1^{D138N}$ protected enterocytes from TNF induced apoptosis, while RIP3 loss was not protective. Similarly, both genetic and pharmacologic RIP1 inactivation protected these mice from LPS induced intestinal cell death *in vivo* (Wong et al., 2020). Together, the increased susceptibility of both the $IKK\beta\ (EE)^{IEC}$ mice and NEMO deficient mice to TNF-induced apoptosis suggests that NF-κB signaling needs to be tightly controlled and dysregulation in either direction may shift TNF signaling from a pro-survival to a pro-death pathway. Interestingly, RIP1 kinase activity is a potent driver of cell death in both scenarios. This further strengthens the hypothesis that RIP1 inhibition may provide a therapeutic benefit to IBD patients.

The $ATG16L1^{T300A}$ polymorphism is associated with Crohn's disease, and ATG16L1 has an important role in Paneth cell survival and function (Cadwell et al., 2008). Norovirus infected mice with reduced ATG16L1 expression have decreased and disorganized Paneth cell granules and decreased lysozyme, and similar defects have been identified in Crohn's disease patients (Cadwell et al., 2008, 2010). ATG16L1 deficient mice also have increased susceptibility to dextran sodium sulfate (DSS)-induced colitis and, in the presence of norovirus infection, develop small intestinal villous atrophy and have loss of Paneth cells. This small intestinal pathology is driven by increased epithelial TNF production and subsequent cell death, and is protected by RIP1 kinase inhibition (Matsuzawa-Ishimoto et al., 2017). Increased Paneth cell death has been identified in the ileum of Crohn's disease patients, and treatment of control patient biopsies with TNF has been shown to reduce Paneth cell-associated *lysozyme* mRNA, which can be rescued by Nec-1, a RIP1 inhibitor (Gunther et al., 2011). Considering the importance of Paneth cells in producing anti-microbial peptides and innate immune responses in the intestine, TNF mediated Paneth cell death may play an important role in the pathogenesis of Crohn's disease. Given the protection observed with RIP1 inhibitors in the survival of mouse and human Paneth cells, and the intrinsic role of RIP1 kinase activity in intestinal pathology secondary to

NFκB dysregulation, RIP1 inhibitors should be further evaluated in the treatment of inflammatory bowel disease.

RIP1 INHIBITORS FOR TREATMENT OF TNF MEDIATED INFLAMMATORY DISEASES

While TNF inhibition is efficacious in the treatment of many inflammatory disease, it is also associated with immunosuppression and increased risk of infections, and many patients are refractory to TNF inhibitors (Taylor and Feldmann, 2009; Adegbola et al., 2018). RIP1 inhibition may provide an alternative mechanism to treat inflammatory diseases with no known risk of immunosuppression (Shan et al., 2018; Yuan et al., 2019). While the *Rip1* knock-out mouse dies in the perinatal period due to RIP3 mediated inflammation and caspase 8 mediated intestinal apoptosis (Kelliher et al., 1998; Dillon et al., 2014; Kaiser et al., 2014), catalytically dead *Rip1* knock-in (RIP1 KD) mice are viable and healthy, even when aged to 18 months (Berger et al., 2014; Kaiser et al., 2014; Newton et al., 2014; Polykratis et al., 2014; Webster et al., 2020). $RIP1^{D138N}$ KD mice were able to clear both vaccinia virus and mouse gammaherpesvirus, MHV68, at a similar rate compared to wild-type mice and these mice showed no immunologic dysfunction following MHV68 infection (Webster et al., 2020). This suggests that while RIP1 scaffolding functions are essential for survival, RIP1 kinase activity can be inhibited without detrimental effects.

As described above, RIP1 kinase inhibition is protective against inflammation in the skin, intestines, and joints secondary to dysfunctions in TNF and NF-κB signaling (Berger et al., 2014; Vlantis et al., 2016; Patel et al., 2020; Webster et al., 2020; Wong et al., 2020). Patients with mutations in these pathways have variably responded to different biologics including anti-IL-1, anti-TNF, and anti-IL-6 molecules (Damgaard et al., 2016; Zhou et al., 2016b; Lalaoui et al., 2020; Tao et al., 2020). It still is to be seen whether these patients would benefit from RIP1 inhibitors. The role of RIP1 kinase activity in inflammation is also evident in the TNF-induced systemic inflammatory response syndrome (SIRS) model, in which genetic or pharmacologic RIP1 inhibition is protective (Newton et al., 2014; Polykratis et al., 2014; Newton et al., 2016; Patel et al., 2020). Interestingly, in some disease models, such as anti-collagen antibody-induced arthritis, combined RIP1 and TNF inhibition does not show a synergistic effect suggesting these proteins are working on a linear pathway (Patel et al., 2020). However, in other models, such as HOIP and HOIL-1L deficient mice, TNF and RIP1 inhibition plays a synergistic role (Taraborrelli et al., 2018), indicating that combination therapies might be efficacious in some diseases. Although RIP1 has been implicated in numerous disease models, the results have not always been reproducible (Newton et al., 2016; Patel et al., 2020; Webster et al., 2020). Therefore, more studies are needed to define the context and potential combination therapies that will provide the maximal benefit for RIP1 inhibition. However, the true test of RIP1 inhibition in inflammatory diseases will be in clinical trials.

To date, GlaxoSmithKline (GSK) and Denali have tested their RIP1 inhibitors in clinical settings and reported that GSK2982772 and DNL104 were generally well tolerated in human subjects (Harris et al., 2017; Weisel et al., 2017; Grievink et al., 2020; Jensen et al., 2020; Martens S. et al., 2020). Denali's brain-penetrant RIP1 inhibitor DNL104 did not cause any central nervous system toxicities but 37% percent of subjects receiving multiple doses of DNL104 had post-dose liver toxicity (Grievink et al., 2020). Denali has, in the meantime, terminated clinical examination of DNL104 and in collaboration with Sanofi entered another RIP1 inhibitor, DNL747, in clinical trials for Alzheimer's disease, amylotrophic lateral sclerosis, and multiple sclerosis (Jensen et al., 2020; Martens S. et al., 2020). GSK2982772 is a systemic, non-brain penetrant RIP1 inhibitor was well-tolerated with no serious adverse events (AEs) and no suggestion of a safety concern (Weisel et al., 2017). Encouraged by favorable safety data, GSK has entered GSK2982772 into small phase 2 clinical trials for psoriasis, rheumatoid arthritis, and ulcerative colitis. So far, GSK2982772 has not shown significant therapeutic benefit in psoriasis or rheumatoid arthritis (clinicatrials.gov), while the data from the ulcerative colitis trial are still pending. GSK has also ventured into cancer trials with a different RIP1 inhibitor, GSK3145095 (Harris et al., 2019). However, that particular trial, designed to test the ability of RIP1 inhibitor to provide benefit in pancreatic and other solid tumors, was relatively quickly terminated (Martens S. et al., 2020). This may not come as a complete surprise given that protective role of RIP1 inhibition in pancreatic cancer was never fully validated (Patel et al., 2020). Thus, although RIP1 inhibition presents an attractive opportunity to target TNF mediated inflammatory diseases, further efforts are needed to fully explore this therapeutic strategy.

AUTHOR CONTRIBUTIONS

JW and DV wrote and contributed to this manuscript and approved this submission.

REFERENCES

Abed, M., Verschueren, E., Budayeva, H., Liu, P., Kirkpatrick, D. S., Reja, R., et al. (2019). The Gag protein PEG10 binds to RNA and regulates trophoblast stem cell lineage specification. *PLoS One* 14:e0214110. doi: 10.1371/journal.pone.0214110

Adegbola, S. O., Sahnan, K., Warusavitarne, J., Hart, A., and Tozer, P. (2018). Anti-TNF Therapy in Crohn's Disease. *Int. J. Mol. Sci.* 19:2244.

Amin, P., Florez, M., Najafov, A., Pan, H., Geng, J., Ofengeim, D., et al. (2018). Regulation of a distinct activated RIPK1 intermediate bridging complex I and complex II in TNFalpha-mediated apoptosis. *Proc. Natl. Acad. Sci. U.S.A.* 115, E5944–E5953. doi: 10.1073/pnas.1806973115

Bamias, G., Dahman, M. I., Arseneau, K. O., Guanzon, M., Gruska, D., Pizarro, T. T., et al. (2013a). Intestinal-specific TNFalpha overexpression induces Crohn's-like ileitis in mice. *PLoS One* 8:e72594. doi: 10.1371/journal.pone.0072594

Bamias, G., Stamatelopoulos, K., Zampeli, E., Protogerou, A., Sigala, F., Papamichael, C., et al. (2013b). Circulating levels of TNF-like cytokine 1A correlate with the progression of atheromatous lesions in patients with rheumatoid arthritis. *Clin. Immunol.* 147, 144–150. doi: 10.1016/j.clim.2013.03.002

Berger, S. B., Kasparcova, V., Hoffman, S., Swift, B., Dare, L., Schaeffer, M., et al. (2014). Cutting Edge: RIP1 kinase activity is dispensable for normal development but is a key regulator of inflammation in SHARPIN-deficient mice. *J. Immunol.* 192, 5476–5480. doi: 10.4049/jimmunol.1400499

Bertrand, M. J., Milutinovic, S., Dickson, K. M., Ho, W. C., Boudreault, A., Durkin, J., et al. (2008). cIAP1 and cIAP2 facilitate cancer cell survival by functioning as E3 ligases that promote RIP1 ubiquitination. *Mol. Cell* 30, 689–700. doi: 10.1016/j.molcel.2008.05.014

Black, R. A., Rauch, C. T., Kozlosky, C. J., Peschon, J. J., Slack, J. L., Wolfson, M. F., et al. (1997). A metalloproteinase disintegrin that releases tumour-necrosis factor-alpha from cells. *Nature* 385, 729–733. doi: 10.1038/385729a0

Boisson, B., Laplantine, E., Dobbs, K., Cobat, A., Tarantino, N., Hazen, M., et al. (2015). Human HOIP and LUBAC deficiency underlies autoinflammation, immunodeficiency, amylopectinosis, and lymphangiectasia. *J. Exp. Med.* 212, 939–951. doi: 10.1084/jem.20141130

Boisson, B., Laplantine, E., Prando, C., Giliani, S., Israelsson, E., Xu, Z., et al. (2012). Immunodeficiency, autoinflammation and amylopectinosis in humans with inherited HOIL-1 and LUBAC deficiency. *Nat. Immunol.* 13, 1178–1186. doi: 10.1038/ni.2457

Brummelkamp, T. R., Nijman, S. M., Dirac, A. M., and Bernards, R. (2003). Loss of the cylindromatosis tumour suppressor inhibits apoptosis by activating NF-κB-. *Nature* 424, 797–801. doi: 10.1038/nature01811

Cadwell, K., Liu, J. Y., Brown, S. L., Miyoshi, H., Loh, J., Lennerz, J. K., et al. (2008). A key role for autophagy and the autophagy gene Atg16l1 in mouse and human intestinal Paneth cells. *Nature* 456, 259–263. doi: 10.1038/nature07416

Cadwell, K., Patel, K. K., Maloney, N. S., Liu, T. C., Ng, A. C., Storer, C. E., et al. (2010). Virus-plus-susceptibility gene interaction determines Crohn's disease gene Atg16L1 phenotypes in intestine. *Cell* 141, 1135–1145. doi: 10.1016/j.cell.2010.05.009

Cai, Z., Jitkaew, S., Zhao, J., Chiang, H. C., Choksi, S., Liu, J., et al. (2014). Plasma membrane translocation of trimerized MLKL protein is required for TNF-induced necroptosis. *Nat. Cell Biol.* 16, 55–65. doi: 10.1038/ncb2883

Chen, W., Zhou, Z., Li, L., Zhong, C. Q., Zheng, X., Wu, X., et al. (2013). Diverse sequence determinants control human and mouse receptor interacting protein 3 (RIP3) and mixed lineage kinase domain-like (MLKL) interaction in necroptotic signaling. *J. Biol. Chem.* 288, 16247–16261. doi: 10.1074/jbc.M112.435545

Chien, S. J., Silva, K. A., Kennedy, V. E., HogenEsch, H., and Sundberg, J. P. (2015). The pathogenesis of chronic eosinophilic esophagitis in SHARPIN-deficient mice. *Exp. Mol. Pathol.* 99, 460–467. doi: 10.1016/j.yexmp.2015.08.012

Cho, Y. S., Challa, S., Moquin, D., Genga, R., Ray, T. D., Guildford, M., et al. (2009). Phosphorylation-driven assembly of the RIP1-RIP3 complex regulates programmed necrosis and virus-induced inflammation. *Cell* 137, 1112–1123. doi: 10.1016/j.cell.2009.05.037

Cuchet-Lourenco, D., Eletto, D., Wu, C., Plagnol, V., Papapietro, O., Curtis, J., et al. (2018). Biallelic RIPK1 mutations in humans cause severe immunodeficiency, arthritis, and intestinal inflammation. *Science* 361, 810–813. doi: 10.1126/science.aar2641

Damgaard, R. B., Elliott, P. R., Swatek, K. N., Maher, E. R., Stepensky, P., Elpeleg, O., et al. (2019). OTULIN deficiency in ORAS causes cell type-specific LUBAC degradation, dysregulated TNF signalling and cell death. *EMBO Mol. Med.* 11:e9324. doi: 10.15252/emmm.201809324

Damgaard, R. B., Jolin, H. E., Allison, M. E. D., Davies, S. E., Titheradge, H. L., McKenzie, A. N. J., et al. (2020). OTULIN protects the liver against cell death, inflammation, fibrosis, and cancer. *Cell Death Differ.* 27, 1457–1474. doi: 10.1038/s41418-020-0532-1

Damgaard, R. B., Walker, J. A., Marco-Casanova, P., Morgan, N. V., Titheradge, H. L., Elliott, P. R., et al. (2016). The deubiquitinase OTULIN Is an essential negative regulator of inflammation and autoimmunity. *Cell* 166, 1215.e20–1230.e20. doi: 10.1016/j.cell.2016.07.019

Degterev, A., Hitomi, J., Germscheid, M., Ch'en, I. L., Korkina, O., Teng, X., et al. (2008). Identification of RIP1 kinase as a specific cellular target of necrostatins. *Nat. Chem. Biol.* 4, 313–321. doi: 10.1038/nchembio.83

Dillon, C. P., Weinlich, R., Rodriguez, D. A., Cripps, J. G., Quarato, G., Gurung, P., et al. (2014). RIPK1 blocks early postnatal lethality mediated by caspase-8 and RIPK3. *Cell* 157, 1189–1202. doi: 10.1016/j.cell.2014.04.018

Doffinger, R., Smahi, A., Bessia, C., Geissmann, F., Feinberg, J., Durandy, A., et al. (2001). X-linked anhidrotic ectodermal dysplasia with immunodeficiency is caused by impaired NF-κB- signaling. *Nat. Genet.* 27, 277–285. doi: 10.1038/85837

Dondelinger, Y., Declercq, W., Montessuit, S., Roelandt, R., Goncalves, A., Bruggeman, I., et al. (2014). MLKL compromises plasma membrane integrity by binding to phosphatidylinositol phosphates. *Cell Rep.* 7, 971–981. doi: 10.1016/j.celrep.2014.04.026

Dynek, J. N., Goncharov, T., Dueber, E. C., Fedorova, A. V., Izrael-Tomasevic, A., Phu, L., et al. (2010). c-IAP1 and UbcH5 promote K11-linked polyubiquitination of RIP1 in TNF signalling. *Embo J.* 29, 4198–4209. doi: 10.1038/emboj.2010.300

Elliott, M. J., Maini, R. N., Feldmann, M., Long-Fox, A., Charles, P., Katsikis, P., et al. (1993). Treatment of rheumatoid arthritis with chimeric monoclonal antibodies to tumor necrosis factor alpha. *Arthritis Rheumatism* 36, 1681–1690. doi: 10.1002/art.23362

Elliott, P. R., Leske, D., Hrdinka, M., Bagola, K., Fiil, B. K., McLaughlin, S. H., et al. (2016). SPATA2 links CYLD to LUBAC, activates CYLD, and controls LUBAC signaling. *Mol. Cell* 63, 990–1005. doi: 10.1016/j.molcel.2016.08.001

Elliott, P. R., Nielsen, S. V., Marco-Casanova, P., Fiil, B. K., Keusekotten, K., Mailand, N., et al. (2014). Molecular basis and regulation of OTULIN-LUBAC interaction. *Mol. Cell* 54, 335–348. doi: 10.1016/j.molcel.2014.03.018

Enesa, K., Zakkar, M., Chaudhury, H., Luong le, A., Rawlinson, L., Mason, J. C., et al. (2008). NF-κB- suppression by the deubiquitinating enzyme Cezanne: a novel negative feedback loop in Pro-inflammatory signaling. *J. Biol, Chem.* 283, 7036–7045. doi: 10.1074/jbc.M708690200

Fiil, B. K., Damgaard, R. B., Wagner, S. A., Keusekotten, K., Fritsch, M., Bekker-Jensen, S., et al. (2013). OTULIN restricts Met1-linked ubiquitination to control innate immune signaling. *Mol. Cell* 50, 818–830. doi: 10.1016/j.molcel.2013.06.004

Gerlach, B., Cordier, S. M., Schmukle, A. C., Emmerich, C. H., Rieser, E., Haas, T. L., et al. (2011). Linear ubiquitination prevents inflammation and regulates immune signalling. *Nature* 471, 591–596. doi: 10.1038/nature09816

Gijbels, M. J., Zurcher, C., Kraal, G., Elliott, G. R., HogenEsch, H., Schijff, G., et al. (1996). Pathogenesis of skin lesions in mice with chronic proliferative dermatitis (cpdm/cpdm). *Am. J. Pathol.* 148, 941–950.

Grell, M., Douni, E., Wajant, H., Lohden, M., Clauss, M., Maxeiner, B., et al. (1995). The transmembrane form of tumor necrosis factor is the prime activating ligand of the 80 kDa tumor necrosis factor receptor. *Cell* 83, 793–802. doi: 10.1016/0092-8674(95)90192-2

Grievink, H. W., Heuberger, J., Huang, F., Chaudhary, R., Birkhoff, W. A. J., Tonn, G. R., et al. (2020). DNL104, a centrally penetrant RIPK1 inhibitor, inhibits RIP1 kinase phosphorylation in a randomized phase I ascending dose study in healthy volunteers. *Cli. Pharmacol. Ther.* 107, 406–414. doi: 10.1002/cpt.1615

Guma, M., Stepniak, D., Shaked, H., Spehlmann, M. E., Shenouda, S., Cheroutre, H., et al. (2011). Constitutive intestinal NF-κB- does not trigger destructive inflammation unless accompanied by MAPK activation. *J. Exp. Med.* 208, 1889–1900. doi: 10.1084/jem.20110242

Gunther, C., Martini, E., Wittkopf, N., Amann, K., Weigmann, B., Neumann, H., et al. (2011). Caspase-8 regulates TNF-alpha-induced epithelial necroptosis and terminal ileitis. *Nature* 477, 335–339. doi: 10.1038/nature10400

Haas, T. L., Emmerich, C. H., Gerlach, B., Schmukle, A. C., Cordier, S. M., Rieser, E., et al. (2009). Recruitment of the linear ubiquitin chain assembly complex stabilizes the TNF-R1 signaling complex and is required for TNF-mediated gene induction. *Mol. Cell* 36, 831–844. doi: 10.1016/j.molcel.2009.10.013

Harris, P. A., Berger, S. B., Jeong, J. U., Nagilla, R., Bandyopadhyay, D., Campobasso, N., et al. (2017). Discovery of a first-in-class receptor interacting protein 1 (RIP1) kinase specific clinical candidate (GSK2982772) for the treatment of inflammatory diseases. *J. Med. Chem.* 60, 1247–1261. doi: 10.1021/acs.jmedchem.6b01751

Harris, P. A., Marinis, J. M., Lich, J. D., Berger, S. B., Chirala, A., Cox, J. A., et al. (2019). Identification of a RIP1 kinase inhibitor clinical Candidate (GSK3145095) for the treatment of pancreatic cancer. *Med. Chem. Lett.* 10, 857–862. doi: 10.1021/acsmedchemlett.9b00108

He, S., Wang, L., Miao, L., Wang, T., Du, F., Zhao, L., et al. (2009). Receptor interacting protein kinase-3 determines cellular necrotic response to TNF-alpha. *Cell* 137, 1100–1111. doi: 10.1016/j.cell.2009.05.021

Heger, K., Wickliffe, K. E., Ndoja, A., Zhang, J., Murthy, A., Dugger, D. L., et al. (2018). OTULIN limits cell death and inflammation by deubiquitinating LUBAC. *Nature* 559, 120–124. doi: 10.1038/s41586-018-0256-2

Hildebrand, J. M., Tanzer, M. C., Lucet, I. S., Young, S. N., Spall, S. K., Sharma, P., et al. (2014). Activation of the pseudokinase MLKL unleashes the four-helix bundle domain to induce membrane localization and necroptotic cell death. *Proc. Natl. Acad. Sci. U.S.A.* 111, 15072–15077. doi: 10.1073/pnas.1408987111

HogenEsch, H., Gijbels, M. J., Offerman, E., van Hooft, J., van Bekkum, D. W., and Zurcher, C. (1993). A spontaneous mutation characterized by chronic proliferative dermatitis in C57BL mice. *Am. J. Pathol.* 143, 972–982.

HogenEsch, H., Janke, S., Boggess, D., and Sundberg, J. P. (1999). Absence of Peyer's patches and abnormal lymphoid architecture in chronic proliferative dermatitis (cpdm/cpdm) mice. *J. Immunol.* 162, 3890–3896.

Ikeda, F., Deribe, Y. L., Skanland, S. S., Stieglitz, B., Grabbe, C., and Franz-Wachtel, M. (2011). SHARPIN forms a linear ubiquitin ligase complex regulating NF-κB-activity and apoptosis. *Nature* 471, 637–641. doi: 10.1038/nature09814

Jensen, S., Seidelin, J. B., LaCasse, E. C., and Nielsen, O. H. (2020). SMAC mimetics and RIPK inhibitors as therapeutics for chronic inflammatory diseases. *Sci. Signal.* 13:aax8295. doi: 10.1126/scisignal.aax8295

Kaiser, W. J., Daley-Bauer, L. P., Thapa, R. J., Mandal, P., Berger, S. B., Huang, C., et al. (2014). RIP1 suppresses innate immune necrotic as well as apoptotic cell death during mammalian parturition. *Proc. Natl. Acad. Sci. U.S.A.* 111, 7753–7758. doi: 10.1073/pnas.1401857111

Kaiser, W. J., Upton, J. W., Long, A. B., Livingston-Rosanoff, D., Daley-Bauer, L. P., Hakem, R., et al. (2011). RIP3 mediates the embryonic lethality of caspase-8-deficient mice. *Nature* 471, 368–372. doi: 10.1038/nature09857

Kato, M., Sanada, M., Kato, I., Sato, Y., Takita, J., Takeuchi, K., et al. (2009). Frequent inactivation of A20 in B-cell lymphomas. *Nature* 459, 712–716.

Kelliher, M. A., Grimm, S., Ishida, Y., Kuo, F., Stanger, B. Z., and Leder, P. (1998). The death domain kinase RIP mediates the TNF-induced NF-κB- signal. *Immunity* 8, 297–303. doi: 10.1016/s1074-7613(00)80535-x

Keusekotten, K., Elliott, P. R., Glockner, L., Fiil, B. K., Damgaard, R. B., Kulathu, Y., et al. (2013). OTULIN antagonizes LUBAC signaling by specifically hydrolyzing Met1-linked polyubiquitin. *Cell* 153, 1312–1326. doi: 10.1016/j.cell.2013.05.014

Khan, N., Lawlor, K. E., Murphy, J. M., and Vince, J. E. (2014). More to life than death: molecular determinants of necroptotic and non-necroptotic RIP3 kinase signaling. *Curr. Opin. Immunol.* 26C, 76–89. doi: 10.1016/j.coi.2013.10.017

Kirisako, T., Kamei, K., Murata, S., Kato, M., Fukumoto, H., Kanie, M., et al. (2006). A ubiquitin ligase complex assembles linear polyubiquitin chains. *Embo J.* 25, 4877–4887. doi: 10.1038/sj.emboj.7601360

Kontoyiannis, D., Pasparakis, M., Pizarro, T. T., Cominelli, F., and Kollias, G. (1999). Impaired on/off regulation of TNF biosynthesis in mice lacking TNF AU-rich elements: implications for joint and gut-associated immunopathologies. *Immunity* 10, 387–398. doi: 10.1016/s1074-7613(00)80038-2

Kovalenko, A., Chable-Bessia, C., Cantarella, G., Israel, A., Wallach, D., and Courtois, G. (2003). The tumour suppressor CYLD negatively regulates NF-κB-signalling by deubiquitination. *Nature* 424, 801–805. doi: 10.1038/nature01802

Kumari, S., Redouane, Y., Lopez-Mosqueda, J., Shiraishi, R., Romanowska, M., and Lutzmayer, S. (2014). Sharpin prevents skin inflammation by inhibiting TNFR1-induced keratinocyte apoptosis. *eLife* 3:e03422. doi: 10.7554/eLife.03422

Kupka, S., De Miguel, D., Draber, P., Martino, L., Surinova, S., Rittinger, K., et al. (2016). SPATA2-Mediated binding of CYLD to HOIP enables CYLD recruitment to signaling complexes. *Cell Rep.* 16, 2271–2280. doi: 10.1016/j.celrep.2016.07.086

Lacey, D., Hickey, P., Arhatari, B. D., O'Reilly, L. A., Rohrbeck, L., Kiriazis, H., et al. (2015). Spontaneous retrotransposon insertion into TNF 3′UTR causes heart valve disease and chronic polyarthritis. *Proc. Natl. Acad .Sci. U.S.A.* 112, 9698–9703. doi: 10.1073/pnas.1508399112

Lalaoui, N., Boyden, S. E., Oda, H., Wood, G. M., Stone, D. L., Chau, D., et al. (2020). Mutations that prevent caspase cleavage of RIPK1 cause autoinflammatory disease. *Nature* 577, 103–108. doi: 10.1038/s41586-019-1828-5

Laurien, L., Nagata, M., Schunke, H., Delanghe, T., Wiederstein, J. L., Kumari, S., et al. (2020). Autophosphorylation at serine 166 regulates RIP kinase 1-mediated cell death and inflammation. *Nat. Commun.* 11:1747. doi: 10.1038/s41467-020-15466-8

Lee, E. G., Boone, D. L., Chai, S., Libby, S. L., Chien, M., Lodolce, J. P., et al. (2000). Failure to regulate TNF-induced NF-κB- and cell death responses in A20-deficient mice. *Science* 289, 2350–2354. doi: 10.1126/science.289.5488.2350

Liang, Y., Seymour, R. E., and Sundberg, J. P. (2011). Inhibition of NF-κB- signaling retards eosinophilic dermatitis in SHARPIN-deficient mice. *J. Invest Dermatol.* 131, 141–149. doi: 10.1038/jid.2010.259

Mahoney, D. J., Cheung, H. H., Mrad, R. L., Plenchette, S., Simard, C., Enwere, E., et al. (2008). Both cIAP1 and cIAP2 regulate TNFalpha-mediated NF-κB-activation. *Proc. Natl. Acad. Sci. U.S.A.* 105, 11778–11783. doi: 10.1073/pnas.0711122105

Majkut, J., Sgobba, M., Holohan, C., Crawford, N., Logan, A. E., Kerr, E., et al. (2014). Longley, differential affinity of FLIP and procaspase 8 for FADD's DED binding surfaces regulates DISC assembly. *Nat. Commun.* 5:3350. doi: 10.1038/ncomms4350

Manthiram, K., Zhou, Q., Aksentijevich, I., and Kastner, D. L. (2017). , The monogenic autoinflammatory diseases define new pathways in human innate immunity and inflammation. *Nat. Immunol.* 18, 832–842. doi: 10.1038/ni1117-1271a

Martens, A., Priem, D., Hoste, E., Vetters, J., Rennen, S., Catrysse, L., et al. (2020). Two distinct ubiquitin-binding motifs in A20 mediate its anti-inflammatory and cell-protective activities. *Nat. Immunol.* 21, 381–387. doi: 10.1038/s41590-020-0621-9

Martens, S., Hofmans, S., Declercq, W., Augustyns, K., and Vandenabeele, P. (2020). Inhibitors targeting RIPK1/RIPK3: Old and new drugs. *Trends Pharmacol. Scie.* 41, 209–224. doi: 10.1016/j.tips.2020.01.002

Matsuzawa-Ishimoto, Y., Shono, Y., Gomez, L. E., Hubbard-Lucey, V. M., Cammer, M., Neil, J., et al. (2017). Autophagy protein ATG16L1 prevents necroptosis in the intestinal epithelium. *J. Exp. Med.* 214, 3687–3705. doi: 10.1084/jem.20170558

Micheau, O., and Tschopp, J. (2003). Induction of TNF receptor I-mediated apoptosis via two sequential signaling complexes. *Cell* 114, 181–190. doi: 10.1016/s0092-8674(03)00521-x

Miot, C., Imai, K., Imai, C., Mancini, A. J., Kucuk, Z. Y., Kawai, T., et al. (2017). Hematopoietic stem cell transplantation in 29 patients hemizygous for hypomorphic IKBKG/NEMO mutations. *Blood* 130, 1456–1467. doi: 10.1182/blood-2017-03-771600

Moss, M. L., Jin, S. L., Milla, M. E., Bickett, D. M., Burkhart, W., and Carter, H. L. (1997). Cloning of a disintegrin metalloproteinase that processes precursor tumour-necrosis factor-alpha. *Nature* 385, 733–736. doi: 10.1038/385733a0

Moulin, M., Anderton, H., Voss, A. K., Thomas, T., Wong, W. W., Bankovacki, A., et al. (2012). IAPs limit activation of RIP kinases by TNF receptor 1 during development. *EMBO J.* 31, 1679–1691. doi: 10.1038/emboj.2012.18

Murphy, J. M., Czabotar, P. E., Hildebrand, J. M., Lucet, I. S., Zhang, J. G., Alvarez-Diaz, S., et al. (2013). The pseudokinase MLKL mediates necroptosis via a molecular switch mechanism. *Immunity* 39, 443–453. doi: 10.1016/j.immuni.2013.06.018

Nabavi, M., Shahrooei, M., Rokni-Zadeh, H., Vrancken, J., Changi-Ashtiani, M., and Darabi, K. (2019). Auto-inflammation in a patient with a novel homozygous OTULIN mutation. *J. Clin. Immunol.* 39, 138–141. doi: 10.1007/s10875-019-00599-3

Nastase, M. V., Zeng-Brouwers, J., Frey, H., Hsieh, L. T., Poluzzi, C., and Beckmann, J. (2016). An Essential role for SHARPIN in the regulation of caspase 1 activity in sepsis. *Am. J. Pathol.* 186, 1206–1220. doi: 10.1016/j.ajpath.2015.12.026

Nenci, A., Becker, C., Wullaert, A., Gareus, R., van Loo, G., Danese, S., et al. (2007). Epithelial NEMO links innate immunity to chronic intestinal inflammation. *Nature* 446, 557–561. doi: 10.1038/nature05698

Newton, K., Dugger, D. L., Maltzman, A., Greve, J. M., Hedehus, M., and Martin-McNulty, B. (2016). RIPK3 deficiency or catalytically inactive RIPK1 provides greater benefit than MLKL deficiency in mouse models of inflammation and tissue injury. *Cell Death Differ.* 23, 1565–1576. doi: 10.1038/cdd.2016.46

Newton, K., Dugger, D. L., Wickliffe, K. E., Kapoor, N., de Almagro, M. C., Vucic, D., et al. (2014). Activity of protein kinase RIPK3 determines whether cells

die by necroptosis or apoptosis. *Science* 343, 1357–1360. doi: 10.1126/science.1249361

Newton, K., Wickliffe, K. E., Dugger, D. L., Maltzman, A., Roose-Girma, M., Dohse, M., et al. (2019). Cleavage of RIPK1 by caspase-8 is crucial for limiting apoptosis and necroptosis. *Nature* 574, 428–431. doi: 10.1038/s41586-019-1548-x

Nilsson, J., Schoser, B., Laforet, P., Kalev, O., Lindberg, C., Romero, N. B., et al. (2013). Polyglucosan body myopathy caused by defective ubiquitin ligase RBCK1. *Ann. Neurol* 74, 914–919. doi: 10.1002/ana.23963

Oda, H., Beck, D. B., Kuehn, H. S., Sampaio Moura, N., Hoffmann, P., Ibarra, M., et al. (2019). Second Case of HOIP deficiency expands clinical features and defines inflammatory transcriptome regulated by LUBAC. *Front. Immunol.* 10:479. doi: 10.3389/fimmu.2019.00479

Oda, H., and Kastner, D. L. (2017). Genomics, biology, and human illness: advances in the monogenic autoinflammatory diseases. *Rheum. Dis. Clin. North Am.* 43, 327–345. doi: 10.1016/j.rdc.2017.04.011

Onizawa, M., Oshima, S., Schulze-Topphoff, U., Oses-Prieto, J. A., Lu, T., Tavares, R., et al. (2015). The ubiquitin-modifying enzyme A20 restricts ubiquitination of the kinase RIPK3 and protects cells from necroptosis. *Nat. Immunol.* 16, 618–627. doi: 10.1038/ni0715-785c

Patel, S., Webster, J. D., Varfolomeev, E., Kwon, Y. C., Cheng, J. H., Zhang, J., et al. (2020). RIP1 inhibition blocks inflammatory diseases but not tumor growth or metastases. *Cell Death Differ.* 27, 161–175. doi: 10.1038/s41418-019-0347-0

Peltzer, N., Darding, M., Montinaro, A., Draber, P., Draberova, H., Kupka, S., et al. (2018). LUBAC is essential for embryogenesis by preventing cell death and enabling haematopoiesis. *Nature* 557, 112–117. doi: 10.1038/s41586-018-0064-8

Peltzer, N., Rieser, E., Taraborrelli, L., Draber, P., Darding, M., Pernaute, B., et al. (2014). AHOIP deficiency causes embryonic lethality by aberrant TNFR1-mediated endothelial cell death. *Cell Rep.* 9, 153–165. doi: 10.1016/j.celrep.2014.08.066

Polykratis, A., Hermance, N., Zelic, M., Roderick, J., Kim, C., Van, T. M., et al. (2014). Cutting edge: RIPK1 Kinase inactive mice are viable and protected from TNF-induced necroptosis in vivo. *J. Immunol.* 193, 1539–1543. doi: 10.4049/jimmunol.1400590

Potter, C. S., Wang, Z., Silva, K. A., Kennedy, V. E., Stearns, T. M., Burzenski, L., et al. (2014). Chronic proliferative dermatitis in Sharpin null mice: development of an autoinflammatory disease in the absence of B and T lymphocytes and IL4/IL13 signaling. *PLoS One* 9:e85666. doi: 10.1371/journal.pone.0085666

Razani, B., Whang, M. I., Kim, F. S., Nakamura, M. C., Sun, X., and dvincula, R. A. (2020). Non-catalytic ubiquitin binding by A20 prevents psoriatic arthritis-like disease and inflammation. *Nat. Immunol.* 21, 422–433. doi: 10.1038/s41590-020-0634-4

Reddy, P., Slack, J. L., Davis, R., Cerretti, D. P., Kozlosky, C. J., Blanton, R. A., et al. (2000). Functional analysis of the domain structure of tumor necrosis factor-alpha converting enzyme. *J. Biol. Chem.* 275, 14608–14614. doi: 10.1074/jbc.275.19.14608

Rickard, J. A., Anderton, H., Etemadi, N., Nachbur, U., Darding, M., Peltzer, N., et al. (2014). TNFR1-dependent cell death drives inflammation in Sharpin-deficient mice. *eLife* 3:e03464. doi: 10.7554/eLife.03464

Rodriguez, D. A., Weinlich, R., Brown, S., Guy, C., Fitzgerald, P., Dillon, C. P., et al. (2016). Characterization of RIPK3-mediated phosphorylation of the activation loop of MLKL during necroptosis. *Cell Death Differ.* 23, 76–88. doi: 10.1038/cdd.2015.70

Roulis, M., Armaka, M., Manoloukos, M., Apostolaki, M., and Kollias, G. (2011). Intestinal epithelial cells as producers but not targets of chronic TNF suffice to cause murine Crohn-like pathology. *Proc. Natl. Acad .Sci. US.A.* 108, 5396–5401. doi: 10.1073/pnas.1007811108

Rubin, B. Y., Smith, L. J., Hellermann, G. R., Lunn, R. M., Richardson, N. K., and Anderson, S. L. (1988). Correlation between the anticellular and DNA fragmenting activities of tumor necrosis factor. *Cancer Res.* 48, 6006–6010.

Scheidereit, C. (2006). IκB kinase complexes: gateways to NF-κB activation and transcription. *Oncogene* 25, 6685–6705. doi: 10.1038/sj.onc.1209934

Schlicher, L., Wissler, M., Preiss, F., Brauns-Schubert, P., Jakob, C., Dumit, V., et al. (2016). SPATA2 promotes CYLD activity and regulates TNF-induced NF-κB- signaling and cell death. *EMBO Rep.* 17, 1485–1497. doi: 10.15252/embr.201642592

Sessler, T., Healy, S., Samali, A., and Szegezdi, E. (2013). Structural determinants of DISC function: new insights into death receptor-mediated apoptosis signalling. *Pharmacol. Ther.* 140, 186–199. doi: 10.1016/j.pharmthera.2013.06.009

Seymour, R. E., Hasham, M. G., Cox, G. A., Shultz, L. D., Hogenesch, H., Roopenian, D. C., et al. (2007). Spontaneous mutations in the mouse Sharpin gene result in multiorgan inflammation, immune system dysregulation and dermatitis. *Genes Immun.* 8, 416–421. doi: 10.1038/sj.gene.6364403

Shan, B., Pan, H., Najafov, A., and Yuan, J. (2018). Necroptosis in development and diseases. *Genes Dev.* 32, 327–340.

Shim, J. H., Xiao, C., Paschal, A. E., Bailey, S. T., Rao, P., Hayden, M. S., et al. (2005). TAK1, but not TAB1 or TAB2, plays an essential role in multiple signaling pathways in vivo. *Genes Dev.* 19, 2668–2681. doi: 10.1101/gad.1360605

Silke, J., and Vucic, D. (2014). IAP family of cell death and signaling regulators. *Methods Enzymol.* 545, 35–65. doi: 10.1016/B978-0-12-801430-1.00002-0

Smahi, A., Courtois, G., Vabres, P., Yamaoka, S., Heuertz, S., Munnich, A., et al. (2000). Genomic rearrangement in NEMO impairs NF-κB- activation and is a cause of incontinentia pigmenti. The International Incontinentia Pigmenti (IP) Consortium. *Nature* 405, 466–472. doi: 10.1038/35013114

Su, L., Quade, B., Wang, H., Sun, L., Wang, X., and Rizo, J. (2014). A plug release mechanism for membrane permeation by MLKL. *Structure* 22, 1489–1500. doi: 10.1016/j.str.2014.07.014

Sun, L., Wang, H., Wang, Z., He, S., Chen, S., Liao, D., et al. (2012). Mixed lineage kinase domain-like protein mediates necrosis signaling downstream of RIP3 kinase. *Cell* 148, 213–227. doi: 10.1016/j.cell.2011.11.031

Sun, X., Yin, J., Starovasnik, M. A., Fairbrother, W. J., and Dixit, V. M. (2002). Identification of a novel homotypic interaction motif required for the phosphorylation of receptor-interacting protein (RIP) by RIP3. *J. Biol. Chem.* 277, 9505–9511. doi: 10.1074/jbc.M109488200

Tao, P., Sun, J., Wu, Z., Wang, S., Wang, J., Li, W., et al. (2020). A dominant autoinflammatory disease caused by non-cleavable variants of RIPK1. *Nature* 577, 109–114. doi: 10.1038/s41586-019-1830-y

Taraborrelli, L., Peltzer, N., Montinaro, A., Kupka, S., Rieser, E., Hartwig, T., et al. (2018). LUBAC prevents lethal dermatitis by inhibiting cell death induced by TNF, TRAIL and CD95L. *Nat. Commun.* 9:3910. doi: 10.1038/s41467-018-06155-8

Targan, S. R., Hanauer, S. B., van Deventer, S. J., Mayer, L., Present, D. H., Braakman, T., et al. (1997). A short-term study of chimeric monoclonal antibody cA2 to tumor necrosis factor alpha for Crohn's disease. Crohn's disease cA2 study group. *N. Engl. J. Med.* 337, 1029–1035. doi: 10.1056/NEJM199710093371502

Taylor, P. C., and Feldmann, M. (2009). Anti-TNF biologic agents: still the therapy of choice for rheumatoid arthritis. *Nat. Rev. Rheumatol.* 5, 578–582. doi: 10.1038/nrrheum.2009.181

Tokunaga, F., and Iwai, K. (2012). LUBAC, a novel ubiquitin ligase for linear ubiquitination, is crucial for inflammation and immune responses. *Microbes Infect.* 14, 563–572. doi: 10.1016/j.micinf.2012.01.011

Tokunaga, F., Nakagawa, T., Nakahara, M., Saeki, Y., Taniguchi, M., Sakata, S., et al. (2011). SHARPIN is a component of the NF-κB–activating linear ubiquitin chain assembly complex. *Nature* 471, 633–636. doi: 10.1038/nature09815

Tokunaga, F., Nishimasu, H., Ishitani, R., Goto, E., Noguchi, T., Mio, K., et al. (2012). Specific recognition of linear polyubiquitin by A20 zinc finger 7 is involved in NF-κB- regulation. *EMBO J.* 31, 3856–3870. doi: 10.1038/emboj.2012.241

Tokunaga, F., Sakata, S., Saeki, Y., Satomi, Y., Kirisako, T., Kamei, K., et al. (2009). Involvement of linear polyubiquitylation of NEMO in NF-κB- activation. *Nat. Cell Biol.* 11, 123–132. doi: 10.1038/ncb1821

Trompouki, E., Hatzivassiliou, E., Tsichritzis, T., Farmer, H., Ashworth, A., and Mosialos, G. (2003). CYLD is a deubiquitinating enzyme that negatively regulates NF-κB- activation by TNFR family members. *Nature* 424, 793–796. doi: 10.1038/nature01803

Uchiyama, Y., Kim, C. A., Pastorino, A. C., Ceroni, J., Lima, P. P., de Barros Dorna, M., et al. (2019). Primary immunodeficiency with chronic enteropathy and developmental delay in a boy arising from a novel homozygous RIPK1 variant. *J. Hum. Genet.* 64, 955–960. doi: 10.1038/s10038-019-0631-3

Van Antwerp, D. J., Martin, S. J., Kafri, T., Green, D. R., and Verma, I. M. (1996). Suppression of TNF-alpha-induced apoptosis by NF-κB-. *Science* 274, 787–789. doi: 10.1126/science.274.5288.787

Varfolomeev, E., Goncharov, T., Fedorova, A. V., Dynek, J. N., Zobel, K., Deshayes, K., et al. (2008). c-IAP1 and c-IAP2 are critical mediators of tumor necrosis factor alpha (TNFα)-induced NF-κB activation. *J. Biol. Chem.* 283, 24295–24299. doi: 10.1074/jbc.C800128200

Varfolomeev, E., and Vucic, D. (2016). Intracellular regulation of TNF activity in health and disease. *Cytokine* 101, 26–32. doi: 10.1016/j.cyto.2016.08.035

Varfolomeev, E. E., Schuchmann, M., Luria, V., Chiannilkulchai, N., Beckmann, J. S., and Mett, I. L. (1998). Targeted disruption of the mouse Caspase 8 gene ablates cell death induction by the TNF receptors, Fas/Apo1, and DR3 and is lethal prenatally. *Immunity* 9, 267–276. doi: 10.1016/s1074-7613(00)80609-3

Vassalli, P. (1992). The pathophysiology of tumor necrosis factors. *Annu. Rev. Immunol.* 10, 411–452.

Verboom, L., Martens, A., Priem, D., Hoste, E., Sze, M., Vikkula, H., et al. (2020). OTULIN prevents liver inflammation and hepatocellular carcinoma by inhibiting FADD- and RIPK1 kinase-mediated hepatocyte apoptosis. *Cell Rep.* 30, 2237.e6–2247.e6. doi: 10.1016/j.celrep.2020.01.028

Vlantis, K., Wullaert, A., Polykratis, A., Kondylis, V., Dannappel, M., Schwarzer, R., et al. (2016). RIP kinase 1-Mediated epithelial cell death and chronic intestinal inflammation by NF-κB–dependent and -independent functions. *Immunity* 44, 553–567. doi: 10.1016/j.immuni.2016.02.020

Wagner, S. A., Satpathy, S., Beli, P., and Choudhary, C. (2016). SPATA2 links CYLD to the TNF-alpha receptor signaling complex and modulates the receptor signaling outcomes. *EMBO J.* 35, 1868–1884. doi: 10.15252/embj.201694300

Wallach, D., Varfolomeev, E. E., Malinin, N. L., Goltsev, Y. V., Kovalenko, A. V., and Boldin, M. P. (1999). Tumor necrosis factor receptor and Fas signaling mechanisms. *Annu. Rev, Immunol.* 17, 331–367. doi: 10.1146/annurev.immunol.17.1.331

Wang, H., Sun, L., Su, L., Rizo, J., Liu, L., Wang, L. F., et al. (2014). Mixed lineage kinase domain-like protein MLKL causes necrotic membrane disruption upon phosphorylation by RIP3. *Mol. Cell* 54, 133–146. doi: 10.1016/j.molcel.2014.03.003

Wang, K., Kim, C., Bradfield, J., Guo, Y., Toskala, E., Otieno, F. G., et al. (2013). Whole-genome DNA/RNA sequencing identifies truncating mutations in RBCK1 in a novel Mendelian disease with neuromuscular and cardiac involvement. *Genome Med.,* 5:67. doi: 10.1186/gm471

Wang, L., Du, F., and Wang, X. (2008). TNF-alpha induces two distinct caspase-8 activation pathways. *Cell* 133, 693–703. doi: 10.1016/j.cell.2008.03.036

Webster, J. D., Kwon, Y. C., Park, S., Zhang, H., Corr, N., Ljumanovic, N., et al. (2020). RIP1 kinase activity is critical for skin inflammation but not for viral propagation. *J. Leukoc Biol.* doi: 10.1002/JLB.3MA1219-398R [Epub ahead of print].

Wei, R., Xu, L. W., Liu, J., Li, Y., Zhang, P., Shan, B., et al. (2017). SPATA2 regulates the activation of RIPK1 by modulating linear ubiquitination. *Genes Dev.* 31, 1162–1176. doi: 10.1101/gad.321075.118

Weisel, K., Scott, N. E., Tompson, D. J., Votta, B. J., Madhavan, S., Povey, K., et al. (2017). Randomized clinical study of safety, pharmacokinetics, and pharmacodynamics of RIPK1 inhibitor GSK2982772 in healthy volunteers. *Pharmacol. Res. Perspect.* 5:e00365. doi: 10.1002/prp2.365

Wertz, I. E., O'Rourke, K. M., Zhou, H., Eby, M., Aravind, L., Seshagiri, S., et al. (2004). De-ubiquitination and ubiquitin ligase domains of A20 downregulate NF-κB signalling. *Nature* 430, 694–699. doi: 10.1038/nature02794

Williams, R. O., Feldmann, M., and Maini, R. N. (1992). Anti-tumor necrosis factor ameliorates joint disease in murine collagen-induced arthritis. *Proc. Natl. Acad. Sci. U.S.A.* 89, 9784–9788. doi: 10.1073/pnas.89.20.9784

Wong, J., Garcia-Carbonell, R., Zelic, M., Ho, S. B., Boland, B. S., Yao, S. J., et al. (2020). RIPK1 mediates TNF-induced intestinal crypt apoptosis during chronic NF-κB- activation. *Cell Mol. Gastroenterol. Hepatol.* 9, 295–312. doi: 10.1016/j.jcmgh.2019.10.002

Wu, X. N., Yang, Z. H., Wang, X. K., Zhang, Y., Wan, H., Song, Y., et al. (2014). Distinct roles of RIP1-RIP3 hetero- and RIP3-RIP3 homo-interaction in mediating necroptosis. *Cell Death Differ.* 21, 1709–1720. doi: 10.1038/cdd.2014.77

Yuan, J., Amin, P., and Ofengeim, D. (2019). Necroptosis and RIPK1-mediated neuroinflammation in CNS diseases. *Nat. Rev. Neurosci.* 20, 19–33. doi: 10.1038/s41583-018-0093-1

Zhang, D. W., Shao, J., Lin, J., Zhang, N., Lu, B. J., Lin, S. C., et al. (2009). RIP3, an energy metabolism regulator that switches TNF-induced cell death from apoptosis to necrosis. *Science* 325, 332–336. doi: 10.1126/science.1172308

Zhang, J., Webster, J. D., Dugger, D. L., Goncharov, T., Roose-Girma, M., Hung, J., et al. (2019). Ubiquitin ligases cIAP1 and cIAP2 limit cell death to prevent inflammation. *Cell Rep.* 27, 2679.e3–2689.e3. doi: 10.1016/j.celrep.2019.04.111

Zhang, X., Dowling, J. P., and Zhang, J. (2019). RIPK1 can mediate apoptosis in addition to necroptosis during embryonic development. *Cell Death Dis.* 10:245. doi: 10.1038/s41419-019-1490-8

Zhou, Q., Wang, H., Schwartz, D. M., Stoffels, M., Park, Y. H., Zhang, Y., et al. (2016a). Loss-of-function mutations in TNFAIP3 leading to A20 haploinsufficiency cause an early-onset autoinflammatory disease. *Nat. Genet.* 48, 67–73. doi: 10.1038/ng.3459

Zhou, Q., Yu, X., Demirkaya, E., Deuitch, N., Stone, D., Tsai, W. L., et al. (2016b). Biallelic hypomorphic mutations in a linear deubiquitinase define otulipenia, an early-onset autoinflammatory disease. *Proc. Natl. Acad. Sci. US.A.* 113, 10127–10132. doi: 10.1073/pnas.1612594113

Zonana, J., Elder, M. E., Schneider, L. C., Orlow, S. J., Moss, C., Golabi, M., et al. (2000). A novel X-linked disorder of immune deficiency and hypohidrotic ectodermal dysplasia is allelic to incontinentia pigmenti and due to mutations in IKK-gamma (NEMO). *Am. J. Hum. Genet.* 67, 1555–1562. doi: 10.1086/316914

Conflict of Interest: JW and DV were employees and shareholders at Genentech-Roche.

frontiers in Cell and Developmental Biology

REVIEW
published: 26 May 2020
doi: 10.3389/fcell.2020.00401

Selective Targeting of TNF Receptors as a Novel Therapeutic Approach

Roman Fischer, Roland E. Kontermann and Klaus Pfizenmaier*

Institute of Cell Biology and Immunology, University of Stuttgart, Stuttgart, Germany

Tumor necrosis factor (TNF) is a central regulator of immunity. Due to its dominant pro-inflammatory effects, drugs that neutralize TNF were developed and are clinically used to treat inflammatory and autoimmune diseases, such as rheumatoid arthritis, inflammatory bowel disease and psoriasis. However, despite their clinical success the use of anti-TNF drugs is limited, in part due to unwanted, severe side effects and in some diseases its use even is contraindicative. With gaining knowledge about the signaling mechanisms of TNF and the differential role of the two TNF receptors (TNFR), alternative therapeutic concepts based on receptor selective intervention have led to the development of novel protein therapeutics targeting TNFR1 with antagonists and TNFR2 with agonists. These antibodies and bio-engineered ligands are currently in preclinical and early clinical stages of development. Preclinical data obtained in different disease models show that selective targeting of TNFRs has therapeutic potential and may be superior to global TNF blockade in several disease indications.

Keywords: TNF, TNFR1, TNFR2, therapy, inflammation, tissue regeneration

OPEN ACCESS

Edited by:
Olivier Micheau,
Université de Bourgogne, France

Reviewed by:
David MacEwan,
University of Liverpool,
United Kingdom
Nathalie Grandvaux,
Université de Montréal, Canada
Patrick Legembre,
INSERM U1262 CRIBL, France

****Correspondence:***
Roman Fischer
roman.fischer@izi.uni-stuttgart.de

Specialty section:
This article was submitted to Signaling, a section of the journal Frontiers in Cell and Developmental Biology

Received: *06 February 2020*
Accepted: *01 May 2020*
Published: *26 May 2020*

Citation:
Fischer R, Kontermann RE and Pfizenmaier K (2020) Selective Targeting of TNF Receptors as a Novel Therapeutic Approach. Front. Cell Dev. Biol. 8:401. doi: 10.3389/fcell.2020.00401

INTRODUCTION

Tumor necrosis factor (TNF) is a key regulatory component of the immune system that regulates innate and adaptive immunity and contributes to initiation and maintenance of inflammation (Aggarwal, 2003). The major cellular source of TNF are macrophages and immune cells that are activated in response to infections or tissue damage (Fischer and Maier, 2015). Therefore, regulated TNF expression is essential to promote tissue homeostasis and fight infections. In contrast, deregulated TNF expression and signaling may induce pathology resulting in chronic inflammation and tissue damage. Indeed, increased levels of TNF were identified in patients with autoimmune and degenerative diseases (Fischer and Maier, 2015; Monaco et al., 2015). To counteract the pro-inflammatory and tissue degenerative effects of TNF signaling, therapeutics have been developed that neutralize TNF. Currently, five structurally different anti-TNF drugs are approved for clinical use: infliximab (Remicade), adalimumab (Humira), certolizumab pegol (Cimzia), golimumab (Simponi), and etanercept (Enbrel) (Monaco et al., 2015). These anti-TNF therapeutics, and biosimilars of infliximab, etanercept and adalimumab that have been approved recently, are successfully used to treat autoimmune diseases, including RA, juvenile RA (JRA), IBD, psoriasis, and ankylosing spondylitis (AS) (Monaco et al., 2015). Despite the clinical success of anti-TNF therapeutics they also show limitations, such as their restricted responsiveness, and severe side-effects, such as opportunistic infections, invasive fungal infections, reactivation of tuberculosis, and development of other autoimmune diseases and lymphomas (Tracey et al., 2008; Monaco et al., 2015). Further, clinical evaluation of anti-TNF therapy in multiple sclerosis failed (van Oosten et al., 1996; Lenercept Study Group, 1999) and anti-TNF therapy of juvenile rheumatoid arthritis

resulted in development of MS-like exacerbations and demyelinating lesions in some patients (Sicotte and Voskuhl, 2001). Altogether this indicates that the use of anti-TNF drugs is limited and contraindicative for several indications, including neurodegenerative diseases.

The limitations of anti-TNF therapy may depend on TNF's pleiotropic biological functions via two distinct TNF receptors (TNFR). Synthesized as a transmembrane protein (tmTNF), the tmTNF form can activate both, TNFR1 and TNFR2. After proteolytical processing, the soluble trimers (sTNF) mainly activate TNFR1 (Fischer et al., 2015). In different animal disease models, genetic deletion of TNFR1 is typically associated with lack or reduced disease, whereas TNFR2 ablation exacerbates disease. These and other data indicate that sTNF/TNFR1 signaling mainly mediates pro-apoptotic and inflammatory responses, whereas TNFR2 contributes to immune regulation and tissue regeneration. Therefore, reagents that selectively target TNFRs might be superior to global TNF blockade because they allow a differential activation and/or inhibition of TNFRs.

Lymphotoxin-α (LTα) is another homotrimeric ligand of the TNF superfamily (TNFSF) that shares 50% homology with TNF (Gray et al., 1984) and can also bind to TNFR1 and TNFR2 (Bodmer et al., 2002). In contrast to TNF, LTα lacks the transmembrane domain and is therefore only expressed as a soluble homotrimeric form (Ruddle, 2014). The close tertiary and quaternary structures indicate that TNF and LTα are functionally redundant. However, the involvement of LTα in inflammatory diseases is less well characterized than sTNF and a RA clinical trial using the anti-lymphotoxin-alpha antibody pateclizumab did not show statistically significant improvement in RA signs and symptoms (Kennedy et al., 2014). Differences between sTNF and LTα have been described elsewhere (Ruddle, 2014; Hirose et al., 2018). In this review, we will summarize the current knowledge of signal pathways emanating from the two TNFRs, their patho-/physiologic role and discuss recent promising results obtained in different disease models in the pre-clinical development of novel TNFR selective drugs.

TUMOR NECROSIS FACTOR

Tumor necrosis factor is synthesized as a 26 kDa type II transmembrane protein that assembles into a homotrimeric molecule (tmTNF) (Kriegler et al., 1988) that can be proteolytically cleavage by the matrix metalloproteases (MMP) TNFα-converting enzyme (TACE/ADAM17) resulting in soluble TNF homotrimers (sTNF; 51 kDa) (Black et al., 1997). TNF binds to the two type I transmembrane receptors TNFR1 and TNFR2. Both TNF receptors contain four cysteine-rich domains (CRD) in their extracellular domains. The membrane distal CRD contains the preligand binding assembly domain (PLAD), which is important for ligand-mediated formation of active receptor complexes. In the absence of a ligand, the PLAD mediates inactive self-association of homo-multimerized receptors (Chan et al., 2000). TNFR1 is constitutively expressed on almost all nucleated cells. In contrast, the expression of TNFR2 is more restricted, highly regulated on various cells of the immune system, and plays an important role, too, on cells of the vasculature, muscle and brain tissues (Wajant et al., 2003; Fischer and Maier, 2015; Pegoretti et al., 2018).

Interestingly, sTNF and tmTNF have different activities to stimulate signaling via TNFR1 and TNFR2. Despite binding sTNF with subnanomolar affinity, TNFR2 needs tmTNF for robust activation (Grell et al., 1995). This difference might be due to different association/dissociation kinetics of the TNF/TNFR complexes. TNF binds to TNFR1 with a higher affinity ($K_d = 1.9 \times 10^{-11}$ M) than TNFR2 ($K_d = 4.2 \times 10^{-10}$ M) (Grell et al., 1998). This high affinity for TNFR1 is dependent on stabilization of the TNF/TNFR1 complex, whereas short-lived signaling-incompetent complexes are formed by transient binding of sTNF to TNFR2 (Grell et al., 1998; Krippner-Heidenreich et al., 2002). Stoichiometry analysis revealed differences in ligand/receptor interactions between TNFR1 and TNFR2 and indicated that avidity is an important factor for TNF-binding and downstream signaling of TNFR2 (Boschert et al., 2010). Indeed, using a system with ligand-immobilization on a surface in a nanoscaled pattern with defined spacings, Ranzinger et al. (2009) showed that mere mechanical fixation of TNF was sufficient to activate TNFR1 but not TNFR2. Whereas, robust TNFR2 activation was dependent on additional stabilization by cluster formation (Ranzinger et al., 2009). Altogether, these data clearly indicate that tmTNF-mediated cluster formation of tmTNF/TNFR2 complexes is necessary for robust activation of TNFR2.

The membrane-proximal extracellular stalk regions were identified as a crucial determinant in controlling responsiveness to sTNF (Richter et al., 2012). Richter et al. (2012) showed that the arrangement of the TNFRs in the plasma membrane in the absence of ligand is a fundamental parameter determining the responsiveness of TNFRs to sTNF. Indeed, the stalk region of TNFR2, in contrast to the corresponding part of TNFR1, efficiently inhibited clustering of TNFR2 in particular cell membrane regions and ligand-independent PLAD-mediated homotypic receptor preassembly resulting in abolished sTNF-, but not tmTNF-induced signaling (Richter et al., 2012). These data are supported by a report suggesting that the two TNFRs are topological segregated in different plasma membrane microcompartments independent of the cytoplasmic signaling domains of the receptors (Gerken et al., 2010). The intracellular structure of the TNFRs is highly different and defines their activity. TNFR1 belongs to the family of death domain (DD)-containing receptors, whereas TNFR2 is a TRAF-interacting receptor without DD (Wajant et al., 2003).

TNFR SIGNALING

TNFR1

Upon TNF binding, TNF receptor 1 associated protein with death domain (TRADD), the receptor interacting protein kinase 1 (RIP1), TNF receptor associated factor 2 (TRAF2), and the cellular inhibitor of apoptosis proteins (cIAPs) 1 and 2 are recruited to the receptor (**Figure 1**). The cIAPs modify intracellular binding partners of the TNFR1 signaling complex

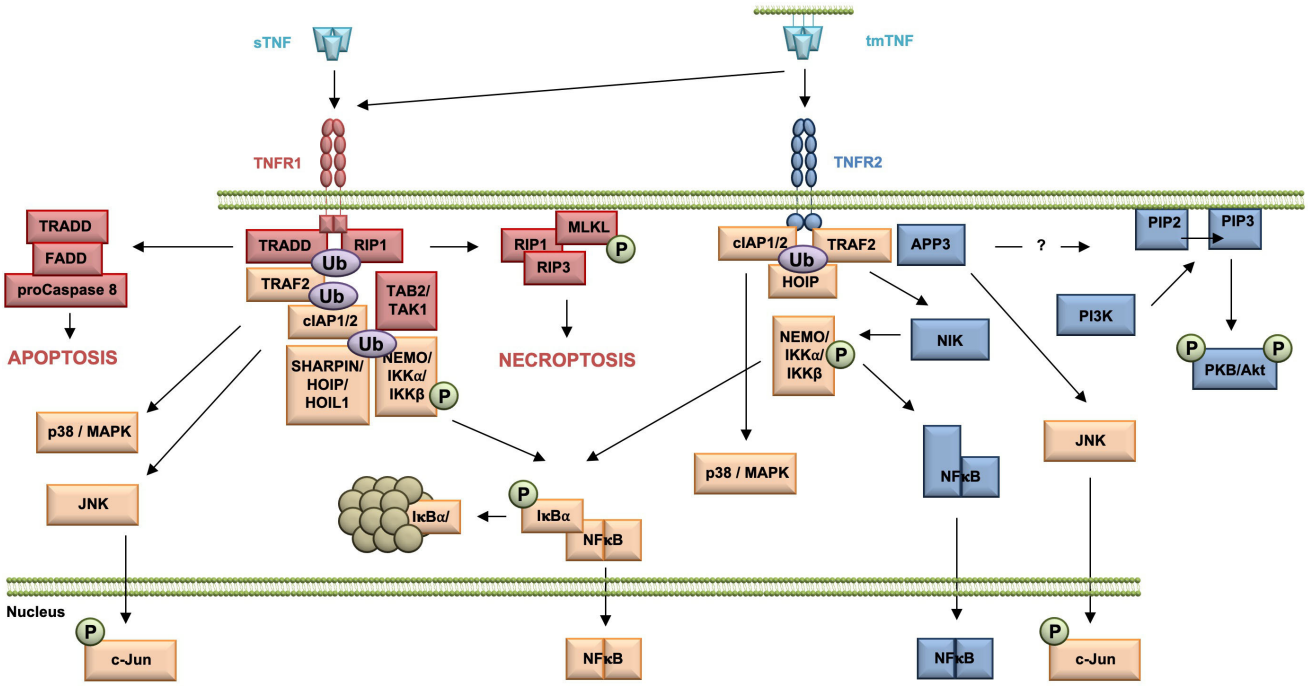

FIGURE 1 | Overview of the TNFR1 and TNFR2 signaling pathway. All TNFR1-exclusive signaling mediators are marked red, whereas all TNFR2-exclusive signaling components are shown in blue. All mediators used by both pathways are labeled orange.

(TNFR1-SC), in particular RIPK1, with K63-linked ubiquitin chains to create a docking platform for the linear ubiquitin assembly complex (LUBAC). LUBAC then adds linearly linked ubiquitin chains to RIPK1 leading to the recruitment of the inhibitor of kappa B kinases (IKK) complex and the MAP3K transforming growth factor-ß (TGFß)–activated kinase-1 (TAK1), which binds to the TNFR1 complex via the adapter protein TAK1-binding protein-2 (TAB2). TAK1 phosphorylates IKKβ and LUBAC adds linear ubiquitin to NEMO, both components of the IKK complex. IKK then phosphorylates inhibitor of kappa B-alpha (IκBα) leading to its ubiquitination and subsequent proteasomal degradation. The dissociation of IκB from the transcription factor nuclear factor kappa B (NFκB) releases its nuclear localization sequence (NLS) resulting in the nuclear translocation of free NFκB dimers and transcription of NFκB-regulated targets (Wajant and Scheurich, 2011; Schmukle and Walczak, 2012). Next to the classical NFκB pathway, the TNFR1 signaling complex I can bind and activate distinct MAP kinase kinases (MKK) resulting in the activation of p38 MAP kinase and JNK pathway (Natoli et al., 1997; Brinkman et al., 1999). The signaling complex I can be internalized, which leads to the dissociation of TRAF2 and the cIAPs and the subsequent recruitment of the adaptor protein Fas associated death domain protein (FADD) and the procaspase 8 to form the secondary pro-apoptotic signaling complex II. Within the death inducing signaling complex (DISC), procaspase 8 is activated by autocatalytic cleavage resulting in activation of the effector caspase cascade ultimately leading to induction of apoptosis (Micheau and Tschopp, 2003; Schneider-Brachert et al., 2004). Using a systems biology approach and mathematical modeling temporal responses of TNFR1-mediated cell death induction were described. A global sensitivity analysis uncovered that concentrations of Caspase-8 and Caspase-3, and their respective inhibitors FLIP, BAR, and XIAP are key elements for deciding the cell's fate. In contrast, NFκB-mediated anti-apoptotic signaling pathways delayed the time of death (Schliemann et al., 2011). When caspase 8 is absent or inactivated, kinase-active RIPK1 recruits and activates RIPK3, resulting in the formation of the necrosome. As a constitutive binding partner of RIPK3, mixed lineage kinase domain-like protein (MLKL) is incorporated in the necrosome (Grootjans et al., 2017). Phosphorylation of MLKL results in a conformational change, recruitment to the plasma membrane and execution of necroptosis via membrane permeabilization (Vanden Berghe et al., 2014; Grootjans et al., 2017).

TNFR2

In contrast to the very well characterized TNFR1 signaling pathways and their physiologic relevance early in TNF research, TNFR2-mediated signaling pathways and in particular their role in TNF biology were uncovered much later (**Figure 1**). TNFR2 activation results in recruitment of TRAF2 (Rothe et al., 1994), cIAP1/cIAP2 (Rothe et al., 1995a), and HOIP, a LUBAC component (Borghi et al., 2018), which form the TNFR2 signaling complex (SC). cIAP-mediated K63-linked polyubiquitination of the SC is required for recruitment of HOIP, which mediates M1-ubiquitination (Borghi et al., 2018). Both HOIP and cIAP1 are required for TNFR2-induced canonical NFκB activation via

IKKβ (Rothe et al., 1995b; Borghi et al., 2018). In addition, in contrast to TNFR1, TNFR2 was shown to be capable to induce the non-canonical NFκB pathway (Rauert et al., 2010). After degradation of TRAF2, probably through receptor internalization and lysosomal degradation (Fischer et al., 2011a), the kinase NIK accumulates, phosphorylates and activates IKKα. This leads to processing of the p100 subunit of NFκB to p52 and the subsequent nuclear translocation of p52/RelB NFκB heterodimers (Sun, 2017).

Similar to TNFR1 and TNFR2 activation may result in induction of the c-Jun N-terminal kinase (JNK) (Jupp et al., 2001) and the p38 MAPK pathway (Inoue et al., 2015; He et al., 2018). Interestingly, recently mitochondrial aminopeptidase P3 (APP3, also known as XPNPEP3) was identified as a novel component of the TNFR2 signal complex, which regulates TNF–TNFR2-dependent phosphorylation of JNK (Inoue et al., 2015). The authors describe that APP3 is released from mitochondria in a TNF-defendant way in the absence of mitochondrial outer membrane permeabilization (MOMP) and suggest that APP3 exerts an anti-apoptotic function (Inoue et al., 2015). Interestingly, it was shown that TNFR2 ligation enhances cell proliferation through the non-canonical NFκB pathway in human regulatory T cells (Tregs) (Wang et al., 2018), whereas in mouse Tregs activation of p38 MAPK was important for TNFR2-induced proliferation (He et al., 2018). Furthermore, TNFR2 promotes phosphatidylinositol 3-kinase (PI3K)-dependent phosphorylation of the protein kinase PKB/Akt via a yet unknown mechanism (Marchetti et al., 2004; Fischer et al., 2011b). Here, PI3K phosphorylates the D3 hydroxyl group of the inositol ring of the plasma membrane lipid phosphatidylinositol-4,5-bisphosphate (PIP2) resulting in the second messenger phosphatidylinositol 3,4,5-bisphosphate (PIP3) (Cantley, 2002). PKB/Akt then is recruited to the plasma membrane by direct binding to PIP3 through its pleckstrin-homology (PH) domains (Lawlor and Alessi, 2001). There, PKB/Akt undergoes a conformational change and is phosphorylated at residue threonine 308 in the activation loop (T loop) of the kinase domain by PDK-1 (Alessi, 2001) and at residue serine 473 in the hydrophobic motif by the Rictor/mammalian target of rapamycin (mTOR) complex (Sarbassov et al., 2005). Activated PKB/Akt then promotes cell survival and proliferation (Fischer et al., 2015; Ortí-Casañ et al., 2019).

OPPOSING ROLES OF TNFR1 AND TNFR2

Inflammatory Diseases

Tumor necrosis factor plays an important role for regulation of the adaptive and innate immune system and thus, is a key player for both infectious and non-infectious inflammatory disorders. Interestingly, TNF induces opposing effects in the immune system, i.e., it plays a key role for the initiation and orchestration of inflammation, while it also suppresses immune cell activity. These antithetic effects often can be explained by the diverse signaling mediated via TNFR1 and TNFR2 (**Figure 1**).

TNFR1 is expressed on a multitude of effector immune cells and most described TNF-mediated proinflammatory functions are predominantly mediated via TNFR1 (Fischer and Maier, 2015; Fischer et al., 2015; Mehta et al., 2018). In contrast, TNFR2 expression is more restricted and highly regulated. In immunity, TNFR2 expression is predominantly found on activated T cells and, in particular, is critically involved in regulation of immune responses through signaling in regulatory T cells (Tregs), a specific immune modulatory lymphocyte subpopulation that suppress development of autoimmune diseases. In particular, it was shown that the expression level of TNFR2 is correlated to the suppressive potential of natural Tregs (nTregs) (Chen et al., 2007, 2008, 2010b), indicating that the most potent suppressors are highly susceptible to TNFR2 activation. It is well recognized now that TNFR2 contributes to the expansion of $CD4^+FoxP3^+$ nTregs *in vitro* and *in vivo* (Chen et al., 2007, 2008; Okubo et al., 2013; Chopra et al., 2016; Fischer et al., 2017, 2018, 2019a,b; Padutsch et al., 2019) and the stabilization of the $CD4^+Foxp3^+$ Treg phenotype in the inflammatory environment (Chen et al., 2013). Like $CD4^+$ Tregs, $CD8^+$ suppressor cells can express FoxP3 and CD25. Similar to $CD4^+$ Tregs, the most potent $CD8^+$ suppressors are characterized by the expression of TNFR2 (Ablamunits et al., 2010; Horwitz et al., 2013).

Infectious Diseases

TNFR1 plays an essential role for host defense against various pathogenic organisms. Rothe et al. described that $TNFR1^{-/-}$ mice were resistant to TNF-mediated toxicity [low-dose lipopolysaccharide (LPS) after sensitization with D-galactosamine (D-GalN)], whereas they are still sensitive to elevated doses of LPS only treatment (Rothe et al., 1993). In addition, they are highly susceptible to infection with the facultative intracellular bacterium *Listeria monocytogenes* (Rothe et al., 1993). A similar study showed that $TNFR1^{-/-}$ mice are resistant to endotoxic shock, but are not able to clear *Listeria monocytogenes* and succumb to the infection (Pfeffer et al., 1993). These studies indicate that TNFR1 plays an essential role in the host's defense against microorganisms and their pathogenic factors. Follow-up studies showed that TNFR1 is also essential to fight *Leishmania major and Candida albicans* infections (Steinshamn et al., 1996; Nashleanas et al., 1998), indicating that TNFR1 signaling also contributes to anti-fungal and parasite defense. Mice deficient for TNFR2 also have a significant reduction in their ability to clear *C. albicans,* although in contrast to $TNFR1^{-/-}$ mice, lethality was not increased (Steinshamn et al., 1996). Similar, in contrast to resistant wild type C57BL/6 mice, *L. major* infected TNFR2-deficient mice develop large skin lesions, which are comparable in size to those in $TNFR1^{-/-}$ mice. However, in contrast to $TNFR1^{-/-}$ mice, $TNFR2^{-/-}$ mice ultimately control the infection (Fromm et al., 2015).

TNFR2 is also upregulated upon T effector cell activation (Chen et al., 2007, 2010a) and acts co-stimulatory for TCR-mediated T cell activation, as well as survival and proliferative expansion of Teff cells (Mehta et al., 2018; Ye et al., 2018). Indeed, TNFR2 expression by $CD4^+$ Teffs is required to induce full-fledged experimental colitis, based on a defective proliferative expansion of TNFR2-deficient Teff cells, as well as their reduced

capacity to mount a full-fledged proinflammatory Th1 cytokine response (Chen et al., 2016). Along the same line, TNFR2 was also shown to control the survival and accumulation of Teffs during the primary response against *L. monocytogenes* infection (Kim et al., 2006), indicating that TNFR2 on Teffs is important for host defense against *L. monocytogenes*. Further, sTNF-deficient transgenic mice that express a non-cleavable form of TNF were partially protected against infections with the pathogens *Mycobacterium tuberculosum* and *Listeria monocytogenes* (Torres et al., 2005; Musicki et al., 2006). Altogether, these data indicate that TNFR2 contributes to protective immune responses following infections, but, in contrast to TNFR1 is not essential for resolving the infection.

Non-infectious Diseases

The essential pro-inflammatory role of TNFR1 is further demonstrated by the observed decreased disease development of TNFR1$^{-/-}$ mice in different models of non-infectious inflammatory diseases. TNFR1$^{-/-}$ mice showed a lower incidence of disease development and an alleviated form collagen-induced arthritis (CIA) (Mori et al., 1996). However, once a joint was affected, disease severity was similar to that in wild-type mice. These data indicate that TNFR1 is the main transducer of TNF-mediated proinflammatory effects in CIA. However, the progression of arthritic disease resulting in tissue destruction and ankylosis seems to be independent of TNFR1 (Mori et al., 1996). Supporting the pro-inflammatory role of TNFR1, Deng et al., recently demonstrated that soluble versions of PLAD (sPLAD) from TNFR1 block TNF-induced responses *in vitro* and potently inhibit arthritis in animal models. In contrast, sPLAD versions from TNFR2 were less potent in inhibiting experimental arthritis (Deng et al., 2005). Because it was shown that PLADs preferentially undergo homotypic interactions, i.e., a TNFR1-sPLAD binds preferentially to a membrane expressed TNFR1, the strong therapeutic effect of TNFR1-sPLAD validates TNFR1 as a therapeutic target for arthritis and potentially other inflammatory diseases as well.

Similar to the arthritis model, TNFR1$^{-/-}$ mice do not develop experimental autoimmune encephalomyelitis (EAE), an animal model of brain inflammation resembling MS. In contrast, TNFR2$^{-/-}$ mice develop an exacerbated form of EAE (Eugster et al., 1999; Suvannavejh et al., 2000; Kassiotis and Kollias, 2001; Williams et al., 2014). Interestingly, it was shown that Treg-TNFR2-deficient mice develop exacerbated EAE motor disease, indicating that intrinsic TNFR2 signaling in Tregs provides protection in CNS autoimmunity (Atretkhany et al., 2018). However, another report demonstrated that TNFR2 expressed on non-hematopoietic cells is necessary for Treg function and suppression of EAE motor disease (Tsakiri et al., 2012), indicating that intrinsic and extrinsic TNFR2 activation impacts Treg functionality in EAE.

Whereas, the function of TNFR2 for nTregs is well-characterized, less is known about the impact of TNFR2 on induced Tregs (iTreg). Recently, Yang et al. (2019) demonstrated that TNFR2 deficiency impeded differentiation, proliferation, and function of iTregs. In contrast, TNFR1 deficiency resulted in reduced differentiation of inflammatory T cells, while the iTregs function was unaltered. Using a colitis model, they confirmed that TNFR2 but not TNFR1 deficiency impaired iTreg functionality (Yang et al., 2019), and proposed that TNFR2 also plays a role of iTreg function.

Next to its immunomodulatory role via Tregs, TNFR2 promotes apoptosis of insulin-specific pathogenic autoreactive CD8$^+$ T cells but not normal T cells isolated from diabetes type I patients (Ban et al., 2008). Confirming, in diabetic mice administration of exogenous TNF resulted in cell death of autoreactive T cells leading to alleviation of clinical symptoms (Kodama et al., 2003). A follow-up study revealed that several defects in TNFR2-dependant activation of NFκB result in impaired anti-apoptotic effects leading to sensibilization for apoptosis (Kodama et al., 2005). Other studies showed that intrinsic TNFR2 signaling in CD4$^+$ T cells impairs the differentiation of Th17 (Miller et al., 2015), outlining other potential immunomodulatory mechanisms regulated by TNFR2 signaling.

Degenerative Diseases

Next to inflammatory diseases, where anti-TNF therapy is approved, increased levels of TNF are found in several degenerative diseases, such as heart failure (HF) or neurodegenerative diseases (Fischer and Maier, 2015; Monaco et al., 2015). Preclinical data in models of heart failure suggested that TNF neutralization in HF would be beneficial. However, clinical trials of TNF antagonists were paradoxically negative and resulted in a time- and dose-related increase in death and disease-dependent hospitalization of anti-TNF treated patients (Mann, 2002). Studies using TNFR$^{-/-}$ mice indicate that in heart failure TNFR1 and TNFR2 induce opposing effects on tissue remodeling, hypertrophy, inflammation, and cell death. Whereas TNFR1 exacerbates these events, TNFR2 leads to amelioration of these events (Hamid et al., 2009). Other studies demonstrate that after myocardial infarction, TNFR1 activation aggravates left ventricular remodeling, whereas it is improved by TNFR2 signaling (Ramani et al., 2004; Monden et al., 2007). Altogether, these data indicate that global blocking of TNF is contraindicative for heart disease due to a protective role of TNFR2.

Similar, TNF contributes to neuropathology, i.e., it was shown that genetic overexpression of TNF in the CNS resulted in T cell infiltration, astrocytosis, and microgliosis, and chronic inflammatory demyelination (Probert et al., 1995). These studies identified TNF as an important contributor to the onset of demyelinating diseases and justified the evaluation of anti-TNF therapies in mouse models of MS. Indeed, neutralization of TNF was therapeutic in EAE mouse models of autoimmune demyelination induced by the adoptive transfer of myelin basic protein−(MBP)−sensitized T lymphocytes (Selmaj et al., 1991, 1995). However, a phase II randomized, multi-center, placebo-controlled clinical trial using the anti-TNF lenercept had to be stopped since exacerbations were significantly increased and neurologic deficits were more severe in the lenercept treatment groups compared with patients receiving placebo (Lenercept Study Group, 1999). Similar, an open-label phase I safety trial showed that two rapidly progressive MS patients showed increased MRI activity

and immune activation after treatment with infliximab (van Oosten et al., 1996), and during anti-TNF therapy some juvenile RA patients developed MS-like demyelinating lesions (Sicotte and Voskuhl, 2001).

Therefore, follow-up studies using TNFR1$^{-/-}$ and TNFR2$^{-/-}$ mice were performed to investigate TNFR-selective responses. Interestingly, using the EAE immunization mouse modelseveral independent groups showed that TNFR1$^{-/-}$-mice do not develop EAE motor disease, whereas TNFR2 deficiency resulted in an exacerbated form of EAE (Eugster et al., 1999; Suvannavejh et al., 2000; Kassiotis and Kollias, 2001; Williams et al., 2014), indicating opposing roles of the TNFRs in EAE. Similar results were obtained using a murine model of retinal ischemia, where TNFR1 promoted neuronal tissue destruction and TNFR2 was neuroprotective via activation of the PKB/Akt pathway (Fontaine et al., 2002).

Interestingly, compared to the vehicle group, local administration of cannabidiol after right middle cerebral artery occlusion (MCAO) resulted in reduced infarction, brain oedema and BBB permeability. Mechanistically, the group showed that cannabinoid treatment downregulated expression of TNF and TNFR1, with TNFR1 expression levels being correlated with the infarct volume (Khaksar and Bigdeli, 2017a,b). Similar studies have shown that cannabinoids inhibit inflammatory TNF activity (Rogers and Hermann, 2012; Tan and Cao, 2018), indicating that TNF/TNFR1 signaling may contribute to neurodegeneration after cerebral ischemia.

The neuroprotective role of TNFR2 was confirmed using *in vitro* studies with primary neurons. Marchetti et al. (2004) compared the impact of TNF stimulation on glutamate-induced excitotoxicity of TNFR1$^{-/-}$ or TNFR2$^{-/-}$ neurons. Only neurons from wild type or TNFR1$^{-/-}$ animals were protected, while TNF activation had no protective effect on neurons from TNFR2$^{-/-}$ mice, indicating that presence of TNFR2 was responsible for TNF-mediated neuroprotection. Mechanistically this study showed TNF-mediated neuroprotection was dependent on prolonged activation of NFκB and activation of the PI3K-PKB/Akt pathway (Marchetti et al., 2004). A follow-up study showed that TNFR2 mediates neuroprotection against glutamate−induced excitotoxicity via NFκB−dependent up−regulation of K_{Ca}2.2, a member of a group of calcium-activated potassium channel known to reduce neuronal excitability (Dolga et al., 2008). Using transgenic AD mice and intracerebroventricular injection of amyloid β oligomers (AβO) into WT mice, Steeland et al. (2018) found that TNFR1 deficiency abrogated inflammation in choroid plexus and hippocampus and protected against AβO-induced morphological alterations of the choroid plexus, indicating that TNFR1 contributes to neurodegeneration.

Using the cuprizone model of toxin-induced controlled de- and remyelination, Arnett et al. (2001) demonstrated that TNFR2, but not TNFR1, is critical for oligodendrocyte regeneration. Further mechanistic studies demonstrated that astrocyte-TNFR2 promotes secretion of the chemokine Cxcl12 resulting in increased oligodendrocyte progenitor cell (OPC) proliferation and differentiation (Patel et al., 2012), supporting the remyelinating role of TNFR2. More mechanistic studies were performed using transgenic CNP-cre:TNFR2$^{fl/fl}$ mice, where TNFR2 is selectively deleted in oligodendrocyte progenitor cells. These mice presented with exacerbated motor disease and neuropathology, including increased demyelination and reduced remyelination. This study thus shows that oligodendroglial-TNFR2 contributes to tmTNF-mediated remyelination, too (Madsen et al., 2016). Interestingly, recent work using the same animals showed that oligodendrocyte-TNFR2 not only promotes myelination, but also modulates the immune-inflammatory response in the early phase of EAE pathogenesis. In particular, specific ablation of oligodendroglial-TNFR2 resulted in increased microglia activation and blood brain barrier permeability, and accelerated infiltration of immune cells into the spinal cord prior to development of motor symptoms (Madsen et al., 2019). Further, opposing functions of microglial and macrophagic TNFR2 in the pathogenesis of EAE were reported. TNFR2-deletion in microglia resulted in increased leukocyte infiltration and demyelination into the spinal cord and early onset of motor symptoms. In contrast, TNFR2 ablation in monocytes/macrophages resulted in impaired peripheral immunity and alleviated neuropathology and EAE motor disease development (Gao et al., 2017). This work revealed an antithetic function for myeloid cells TNFR2 in EAE, with protective microglial TNFR2 signals to counteract disease development, and monocyte/macrophagic TNFR2 contributing to pathology and EAE development. These opposing effects mediated via the TNFRs indicate that inhibition of tmTNF/TNFR2 signaling was responsible for the exacerbated symptoms and may explain the failure of anti-TNF therapy in MS patients. Indeed, studies using transgenic animals that exclusively express physiologically regulated levels of tmTNF demonstrated that tmTNF is sufficient for antibacterial defense and has an important role to control chronic inflammation and autoimmunity (Alexopoulou et al., 2006).

Chronic Neuropathic Pain

Tumor necrosis factor also plays an important role for the development of chronic neuropathic pain (CNP), a long-lasting chronic pain that is caused by damage to the somatosensory nervous system and is associated with various diseases/conditions, including neurodegenerative and inflammatory diseases, diabetes, cancer and chemotherapy (Scholz and Woolf, 2007; Murphy et al., 2017). Indeed, intra-sciatic injection of TNF in rats was shown to reproduce pain hypersensitivity similar to human neuropathic pain (Wagner and Myers, 1996; Sorkin and Doom, 2000). Studies using TNFR1/TNFR2 knock-out mice indicate that TNFR1 plays a role for death of hippocampal neurons, whereas TNFR2 played a neuroprotective role (Yang et al., 2002). However, the relative roles of TNFR1 and TNFR2 in chronic pain are still controversially discussed. TNFR1$^{-/-}$ mice do not develop mechanical allodynia (Dellarole et al., 2014) and thermal hyperalgesia (Sommer et al., 1998), highlighting an essential role of TNFR1 for development of neuropathic pain. Interestingly, CCI did not result in pain development in male TNFR1$^{-/-}$ mice. In contrast, female TNFR1$^{-/-}$ mice developed

CNP, however less intense than wildtype females (del Rivero et al., 2019), indicating sex-differences in TNFR1-mediated pain development.

Vogel et al. (2006) showed that thermal hyperalgesia was absent in mice deficient of TNFR1 and that both TNFR1$^{-/-}$ and TNFR2$^{-/-}$ mice developed an alleviated form of mechanical and cold allodynia compared to wild type mice. Another study demonstrated that TNFR1/TNFR2-double knockout mice showed reduced tactile hypersensitivity, while spontaneous pain behavior was transiently increased in a model of bone-cancer related pain. In contrast, TNFR1 or TNFR2 single knockout did not show an effect on pain sensitivity (Geis et al., 2010), indicating an interplay of TNFR1 and TNFR2 signaling for pain development in this model. In a mouse cancer model, it was shown that endogenous TNF requires TNFR2 to generate thermal hyperalgesia (Constantin et al., 2008). In particular, experimental tumor-induced thermal hyperalgesia and nociceptor sensitization were prevented by systemic administration of the anti-TNF drug etanercept. While in this model, TNFR1 gene deletion played a minor role, deletion of the TNFR2 gene reduced the painful response (Constantin et al., 2008).

In a spared nerve injury (SNI) model, immunohistochemistry analysis demonstrated that both TNFR1 and TNFR2 levels were significantly increased in the red nucleus after SNI, compared to sham-operated and normal rats (Zeng et al., 2014). A temporal analysis showed that TNFR1 expression was increased starting at 2 weeks after SNI, whereas TNFR2 expression was already elevated 1 week after injury but began to decrease by 2 weeks after injury (Zeng et al., 2014). Microinjection of anti-TNFR1 or anti-TNFR2 blocking antibodies into the red nucleus correlated with the nerve injury site increased paw withdrawal threshold in a dose-dependent manner. Combination of both anti-TNFR1 and anti-TNFR2 had the largest effect (Zeng et al., 2014). This study showed that, while TNFR1 is important throughout the development and maintenance phase of disease, TNFR2 seems to play a role for development of CNP. Similar, using a model of inflammatory pain, Zhang et al. (2011) showed that TNFR2 plays a role for mediating early-phase inflammatory pain. In particular, after intraplantar injection of complete Freund's adjuvant (CFA), heat hyperalgesia was only alleviated early in TNFR2$^{-/-}$ mice but reduced in both early and later phases in TNFR1$^{-/-}$ mice (Zhang et al., 2011). In a model of experimental arthritis, chronic joint inflammation was associated with a persistent increase in TNFR1 and TNFR2 expression on dorsal root ganglion (DRG) cells. Here, after induction of arthritis, expression of TNFR1 was elevated bilaterally in neuronal cells of the DRG. In contrast, TNFR2 expression was restricted to non-neuronal cells of the macrophage-monocyte lineage that increased dependent on TNF during experimental arthritis (Inglis et al., 2005). Interestingly, the numbers of macrophages was strongly correlated to the development of mechanical hyperalgesia (Inglis et al., 2005), indicating that TNFR2-expressing macrophages may contribute to pain modulation. Summarizing, while studies demonstrate that TNFR1 plays a role for development and maintenance of neuropathic pain, the role of TNFR2 seems to be more restricted to the early phase of pain development, potentially by promoting inflammation through macrophages. Interestingly, we recently demonstrated that TNFR2$^{-/-}$ mice have chronic non-resolving pain after CCI, a phenotype that is mirrored by depletion of Tregs (Fischer et al., 2019b), suggesting that TNFR2 may also promote analgesic responses via Tregs.

NOVEL THERAPEUTICS TO TARGET TNFR SIGNALING

The activities mediated by TNFR1 and TNFR2 can be modulated in several ways and adapted to the desired therapeutic effects. Inhibition of the proinflammatory activities induced by TNFR1 can be achieved either at the level of ligand or receptor. Most of the approved therapeutics interfering with the proinflammatory activity are antibodies directed against TNF, including three IgG molecules (infliximab, adalimumab, golimumab, and several biosimilars thereof) and a PEGylated Fab fragment (certolizumab-pegol) (Kontermann et al., 2009; Monaco et al., 2015). These antibodies neutralize activation of TNFR1 and TNFR2 by inhibiting binding of TNF to its receptors, however, do not affect the activity of lymphotoxin-alpha (LTα). In contrast, a soluble TNFR2-Fc fusion protein (etanercept, and its biosimilars) is capable of inhibiting binding of TNF and LTα to its receptors (Monaco et al., 2015). Approved indications of these molecules include the treatment of chronic inflammatory diseases of the joints, digestive tract, the eye and the skin, such as rheumatoid arthritis, psoriatic arthritis, ankylosing spondylitis, Crohn's disease, ulcerative colitis, psoriasis, hidradenitis suppurativa, uveitis, and juvenile idiopathic arthritis (Fischer et al., 2015; Monaco et al., 2015). Obviously, all these therapeutics globally affect activation of TNFR1 and TNFR2 by TNF.

Novel therapeutics currently in development aim at a more selective inhibition of TNFR1 or are developed for a selective activation of TNFR2 (**Figure 2**). Selective inhibition of TNFR1 can be achieved using TNFR1 specific antibodies or modified ligands, while selective activation of TNFR2 requires (i) a specific binding to TNFR2, and (ii) the capability of activating the receptor through clustering, i.e., formation of higher order complexes (Grell et al., 1995; Fischer et al., 2017). This can be achieved using receptor-specific monoclonal antibodies or using modified ligands.

Targeting TNFR1

Various TNFR1-selective, neutralizing molecules have been developed in recent years, including monoclonal antibodies, antibody derivatives and TNF muteins (**Figure 3**). Atrosab is a humanized IgG1 derived from the mouse monoclonal antibody H398 (Kontermann et al., 2008). H398 was generated by the hybridoma technology from mice immunized with human TNFR1 and shown to compete for receptor binding with TNF and LTα (Thoma et al., 1990). Humanization was achieved by CDR grafting into human germline sequences. The humanized antibody retained the neutralizing capacity of H398 and was further developed into a human IgG1 molecule comprising an effector-deficient Fc region derived from the FcΔab sequence

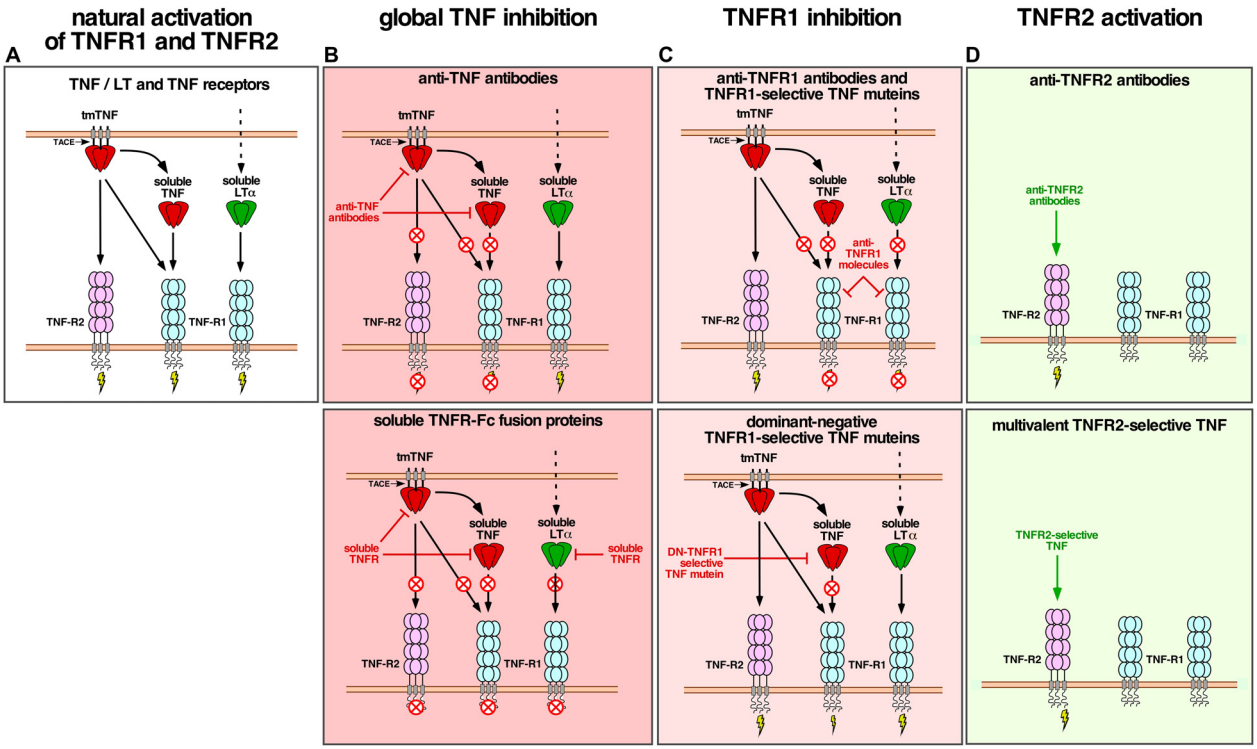

FIGURE 2 | (A) Activation of TNFR1 and TNFR2 by membrane-bound TNF (mTNF), soluble TNF and LTα. **(B)** Global inhibition of TNFR1 and TNFR2 by anti-TNF antibodies and soluble TNFR2-Fc fusion proteins. **(C)** Selective inhibition of TNFR1 by anti-TNFR1 antibodies and dominant-negative TNFR1-selective TNF muteins. **(D)** Selective activation of TNFR2 by anti-TNFR2 antibodies and multivalent TNFR2-selective TNF muteins.

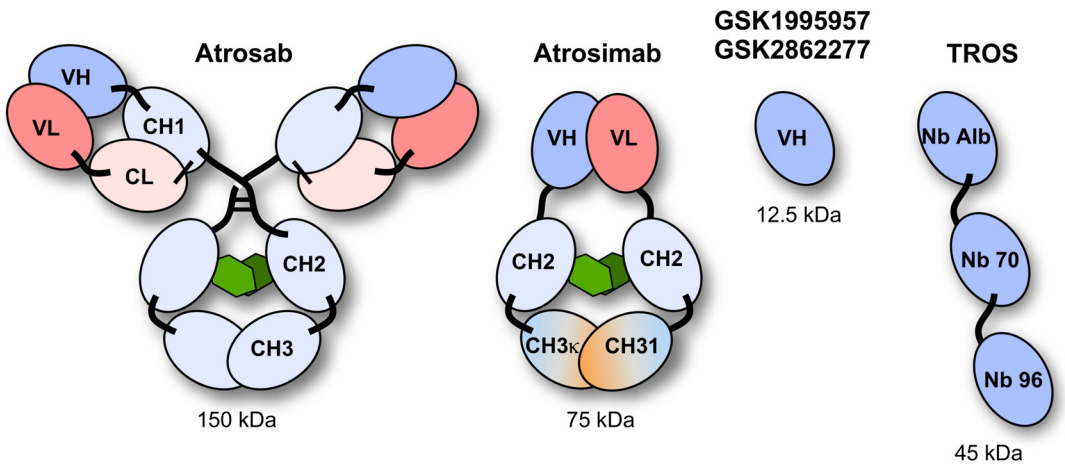

FIGURE 3 | Schematic representation of the TNFR1 antagonists Atrosab (full human IgG1), Atrosimab (monovalent antibody derivate of Atrosab), GSK1995957/GS2862277 (domain antibody), and TROS (a nanobody fusion protein).

(Armour et al., 1999). Atrosab recognizes human and rhesus TNFR1, but not mouse TNFR1, and is capable of inhibiting TNFR1-activation by TNF and LTα with EC_{50} values in the low nanomolar range (Zettlitz et al., 2010). The epitope of Atrosab was mapped to CRD1 and CRD2 of TNFR1, with residues P23, R68, H69, located within the TNF binding site, contributing to binding (Richter et al., 2013). Atrosab could be safely administered at therapeutic doses to mice and cynomolgus monkeys and demonstrated therapeutic efficacy in various disease models (Dong et al., 2016; Williams et al., 2018). However, a first clinical phase 1 study revealed dose-limiting side effects at rather low doses, which was subsequently attributed to a marginal agonistic activity in a small concentration range observed *in vitro* due to bivalent TNFR1 binding of the IgG molecule.

This led to the development of Atrosimab, a monovalent derivative of Atrosab (Richter et al., 2019b). Atrosimab is an Fv-Fc fusion protein with approximately half the size of an antibody. The Fv fragment was generated from an alternative humanized version of H398, which was further affinity matured by CDR and random mutagenesis using phage display (Richter et al., 2019a). In order to force heterodimerization of the Fc region, a novel strategy was employed using CH3 domains engineered to comprise the CH1-CL interface of a Fab fragment. This resulted in a monovalent antibody with improved binding and neutralizing activity compared to Atrosab (Richter et al., 2019a).

Another monovalent anti-TNFR1 binder was generated using a single antibody heavy chain domain (VH; domain antibody − dAb), which acts a competitive antagonist and lacks agonistic activity (Holland et al., 2013). This molecule was developed by GSK (GSK1995057) and had entered preclinical and clinical testing, including i.v. and pulmonary delivery (Proudfoot et al., 2018). Surprisingly, a novel type of autoantibody (HAVH) reacting with the human VH framework used in GSK1995957 was identified in approximately 50% of healthy human serum samples. *In vitro* studies showed that these pre-existing anti-drug antibodies led to TNFR1 activation and infusion reactions consistent with cytokine release, limiting its therapeutic use (Holland et al., 2013; Cordy et al., 2015). Information derived from the HAVH binding epitope on the VH was used to generate a derivative (GSK2862277) with reduced binding of HAVH autoantibodies reducing the frequency of donors with pre-existing autoantibodies to 7%. However, in a phase 1 trial adverse effects due to presence of high levels of novel pre-existing antibodies were observed in one subject (Cordy et al., 2015). Another obstacle for use in patients comes from the rather short serum half-life of these domain antibodies with a size of approximately 10−13 kDa. This can be circumvented by implementing half-life extension strategies (Kontermann, 2011). In one approach, an anti-mouse TNFR1 domain antibody (DOM1m-21-23) was fused to an albumin-binding domain antibody, resulting in a bispecific fusion protein (DMS5540) which showed dose-depended extension of half-life in mice (from 3.3 h at 0.1 mg/kg to 23.2 h at a dose of 10 m/kg), indicative of target-mediated clearance. Furthermore, protective activity in a prophylactic mouse challenge study with bolus injected TNF was observed starting with doses of 0.3 mg/kg (Goodall et al., 2015).

Similarly, two anti-TNFR1 Nanobodies (Nb) isolated from an alpaca immunized with recombinant human soluble TNFR1 were genetically linked to an albumin-binding Nb to generate a bispecific half-life extended molecule named "TNF Receptor-One Silencer" (TROS) (Steeland et al., 2015). TROS competes with TNF for binding to TNFR1, inhibits its activity with IC_{50} values in the nanomolar range and showed therapeutic activity in *ex vivo* and *in vivo* models of inflammation, e.g., in a EAE model in human TNFR1 transgenic in a mouse TNFR1-k/o-background (Steeland et al., 2017). In these mice, TROS exhibited a serum half-life of >24 h after i.p., injections requiring administration every 2nd day.

Others have developed small molecular inhibitors of TNFR1, including antisense oligonucleotides (ASO) and small-molecule inhibitors identified by screening compounds of the NIH Clinical Collection (Lo et al., 2017, 2019). The ASO approach was used to induce downregulation of TNFR1, allowing tumor therapy with high dose TNF, i.e., protecting animals from systemic TNF-induced toxicity (van Hauwermeiren et al., 2015). The small-molecule inhibitors either disrupted the interaction of the TNFR1 pre-ligand assembly domain (PLAD) or acted allosterically on TNFR1 (Lo et al., 2017). In a recent study, the cheminformatics pipeline was used to identify compounds in the Zinc database that inhibit TNFR1 using a pharmacophore-based screening, molecular docking and *in silico* ADMET (absorption, distribution, metabolism, excretion and toxicity) prediction (Saddala and Huang, 2019).

The use of TNF muteins represents another approach for selective interference with TNFR1 activity. R1antTNF is a modified TNF with specificity for TNFR1 isolated from a TNF phage display library (Shibata et al., 2008a). This TNF mutein, with an affinity for TNFR1 similar to that of the wild-type TNF, carries the mutations A84S, V85T, S86T, Y87H, Q88N, and T89Q, and inhibits TNFR1-mediated activity without affecting TNFR2. It was reasoned from x-ray crystallographic studies that one of the mutations, Y87H, which changes the binding mode from a hydrophobic to an electrostatic interaction, causing an unstable, rapid TNFR1 binding pattern, is responsible for the antagonistic activity (Shibata et al., 2008b), which was also confirmed for another TNF mutein, R1antTNF-T8, bearing in addition a T89R mutation (Mukai et al., 2009). Therapeutic activity of R1antTNF was demonstrated in various animal models. Another study revealed that R1antiTNF binds TNFR1 with fast association and dissociation rates, resulting in a shortened nuclear duration of NFκB and a gene expression profile biased toward early response genes (Zhang et al., 2017). Interestingly, at higher concentrations R1antTNF selectively activates the apoptosis pathway and not the NFκB pathway. Half-life of this short-lived TNF mutein was improved through PEGylation (PEG-R1antTNF), which improved furthermore the therapeutic activity, e.g., in an EAE model of MS (Nomura et al., 2011). Furthermore, the molecular stability and bioactivity was improved by converting the homotrimeric R1antTNF into a single-chain derivative (scR1antTNF) by introducing short peptide linkers of 5 or 7 residues between the three protomers (Inoue et al., 2017).

One of the most studied TNF muteins is XPro1595 and a PEGylated derivative thereof. XPRo1595 is a dominant-negative mutant of TNF developed by Xencor applying an *in silico* method to predict and design homotrimeric TNF variants exhibiting decreased receptor binding and being capable of sequestering native TNF homotrimers into inactive native:variant heterotrimers leading to inhibition of TNF-mediated signaling (Steed et al., 2003). XPro1595 carries two mutations, A145R and Y87H, located at the TNF-TNFR interface, and is unable to bind TNFR1 or TNFR2 and to activate downstream signals as homotrimer. XPro1595 efficiently blocks the activity of TNF by exchanging individual subunits and forming heterotrimers. Thus, exchange of one subunit already leads to an inactive TNF molecule, which can bind only one TNF receptor chain, insufficient for receptor activation. At a ratio of 10:1 XPro1595 to wt TNF already 99% of the TNF molecules are inactivated.

XPro1595 was further modified into a PEGylated derivative (XENP1595) for increased half-life and reduced immunogenicity. This involved the introduction of three mutations, C69V, C101A, and R31C, allowing a site-directed PEGylation at C31 (Zalevsky et al., 2007; Olleros et al., 2009). Of note, membrane TNF is not affected by XPro1595 and its derivatives.

Targeting TNFR2

Besides selective binding to TNFR2, activation of TNFR2 requires efficient receptor clustering, which is mediated by membrane TNF or secondary receptor cross-linking, e.g., with anti-TNFR2 antibodies (Wajant et al., 2001). Various TNF muteins selectively binding to TNFR2 have been generated by site-directed mutagenesis or using phage display (Loetscher et al., 1993; Abe et al., 2011; Ando et al., 2016). One of the most commonly used variant is a double mutation in human TNF, D143N and A145R, which lacks complete binding to human or mouse TNFR1 (Loetscher et al., 1993). The soluble, homotrimeric TNF molecule comprising the receptor-binding TNF-homology domain (aa 80 - 233) was further converted into a single-chain derivative (scTNF) by connecting the three subunits (protomers) with 2 flexible linkers, e.g., composed of glycines and serines (Krippner-Heidenreich et al., 2008). This increased the stability under physiological conditions *in vitro* and *in vivo*, while maintaining receptor selectivity. Furthermore, the scTNF moiety allows to generate fusion proteins to increase valency for TNFR2. One of the first approached was fusion of the trimerization of domain of tenascin C (TNC) to the N-terminus of TNFR2-selective scTNF, resulting in a nonavalent molecule capable of clustering TNFR2 (Fischer et al., 2011b). This approach was also applied to generate a mouse TNFR2-selective mouse TNC-scTNF. Here, two mutations, D221N and A223R, were introduced into mouse TNF (Fischer et al., 2014; Chopra et al., 2016). In an alternative approach, the homodimerization heavy chain domain 2 of human IgE (EHD2) was used to generate a hexavalent fusion protein (EHD2-scTNF$_{R2}$), which was also capable of specifically binding to TNFR2 and inducing efficient receptor activation (Dong et al., 2016). Furthermore, the use of tetramerization domains, e.g., derived from p53 and GCN4, was applied to obtain dodecavalent fusion proteins with further improved crosslinking activity (Fischer et al., 2017). The use of Fc-regions or whole antibodies represents another option to generate hexavalent molecules and, in addition, allows to obtain targeted derivatives, e.g., as has been shown for scTRAIL fusion proteins (Hutt et al., 2018; Siegemund et al., 2018).

Selective TNFR2 activation was also described for a homotrimeric TNF variant (TNF07) carrying 2 mutations, S95C and G148C, which result in disulfide-linked TNF molecules with increased stability and, surprisingly, the capability to activation TNFR2 without further crosslinking, as shown in CD4$^+$ T-regulatory expansion assays, although the molecular composition and absence of TNF07 multimers was not analyzed (Ban et al., 2015).

TNFR2 agonism can also be induced by TNFR2-selective antibodies. Screening available anti-TNFR2 monoclonal antibodies, one agonistic antibody was identified leading, e.g., in activation and expansion of T_{reg} cells, capable of correcting type 1 diabetes-associated Treg activation defects (Okubo et al., 2013, 2016). Mechanistically, it has been proposed that antagonistic anti-TNFR2 antibodies block ligand binding and lock membrane receptors in a resting (non-signaling), antiparallel dimer arrangement, while agonistic, cross-linking antibodies stabilize parallel TNF-TNFR2 complexes, i.e., provide a structural stabilization of the active signaling network (Vanamee and Faustman, 2018). Ligand-independent activation of TNFR2 by antibodies can, furthermore, be induced by Fc-mediated binding to FcγR on neighboring cells resulting in multivalent membrane display, thus mimicking membrane TNF. A potent, Fc-dependent T-cell co-stimulation and robust antitumor effects of these type of antibodies were described (Tam et al., 2019). Alternatively, combining an anti-TNFR2 antibody with an anchoring domain mediating binding to a membrane protein has also been described to allow a FcγR-independent TNFR2 activation. This was exemplarily shown fusing co-stimulatory members of the TNFSF, such as scGITRL, sc4-1BBL and IL-2, to the C-terminus of an anti-TNFR2 monoclonal antibody (Medler et al., 2019). Similarly, bispecific antibodies could be used to retarget the TNFR2 binding site and to induce a multivalent presentation, as shown for a tetravalent bispecific anti-TRAILR2 antibody targeting fibroblast activation protein (FAP) on tumor stroma fibroblasts (Brünker et al., 2016).

SELECTIVE NEUTRALIZATION OF sTNF BY DOMINANT-NEGATIVE TNF MUTEINS

Since tmTNF is sufficient to promote important immune functions like self-tolerance and resistance to infection (Alexopoulou et al., 2006), selective neutralization of sTNF may be a superior therapeutic strategy to treat chronic inflammatory and autoimmune diseases compared to non-selective blocking of TNF. The dominant-negative TNF mutein XPro1595 has shown therapeutic activity in disease models of inflammatory and degenerative diseases. It was first shown in 2007 that sTNF neutralization attenuates experimental arthritis in two rodent arthritis models without suppressing innate immunity to *Listeria* infection (Zalevsky et al., 2007), indicating that inflammation in mouse arthritis models is primarily driven by sTNF, and suggest that sTNF inhibitors might have a superior safety profile compared to conventional non-selective anti-TNF therapeutics. A follow-up study using XPro1595 showed that selective inhibition of sTNF protected mice from Bacillus Calmette-Guérin (BCG)/LPS and D-GALN/LPS-induced liver damage, indicating that sTNF, but not tmTNF, is critical for LPS-induced hepatitis (Olleros et al., 2010).

The main focus of pre-clinical studies using DN-TNFs is on treatment of neurodegenerative diseases where elevated TNF levels are found at the site of injuries, such as MS, Parkinson's disease (PD) and spinal cord injury (SCI). XPro1595 was evaluated in two parallel studies by the groups of Lesley Probert and John Bethea in the EAE mouse model of MS. Both studies showed that blocking the action of sTNF by XPro1595, but not of sTNF/tmTNF by the non-selective anti-TNF therapeutic etanercept, protected mice against the clinical

symptoms of EAE. Taoufik et al. (2011) treated at time of disease onset and demonstrated that the therapeutic effect in this study was associated with reduced CNS immunoreactivity and increased expression of neuroprotective mediators but independent of changes in antigen-specific immune responses and focal inflammatory spinal cord lesions, but was (Taoufik et al., 2011). Brambilla et al. (2011) treated the EAE mice at peak of disease, when marked demyelination was already in progress, and showed that XPro1595 administration resulted in reduced axon damage, preservation of axons and improved myelin compaction and significant remyelination. Mechanistic studies showed that therapeutic inhibition of soluble brain TNF promotes remyelination due to improved phagocytosis of myelin debris by microglia and prevented disease-associated decline in motor performance in cuprizone-fed mice (Karamita et al., 2017). These results demonstrate that sTNF promotes CNS inflammation in EAE and indicate that blocking of neuroprotective tmTNF might have been the cause of the failed lenercept trial.

The laboratory of Malú Tansey has demonstrated that blocking sTNF signaling attenuates loss of dopaminergic neurons in models of Parkinson's disease. Local administration of the dominant-negative TNF inhibitor XENP345, an earlier version of XPro1595 that works via the same mechanism of action, reduced the retrograde nigral degeneration induced by a striatal injection of the oxidative neurotoxin 6-hydroxydopamine (6-OHDA) by 50%. Similar neuroprotective effects were observed after chronic co-infusion of XENP345 with bacterial lipopolysaccharide (LPS) into the substantia nigra (McCoy et al., 2006). Another study from the same laboratory showed that intranigral lentiviral delivery of dominant-negative TNF administered concomitant with 6-OHDA attenuated neurotoxin-induced DA neuron loss and associated behavioral deficits in hemiparkinsonian rats (McCoy et al., 2008). Similar, delayed injection of DN-TNF encoding lentivirus 2 weeks after receiving a 6-OHDA lesion attenuated microglia activation and halted progressive loss of nigral dopaminergic neurons (Harms et al., 2011). Interestingly, peripheral administration of XPro1595 resulted in significant CSF levels of the TNF mutein and attenuated glial activation and nigral cell loss and in 6-OHDA hemiparkinsonian rats (Barnum et al., 2014). Collectively, these data clearly demonstrate a role for sTNF in PD pathology, and indicate that selective inhibition of sTNF may be therapeutic in early stages of PD.

Other work from the Tansey laboratory indicates the therapeutic potential of XPro1595 for Alzheimer's disease (AD). Using 5xFAD mice, which express human *a*myloid precursor protein (*APP*) and presenilin-1 (PSEN1) transgenes and recapitulate many AD-related phenotypes, they showed that peripheral injection of XPro1595 alleviated the age-dependent increase in activated immune cells in the brain of transgenic mice, decreased beta-amyloid plaque load, and rescued impaired long-term potentiation (LTP). This indicates that sTNF neutralization may impact brain immune cell infiltration and prevent or delay neuronal dysfunction in AD (MacPherson et al., 2017). Similar, chronic infusion of XENP345 or single injection of a lentivirus encoding DN-TNF abrogated AD-like pathology in LPS-treated 3xTgAD mice (McAlpine et al., 2009). Further data indicate that XPro1595 administration lowers the risk for late-onset Alzheimer's disease associated with obesity, metabolic syndrome, and type 2 diabetes (Sousa Rodrigues et al., 2019).

Interestingly, genetic ablation of sTNF did not reduce lesion size and improve functional recovery after moderate SCI in mice (Ellman et al., 2016). In contrast, epidural administration of XPro1595 to the contused spinal cord decreased anxiety-related behavior, and reduced neuronal damage at the site of injury resulting in improved locomotor function, whereas central administration of the non-selective anti-TNF drug etanercept had no therapeutic effects (Novrup et al., 2014). Further studies in rats demonstrated that intrathecally administered XPro1595 directly post-high-level SCI improved the intensification of colorectal distension-induced and naturally occurring autonomic dysreflexia, a life-threatening syndrome experienced by SCI patients. This effect was mediated via decreased sprouting of nociceptive primary afferents and activation of the spinal sympathetic reflex circuit (Mironets et al., 2018). A follow-up study from the same laboratory further demonstrated that delayed (3 days after injury) local administration of XPro1595 still improved autonomic dysreflexia for months postinjury. Further, XPro1595 administration also prevented sympathetic hyperreflexia-associated splenic atrophy and loss of leukocytes to dramatically improve the ability of chronic SCI rats to fight off pneumonia, a common cause of hospitalization after injury (Mironets et al., 2020). Interestingly, subcutaneous administration of XPro1595 caused an exacerbation of SCI-associated depressive phenotype in rats, whereas intracerebroventricular administration of the drug did not impact the development of depression after injury (Farrell and Houle, 2019). This suggests a complex contribution of TNF-based neuroinflammation in SCI−induced depression.

Clausen et al. studied systemic administration of Xpro1595 and etanercept on infarct volume, functional recovery and inflammation after focal cerebral ischemia in mice. They found that systemically administered XPro1595 and etanercept significantly improved functional outcomes, such as brain inflammation and liver acute phase response (APR), but did not affect infarct volumes (Clausen et al., 2014). In a follow-up study, mice were treated topically or intracerebroventricularly with saline, XPro1595, or etanercept immediately after permanent MCAO. Topical, but not intracerebroventricular XPro1595 treatment reduced infarct volume after pMCAO, whereas etanercept administration had no effect (Yli-Karjanmaa et al., 2019). Altogether, these data indicate that inhibition of sTNF signaling holds promise as a novel treatment for ischemic stroke.

Genetic data indicate that TNFR1 plays an essential role for pain development in males (Dellarole et al., 2014). Accordingly, it was shown that intraperitoneal administration of XPro1595 prevented complete Freund's adjuvant (CFA)-induced mechanical hypersensitivity in male mice in a model of local CFA-induced model of orofacial pain (Lis et al., 2017). Similar, after CCI, systemic application of XPro1595 alleviated mechanical allodynia in males. However, no therapeutic response was observed in females. Mechanistically this study showed that presence of estrogen inhibited the therapeutic response of XPro1595 in females, i.e., XPro1595 was therapeutic in

ovariectomized mice, whereas the therapeutic effect was lost after estrogen replacement therapy in ovariectomized mice (del Rivero et al., 2019). This study indicates sex-difference in the response to DN-TNFs. Since most disease models are limited to analysis of one sex, further investigations are needed to evaluate sex differences in other disease models, such as EAE or PD/AD models.

Shibata et al. (2008a) studies the therapeutic effect of R1antTNF in chemically induced acute hepatitis models. In a carbon tetrachloride (CCl_4)-induced model, R1antTNF administration significantly reduced serum levels of ALT (alanine aminotransferase), a marker for liver damage. In a concanavalin A (ConA)-induced T-cell-dependent model, R1antTNF administration reduced serum levels of the inflammatory cytokines IL-2 and IL-6 (Shibata et al., 2008a). Importantly, the efficacy of R1antTNF treatment was superior to antagonistic anti-TNF antibodies, indicating that blocking of TNFR1 might be superior to non-specific neutralization of sTNF/tmTNF. The therapeutic effect of pegylated R1-antTNF was then evaluated in animal models of chronic inflammation. In a murine collagen-induced arthritis model XPro1595 showed a comparable therapeutic effect to etanercept in a prophylactic treatment setting. However, in therapeutic protocols, PEG-R1antTNF showed a greater therapeutic effect than etanercept. Moreover, PEG-R1antTNF did not affect the clearance of injected adenovirus. In contrast, virus load strongly accumulated during etanercept treatment (Shibata et al., 2009). Further, PEG-R1antTNF treatment at time of disease induction significantly improved the clinical score and suppressed peripheral and central Th1 and Th17-type response as well as cerebral demyelination in EAE mice (Nomura et al., 2011). Similar, PEG-R1antTNF treatment attenuated arterial inflammation and intimal hyperplasia in IL-1 receptor antagonist-deficient mice (Kitagaki et al., 2012). Altogether, these data indicate that inhibition of sTNF/TNFR1 seems to be superior to unspecific sTNF/tmTNF neutralization by conventional anti-TNF drugs (**Table 1**).

BLOCKING OF TNFR1 BY TNFR1-SELECTIVE ANTAGONISTS

To neutralize pro-inflammatory TNFR1 signaling, we have developed the human TNFR1 specific antagonist Atrosab. Similar to sTNF neutralization, Atrosab ameliorated EAE motor disease. To study long-term efficacy of TNFR1 antagonist treatment the parental mouse anti-human TNFR1 antibody H398 was administered. Interestingly, our data indicate that TNFR1 blocking restricts CNS-infiltration of peripheral immune cell through down-regulation of TNF-induced adhesion molecules and not by impacting peripheral immunity (Williams et al., 2018). Further, in a CIA rhesus monkey model, Atrosab administration resulted in reduced acute-phase C-reactive protein (CRP) and IL-6 levels in serum, prevented body weight loss, delayed the onset of arthritic symptoms and improved the clinical arthritis score (Guenzi et al., 2013). Moreover, therapeutic efficacy of Atrosab was superior to the clinically used anti-TNF drugs etanercept and infliximab (Guenzi et al., 2013). Importantly, using a mouse model of NMDA-induced acute neurodegeneration, we demonstrated that co-administration of Atrosab together with glutamate into the magnocellular nucleus basalis resulted in protection of cholinergic neurons from glutamate-induced excitotoxic cell death and reverted the neurodegeneration-associated memory impairment tested by a passive avoidance paradigm (Dong et al., 2016). Interestingly, administration of Atrosab together with a TNFR1 antagonist abrogated the therapeutic effect of Atrosab, indicating that the therapeutic activity of Atrosab depends on functional TNFR2 signaling, which appears essential for neuroprotection (Dong et al., 2016).

TABLE 1 | Preclinical Use of sTNF neutralizing therapeutics.

Molecule	Disease model	References
Dominant-negative TNF muteins (DN-TNF)		
XENP345/XPro1595	Experimental arthritis	Zalevsky et al., 2007
XPro1595	(BCG)/LPS and D-GALN/LPS-induced liver damage	Olleros et al., 2009, 2010
XPro1595	Experimental autoimmune encephalomyelitis (EAE)	Brambilla et al., 2011; Taoufik et al., 2011; Karamita et al., 2017
XENP345, lentiviral DN-TNF delivery, XPro1595	6-OHDA- and LPS-induced models of Parkinson disease	McCoy et al., 2006, 2008; Harms et al., 2011; Barnum et al., 2014
XPro1595	5xFAD transgenic mice as a model of Alzheimer's disease	MacPherson et al., 2017
XENP345, lentiviral DN-TNF delivery	LPS-treated 3xTgAD transgenic mice as a model of Alzheimer's disease	McAlpine et al., 2009
XPro1595	high-fat high-carbohydrate diet induced model of insulin impairment	Sousa Rodrigues et al., 2019
XPro1595	Spinal cord injury: motor impairment	Novrup et al., 2014
XPro1595	Spinal cord injury: autonomic dysreflexia and antibacterial immunity	Mironets et al., 2018, 2020
XPro1595	Focal cerebral ischemia: neuroinflammation and liver acute phase response	Clausen et al., 2014
XPro1595	Permanent Middle Cerebral Artery Occlusion (pMCAO): infarct volume	Yli-Karjanmaa et al., 2019
XPro1595	CFA-induced orofacial pain	Lis et al., 2017
XPro1595	Chronic constriction injury (CCI)	del Rivero et al., 2019
R1antTNF	CCl_4- and ConA-induced hepatitis	Shibata et al., 2008a
PEG-R1antTNF	Collagen-induced arthritis	Shibata et al., 2009
PEG-R1antTNF	Experimental autoimmune encephalomyelitis (EAE)	Nomura et al., 2011
PEG-R1antTNF	femoral artery injury in IL1R-deficient mice: arterial inflammation and intimal hyperplasia	Kitagaki et al., 2012

Recently, we further demonstrated that Atrosab might be a promising novel therapeutic for non-alcoholic fatty liver disease (NAFLD), a wide-spread disease with increasing prevalence that is associated with the development of liver fibrosis/cirrhosis, a major risk factor of liver-related and all-cause mortality in this disease (Chalasani et al., 2018). Activation of pro-inflammatory cytokines, such as TNF, in adipose and liver tissues has been implicated to play an important role in the pathogenesis and disease progression of NAFLD (Hotamisligil et al., 1993; Crespo et al., 2001). Indeed, higher serum levels of TNF correlate with insulin resistance patients and were observed in samples from non-alcoholic steatohepatitis (NASH) patients compared to samples from patients with simple steatosis (Hui et al., 2004; Wellen and Hotamisligil, 2005). Moreover, in liver tissues of NASH patients enhanced TNF/TNFR1 expression was found in correlation with disease activity and fibrosis stages (Crespo et al., 2001). Vice versa, in various diet-induced or genetic NAFLD models, TNF- or TNFR-deficient mice showed improved insulin sensitivity and less pronounced liver steatosis and fibrosis (Uysal et al., 1997, 1998; Tomita et al., 2006). Our data show that blocking of TNFR1 by Atrosab results in alleviation of liver steatosis and insulin resistance as well as liver injury and fibrosis (Wandrer et al., 2020). Selective TNFR1 inhibition might therefore represent a promising treatment strategy in NAFLD.

The nanobody-based selective inhibitor of TNFR1 TROS reduced secretion of IL-6, IL-8 and TNF in *ex vivo* cultured inflamed colon biopsies from patients suffering from active Crohn's disease. Similar, in liver chimeric humanized mice, TROS antagonized inflammation in a model of acute TNF-induced liver inflammation (Steeland et al., 2015). The neuroprotective effect of TROS was affirmed using transgenic AD mice and icv injection of AβO into WT mice. Here, Steeland et al. (2018) showed that therapeutic blockage of TNFR1 by TROS prevented the cognitive decline in APP/PS1$^{tg/wt}$ mice and upon icv AβO injection, outlining the therapeutic potential of TNFR1 antagonists for AD. Similar to Atrosab, TROS was therapeutic in a model of MS. It was shown that prophylactic TROS treatment significantly delayed disease onset and ameliorated EAE symptoms in mice. Treatment initiated early after disease onset prevented further disease development. Altogether, TROS administration reduced neuroinflammation and preserved myelin and neurons (Steeland et al., 2017). The therapeutic responses of TROS and Atrosab in EAE indicate that TNFR1 blocking might be therapeutic in MS. Indeed, through genome-wide association studies, a single nucleotide polymorphism (SNP) in the TNFRSF1A gene encoding TNFR1 was discovered to be associated with MS, but not with other autoimmune conditions such as rheumatoid arthritis, psoriasis and Crohn's disease. Functional studies showed that this MS risk allele directs expression of a novel, soluble form of TNFR1 that can neutralize TNF, similar to anti-TNF therapeutics (Gregory et al., 2012). Together with the overwhelming data describing TNFR2 as an essential mediator of neuroprotection this indicated that maintenance of functional TNFR2 signaling is important during MS therapy. Therefore, selective blocking of TNFR1 might be superior to anti-TNF therapeutics like lenercept, which failed in clinical trials of MS (**Table 2**).

SELECTIVE ACTIVATION OF TNFR2 USING AGONISTIC TNF MUTEINS AND ANTIBODIES

TNFR2 agonist may work via a dual mode of action, modulation of immunity and direct neuroprotection. Therefore, TNFR2 agonists were evaluated in models of inflammation and neurodegeneration (**Table 3**). Indeed, several articles using different TNFR2 agonists demonstrated that TNFR2 activation results in expansion of Tregs *ex vivo* and *in vivo* (Okubo et al., 2013; Chopra et al., 2016; Fischer et al., 2017, 2018, 2019a,b). Using the mouse TNFR2 agonist STAR2, Chopra et al. (2016) showed that exogenous TNFR2 activation protected from acute graft-versus-host disease (GvHD) after allogeneic hematopoietic stem cell transplantation (allo-HCT) via host Treg cell expansion. In this model, Tregs were first expanded via STAR2 administration in recipient mice before allo-HCT, which led to a significantly prolonged survival and reduced GvHD severity in a TNFR2- and Treg-dependent manner. Importantly, the beneficial effects of transplanted T cells to attack leukemic cells and infectious pathogens remained unaffected (Chopra et al., 2016). Another study using a human TNFR2 selective STAR2 variant demonstrated that TNFR2 impeded differentiation of bone marrow-derived immature myeloid cells in culture and dampened their suppressor function *in vitro*. *In vivo* administration of STAR2 resulted in mild myelopoiesis in naïve mice but did not affect immune cell composition. In mice with chronic inflammation, STAR2 treatment expanded CD4$^+$ Tregs and improved their suppressive function (Schmid et al., 2017).

Using the mouse TNFR2 agonist EHD2-sc-mTNF$_{R2}$, we demonstrated that selective activation of TNFR2 induces anti-inflammatory responses and alleviates experimental arthritis. Interestingly, we observed that TNFR2 agonism expands both CD4$^+$ and CD8$^+$ FoxP3$^+$ Tregs both *ex vivo* and in CIA mice (Fischer et al., 2018). This might be important for the therapeutic effect of TNFR2 agonists, since CD8$^+$ suppressor cells were shown to be more suppressive in arthritic mice than their CD4$^+$ counterparts (Notley et al., 2010). In the applied 10-day observation protocol, we only observed a therapeutic response by EHD2-sc-mTNF$_{R2}$ in a prophylactic setting, whereas treatment

TABLE 2 | Preclinical Use of TNFR1 blocking therapeutics.

Molecule	Disease model	References
TNFR1 blocking reagents		
Atrosab	Experimental autoimmune encephalomyelitis (EAE)	Williams et al., 2018
Atrosab	Collagen-induced arthritis	Guenzi et al., 2013
Atrosab	NMDA-induced neurodegeneration model of Alzheimer's disease	Dong et al., 2016
Atrosab	non-alcoholic steatohepatitis (NASH)	Wandrer et al., 2020
TROS	Acute TNF-induced liver inflammation	Steeland et al., 2015
TROS	AβO injection into APP/PS1$^{tg/wt}$ mouse model of Alzheimer's disease	Steeland et al., 2018
TROS	Experimental autoimmune encephalomyelitis (EAE)	Steeland et al., 2017

TABLE 3 | Preclinical Use of TNFR2 agonists and antagonists.

Molecule	Disease model	References
TNFR2 agonists		
STAR2	Graft versus host disese (GvHD)	Chopra et al., 2016
STAR2, EHD2-sc-mTNF$_{R2}$	Collagen-induced arthritis	Fischer et al., 2018; Lamontain et al., 2019
EHD2-scTNF$_{R2}$	NMDA-induced neurodegeneration model of Alzheimer's disease	Dong et al., 2016
EHD2-sc-mTNF$_{R2}$	Spinal cord injury (SCI)	Gerald et al., 2019
EHD2-sc-mTNF$_{R2}$	Chronic constriction injury (CCI) model of neuropathic pain	Fischer et al., 2019b
EHD2-sc-mTNF$_{R2}$	Experimental autoimmune encephalomyelitis (EAE)	Fischer et al., 2019a
Y9 (agonistic anti-TNFR2 antibody)	Syngeneic mouse tumor models	Tam et al., 2019
TNFR2 antagonists		
TNFR2 antagonistic antibodies	Ovarian cancer (patient material)	Torrey et al., 2017
TNFR2 antagonistic antibodies	Sézary syndrome (patient material)	Torrey et al., 2019

after onset of arthritis did not impact arthritic disease within the observation period. However, another study using STAR2 in CIA mice showed that TNFR2 agonist treatment ameliorates established collagen-induced arthritis in mice (Lamontain et al., 2019). Of note, in this protocol, TNFR2 agonist treated mice showed amelioration of arthritic disease only after more than 10 days observation period. Together, these two independent studies suggest a therapeutic potential of TNFR2 agonists for arthritis and other chronic inflammatory diseases.

Using EHD2-scTNF$_{R2}$ we confirmed the neuroprotective role of TNFR2 and demonstrated that selective activation of TNFR2 rescued dopaminergic neurons (Fischer et al., 2011b) and oligodendrocytes (Maier et al., 2013) from oxidative stress induced cell death and promoted myelination via astrocyte-dependent secretion of neurotrophic factors (Fischer et al., 2014). In this line, we showed that coadministration of glutamate and EHD2-scTNF$_{R2}$ into the magnocellular nucleus basalis of mice protected cholinergic neurons and their cortical projections from excitotoxic cell death induced by glutamate and reverted the injury-associated memory impairment testes by a passive avoidance paradigm (Dong et al., 2016). Similar, using a mouse model of contusive injury, Gerald et al. showed that EHD2-sc-mTNF$_{R2}$-mediated activation of TNFR2 in the spinal cord improved locomotion and cortical neural activity (Gerald et al., 2019). Due to the important role of TNFR2 for neuroprotection, we went on to study the neuroprotective role of TNFR2 in models of CNP. Here, we showed that pharmacological activation of TNFR2 using EHD2-sc-mTNF$_{R2}$ in mice promoted long-lasting pain recovery after CCI. TNFR2 agonist treatment alleviated peripheral and central inflammation and reduced neuronal injury. Importantly, depletion of Tregs abolished the therapeutic effect of TNFR2 agonist treatment (Fischer et al., 2019b), indicating that Treg-TNFR2 mediated responses are essential for the analgesic effect of EHD2-sc-mTNF$_{R2}$. Similar, we demonstrated that in EAE mice systemic administration of EHD2-sc-mTNF$_{R2}$ alleviated inflammation resulting in reduced demyelination and neurodegeneration. The behavioral data showed that TNFR2 agonist treatment alleviated motor disease and promoted long-term recovery from CNP. Mechanistically, this study indicated that TNFR2 agonist treatment in EAE mice follows a dual mode of action and promotes suppression of CNS autoimmunity as well as remyelination (Fischer et al., 2019a).

The group of Denise Faustman used an agonistic TNFR2-selective antibody to demonstrate that a subpopulation of insulin-specific CD8$^+$, but not CD4$^+$, T cells in blood samples from patients with type 1 diabetes was vulnerable to TNFR2 induced death. However, other activated and memory T cell populations were resistant to TNFR2-triggered cell death (Ban et al., 2008). This indicates that autoreactive T cells in type 1 diabetes patients can be selectively destroyed by TNFR2 agonism. TNFR2 agonist may offer highly targeted therapies, with a potentially reduced risk of systemic toxicity. Using their agonistic αTNFR2 antibody, Okubo et al. further established a protocol for homogenous expansion of Tregs from human donors (Okubo et al., 2013). Therefore, TNFR2 agonists might work via two different mode of action in diabetes, killing of autoreactive T cells and expansion of immunomodulatory Tregs.

SELECTIVE MODULATION OF TNFR2 SIGNALING FOR CANCER THERAPY

Next to its potential use as a therapeutic target in inflammatory and degenerative diseases, TNFR2 was recently identified as a novel drug target for the treatment of cancer (**Table 3**). Next to its function on immunosuppressive Tregs and myeloid-derived suppressor cells, which may inhibit immune responses to combat tumor development, TNFR2 is expressed on certain tumor cells and directly promotes their proliferation (Vanamee and Faustman, 2017; Sheng et al., 2018). Indeed, TNFR2 plays important roles in multiple aspects of tumor progression, including tumor cell proliferation, bypassing of immune surveillance, promotion of angiogenesis, the formation of a pre-metastasis milieu (reviewed in Sheng et al., 2018). Therefore, therapeutic strategies targeting TNFR2-mediated tumor growth include depletion of TNFR2-expressing Tregs (van der Most et al., 2009) and antagonistic antibodies targeting TNFR2 over-expressed on tumor cells. Several antagonistic antibodies were shown to directly kill human ovarian tumor cells and Tregs by blocking ligation of TNF to TNFR2. Importantly, these antagonistic TNFR2 antibodies depleted Tregs isolated from ovarian cancer ascites more potently than Tregs from healthy donor samples, implying increased tumor specificity (Torrey et al., 2017). A follow-up study indicated that targeted killing of TNFR2-expressing tumor cells and Tregs using TNFR2 antagonistic antibodies is therapeutic in advanced Sézary syndrome, a rare form of cutaneous T-cell lymphoma that is often refractory to treatment (Torrey et al., 2019). Interestingly, next to TNFR2 antagonists, agonistic monoclonal anti-TNFR2 antibodies yielded robust antitumor activity and

durable protective antitumor immunity in multiple mouse cancer cell line models. These antibodies mediated potent Fc-dependent T cell co-stimulation but did not impact numbers or function of Tregs (Tam et al., 2019). These and other studies indicate the complex role of TNFR2 for tumor growth and therapy and suggest that selection of a therapeutic approach with either agonistic or antagonistic TNFR2 targeting reagents depends on the individual context, such as immune status, tumor type and more factors.

CONCLUSION AND OUTLOOK

Tumor necrosis factor blockers have demonstrated their clinical effectiveness, are successfully used to treat autoimmune diseases and are under the top-selling biologics world-wide. However, despite this success the development of serious side-effects and the failure of clinical trials in specific indications such as heart disease and MS revealed the limitations of anti-TNF therapy. Research of the last two decades has established that TNF mediates inflammation and tissue degeneration via TNFR1 signaling and immunomodulation and tissue regeneration via TNFR2. Accordingly, a novel class of drugs that selectively target TNF signaling at the level of the ligand or receptor has emerged. As outlined in this review, selective blocking of sTNF/TNFR1 signaling, which will preserve functional tmTNF/TNFR2 signaling, seems to be sufficient to interfere with pathological TNF signaling. In contrast to global TNF blockers that neutralize sTNF and tmTNF, this class of therapeutics may induce less severe side-effects and may be therapeutic for other diseases such as MS or neurodegenerative diseases, where complete TNF inhibition is contraindicative. Indeed, preclinical evaluation of DN-TNF muteins and TNFR1 antagonists was promising and often superior to conventional anti-TNF therapeutics. Similar, TNFR2 agonists were developed and first pre-clinical evaluation using prototype molecules was successful. However, development of completely human clinical grade products will be necessary to succeed into clinical trials. Ultimately, combination therapies, using sTNF/TNFR1 antagonists together with TNFR2 agonists, may rebalance pathologically deregulated TNF signaling and induce tissue repair and might be a novel superior therapeutic concept to treat a multitude of inflammatory and degenerative diseases.

AUTHOR CONTRIBUTIONS

RF and RK wrote the review and generated the figures. KP reviewed and revised the manuscript.

FUNDING

The authors received funding from Baliopharm AG for clinical development of TNFR1 antagonists.

REFERENCES

Abe, Y., Yoshikawa, T., Inoue, M., Nomura, T., Furuya, T., Yamashita, T., et al. (2011). Fine tuning of receptor-selectivity for tumor necrosis factor-α using a phage display system with one-step competitive panning. *Biomaterials* 32, 5498–5504. doi: 10.1016/j.biomaterials.2011.04.018

Ablamunits, V., Bisikirska, B., and Herold, K. C. (2010). Acquisition of regulatory function by human CD8(+) T cells treated with anti-CD3 antibody requires TNF. *Eur. J. Immunol.* 40, 2891–2901. doi: 10.1002/eji.201040485

Aggarwal, B. B. (2003). Signalling pathways of the TNF superfamily: a double-edged sword. *Nat. Rev. Immunol.* 3, 745–756. doi: 10.1038/nri1184

Alessi, D. R. (2001). Discovery of PDK1, one of the missing links in insulin signal transduction. Colworth Medal Lecture. *Biochem. Soc. Trans.* 29, 1–14. doi: 10.1042/0300-5127:0290001

Alexopoulou, L., Kranidioti, K., Xanthoulea, S., Denis, M., Kotanidou, A., Douni, E., et al. (2006). Transmembrane TNF protects mutant mice against intracellular bacterial infections, chronic inflammation and autoimmunity. *Eur. J. Immunol.* 36, 2768–2780. doi: 10.1002/eji.200635921

Ando, D., Inoue, M., Kamada, H., Taki, S., Furuya, T., Abe, Y., et al. (2016). Creation of mouse TNFR2-selective agonistic TNF mutants using a phage display technique. *Biochem. Biophys. Rep.* 7, 309–315. doi: 10.1016/j.bbrep.2016.06.008

Armour, K. L., Clark, M. R., Hadley, A. G., and Williamson, L. M. (1999). Recombinant human IgG molecules lacking Fcgamma receptor I binding and monocyte triggering activities. *Eur. J. Immunol.* 29, 2613–2624. doi: 10.1002/(SICI)1521-4141(199908)29:08<2613::AID-IMMU2613>3.0.CO;2-J

Arnett, H. A., Mason, J., Marino, M., Suzuki, K., Matsushima, G. K., and Ting, J. P. (2001). TNF alpha promotes proliferation of oligodendrocyte progenitors and remyelination. *Nat. Neurosci.* 4, 1116–1122. doi: 10.1038/nn738

Atretkhany, K.-S. N., Mufazalov, I. A., Dunst, J., Kuchmiy, A., Gogoleva, V. S., Andruszewski, D., et al. (2018). Intrinsic TNFR2 signaling in T regulatory cells provides protection in CNS autoimmunity. *Proc. Natl. Acad. Sci. U.S.A.* 115, 13051–13056. doi: 10.1073/pnas.1807499115

Ban, L., Kuhtreiber, W., Butterworth, J., Okubo, Y., Vanamee, ÉS., and Faustman, D. L. (2015). Strategic internal covalent cross-linking of TNF produces a stable TNF trimer with improved TNFR2 signaling. *Mol. Cell. Ther.* 3:7. doi: 10.1186/s40591-015-0044-4

Ban, L., Zhang, J., Wang, L., Kuhtreiber, W., Burger, D., and Faustman, D. L. (2008). Selective death of autoreactive T cells in human diabetes by TNF or TNF receptor 2 agonism. *Proc. Natl. Acad. Sci. U.S.A.* 105, 13644–13649. doi: 10.1073/pnas.0803429105

Barnum, C. J., Chen, X., Chung, J., Chang, J., Williams, M., Grigoryan, N., et al. (2014). Peripheral administration of the selective inhibitor of soluble tumor necrosis factor (TNF) XPro® 1595 attenuates nigral cell loss and glial activation in 6-OHDA hemiparkinsonian rats. *J. Parkinsons Dis.* 4, 349–360. doi: 10.3233/JPD-140410

Black, R. A., Rauch, C. T., Kozlosky, C. J., Peschon, J. J., Slack, J. L., Wolfson, M. F., et al. (1997). A metalloproteinase disintegrin that releases tumour-necrosis factor-alpha from cells. *Nature* 385, 729–733. doi: 10.1038/385729a0

Bodmer, J.-L., Schneider, P., and Tschopp, J. (2002). The molecular architecture of the TNF superfamily. *Trends Biochem. Sci.* 27, 19–26. doi: 10.1016/s0968-0004(01)01995-8

Borghi, A., Haegman, M., Fischer, R., Carpentier, I., Bertrand, M. J. M., Libert, C., et al. (2018). The E3 ubiquitin ligases HOIP and cIAP1 are recruited to the TNFR2 signaling complex and mediate TNFR2-induced canonical NF-κB signaling. *Biochem. Pharmacol.* 153, 292–298. doi: 10.1016/j.bcp.2018.01.039

Boschert, V., Krippner-Heidenreich, A., Branschädel, M., Tepperink, J., Aird, A., and Scheurich, P. (2010). Single chain TNF derivatives with individually mutated receptor binding sites reveal differential stoichiometry of ligand receptor complex formation for TNFR1 and TNFR2. *Cell. Signal.* 22, 1088–1096. doi: 10.1016/j.cellsig.2010.02.011

Brambilla, R., Ashbaugh, J. J., Magliozzi, R., Dellarole, A., Karmally, S., Szymkowski, D. E., et al. (2011). Inhibition of soluble tumour necrosis factor is therapeutic in experimental autoimmune encephalomyelitis and promotes axon preservation and remyelination. *Brain* 134, 2736–2754. doi: 10.1093/brain/awr199

Brinkman, B. M., Telliez, J. B., Schievella, A. R., Lin, L. L., and Goldfeld, A. E. (1999). Engagement of tumor necrosis factor (TNF) receptor 1 leads to ATF-2- and p38 mitogen-activated protein kinase-dependent TNF-alpha gene expression. *J. Biol. Chem.* 274, 30882–30886. doi: 10.1074/jbc.274.43.30882

Brünker, P., Wartha, K., Friess, T., Grau-Richards, S., Waldhauer, I., Koller, C. F., et al. (2016). RG7386, a novel tetravalent FAP-DR5 antibody, effectively triggers FAP-dependent, avidity-driven DR5 hyperclustering and tumor cell apoptosis. *Mol. Cancer Ther.* 15, 946–957. doi: 10.1158/1535-7163.MCT-15-0647

Cantley, L. C. (2002). The phosphoinositide 3-kinase pathway. *Science* 296, 1655–1657.

Chalasani, N., Younossi, Z., Lavine, J. E., Charlton, M., Cusi, K., Rinella, M., et al. (2018). The diagnosis and management of nonalcoholic fatty liver disease: practice guidance from the American Association for the Study of liver diseases. *Hepatology* 67, 328–357. doi: 10.1002/cld.722

Chan, F. K., Chun, H. J., Zheng, L., Siegel, R. M., Bui, K. L., and Lenardo, M. J. (2000). A domain in TNF receptors that mediates ligand-independent receptor assembly and signaling. *Science* 288, 2351–2354. doi: 10.1126/science.288.5475.2351

Chen, X., Bäumel, M., Männel, D. N., Howard, O. M. Z., and Oppenheim, J. J. (2007). Interaction of TNF with TNF receptor type 2 promotes expansion and function of mouse CD4+CD25+ T regulatory cells. *J. Immunol.* 179, 154–161. doi: 10.4049/jimmunol.179.1.154

Chen, X., Hamano, R., Subleski, J. J., Hurwitz, A. A., Howard, O. M. Z., and Oppenheim, J. J. (2010a). Expression of costimulatory TNFR2 induces resistance of CD4+FoxP3- conventional T cells to suppression by CD4+FoxP3+ regulatory T cells. *J. Immunol.* 185, 174–182. doi: 10.4049/jimmunol.0903548

Chen, X., Nie, Y., Xiao, H., Bian, Z., Scarzello, A. J., Song, N.-Y., et al. (2016). TNFR2 expression by CD4 effector T cells is required to induce full-fledged experimental colitis. *Sci. Rep.* 6:32834. doi: 10.1038/srep32834

Chen, X., Subleski, J. J., Hamano, R., Howard, O. Z., Wiltrout, R. H., and Oppenheim, J. J. (2010b). Co-expression of TNFR2 and CD25 identifies more of the functional CD4+FoxP3+ regulatory T cells in human peripheral blood. *Eur. J. Immunol.* 40, 1099–1106. doi: 10.1002/eji.200940022

Chen, X., Subleski, J. J., Kopf, H., Howard, O. M. Z., Männel, D. N., and Oppenheim, J. J. (2008). Cutting edge: expression of TNFR2 defines a maximally suppressive subset of mouse CD4+CD25+FoxP3+ T regulatory cells: applicability to tumor-infiltrating T regulatory cells. *J. Immunol.* 180, 6467–6471. doi: 10.4049/jimmunol.180.10.6467

Chen, X., Wu, X., Zhou, Q., Howard, O. M. Z., Netea, M. G., and Oppenheim, J. J. (2013). TNFR2 is critical for the stabilization of the CD4+Foxp3+ regulatory T. cell phenotype in the inflammatory environment. *J. Immunol.* 190, 1076–1084. doi: 10.4049/jimmunol.1202659

Chopra, M., Biehl, M., Steinfatt, T., Brandl, A., Kums, J., Amich, J., et al. (2016). Exogenous TNFR2 activation protects from acute GvHD via host T reg cell expansion. *J. Exp. Med.* 213, 1881–1900. doi: 10.1084/jem.20151563

Clausen, B. H., Degn, M., Martin, N. A., Couch, Y., Karimi, L., Ormhøj, M., et al. (2014). Systemically administered anti-TNF therapy ameliorates functional outcomes after focal cerebral ischemia. *J. Neuroinflammation* 11:203. doi: 10.1186/s12974-014-0203-6

Constantin, C. E., Mair, N., Sailer, C. A., Andratsch, M., Xu, Z.-Z., Blumer, M. J. F., et al. (2008). Endogenous tumor necrosis factor alpha (TNFalpha) requires TNF receptor type 2 to generate heat hyperalgesia in a mouse cancer model. *J. Neurosci.* 28, 5072–5081. doi: 10.1523/JNEUROSCI.4476-07.2008

Cordy, J. C., Morley, P. J., Wright, T. J., Birchler, M. A., Lewis, A. P., Emmins, R., et al. (2015). Specificity of human anti-variable heavy (VH) chain autoantibodies and impact on the design and clinical testing of a VH domain antibody antagonist of tumour necrosis factor-α receptor 1. *Clin. Exp. Immunol.* 182, 139–148. doi: 10.1111/cei.12680

Crespo, J., Cayón, A., Fernández-Gil, P., Hernández-Guerra, M., Mayorga, M., Domínguez-Díez, A., et al. (2001). Gene expression of tumor necrosis factor alpha and TNF-receptors, p55 and p75, in nonalcoholic steatohepatitis patients. *Hepatology* 34, 1158–1163. doi: 10.1053/jhep.2001.29628

del Rivero, T., Fischer, R., Yang, F., Swanson, K. A., and Bethea, J. R. (2019). Tumor necrosis factor receptor 1 inhibition is therapeutic for neuropathic pain in males but not in females. *Pain* 160, 922–931. doi: 10.1097/j.pain.0000000000001470

Dellarole, A., Morton, P., Brambilla, R., Walters, W., Summers, S., Bernardes, D., et al. (2014). Neuropathic pain-induced depressive-like behavior and hippocampal neurogenesis and plasticity are dependent on TNFR1 signaling. *Brain Behav. Immun.* 41, 65–81. doi: 10.1016/j.bbi.2014.04.003

Deng, G.-M., Zheng, L., Chan, F. K.-M., and Lenardo, M. (2005). Amelioration of inflammatory arthritis by targeting the pre-ligand assembly domain of tumor necrosis factor receptors. *Nat. Med.* 11, 1066–1072. doi: 10.1038/nm1304

Dolga, A. M., Granic, I., Blank, T., Knaus, H.-G., Spiess, J., Luiten, P. G. M., et al. (2008). TNF-alpha-mediates neuroprotection against glutamate-induced excitotoxicity via NF-kappaB-dependent up-regulation of K2.2 channels. *J. Neurochem.* 107, 1158–1167. doi: 10.1111/j.1471-4159.2008.05701.x

Dong, Y., Fischer, R., Naudé, P. J. W., Maier, O., Nyakas, C., Duffey, M., et al. (2016). Essential protective role of tumor necrosis factor receptor 2 in neurodegeneration. *Proc. Natl. Acad. Sci. U.S.A.* 113, 12304–12309. doi: 10.1073/pnas.1605195113

Ellman, D. G., Degn, M., Lund, M. C., Clausen, B. H., Novrup, H. G., Flæng, S. B., et al. (2016). Genetic ablation of soluble TNF does not affect lesion size and functional recovery after moderate spinal cord injury in mice. *Mediators Inflamm.* 2016:2684098. doi: 10.1155/2016/2684098

Eugster, H. P., Frei, K., Bachmann, R., Bluethmann, H., Lassmann, H., and Fontana, A. (1999). Severity of symptoms and demyelination in MOG-induced EAE depends on TNFR1. *Eur. J. Immunol.* 29, 626–632. doi: 10.1002/(SICI)1521-4141(199902)29:02<626::AID-IMMU626>3.0.CO;2-A

Farrell, K., and Houle, J. D. (2019). Systemic inhibition of soluble tumor necrosis factor with XPro1595 exacerbates a post-spinal cord injury depressive phenotype in female rats. *J. Neurotrauma* 36, 2964–2976. doi: 10.1089/neu.2019.6438

Fischer, R., Kontermann, R., and Maier, O. (2015). Targeting sTNF/TNFR1 signaling as a new therapeutic strategy. *Antibodies* 4, 48–70.

Fischer, R., and Maier, O. (2015). Interrelation of oxidative stress and inflammation in neurodegenerative disease: role of TNF. *Oxid. Med. Cell. Longev.* 2015:610813. doi: 10.1155/2015/610813

Fischer, R., Maier, O., Naumer, M., Krippner-Heidenreich, A., Scheurich, P., and Pfizenmaier, K. (2011a). Ligand-induced internalization of TNF receptor 2 mediated by a di-leucin motif is dispensable for activation of the NFκB pathway. *Cell. Signal.* 23, 161–170. doi: 10.1016/j.cellsig.2010.08.016

Fischer, R., Maier, O., Siegemund, M., Wajant, H., Scheurich, P., and Pfizenmaier, K. (2011b). A TNF receptor 2 selective agonist rescues human neurons from oxidative stress-induced cell death. *PLoS One* 6:e27621. doi: 10.1371/journal.pone.0027621

Fischer, R., Marsal, J., Guttà, C., Eisler, S. A., Peters, N., Bethea, J. R., et al. (2017). Novel strategies to mimic transmembrane tumor necrosis factor-dependent activation of tumor necrosis factor receptor 2. *Sci. Rep.* 7:6607. doi: 10.1038/s41598-017-06993-4

Fischer, R., Padutsch, T., Bracchi-Ricard, V., Murphy, K. L., Martinez, G. F., Delguercio, N., et al. (2019a). Exogenous activation of tumor necrosis factor receptor 2 promotes recovery from sensory and motor disease in a model of multiple sclerosis. *Brain Behav. Immun.* 81, 247–259. doi: 10.1016/j.bbi.2019.06.021

Fischer, R., Proske, M., Duffey, M., Stangl, H., Martinez, G. F., Peters, N., et al. (2018). Selective activation of tumor necrosis factor receptor II induces antiinflammatory responses and alleviates experimental arthritis. *Arthr. Rheumatol.* 70, 722–735. doi: 10.1002/art.40413

Fischer, R., Sendetski, M., del Rivero, T., Martinez, G. F., Bracchi-Ricard, V., Swanson, K. A., et al. (2019b). TNFR2 promotes Treg-mediated recovery from neuropathic pain across sexes. *Proc. Natl. Acad. Sci. U.S.A.* 116, 17045–17050. doi: 10.1073/pnas.1902091116

Fischer, R., Wajant, H., Kontermann, R., Pfizenmaier, K., and Maier, O. (2014). Astrocyte-specific activation of TNFR2 promotes oligodendrocyte maturation by secretion of leukemia inhibitory factor. *Glia* 62, 272–283. doi: 10.1002/glia.22605

Fontaine, V., Mohand-Said, S., Hanoteau, N., Fuchs, C., Pfizenmaier, K., and Eisel, U. (2002). Neurodegenerative and neuroprotective effects of tumor Necrosis factor (TNF) in retinal ischemia: opposite roles of TNF receptor 1 and TNF receptor 2. *J. Neurosci.* 22:RC216. doi: 10.1523/JNEUROSCI.22-07-j0001.2002

Fromm, P. D., Kling, J. C., Remke, A., Bogdan, C., and Körner, H. (2015). Fatal leishmaniasis in the absence of TNF despite a strong Th1 response. *Front. Microbiol.* 6:1520. doi: 10.3389/fmicb.2015.01520

Gao, H., Danzi, M. C., Choi, C. S., Taherian, M., Dalby-Hansen, C., Ellman, D. G., et al. (2017). Opposing functions of microglial and macrophagic TNFR2 in the pathogenesis of experimental autoimmune encephalomyelitis. *Cell Rep.* 18, 198–212. doi: 10.1016/j.celrep.2016.11.083

Geis, C., Graulich, M., Wissmann, A., Hagenacker, T., Thomale, J., Sommer, C., et al. (2010). Evoked pain behavior and spinal glia activation is dependent on tumor necrosis factor receptor 1 and 2 in a mouse model of bone cancer pain. *Neuroscience* 169, 463–474. doi: 10.1016/j.neuroscience.2010.04.022

Gerald, M. J., Bracchi-Ricard, V., Ricard, J., Fischer, R., Nandakumar, B., Blumenthal, G. H., et al. (2019). Continuous infusion of an agonist of the tumor necrosis factor receptor 2 in the spinal cord improves recovery after traumatic contusive injury. *CNS Neurosci. Ther.* 25, 884–893. doi: 10.1111/cns.13125

Gerken, M., Krippner-Heidenreich, A., Steinert, S., Willi, S., Neugart, F., Zappe, A., et al. (2010). Fluorescence correlation spectroscopy reveals topological segregation of the two tumor necrosis factor membrane receptors. *Biochim. Biophys. Acta* 1798, 1081–1089. doi: 10.1016/j.bbamem.2010.02.021

Goodall, L. J., Ovecka, M., Rycroft, D., Friel, S. L., Sanderson, A., Mistry, P., et al. (2015). Pharmacokinetic and pharmacodynamic characterisation of an anti-mouse TNF receptor 1 domain antibody formatted for in vivo half-life extension. *PLoS One* 10:e0137065. doi: 10.1371/journal.pone.0137065

Gray, P. W., Aggarwal, B. B., Benton, C. V., Bringman, T. S., Henzel, W. J., Jarrett, J. A., et al. (1984). Cloning and expression of cDNA for human lymphotoxin, a lymphokine with tumour necrosis activity. *Nature* 312, 721–724. doi: 10.1038/312721a0

Gregory, A. P., Dendrou, C. A., Attfield, K. E., Haghikia, A., Xifara, D. K., Butter, F., et al. (2012). TNF receptor 1 genetic risk mirrors outcome of anti-TNF therapy in multiple sclerosis. *Nature* 488, 508–511. doi: 10.1038/nature11307

Grell, M., Douni, E., Wajant, H., Löhden, M., Clauss, M., Maxeiner, B., et al. (1995). The transmembrane form of tumor necrosis factor is the prime activating ligand of the 80 kDa tumor necrosis factor receptor. *Cell* 83, 793–802. doi: 10.1016/0092-8674(95)90192-2

Grell, M., Wajant, H., Zimmermann, G., and Scheurich, P. (1998). The type 1 receptor (CD120a) is the high-affinity receptor for soluble tumor necrosis factor. *Proc. Natl. Acad. Sci. U.S.A.* 95, 570–575. doi: 10.1073/pnas.95.2.570

Grootjans, S., Vanden Berghe, T., and Vandenabeele, P. (2017). Initiation and execution mechanisms of necroptosis: an overview. *Cell Death Differ.* 24, 1184–1195. doi: 10.1038/cdd.2017.65

Guenzi, E., Stroissnig, H., Vierboom, M., and Herrmann, A. (2013). FRI0231 Atrosab, a humanized antibody directed against tnf-receptor 1, hold great promises for the treatment of rheumatoid arthritis. *Ann. Rheum. Dis.* 72, 2–451.

Hamid, T., Gu, Y., Ortines, R. V., Bhattacharya, C., Wang, G., Xuan, Y.-T., et al. (2009). Divergent tumor necrosis factor receptor-related remodeling responses in heart failure: role of nuclear factor-kappaB and inflammatory activation. *Circulation* 119, 1386–1397. doi: 10.1161/CIRCULATIONAHA.108.802918

Harms, A. S., Barnum, C. J., Ruhn, K. A., Varghese, S., Treviño, I., Blesch, A., et al. (2011). Delayed dominant-negative TNF gene therapy halts progressive loss of nigral dopaminergic neurons in a rat model of Parkinson's disease. *Mol. Ther.* 19, 46–52. doi: 10.1038/mt.2010.217

He, T., Liu, S., Chen, S., Ye, J., Wu, X., Bian, Z., et al. (2018). The p38 MAPK inhibitor SB203580 abrogates tumor necrosis factor-induced proliferative expansion of mouse CD4+Foxp3+ regulatory T cells. *Front. Immunol.* 9:1556. doi: 10.3389/fimmu.2018.01556

Hirose, T., Fukuma, Y., Takeshita, A., and Nishida, K. (2018). The role of lymphotoxin-α in rheumatoid arthritis. *Inflamm. Res.* 67, 495–501. doi: 10.1007/s00011-018-1139-6

Holland, M. C., Wurthner, J. U., Morley, P. J., Birchler, M. A., Lambert, J., Albayaty, M., et al. (2013). Autoantibodies to variable heavy (VH) chain Ig sequences in humans impact the safety and clinical pharmacology of a VH domain antibody antagonist of TNF-α receptor 1. *J. Clin. Immunol.* 33, 1192–1203. doi: 10.1007/s10875-013-9915-0

Horwitz, D. A., Pan, S., Ou, J.-N., Wang, J., Chen, M., Gray, J. D., et al. (2013). Therapeutic polyclonal human CD8+ CD25+ Fox3+ TNFR2+ PD-L1+ regulatory cells induced ex-vivo. *Clin. Immunol.* 149, 450–463. doi: 10.1016/j.clim.2013.08.007

Hotamisligil, G. S., Shargill, N. S., and Spiegelman, B. M. (1993). Adipose expression of tumor necrosis factor-alpha: direct role in obesity-linked insulin resistance. *Science* 259, 87–91. doi: 10.1126/science.7678183

Hui, J. M., Hodge, A., Farrell, G. C., Kench, J. G., Kriketos, A., and George, J. (2004). Beyond insulin resistance in NASH: TNF-alpha or adiponectin? *Hepatology* 40, 46–54. doi: 10.1002/hep.20280

Hutt, M., Fellermeier-Kopf, S., Seifert, O., Schmitt, L. C., Pfizenmaier, K., and Kontermann, R. E. (2018). Targeting scFv-Fc-scTRAIL fusion proteins to tumor cells. *Oncotarget* 9, 11322–11335. doi: 10.18632/oncotarget.24379

Inglis, J. J., Nissim, A., Lees, D. M., Hunt, S. P., Chernajovsky, Y., and Kidd, B. L. (2005). The differential contribution of tumour necrosis factor to thermal and mechanical hyperalgesia during chronic inflammation. *Arthritis Res. Ther.* 7, R807–R816. doi: 10.1186/ar1743

Inoue, M., Ando, D., Kamada, H., Taki, S., Niiyama, M., Mukai, Y., et al. (2017). A trimeric structural fusion of an antagonistic tumor necrosis factor-α mutant enhances molecular stability and enables facile modification. *J. Biol. Chem.* 292, 6438–6451. doi: 10.1074/jbc.M117.779686

Inoue, M., Kamada, H., Abe, Y., Higashisaka, K., Nagano, K., Mukai, Y., et al. (2015). Aminopeptidase P3, a new member of the TNF-TNFR2 signaling complex, induces phosphorylation of JNK1 and JNK2. *J. Cell Sci.* 128, 656–669. doi: 10.1242/jcs.149385

Jupp, O. J., McFarlane, S. M., Anderson, H. M., Littlejohn, A. F., Mohamed, A. A., MacKay, R. H., et al. (2001). Type II tumour necrosis factor-alpha receptor (TNFR2) activates c-Jun N-terminal kinase (JNK) but not mitogen-activated protein kinase (MAPK) or p38 MAPK pathways. *Biochem. J.* 359, 525–535. doi: 10.1042/0264-6021:3590525

Karamita, M., Barnum, C., Möbius, W., Tansey, M. G., Szymkowski, D. E., Lassmann, H., et al. (2017). Therapeutic inhibition of soluble brain TNF promotes remyelination by increasing myelin phagocytosis by microglia. *JCI Insight* 2:e87455. doi: 10.1172/jci.insight.87455

Kassiotis, G., and Kollias, G. (2001). Uncoupling the proinflammatory from the immunosuppressive properties of tumor necrosis factor (TNF) at the p55 TNF receptor level: implications for pathogenesis and therapy of autoimmune demyelination. *J. Exp. Med.* 193, 427–434. doi: 10.1084/jem.193.4.427

Kennedy, W. P., Simon, J. A., Offutt, C., Horn, P., Herman, A., Townsend, M. J., et al. (2014). Efficacy and safety of pateclizumab (anti-lymphotoxin-α) compared to adalimumab in rheumatoid arthritis: a head-to-head phase 2 randomized controlled study (The ALTαRA Study). *Arthritis Res. Ther.* 16:467. doi: 10.1186/s13075-014-0467-3

Khaksar, S., and Bigdeli, M. R. (2017a). Correlation between cannabidiol-induced reduction of infarct volume and inflammatory factors expression in ischemic stroke model. *Basic Clin. Neurosci.* 8, 139–146. doi: 10.18869/nirp.bcn.8.2.139

Khaksar, S., and Bigdeli, M. R. (2017b). Intra-cerebral cannabidiol infusion-induced neuroprotection is partly associated with the TNF-α/TNFR1/NF-κB pathway in transient focal cerebral ischaemia. *Brain Inj.* 31, 1932–1943. doi: 10.1080/02699052.2017.1358397

Kim, E. Y., Priatel, J. J., Teh, S.-J., and Teh, H.-S. (2006). TNF receptor type 2 (p75) functions as a costimulator for antigen-driven T cell responses in vivo. *J. Immunol.* 176, 1026–1035. doi: 10.4049/jimmunol.176.2.1026

Kitagaki, M., Isoda, K., Kamada, H., Kobayashi, T., Tsunoda, S., Tsutsumi, Y., et al. (2012). Novel TNF-α receptor 1 antagonist treatment attenuates arterial inflammation and intimal hyperplasia in mice. *J. Atheroscler Thromb.* 19, 36–46. doi: 10.5551/jat.9746

Kodama, S., Davis, M., and Faustman, D. L. (2005). The therapeutic potential of tumor necrosis factor for autoimmune disease: a mechanistically based hypothesis. *Cell. Mol. Life Sci.* 62, 1850–1862. doi: 10.1007/s00018-005-5022-6

Kodama, S., Kühtreiber, W., Fujimura, S., Dale, E. A., and Faustman, D. L. (2003). Islet regeneration during the reversal of autoimmune diabetes in NOD mice. *Science* 302, 1223–1227. doi: 10.1126/science.1088949

Kontermann, R. E. (2011). Strategies for extended serum half-life of protein therapeutics. *Curr. Opin. Biotechnol.* 22, 868–876. doi: 10.1016/j.copbio.2011.06.012

Kontermann, R. E., Münkel, S., Neumeyer, J., Müller, D., Branschädel, M., Scheurich, P., et al. (2008). A humanized tumor necrosis factor receptor 1 (TNFR1)-specific antagonistic antibody for selective inhibition of tumor necrosis factor (TNF) action. *J. Immunother.* 31, 225–234. doi: 10.1097/CJI.0b013e31816a88f9

Kontermann, R. E., Scheurich, P., and Pfizenmaier, K. (2009). Antagonists of TNF action: clinical experience and new developments. *Expert Opin. Drug Discov.* 4, 279–292. doi: 10.1517/17460440902785167

Kriegler, M., Perez, C., DeFay, K., Albert, I., and Lu, S. D. (1988). A novel form of TNF/cachectin is a cell surface cytotoxic transmembrane protein: ramifications for the complex physiology of TNF. *Cell* 53, 45–53. doi: 10.1016/0092-8674(88)90486-2

Krippner-Heidenreich, A., Grunwald, I., Zimmermann, G., Kühnle, M., Gerspach, J., Sterns, T., et al. (2008). Single-chain TNF, a TNF derivative with enhanced stability and antitumoral activity. *J. Immunol.* 180, 8176–8183. doi: 10.4049/jimmunol.180.12.8176

Krippner-Heidenreich, A., Tübing, F., Bryde, S., Willi, S., Zimmermann, G., and Scheurich, P. (2002). Control of receptor-induced signaling complex formation by the kinetics of ligand/receptor interaction. *J. Biol. Chem.* 277, 44155–44163. doi: 10.1074/jbc.M207399200

Lamontain, V., Schmid, T., Weber-Steffens, D., Zeller, D., Jenei-Lanzl, Z., Wajant, H., et al. (2019). Stimulation of TNF receptor type 2 expands regulatory T cells and ameliorates established collagen-induced arthritis in mice. *Cell. Mol. Immunol.* 16, 65–74. doi: 10.1038/cmi.2017.138

Lawlor, M. A., and Alessi, D. R. (2001). PKB/Akt: a key mediator of cell proliferation, survival and insulin responses? *J. Cell Sci.* 114, 2903–2910.

Lenercept Study Group (1999). TNF neutralization in MS: results of a randomized, placebo-controlled multicenter study. The lenercept multiple sclerosis study group and the University of British Columbia MS/MRI analysis group. *Neurology* 53, 457–465.

Lis, K., Grygorowicz, T., Cudna, A., Szymkowski, D. E., and Bałkowiec-Iskra, E. (2017). Inhibition of TNF reduces mechanical orofacial hyperalgesia induced by complete Freund's adjuvant by a TRPV1-dependent mechanism in mice. *Pharmacol. Rep.* 69, 1380–1385. doi: 10.1016/j.pharep.2017.05.013

Lo, C. H., Schaaf, T. M., Grant, B. D., Lim, C. K.-W., Bawaskar, P., Aldrich, C. C., et al. (2019). Noncompetitive inhibitors of TNFR1 probe conformational activation states. *Sci. Signal.* 12:eaav5637. doi: 10.1126/scisignal.aav5637

Lo, C. H., Vunnam, N., Lewis, A. K., Chiu, T.-L., Brummel, B. E., Schaaf, T. M., et al. (2017). An innovative high-throughput screening approach for discovery of small molecules that inhibit TNF receptors. *SLAS Discov.* 22, 950–961. doi: 10.1177/2472555217706478

Loetscher, H., Stueber, D., Banner, D., Mackay, F., and Lesslauer, W. (1993). Human tumor necrosis factor alpha (TNF alpha) mutants with exclusive specificity for the 55-kDa or 75-kDa TNF receptors. *J. Biol. Chem.* 268, 26350–26357.

MacPherson, K. P., Sompol, P., Kannarkat, G. T., Chang, J., Sniffen, L., Wildner, M. E., et al. (2017). Peripheral administration of the soluble TNF inhibitor XPro1595 modifies brain immune cell profiles, decreases beta-amyloid plaque load, and rescues impaired long-term potentiation in 5xFAD mice. *Neurobiol. Dis.* 102, 81–95. doi: 10.1016/j.nbd.2017.02.010

Madsen, P. M., Desu, H. L., Pablo de Rivero Vaccari, J., Florimon, Y., Ellman, D. G., Keane, R. W., et al. (2019). Oligodendrocytes modulate the immune-inflammatory response in EAE via TNFR2 signaling. *Brain Behav. Immun.* 84, 132–146. doi: 10.1016/j.bbi.2019.11.017

Madsen, P. M., Motti, D., Karmally, S., Szymkowski, D. E., Lambertsen, K. L., Bethea, J. R., et al. (2016). Oligodendroglial TNFR2 mediates membrane TNF-dependent repair in experimental autoimmune encephalomyelitis by promoting oligodendrocyte differentiation and remyelination. *J. Neurosci.* 36, 5128–5143. doi: 10.1523/JNEUROSCI.0211-16.2016

Maier, O., Fischer, R., Agresti, C., and Pfizenmaier, K. (2013). TNF receptor 2 protects oligodendrocyte progenitor cells against oxidative stress. *Biochem. Biophys. Res. Commun.* 440, 336–341. doi: 10.1016/j.bbrc.2013.09.083

Mann, D. L. (2002). Inflammatory mediators and the failing heart: past, present, and the foreseeable future. *Circ. Res.* 91, 988–998. doi: 10.1161/01.res.0000043825.01705.1b

Marchetti, L., Klein, M., Schlett, K., Pfizenmaier, K., and Eisel, U. L. M. (2004). Tumor necrosis factor (TNF)-mediated neuroprotection against glutamate-induced excitotoxicity is enhanced by N-methyl-D-aspartate receptor activation. Essential role of a TNF receptor 2-mediated phosphatidylinositol 3-kinase-dependent NF-kappa B pathway. *J. Biol. Chem.* 279, 32869–32881. doi: 10.1074/jbc.M311766200

McAlpine, F. E., Lee, J.-K., Harms, A. S., Ruhn, K. A., Blurton-Jones, M., Hong, J., et al. (2009). Inhibition of soluble TNF signaling in a mouse model of Alzheimer's disease prevents pre-plaque amyloid-associated neuropathology. *Neurobiol. Dis.* 34, 163–177. doi: 10.1016/j.nbd.2009.01.006

McCoy, M. K., Martinez, T. N., Ruhn, K. A., Szymkowski, D. E., Smith, C. G., Botterman, B. R., et al. (2006). Blocking soluble tumor necrosis factor signaling with dominant-negative tumor necrosis factor inhibitor attenuates loss of dopaminergic neurons in models of Parkinson's disease. *J. Neurosci.* 26, 9365–9375. doi: 10.1523/JNEUROSCI.1504-06.2006

McCoy, M. K., Ruhn, K. A., Martinez, T. N., McAlpine, F. E., Blesch, A., and Tansey, M. G. (2008). Intranigral lentiviral delivery of dominant-negative TNF attenuates neurodegeneration and behavioral deficits in hemiparkinsonian rats. *Mol. Ther.* 16, 1572–1579. doi: 10.1038/mt.2008.146

Medler, J., Nelke, J., Weisenberger, D., Steinfatt, T., Rothaug, M., Berr, S., et al. (2019). TNFRSF receptor-specific antibody fusion proteins with targeting controlled FcγR-independent agonistic activity. *Cell Death Dis.* 10, 224. doi: 10.1038/s41419-019-1456-x

Mehta, A. K., Gracias, D. T., and Croft, M. (2018). TNF activity and T cells. *Cytokine* 101, 14–18. doi: 10.1016/j.cyto.2016.08.003

Micheau, O., and Tschopp, J. (2003). Induction of TNF receptor I-mediated apoptosis via two sequential signaling complexes. *Cell* 114, 181–190. doi: 10.1016/s0092-8674(03)00521-x

Miller, P. G., Bonn, M. B., and McKarns, S. C. (2015). Transmembrane TNF-TNFR2 Impairs Th17 Differentiation by Promoting Il2 Expression. *J. Immunol.* 195, 2633–2647. doi: 10.4049/jimmunol.1500286

Mironets, E., Fischer, R., Bracchi-Ricard, V., Saltos, T. M., Truglio, T. S., O'Reilly, M. L., et al. (2020). Attenuating neurogenic sympathetic hyperreflexia robustly improves antibacterial immunity after chronic spinal cord injury. *J. Neurosci.* 40, 478–492. doi: 10.1523/JNEUROSCI.2417-19.2019

Mironets, E., Osei-Owusu, P., Bracchi-Ricard, V., Fischer, R., Owens, E. A., Ricard, J., et al. (2018). Soluble TNFα signaling within the spinal cord contributes to the development of autonomic dysreflexia and ensuing vascular and immune dysfunction after spinal cord injury. *J. Neurosci.* 38, 4146–4162. doi: 10.1523/JNEUROSCI.2376-17.2018

Monaco, C., Nanchahal, J., Taylor, P., and Feldmann, M. (2015). Anti-TNF therapy: past, present and future. *Int. Immunol.* 27, 55–62. doi: 10.1093/intimm/dxu102

Monden, Y., Kubota, T., Inoue, T., Tsutsumi, T., Kawano, S., Ide, T., et al. (2007). Tumor necrosis factor-alpha is toxic via receptor 1 and protective via receptor 2 in a murine model of myocardial infarction. *Am. J. Physiol. Heart Circ. Physiol.* 293, H743–H753. doi: 10.1152/ajpheart.00166.2007

Mori, L., Iselin, S., De Libero, G., and Lesslauer, W. (1996). Attenuation of collagen-induced arthritis in 55-kDa TNF receptor type 1 (TNFR1)-IgG1-treated and TNFR1-deficient mice. *J. Immunol.* 157, 3178–3182.

Mukai, Y., Shibata, H., Nakamura, T., Yoshioka, Y., Abe, Y., Nomura, T., et al. (2009). Structure-function relationship of tumor necrosis factor (TNF) and its receptor interaction based on 3D structural analysis of a fully active TNFR1-selective TNF mutant. *J. Mol. Biol.* 385, 1221–1229. doi: 10.1016/j.jmb.2008.11.053

Murphy, K. L., Bethea, J. R., and Fischer, R. (2017). "Neuropathic pain in multiple sclerosis–current therapeutic intervention and future treatment perspectives," in *Multiple Sclerosis: Perspectives in Treatment and Pathogenesis*, eds I. S. Zagon, and P. J. McLaughlin, (Brisbane, QLD: Codon Publications). doi: 10.15586/codon.multiplesclerosis.2017.ch4

Musicki, K., Briscoe, H., Tran, S., Britton, W. J., and Saunders, B. M. (2006). Differential requirements for soluble and transmembrane tumor necrosis factor in the immunological control of primary and secondary Listeria monocytogenes infection. *Infect. Immun.* 74, 3180–3189. doi: 10.1128/IAI.02004-05

Nashleanas, M., Kanaly, S., and Scott, P. (1998). Control of Leishmania major infection in mice lacking TNF receptors. *J. Immunol.* 160, 5506–5513.

Natoli, G., Costanzo, A., Ianni, A., Templeton, D. J., Woodgett, J. R., Balsano, C., et al. (1997). Activation of SAPK/JNK by TNF receptor 1 through a noncytotoxic TRAF2-dependent pathway. *Science* 275, 200–203. doi: 10.1126/science.275.5297.200

Nomura, T., Abe, Y., Kamada, H., Shibata, H., Kayamuro, H., Inoue, M., et al. (2011). Therapeutic effect of PEGylated TNFR1-selective antagonistic mutant TNF in experimental autoimmune encephalomyelitis mice. *J. Control Release* 149, 8–14. doi: 10.1016/j.jconrel.2009.12.015

Notley, C. A., McCann, F. E., Inglis, J. J., and Williams, R. O. (2010). ANTI-CD3 therapy expands the numbers of CD4+ and CD8+ Treg cells and induces sustained amelioration of collagen-induced arthritis. *Arthritis Rheum.* 62, 171–178. doi: 10.1002/art.25058

Novrup, H. G., Bracchi-Ricard, V., Ellman, D. G., Ricard, J., Jain, A., Runko, E., et al. (2014). Central but not systemic administration of XPro1595 is therapeutic following moderate spinal cord injury in mice. *J. Neuroinflammation* 11:159. doi: 10.1186/s12974-014-0159-6

Okubo, Y., Mera, T., Wang, L., and Faustman, D. L. (2013). Homogeneous expansion of human T-regulatory cells via tumor necrosis factor receptor 2. *Sci. Rep.* 3:3153. doi: 10.1038/srep03153

Okubo, Y., Torrey, H., Butterworth, J., Zheng, H., and Faustman, D. L. (2016). Treg activation defect in type 1 diabetes: correction with TNFR2 agonism. *Clin. Transl. Immunol.* 5:e56. doi: 10.1038/cti.2015.43

Olleros, M. L., Vesin, D., Fotio, A. L., Santiago-Raber, M.-L., Tauzin, S., Szymkowski, D. E., et al. (2010). Soluble TNF, but not membrane TNF, is critical in LPS-induced hepatitis. *J. Hepatol.* 53, 1059–1068. doi: 10.1016/j.jhep.2010.05.029

Olleros, M. L., Vesin, D., Lambou, A. F., Janssens, J.-P., Ryffel, B., Rose, S., et al. (2009). Dominant-negative tumor necrosis factor protects from *Mycobacterium bovis* Bacillus Calmette Guérin (BCG) and endotoxin-induced liver injury without compromising host immunity to BCG and Mycobacterium tuberculosis. *J. Infect Dis.* 199, 1053–1063. doi: 10.1086/597204

Ortí-Casañ, N., Wu, Y., Naudé, P. J. W., Deyn, P. P., de Zuhorn, I. S., and Eisel, U. L. M. (2019). Targeting TNFR2 as a novel therapeutic strategy for Alzheimer's disease. *Front. Neurosci.* 13:49. doi: 10.3389/fnins.2019.00049

Padutsch, T., Sendetski, M., Huber, C., Peters, N., Pfizenmaier, K., Bethea, J. R., et al. (2019). Superior Treg-expanding properties of a novel dual-acting cytokine fusion protein. *Front. Pharmacol.* 10:1490. doi: 10.3389/fphar.2019.01490

Patel, J. R., Williams, J. L., Muccigrosso, M. M., Liu, L., Sun, T., Rubin, J. B., et al. (2012). Astrocyte TNFR2 is required for CXCL12-mediated regulation of oligodendrocyte progenitor proliferation and differentiation within the adult CNS. *Acta Neuropathol.* 124, 847–860. doi: 10.1007/s00401-012-1034-0

Pegoretti, V., Baron, W., Laman, J. D., and Eisel, U. L. M. (2018). Selective modulation of TNF-TNFRs signaling: insights for multiple sclerosis treatment. *Front. Immunol.* 9:925. doi: 10.3389/fimmu.2018.00925

Pfeffer, K., Matsuyama, T., Kündig, T. M., Wakeham, A., Kishihara, K., Shahinian, A., et al. (1993). Mice deficient for the 55 kd tumor necrosis factor receptor are resistant to endotoxic shock, yet succumb to L. monocytogenes infection. *Cell* 73, 457–467. doi: 10.1016/0092-8674(93)90134-c

Probert, L., Akassoglou, K., Pasparakis, M., Kontogeorgos, G., and Kollias, G. (1995). Spontaneous inflammatory demyelinating disease in transgenic mice showing central nervous system-specific expression of tumor necrosis factor alpha. *Proc. Natl. Acad. Sci. U.S.A.* 92, 11294–11298. doi: 10.1073/pnas.92.24.11294

Proudfoot, A., Bayliffe, A., O'Kane, C. M., Wright, T., Serone, A., Bareille, P. J., et al. (2018). Novel anti-tumour necrosis factor receptor-1 (TNFR1) domain antibody prevents pulmonary inflammation in experimental acute lung injury. *Thorax* 73, 723–730. doi: 10.1136/thoraxjnl-2017-210305

Ramani, R., Mathier, M., Wang, P., Gibson, G., Tögel, S., Dawson, J., et al. (2004). Inhibition of tumor necrosis factor receptor-1-mediated pathways has beneficial effects in a murine model of postischemic remodeling. *Am. J. Physiol. Heart Circ. Physiol.* 287, H1369–H1377. doi: 10.1152/ajpheart.00641.2003

Ranzinger, J., Krippner-Heidenreich, A., Haraszti, T., Bock, E., Tepperink, J., Spatz, J. P., et al. (2009). Nanoscale arrangement of apoptotic ligands reveals a demand for a minimal lateral distance for efficient death receptor activation. *Nano Lett.* 9, 4240–4245. doi: 10.1021/nl902429b

Rauert, H., Wicovsky, A., Müller, N., Siegmund, D., Spindler, V., Waschke, J., et al. (2010). Membrane tumor necrosis factor (TNF) induces p100 processing via TNF receptor-2 (TNFR2). *J. Biol. Chem.* 285, 7394–7404. doi: 10.1074/jbc.M109.037341

Richter, C., Messerschmidt, S., Holeiter, G., Tepperink, J., Osswald, S., Zappe, A., et al. (2012). The tumor necrosis factor receptor stalk regions define responsiveness to soluble versus membrane-bound ligand. *Mol. Cell. Biol.* 32, 2515–2529. doi: 10.1128/MCB.06458-11

Richter, F., Liebig, T., Guenzi, E., Herrmann, A., Scheurich, P., Pfizenmaier, K., et al. (2013). Antagonistic TNF receptor one-specific antibody (ATROSAB): receptor binding and in vitro bioactivity. *PLoS One* 8:e72156. doi: 10.1371/journal.pone.0072156

Richter, F., Seifert, O., Herrmann, A., Pfizenmaier, K., and Kontermann, R. E. (2019a). Improved monovalent TNF receptor 1-selective inhibitor with novel heterodimerizing Fc. *MAbs* 11, 653–665. doi: 10.1080/19420862.2019.1596512

Richter, F., Zettlitz, K. A., Seifert, O., Herrmann, A., Scheurich, P., Pfizenmaier, K., et al. (2019b). Monovalent TNF receptor 1-selective antibody with improved affinity and neutralizing activity. *MAbs* 11, 166–177. doi: 10.1080/19420862.2018.1524664

Rogers, R. C., and Hermann, G. E. (2012). Tumor necrosis factor activation of vagal afferent terminal calcium is blocked by cannabinoids. *J. Neurosci.* 32, 5237–5241. doi: 10.1523/JNEUROSCI.6220-11.2012

Rothe, J., Lesslauer, W., Lötscher, H., Lang, Y., Koebel, P., Köntgen, F., et al. (1993). Mice lacking the tumour necrosis factor receptor 1 are resistant to TNF-mediated toxicity but highly susceptible to infection by Listeria monocytogenes. *Nature* 364, 798–802. doi: 10.1038/364798a0

Rothe, M., Pan, M. G., Henzel, W. J., Ayres, T. M., and Goeddel, D. V. (1995a). The TNFR2-TRAF signaling complex contains two novel proteins related to baculoviral inhibitor of apoptosis proteins. *Cell* 83, 1243–1252. doi: 10.1016/0092-8674(95)90149-3

Rothe, M., Sarma, V., Dixit, V. M., and Goeddel, D. V. (1995b). TRAF2-mediated activation of NF-kappa B by TNF receptor 2 and CD40. *Science* 269, 1424–1427. doi: 10.1126/science.7544915

Rothe, M., Wong, S. C., Henzel, W. J., and Goeddel, D. V. (1994). A novel family of putative signal transducers associated with the cytoplasmic domain of the 75 kDa tumor necrosis factor receptor. *Cell* 78, 681–692. doi: 10.1016/0092-8674(94)90532-0

Ruddle, N. H. (2014). Lymphotoxin and TNF: how it all began-a tribute to the travelers. *Cytokine Growth Factor Rev.* 25, 83–89. doi: 10.1016/j.cytogfr.2014.02.001

Saddala, M. S., and Huang, H. (2019). Identification of novel inhibitors for TNFα, TNFR1 and TNFα-TNFR1 complex using pharmacophore-based approaches. *J. Transl. Med.* 17, 215. doi: 10.1186/s12967-019-1965-5

Sarbassov, D. D., Guertin, D. A., Ali, S. M., and Sabatini, D. M. (2005). Phosphorylation and regulation of Akt/PKB by the rictor-mTOR complex. *Science* 307, 1098–1101. doi: 10.1126/science.1106148

Schliemann, M., Bullinger, E., Borchers, S., Allgöwer, F., Findeisen, R., and Scheurich, P. (2011). Heterogeneity reduces sensitivity of cell death for TNF-stimuli. *BMC Syst. Biol.* 5:204. doi: 10.1186/1752-0509-5-204

Schmid, T., Falter, L., Weber, S., Müller, N., Molitor, K., Zeller, D., et al. (2017). Chronic inflammation increases the sensitivity of mouse Treg for TNFR2 costimulation. *Front. Immunol.* 8:1471. doi: 10.3389/fimmu.2017.01471

Schmukle, A. C., and Walczak, H. (2012). No one can whistle a symphony alone - how different ubiquitin linkages cooperate to orchestrate NF-κB activity. *J. Cell. Sci.* 125, 549–559. doi: 10.1242/jcs.091793

Schneider-Brachert, W., Tchikov, V., Neumeyer, J., Jakob, M., Winoto-Morbach, S., Held-Feindt, J., et al. (2004). Compartmentalization of TNF receptor 1 signaling: internalized TNF receptosomes as death signaling vesicles. *Immunity* 21, 415–428. doi: 10.1016/j.immuni.2004.08.017

Scholz, J., and Woolf, C. J. (2007). The neuropathic pain triad: neurons, immune cells and glia. *Nat. Neurosci.* 10, 1361–1368. doi: 10.1038/nn1992

Selmaj, K., Papierz, W., Glabiński, A., and Kohno, T. (1995). Prevention of chronic relapsing experimental autoimmune encephalomyelitis by soluble tumor necrosis factor receptor I. *J. Neuroimmunol.* 56, 135–141. doi: 10.1016/0165-5728(94)00139-f

Selmaj, K., Raine, C. S., and Cross, A. H. (1991). Anti-tumor necrosis factor therapy abrogates autoimmune demyelination. *Ann. Neurol.* 30, 694–700. doi: 10.1002/ana.410300510

Sheng, Y., Li, F., and Qin, Z. (2018). TNF receptor 2 makes tumor necrosis factor a friend of tumors. *Front. Immunol.* 9:1170. doi: 10.3389/fimmu.2018.01170

Shibata, H., Yoshioka, Y., Abe, Y., Ohkawa, A., Nomura, T., Minowa, K., et al. (2009). The treatment of established murine collagen-induced arthritis with a TNFR1-selective antagonistic mutant TNF. *Biomaterials* 30, 6638–6647. doi: 10.1016/j.biomaterials.2009.08.041

Shibata, H., Yoshioka, Y., Ohkawa, A., Abe, Y., Nomura, T., Mukai, Y., et al. (2008a). The therapeutic effect of TNFR1-selective antagonistic mutant TNF-alpha in murine hepatitis models. *Cytokine* 44, 229–233. doi: 10.1016/j.cyto.2008.07.003

Shibata, H., Yoshioka, Y., Ohkawa, A., Minowa, K., Mukai, Y., Abe, Y., et al. (2008b). Creation and X-ray structure analysis of the tumor necrosis factor receptor-1-selective mutant of a tumor necrosis factor-alpha antagonist. *J. Biol. Chem.* 283, 998–1007. doi: 10.1074/jbc.M707933200

Sicotte, N. L., and Voskuhl, R. R. (2001). Onset of multiple sclerosis associated with anti-TNF therapy. *Neurology* 57, 1885–1888. doi: 10.1212/wnl.57.10.1885

Siegemund, M., Schneider, F., Hutt, M., Seifert, O., Müller, I., Kulms, D., et al. (2018). IgG-single-chain TRAIL fusion proteins for tumour therapy. *Sci. Rep.* 8:7808. doi: 10.1038/s41598-018-24450-8

Sommer, C., Schmidt, C., and George, A. (1998). Hyperalgesia in experimental neuropathy is dependent on the TNF receptor 1. *Exp. Neurol.* 151, 138–142. doi: 10.1006/exnr.1998.6797

Sorkin, L. S., and Doom, C. M. (2000). Epineurial application of TNF elicits an acute mechanical hyperalgesia in the awake rat. *J. Peripher. Nerv. Syst.* 5, 96–100. doi: 10.1046/j.1529-8027.2000.00012.x

Sousa Rodrigues, M. E., de Houser, M. C., Walker, D. I., Jones, D. P., Chang, J., Barnum, C. J., et al. (2019). Targeting soluble tumor necrosis factor as a potential intervention to lower risk for late-onset Alzheimer's disease associated with obesity, metabolic syndrome, and type 2 diabetes. *Alzheimers Res. Ther.* 12:1. doi: 10.1186/s13195-019-0546-4

Steed, P. M., Tansey, M. G., Zalevsky, J., Zhukovsky, E. A., Desjarlais, J. R., Szymkowski, D. E., et al. (2003). Inactivation of TNF signaling by rationally designed dominant-negative TNF variants. *Science* 301, 1895–1898. doi: 10.1126/science.1081297

Steeland, S., Gorlé, N., Vandendriessche, C., Balusu, S., Brkic, M., van Cauwenberghe, C., et al. (2018). Counteracting the effects of TNF receptor-1 has therapeutic potential in Alzheimer's disease. *EMBO Mol. Med.* 10:e8300. doi: 10.15252/emmm.201708300

Steeland, S., Puimège, L., Vandenbroucke, R. E., van Hauwermeiren, F., Haustraete, J., Devoogdt, N., et al. (2015). Generation and characterization of small single domain antibodies inhibiting human tumor necrosis factor receptor 1. *J. Biol. Chem.* 290, 4022–4037. doi: 10.1074/jbc.M114.617787

Steeland, S., van Ryckeghem, S., van Imschoot, G., Rycke, R., de, Toussaint, W., Vanhoutte, L., et al. (2017). TNFR1 inhibition with a nanobody protects against EAE development in mice. *Sci. Rep.* 7:13646. doi: 10.1038/s41598-017-13984-y

Steinshamn, S., Bemelmans, M. H., van Tits, L. J., Bergh, K., Buurman, W. A., and Waage, A. (1996). TNF receptors in murine Candida albicans infection: evidence for an important role of TNF receptor p55 in antifungal defense. *J. Immunol.* 157, 2155–2159.

Sun, S.-C. (2017). The non-canonical NF-κB pathway in immunity and inflammation. *Nat. Rev. Immunol.* 17, 545–558. doi: 10.1038/nri.2017.52

Suvannavejh, G. C., Lee, H. O., Padilla, J., Dal Canto, M. C., Barrett, T. A., and Miller, S. D. (2000). Divergent roles for p55 and p75 tumor necrosis factor receptors in the pathogenesis of MOG(35-55)-induced experimental autoimmune encephalomyelitis. *Cell. Immunol.* 205, 24–33. doi: 10.1006/cimm.2000.1706

Tam, E. M., Fulton, R. B., Sampson, J. F., Muda, M., Camblin, A., Richards, J., et al. (2019). Antibody-mediated targeting of TNFR2 activates CD8+ T cells in mice and promotes antitumor immunity. *Sci. Transl. Med.* 11:eaax0720. doi: 10.1126/scitranslmed.aax0720

Tan, R., and Cao, L. (2018). Cannabinoid WIN-55,212-2 mesylate inhibits tumor necrosis factor-α-induced expression of nitric oxide synthase in dorsal root ganglion neurons. *Int. J. Mol. Med.* 42, 919–925. doi: 10.3892/ijmm.2018.3687

Taoufik, E., Tseveleki, V., Chu, S. Y., Tselios, T., Karin, M., Lassmann, H., et al. (2011). Transmembrane tumour necrosis factor is neuroprotective and regulates experimental autoimmune encephalomyelitis via neuronal nuclear factor-kappaB. *Brain* 134, 2722–2735. doi: 10.1093/brain/awr203

Thoma, B., Grell, M., Pfizenmaier, K., and Scheurich, P. (1990). Identification of a 60-kD tumor necrosis factor (TNF) receptor as the major signal transducing component in TNF responses. *J. Exp. Med.* 172, 1019–1023. doi: 10.1084/jem.172.4.1019

Tomita, K., Tamiya, G., Ando, S., Ohsumi, K., Chiyo, T., Mizutani, A., et al. (2006). Tumour necrosis factor alpha signalling through activation of Kupffer cells plays an essential role in liver fibrosis of non-alcoholic steatohepatitis in mice. *Gut* 55, 415–424. doi: 10.1136/gut.2005.071118

Torres, D., Janot, L., Quesniaux, V. F. J., Grivennikov, S. I., Maillet, I., Sedgwick, J. D., et al. (2005). Membrane tumor necrosis factor confers partial protection to Listeria infection. *Am. J. Pathol.* 167, 1677–1687. doi: 10.1016/S0002-9440(10)61250-3

Torrey, H., Butterworth, J., Mera, T., Okubo, Y., Wang, L., Baum, D., et al. (2017). Targeting TNFR2 with antagonistic antibodies inhibits proliferation of ovarian cancer cells and tumor-associated Tregs. *Sci. Signal.* 10:eaaf8608. doi: 10.1126/scisignal.aaf8608

Torrey, H., Khodadoust, M., Tran, L., Baum, D., Defusco, A., Kim, Y. H., et al. (2019). Targeted killing of TNFR2-expressing tumor cells and Tregs by TNFR2 antagonistic antibodies in advanced Sézary syndrome. *Leukemia* 33, 1206–1218. doi: 10.1038/s41375-018-0292-9

Tracey, D., Klareskog, L., Sasso, E. H., Salfeld, J. G., and Tak, P. P. (2008). Tumor necrosis factor antagonist mechanisms of action: a comprehensive review. *Pharmacol. Ther.* 117, 244–279. doi: 10.1016/j.pharmthera.2007.10.001

Tsakiri, N., Papadopoulos, D., Denis, M. C., Mitsikostas, D.-D., and Kollias, G. (2012). TNFR2 on non-haematopoietic cells is required for Foxp3+ Treg-cell function and disease suppression in EAE. *Eur. J. Immunol.* 42, 403–412. doi: 10.1002/eji.201141659

Uysal, K. T., Wiesbrock, S. M., and Hotamisligil, G. S. (1998). Functional analysis of tumor necrosis factor (TNF) receptors in TNF-alpha-mediated insulin resistance in genetic obesity. *Endocrinology* 139, 4832–4838. doi: 10.1210/endo.139.12.6337

Uysal, K. T., Wiesbrock, S. M., Marino, M. W., and Hotamisligil, G. S. (1997). Protection from obesity-induced insulin resistance in mice lacking TNF-alpha function. *Nature* 389, 610–614. doi: 10.1038/39335

van der Most, R. G., Currie, A. J., Mahendran, S., Prosser, A., Darabi, A., Robinson, B. W. S., et al. (2009). Tumor eradication after cyclophosphamide depends on concurrent depletion of regulatory T cells: a role for cycling TNFR2-expressing effector-suppressor T cells in limiting effective chemotherapy. *Cancer Immunol. Immunother.* 58, 1219–1228. doi: 10.1007/s00262-008-0628-9

van Hauwermeiren, F., Vandenbroucke, R. E., Grine, L., Lodens, S., van Wonterghem, E., de Rycke, R., et al. (2015). TNFR1-induced lethal inflammation is mediated by goblet and Paneth cell dysfunction. *Mucosal. Immunol.* 8, 828–840. doi: 10.1038/mi.2014.112

van Oosten, B. W., Barkhof, F., Truyen, L., Boringa, J. B., Bertelsmann, F. W., von Blomberg, B. M., et al. (1996). Increased MRI activity and immune activation in two multiple sclerosis patients treated with the monoclonal anti-tumor necrosis factor antibody cA2. *Neurology* 47, 1531–1534. doi: 10.1212/wnl.47.6.1531

Vanamee, ÉS., and Faustman, D. L. (2017). TNFR2: a novel target for cancer immunotherapy. *Trends Mol. Med.* 23, 1037–1046. doi: 10.1016/j.molmed.2017.09.007

Vanamee, ÉS., and Faustman, D. L. (2018). Structural principles of tumor necrosis factor superfamily signaling. *Sci. Signal.* 11:eaao4910. doi: 10.1126/scisignal.aao4910

Vanden Berghe, T., Linkermann, A., Jouan-Lanhouet, S., Walczak, H., and Vandenabeele, P. (2014). Regulated necrosis: the expanding network of non-apoptotic cell death pathways. *Nat. Rev. Mol. Cell. Biol.* 15, 135–147. doi: 10.1038/nrm3737

Vogel, C., Stallforth, S., and Sommer, C. (2006). Altered pain behavior and regeneration after nerve injury in TNF receptor deficient mice. *J. Peripher. Nerv. Syst.* 11, 294–303. doi: 10.1111/j.1529-8027.2006.00101.x

Wagner, R., and Myers, R. R. (1996). Endoneurial injection of TNF-alpha produces neuropathic pain behaviors. *Neuroreport* 7, 2897–2901. doi: 10.1097/00001756-199611250-00018

Wajant, H., Henkler, F., and Scheurich, P. (2001). The TNF-receptor-associated factor family: scaffold molecules for cytokine receptors, kinases and their regulators. *Cell. Signal.* 13, 389–400. doi: 10.1016/s0898-6568(01)00160-7

Wajant, H., Pfizenmaier, K., and Scheurich, P. (2003). Tumor necrosis factor signaling. *Cell Death Differ* 10, 45–65.

Wajant, H., and Scheurich, P. (2011). TNFR1-induced activation of the classical NF-κB pathway. *FEBS J.* 278, 862–876. doi: 10.1111/j.1742-4658.2011.08015.x

Wandrer, F., Liebig, S., Marhenke, S., Vogel, A., Manns, M. P., Teufel, A., et al. (2020). TNF-receptor-1 inhibition reduces liver steatosis, hepatocellular injury and fibrosis in NAFLD mice. *Cell Death Dis.* 11:212. doi: 10.1038/s41419-020-2411-6

Wang, J., Ferreira, R., Lu, W., Farrow, S., Downes, K., Jermutus, L., et al. (2018). TNFR2 ligation in human T regulatory cells enhances IL2-induced cell proliferation through the non-canonical NF-κB pathway. *Sci. Rep.* 8:12079. doi: 10.1038/s41598-018-30621-4

Wellen, K. E., and Hotamisligil, G. S. (2005). Inflammation, stress, and diabetes. *J. Clin. Invest.* 115, 1111–1119.

Williams, S. K., Fairless, R., Maier, O., Liermann, P. C., Pichi, K., Fischer, R., et al. (2018). Anti-TNFR1 targeting in humanized mice ameliorates disease in a model of multiple sclerosis. *Sci. Rep.* 8:13628. doi: 10.1038/s41598-018-31957-7

Williams, S. K., Maier, O., Fischer, R., Fairless, R., Hochmeister, S., Stojic, A., et al. (2014). Antibody-mediated inhibition of TNFR1 attenuates disease in a mouse model of multiple sclerosis. *PLoS One* 9:e90117. doi: 10.1371/journal.pone.0090117

Yang, L., Lindholm, K., Konishi, Y., Li, R., and Shen, Y. (2002). Target depletion of distinct tumor necrosis factor receptor subtypes reveals hippocampal neuron death and survival through different signal transduction pathways. *J. Neurosci.* 22, 3025–3032. doi: 10.1523/JNEUROSCI.22-08-03025.2002

Yang, S., Xie, C., Chen, Y., Wang, J., Chen, X., Lu, Z., et al. (2019). Differential roles of TNFα-TNFR1 and TNFα-TNFR2 in the differentiation and function of CD4+Foxp3+ induced Treg cells in vitro and in vivo periphery in autoimmune diseases. *Cell Death Dis.* 10:27. doi: 10.1038/s41419-018-1266-6

Ye, L.-L., Wei, X.-S., Zhang, M., Niu, Y.-R., and Zhou, Q. (2018). The significance of tumor necrosis factor receptor type II in CD8+ regulatory T cells and CD8+ effector T cells. *Front. Immunol.* 9:583. doi: 10.3389/fimmu.2018.00583

Yli-Karjanmaa, M., Clausen, B. H., Degn, M., Novrup, H. G., Ellman, D. G., Toft-Jensen, P., et al. (2019). Topical administration of a soluble TNF inhibitor reduces infarct volume after focal cerebral ischemia in mice. *Front. Neurosci.* 13:781. doi: 10.3389/fnins.2019.00781

Zalevsky, J., Secher, T., Ezhevsky, S. A., Janot, L., Steed, P. M., O'Brien, C., et al. (2007). Dominant-negative inhibitors of soluble TNF attenuate experimental arthritis without suppressing innate immunity to infection. *J. Immunol.* 179, 1872–1883. doi: 10.4049/jimmunol.179.3.1872

Zeng, X.-Y., Zhang, Q., Wang, J., Yu, J., Han, S.-P., and Wang, J.-Y. (2014). Distinct role of tumor necrosis factor receptor subtypes 1 and 2 in the red nucleus in the development of neuropathic pain. *Neurosci. Lett.* 569, 43–48. doi: 10.1016/j.neulet.2014.03.048

Zettlitz, K. A., Lorenz, V., Landauer, K., Münkel, S., Herrmann, A., Scheurich, P., et al. (2010). ATROSAB, a humanized antagonistic anti-tumor necrosis factor receptor one-specific antibody. *MAbs* 2, 639–647. doi: 10.4161/mabs.2.6.13583

Zhang, L., Berta, T., Xu, Z.-Z., Liu, T., Park, J. Y., and Ji, R.-R. (2011). TNF-α contributes to spinal cord synaptic plasticity and inflammatory pain: distinct role of TNF receptor subtypes 1 and 2. *Pain* 152, 419–427. doi: 10.1016/j.pain.2010.11.014

Zhang, X., Yin, N., Guo, A., Zhang, Q., Zhang, Y., Xu, Y., et al. (2017). NF-κB signaling and cell-fate decision induced by a fast-dissociating tumor necrosis factor mutant. *Biochem. Biophys. Res. Commun.* 489, 287–292. doi: 10.1016/j.bbrc.2017.05.149

Conflict of Interest: RK and KP are named inventors on patent applications covering TNFR1 specific antagonists. RF, RK, and KP are named inventors on patent applications covering the TNFR2 agonist technology.

frontiers in Cell and Developmental Biology

BRIEF RESEARCH REPORT
published: 14 October 2020
doi: 10.3389/fcell.2020.569684

The Diversity and Similarity of Transmembrane Trimerization of TNF Receptors

*Linlin Zhao, Qingshan Fu, Liqiang Pan, Alessandro Piai and James J. Chou**

Department of Biological Chemistry and Molecular Pharmacology, Harvard Medical School, Boston, MA, United States

Receptors in the tumor necrosis factor receptor superfamily (TNFRSF) regulate proliferation of immune cells or induce programmed cell death, and many of them are candidates for antibody-based immunotherapy. Previous studies on several death receptors in the TNFRSF including Fas, p75NTR, and DR5 showed that the transmembrane helix (TMH) of these receptors can specifically oligomerize and their oligomeric states have direct consequences on receptor activation, suggesting a much more active role of TMH in receptor signaling than previously appreciated. Here, we report the structure of the TMH of TNFR1, another well studied member of the TNFRSF, in neutral bicelles that mimic a lipid bilayer. We find that TNFR1 TMH forms a defined trimeric complex in bicelles, and no evidences of higher-order clustering of trimers have been detected. Unexpectedly, a conserved proline, which is critical for Fas TMH trimerization, does not appear to play an important role in TNFR1 TMH trimerization, which is instead mediated by a glycine near the middle of the TMH. Further, TNFR1 TMH trimer shows a larger hydrophobic core than that of Fas or DR5, with four layers of hydrophobic interaction along the threefold axis. Comparison of the TNFR1 TMH structure with that of Fas and DR5 reveals reassuring similarities that have functional implications but also significant structural diversity that warrants systematic investigation of TMH oligomerization property for other members of the TNFRSF.

Keywords: TNFR1, transmembrane domain, oligomerization, receptor activation, NMR

OPEN ACCESS

Edited by:
Marta Rizzi,
University of Freiburg Medical Center, Germany

Reviewed by:
Alastair D. G. Lawson,
UCB Pharma, United Kingdom
Pascal Schneider,
University of Lausanne, Switzerland

***Correspondence:**
James J. Chou
james_chou@hms.harvard.edu

Specialty section:
This article was submitted to Signaling, a section of the journal Frontiers in Cell and Developmental Biology

Received: *04 June 2020*
Accepted: *17 September 2020*
Published: *14 October 2020*

Citation:
Zhao L, Fu Q, Pan L, Piai A and Chou JJ (2020) The Diversity and Similarity of Transmembrane Trimerization of TNF Receptors. Front. Cell Dev. Biol. 8:569684. doi: 10.3389/fcell.2020.569684

INTRODUCTION

Receptors in the tumor necrosis factor receptor superfamily (TNFRSF) are Type I transmembrane proteins with an ectodomain (ECD) composed of multiple cysteine-rich domains (CRDs), a transmembrane helix (TMH), and an intracellular region that specifically interacts with signaling adaptors such as the Fas-associated death domain (FADD), the TNFR1-associated death domain (TRADD), or the TNFR-associated factors (TRAFs) (Baker and Reddy, 1998). In-depth understanding of the mechanism by which these receptors are activated is becoming increasingly important, as many of them are targets for antibody-based immunotherapy (Chaudhary et al., 1997; Sheridan et al., 1997; Hatzoglou et al., 2000; Rogers et al., 2001; Cooper et al., 2002; Ashkenazi, 2008; Croft et al., 2013). Early functional and structural studies on TNFR1 and Fas have suggested a general model of receptor activation in which the binding of the trimeric ligand causes the receptor ECD to trimerize, allowing subsequent clustering of the intracellular domains that recruits and activates downstream signaling proteins (Wajant, 2002; Vanamee and Faustman, 2018) (**Figure 1A**;

schematic of the receptor activation model without considering the TMH). This mechanism, however, did not include the role of the TMH but disease mutations in the TMH of Fas have been documented (Gronbaek et al., 1998; Lee et al., 2000). We have thus undertaken structural and functional investigation of the TMHs of members of the TNFRSF.

Previous studies have already suggested the function of TMH dimerization in the signaling of death receptors p75NTR (Goh et al., 2018) and DR5 (Valley et al., 2012). We found that Fas TMH in bicelles (q = 0.5) forms a defined trimer around a proline-containing signature sequence, and disruptive mutations for TMH trimerization severely attenuate Fas ligand (FasL)-induced signaling (Fu et al., 2016), suggesting that specific trimerization of TMH is essential for positioning the intracellular DDs to cluster and form the signaling-compatible complex. More recently, we made another unexpected finding that the TMH of DR5 not only trimerizes but also dimerizes via a GXXXG motif (MacKenzie et al., 1997; Trenker et al., 2015), resulting in the formation of dimer–trimer interaction network (Pan et al., 2019). This higher-order clustering of TMH is also critical for DR5 activation as single mutations that disrupt either trimerization or dimerization abolish ligand-induced receptor activation (Pan et al., 2019). More strikingly, proteolytic removal of the ECD of DR5, which deletes the extracellular constraints on the TMH, can activate DR5 to the same extent as its native ligand (TRAIL) (Pan et al., 2019). This result, combined with TMH clustering, suggests that the ECD adopts a preligand conformation that precludes the TMH oligomerization essential for downstream signaling and that the primary consequence of ligand binding is to overcome this inhibitory constraint (**Figure 1B**; schematic of receptor activation including the role of the TMH).

The mechanism in **Figure 1B** could have major therapeutic implication, as it suggests that a true agonistic antibody must be able to break the autoinhibitory, preligand association of receptor ECD so that the TMH can freely oligomerize, positioning the intracellular region for efficient formation of signaling capable clusters. Consistent with this mechanism, proteolytic removal of ECD can directly activate DR5 because DR5 TMH alone can form cluster of trimers via the GXXXG dimerization motif. TNFR2 and OX40 can also be activated by proteolytic removal of ECD (Pan et al., 2019), and interestingly, their TMHs also contain GXXXG. Conversely, if the TMH can form multimer of trimers, then disrupting the preligand ECD association by either soluble ligand or antibody should be sufficient to activate the receptor. Thus, a broader survey of the clustering properties of TMHs in the TNFRSF would evaluate the generality of

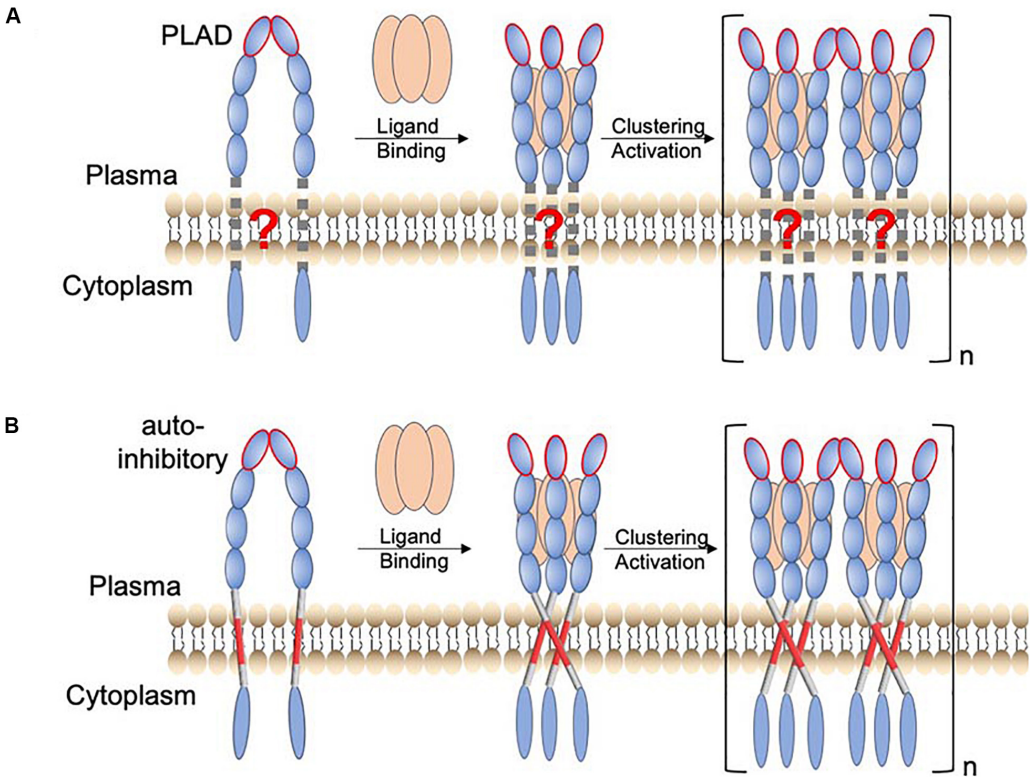

FIGURE 1 | Proposed function of TMH oligomerization in receptor activation of the TNFRSF. **(A)** Schematic of a TNFR activation mechanism in which the TMH only plays the passive role of membrane anchoring. The resting state involves preligand receptor association mediated mainly by the homodimeric interaction of the pre-ligand association domain (PLAD; ellipsoid with red edge). Binding of the trimeric ligand causes receptor trimerization, which in turn leads to higher-order receptor clustering and activation. **(B)** A revised receptor activation mechanism in which the TMH specifically oligomerizes, positioning the intracellular domains to form signaling-compatible complexes. In this case, the preligand receptor association prevents the specific TMH oligomerization that drives downstream signaling. The consequence of ligand binding is to overcome this inhibitory constraint.

the mechanism in **Figure 1B** while potentially discovering exceptions to the rule.

In this study, we examined the TMH of TNFR1 in bicelles that mimic a lipid bilayer. We used biochemical method to show that TNFR1 TMH forms homogeneous trimers in neutral lipid bicelles. We then used NMR to determine the structure of the TMH trimer. The TMH trimerization of TNFR1 shows features that are strongly distinct from that of Fas and DR5, implying the general unpredictability of TMH trimerization for receptors in the TNFRSF.

RESULTS

Amino Acid Sequences of TNFR1 TMH

Sequence alignment of TNFR1 TMH from different organisms shows a few interesting and useful features (**Figure 2A**). The N-terminal half (residues 212-222) is much more conserved than the C-terminal half (residues 223-234). Previous structural analysis of the TMHs of Fas and DR5 revealed proline and threonine/alanine-based motifs, respectively, that mediate TMH trimerization, and these motifs indeed can be found in many of the TNFRSF members, including TNFR1 (**Figure 2B**). The Fas TMH structure shows a proline-containing signature sequence (ΦPxΦ) that drives TMH trimerization, where Φ represents hydrophobic residues, P is proline, and x can be any apolar residues except for proline and glycine. TNFR1 TMH also contains a $LP^{215}LV$ that fits the ΦPxΦ description but is suspiciously close to the N-terminal end of the TMH. Hence, it is important to examine whether the proline plays a role in TNFR1 TMH oligomerization.

Protein Construct for Structural Analysis

The human TNFR1 TM fragment, residue 209–238, designated TNFR1 TMH, was selected for structural study. The residue C223 in the middle of the TM region was mutated to alanine to avoid artificial disulfide bond formation in solution during protein reconstitution. In addition, M233 is incompatible with the TrpLE expression system, which requires cleavage at the N-terminal methionine to separate the TrpLE and the TM fragment; it is also poorly conserved (**Supplementary Figure S1A**). Therefore, M233 was mutated to alanine as well. The C223, however, is quite conserved as shown in **Supplementary Figure S1A**, suggesting that it could participate in oligomerization. Hence, this was initially a risky mutation for facilitating sample preparation but, in retrospect, turned out to be harmless as residue 223 is lipid-facing (**Supplementary Figure S1B**) and on the opposite side of the helix–helix packing interface (described later in the article after structure determination).

Structure Determination in Bicelles That Mimic a Lipid Bilayer

TNFR1 TMH was expressed, purified, and reconstituted in neutral lipid bicelles as previously described (Fu et al., 2019). The purified protein fragment was reconstituted in DMPC-DH_6PC bicelles with q = 0.5, where q is the molar ratio of DMPC/DH_6PC. The final NMR sample contains ∼0.7 mM TNFR1, 50 mM DMPC, 100 mM DH_6PC, and 20 mM phosphate

FIGURE 2 | Amino acid conservation of TNFR1 TMH and TMH sequences of other members of the TNFRSF. **(A)** Alignment of TNFR1 TMH sequences from various organisms generated using the ClustalX2 program (Larkin et al., 2007). The most conserved positions are shaded in light red; the secondary higher identity positions are shaded in light orange. **(B)** Comparison of TMH sequences from the TNFRSF. Proposed trimerization and dimerization motifs are shown in red and blue, respectively. The "?" indicates unknown or highly speculative.

buffer (pH 6.8). At q = 0.5, the diameter of the planar bilayer region of the bicelles is ∼45 Å (Sanders and Schwonek, 1992; Glover et al., 2001). As in the case of Fas TMH, the bicelle-reconstituted TNFR1 TMH ran on SDS-PAGE as trimers (theoretical MW of TNFR1 TMH is ∼3.4 kDa; trimer is between 14 and 18 KDa), whereas unreconstituted peptide migrated as monomers on the gel (**Figure 3A**), providing the direct evidence that TNFR1 TMH spontaneously formed homotrimers in bicelles and that the trimeric complexes, once formed, can resist the strong denaturing environment of SDS-PAGE. The reconstituted TNFR1 TMH in bicelles generated TROSY-HSQC spectrum with good chemical shift dispersion and peak homogeneity (**Figure 3B** and **Supplementary Figure S2**) and in combination with the SDS-PAGE result indicates that TNFR1 TMH in bicelles is a homogeneous trimer suitable for full-scale structure determination.

The NMR structure of the TNFR1 TMH trimer was determined using a published protocol (Fu et al., 2019). Briefly, the protocol involves (1) construction of a preliminary monomer structure with local nuclear Overhauser effect (NOE) restraints and backbone dihedral angles derived from chemical shift values (using TALOS+ Shen et al., 2009), (2) obtaining a unique structural solution of the trimer with inter-chain NOE restraints derived from mixed isotopically labeled sample, and (3) refinement of the trimer structure by further assignment of self-consistent NOE restraints. Assignment of the H^N, N, C', and C^α resonances was achieved for residues 212–238 except for that of P215. For initially identifying inter-chain contacts, we used mixed samples in which half of the monomers are (^{15}N, ^{2}H)-labeled and the other half ^{13}C-labeled, and performed the J_{CH}-modulated NOE experiment (Fu et al., 2016, 2018) to detect exclusively NOEs between the ^{15}N-attached protons of one subunit and ^{13}C-attached protons of the neighboring subunits. This type of inter-chain NOE peaks is positive in J_{CH}-unmodulated spectrum and negative in the J_{CH}-modulated spectrum (see examples in **Figure 3C**). The 15 lowest energy structures of 100 calculated converged to root-mean-square deviation (RMSD) of ∼0.862 and ∼1.411 Å for backbone and all heavy atoms, respectively (**Supplementary Figure S3** and **Supplementary Table S1**).

Structure of the TMH Trimer of Human TNFR1

The trimeric structure of TNFR1 TMH shows an extensive hydrophobic core formed by bulky hydrophobic amino acids such as leucine and isoleucine. In this regard, it is similar to the Fas TMH structure. TNFR1 TMH trimer, however, shows a more extended hydrophobic core as there appears to be four layers of hydrophobic interaction along the 3-fold axis, including interactions between F219 and I218, between L222 and G221, between L225 and L224, and between F229 and L228 (**Figure 4A**). The core interactions involving I218 and L228 are likely weaker than those of central residues (e.g., G221, L225) because their associated inter-chain NOEs are much weaker (see **Figure 3C**). The hydrophobic core of the Fas TMH trimer comprises three layers of hydrophobic interaction: L181-L180, P185-I184, and V188-I187 (**Figure 4B**). It is also interesting to mention that the hydrophobic core the DR5 TMH trimer is formed mostly with small amino acids such as alanine and threonine (**Figure 4C**). Another major difference of DR5 TMH is the presence of the GXXXG motif (MacKenzie et al., 1997; Trenker et al., 2015) that allows DR5 TMH to form multimer of trimers.

Although the LP^{215}LV fits the ΦPxΦ motif that mediates Fas TMH trimerization, we did not detect any significant inter-chain NOEs around P215, and this is consistent with the fact that P215 is not involved in helix-helix packing in our structure. Instead, the structure suggests that G221 near the middle of the TMH plays the important role of allowing close van der Waals (VDW) contact with L222 of the neighboring chain, which appears to allow close packing of I218 and L225 above and below it, respectively, from the three chains (**Figure 4D**). In this regard, G221 seems to serve the role of P185 in the Fas TMH trimer in allowing VDW contact with I184 of the neighboring chain (**Figure 4D**).

Residues Important for TNFR1 TMH Trimerization

To examine the structure independently by mutagenesis, we generated three single mutations—P215Y, G221Y, and L225Y—and evaluated their effect on TMH trimerization (**Supplementary Figure S4**). Mutating P215 to tyrosine has essentially no effect on TMH trimerization in bicelles, further supporting the structural conclusion in **Figure 4D** that this relatively conserved proline does not play a role in helix–helix packing. As shown in **Figure 4A**, G221 is involved in close inter-helical packing with L222 and mutating G221 to the bulky tyrosine is expected to disrupt such packing. Indeed, the G221Y mutant showed a dominant dimer band and a very minor trimer band in SDS-PAGE, suggesting that this mutant cannot form specific trimers but could aggregate as non-specific dimers. Finally, the mutation L225Y almost completely abolished trimerization and migrated as monomers. This is consistent with L225 forming the most compact hydrophobic core along the TMH (**Figure 4A**). Overall, the oligomeric properties of the three mutants agree well with the NMR structure.

DISCUSSION

We have shown that the TMH of TNFR1 forms intimately assembled trimeric complex in a lipid bilayer environment. We initially thought that the LP^{215}LV sequence near the N-terminal end fits the description of the ΦPxΦ motif that mediates Fas TMH trimerization and thus could be the key element of TMH trimerization. But our structure and mutagenesis data indicate otherwise. Instead, G221 near the middle of the TMH appears to be important as it allows intimate contact with the adjacent chain at this position. In this context, the structural role of the glycine is similar to the proline of the ΦPxΦ motif, which is to permit VDW contact with the neighboring chain such that the hydrophobic core of the trimer can form. We also emphasize that although the hydrophobic packing along the threefold axis of the TNFR1 TMH trimer appears to be quite

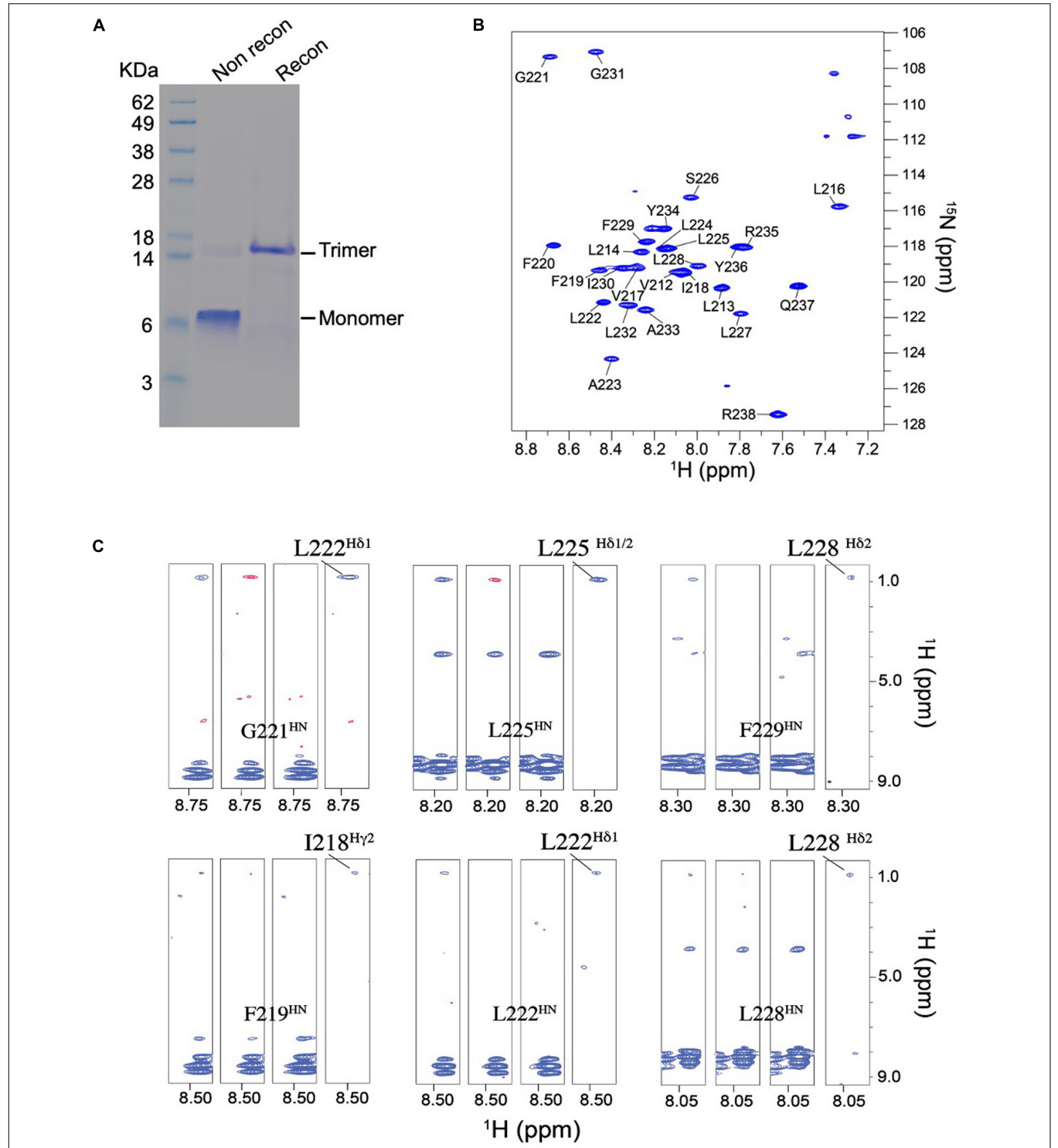

FIGURE 3 | Biochemical and NMR characterizations of the TNFR1 TMH. **(A)** Oligomerization of TNFR1 TMH in bicelles analyzed by standard SDS-PAGE. The gel lanes from left to right are: (1) MW markers; (2) purified TNFR1 TMH powder without reconstitution; (3) TNFR1 TMH reconstituted in DMPC- DH_6PC bicelles (q = 0.5). Both TNFR1 TMH samples were dissolved in gel loading buffer prior to SDS-PAGE. **(B)** The ^{1}H-^{15}N TROSY-HSQC spectrum of (^{15}N,^{13}C, ^{2}H)-labeled TNFR TMH reconstituted in same bicelles, recorded at ^{1}H frequency of 600 MHz at 303 K. **(C)** Detection of inter-chain NOEs. Residue-specific strips from the J_{CH}-modulated NOESY (NOE mixing time = 200 ms) recorded at 800 MHz and 303 K. The sample comprises 50% (^{15}N,^{2}H)-labeled and 50% (^{1}H,^{13}C)-labeled TNFR1 TMH. For each selected residue, four strips are shown from left to right: (1) positive inter-NOEs, blue; (2) negative inter-NOEs, red; (3) inter-NOEs are canceled [(1) + (2)]; (4) inter-NOEs are selected [(1) - (2)].

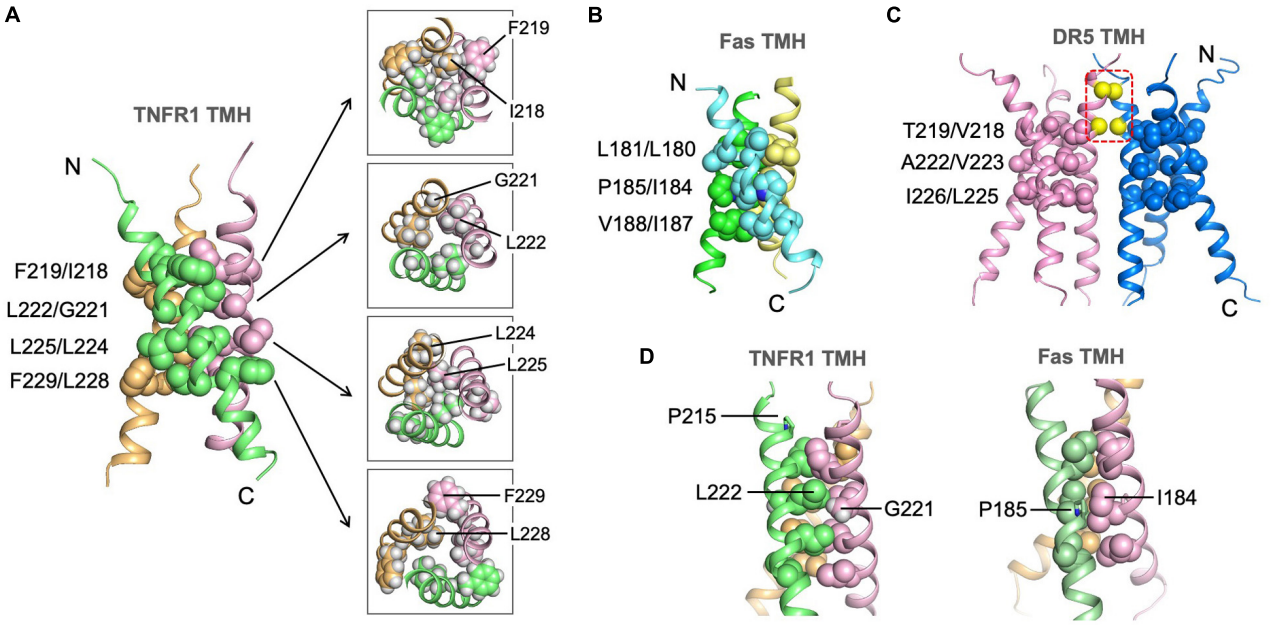

FIGURE 4 | Structure of the TNFR1 TMH trimer in bicelles and comparison with TMHs of Fas and DR5. **(A)** Ribbon representation (left) of the trimeric TNFR1 TMH with core residues highlighted (side-chain heavy atoms shown as spheres). The sidechain packing at four different levels along the threefold axis is further illustrated with sectional top views of the trimer (right) (sidechain heavy atoms and protons included). **(B)** The structure of the Fas TMH trimer with core residues at three layers along the TM helices. The sidechain heavy atoms are shown as spheres. **(C)** The dimer-of-trimer structure of DR5 TMH. The trimer packing is displayed as in **(A)** and **(B)**. In addition, the Cα atoms of G213 and G217 in the dimer interface are shown as yellow spheres. **(D)** Comparison of the glycine-mediated helical packing of TNFR1 TMH (left) and the proline-mediated helical packing of Fas TMH (right). Residues in the hydrophobic core are highlighted (side-chain heavy atoms shown as spheres).

extensive (comprising four layers of interactions), only the central interactions L222-G221 and L225-L224 show very intense inter-chain NOEs, suggesting the trimerization at the levels of I218 and L228 are weak and possibly more dynamic. In particular, L228 and generally the C-terminal region of the TMH after L225 are poorly conserved.

Like Fas, TNFR1 TMH can only form trimer but not higher order cluster of trimers as the dimeric interaction is lacking. But unlike Fas, TNFR1 can be activated by soluble TNF ligand, whereas Fas can only be efficiently activated by crosslinked Fas ligand (FasL) (Banner et al., 1993; Wajant et al., 2003); when the membrane-bound FasL is shedded to become soluble, it can no longer activate Fas (Schneider et al., 1998; Tanaka et al., 1998). In the context of ligand requirement, TNFR1 is more similar to DR5, which can be efficiently activated by soluble ligand (TRAIL). We have previously shown that DR5 can be activated by soluble TRAIL owing to its TMH's capacity to form higher-order dimer-trimer network to drive receptor clustering when unconstrained by the autoinhibitory, preligand association of the ECD (Pan et al., 2019). TNFR1 TMH, however, does not have the capacity to form cluster of trimers. We thus speculate that the previously suggested dimeric interactions of TNFR1 ECD in crystal structures (Naismith et al., 1996) could complement TMH trimerization by allowing clustering of trimeric receptors. It has been shown that the first CRD of TNFR1 (CDR1) is responsible for mediating receptor association on the cell surface in the absence of ligand and is thus known as the preligand association domain (PLAD) (Chan, 2000; Karathanasis et al., 2020; Weinelt et al., 2020). Further, the crystal structure of receptor–ligand complex (Banner et al., 1993) shows that the CDR1 of TNFR1 is not involved in ligand binding, although its presence appears to be important for the optimal binding of the ligand by CRD2 and CRD3 (Branschadel et al., 2010). These evidences suggest that the CRD1 of TNFR1 can provide the dimeric interaction for achieving higher-order receptor dimer–trimer network. Indeed, soluble TNFR1 CRD1 has been used to compete with CRD1-mediated receptor association, which inhibits receptor clustering and activation, as a new anti-arthritis treatment strategy (Deng, 2007). In addition to the ECD, the self-interaction of the intracellular domains could also contribute to receptor clustering and this type of interaction has been well characterized, for example, for death receptors such as DR3 and Fas (Scott et al., 2009; Wang et al., 2010; Yin et al., 2019).

Finally, the premise of the above analysis is that the trimerization of TNFR1 TMH is required for ligand-induced signaling. Unfortunately, to the best of our knowledge, there have been no report of naturally occurring, disease-causing mutations in the TMH of TNFR1 that would indicate the function of TMH oligomerization in receptor activation. It is thus important to perform functional mutagenesis of the TMH in the context of the full-length TNFR1. The TMH structure reported in this article should guide this effort.

CONCLUSION

We have thus far determined the TMH structures for Fas, DR5, and TNFR1 in essentially lipid bilayer environment. While they show obvious similarities, there are significant differences that make sequence-based structural prediction extremely difficult. One fundamental property shared by the three receptors is the ability of the TMH to spontaneously form defined trimer in lipid bilayer, although the TMH of DR5, in addition, can dimerize via the GXXXG signature sequence. Another similarity is that these trimers are all stabilized by hydrophobic interactions in the core of the assembly, and the intimate helical packing is made possible by small amino acids such as proline, glycine, alanine, or threonine. But, the nature of the hydrophobic core formation is where the biggest differences reside among these TMH structures. While the larger hydrophobic amino acids such as leucine, isoleucine, and valine make up the cores of Fas and TNFR1 TMH trimers, the small alanine and threonine appear to dominate the hydrophobic core of DR5 TMH trimer. In the case of Fas TMH, the critical proline not only facilitates close helix–helix packing but also introduces backbone malleability for accommodating the hydrophobic core (Fu et al., 2016). Although TNFR1 TMH also has a relatively conserved proline, it is the glycine that permits intimate helical packing. The GXXXG or small-XXX-small motif has been rather consistent in predicting TMH dimerization. Determinants for TMH trimerization, however, could be highly diverse. Hence, it remains important to experimentally survey the oligomerization properties of TMHs of other members of the TNFRSF to gain a broad understanding of the functional roles of TMH in receptor activation.

MATERIALS AND METHODS

Protein Expression and Purification

The DNA corresponding to the human TNFR1 (isoform 1) fragment, residues 209–238, designated TNFR1 TMH, was synthesized by GenScript (Piscataway, NJ, United States). Residues C223 and M233 were mutated to alanines to facilitate expression and purification. The protein expression construct was created by fusing the TNFR1 TMH fragment to the C terminus of the His9-TrpLE expression sequence in the pMM-LR6 vector, with an added methionine in-between for cleavage by cyanogen bromide. For NMR sample preparation, transformed *Escherichia coli* strain BL21 (DE3) bacteria were grown in M9 minimal media supplemented with centrum multivitamins and stable isotopes. Cultures were grown at 37°C to an absorbance of ∼0.6 at 600 nm and cooled to 25°C before induction with 500 μM isopropyl β-D-thiogalactopyranoside at 25°C for overnight. For fully deuterated proteins, bacterial cultures were grown in 99.8% D_2O (Sigma Aldrich, St. Louis, MO, United States) with deuterated glucose (Cambridge Isotope Laboratories, Tewksbury, MA, United States). The TNFR1 TMH protein was extracted, cleaved by cyanogen bromide, purified and lyophilized as described (Fu et al., 2016). Bacteria were harvested and resuspended in 50 mM Tris-HCl (pH 8.0) and 200 mM NaCl. The bacteria were sonicated twice and centrifuged at 40,000×g for 30 min to collect inclusion body pellets. The inclusion body pellets were dissolved in 6 M guanidine HCl, 50 mM Tris (pH 8.0), 100 mM NaCl, and 1% (v/v) Triton X-100. The solubilized solution of inclusion body was loaded to a Ni^{2+} affinity column (Sigma), washed with 8 M urea solution and distilled water, and eluted with 70% (v/v) formic acid. The fusion protein was cleaved at the methionine position by cyanogen bromide (0.1 g/mL) to release the TNFR1 TMH peptide. The cleaved peptide was then precipitated in water, lyophilized, dissolved in 50% formic acid, and loaded to a Zorbax SB-C3 column (Agilent), equilibrated in Buffer A [5% isopropanol, 0.1% trifluoroacetic acid (TFA)]. TNFR1 TMH was separated from the unwanted species in a gradient of 50–100% Buffer B (25% acetonitrile, 75% isopropanol, 0.1% TFA). The eluted TNFR1 TMH was lyophilized for storage.

NMR Sample Preparation in Bicelle

To reconstitute TNFR1 TMH in bicelles, 1∼2 mg of the purified and lyophilized protein was mixed with 9 mg 1,2-Dimyristoyl-sn-Glycero-3-Phosphocholine (DMPC, protonated or deuterated from Avanti Polar Lipids, Alabaster, AL, United States) and dissolved in 1,1,1,3,3,3-hexafluoro-2-propanol. The mixture was slowly dried to a thin film under nitrogen stream, followed by overnight lyophilization. The dried thin film was redissolved in 2 mL of 8 M urea containing ∼27 mg 1,2-Dihexanoyl-sn-Glycero-3-Phosphocholine (DH_6PC, protonated or deuterated from Avanti Polar Lipids). The mixture was dialyzed twice against a 20 mM phosphate buffer (pH 6.8) (1 L each time) to remove the denaturant, and 10 mg DH_6PC was added to the sample before the second dialysis to compensate its loss. The DMPC:DH_6PC ratio was monitored by 1D NMR throughout the reconstitution process. If needed, additional DH_6PC was added to make the final DMPC:DH_6PC ratio between 0.5 and 0.6. The sample was concentrated using Centricon (EMD Millipore, Billerica, MA, United States) to ∼350 μL. The final NMR sample contained ∼0.7 mM TNFR1 TMH (monomer), ∼50 mM DMPC, ∼100 mM DH_6PC, 20 mM phosphate buffer (pH 6.8), 0.02% NaN_3 and 5% D_2O. For all NOE experiments, the protein was reconstituted using DMPC and DH_6PC with deuterated acyl chains (Avanti Polar Lipids).

SDS-PAGE Analysis of TMH Oligomerization

For SDS-PAGE analysis of the bicelle-reconstituted samples, lyophilized protein (2 mg) was dissolved in hexafluoro-isopropanol (HFIP) with 2 mg DMPC, followed by drying of the solution under a nitrogen stream to achieve a thin film. The thin film was then dissolved in 1 ml of an 8 M urea solution containing approximately 6 mg DH_6PC, followed by dialysis against 20 mM sodium phosphate buffer (pH 6.8) to remove the denaturant. After dialysis, DH_6PC was added to adjust the ratio of DMPC:DH_6PC to approximately 1:2. To perform gel electrophoresis, 20 μL of the reconstitution sample was mixed with 5 μL of 4× (dilution) LDS loading buffer (Invitrogen, Catalog No.: NP0007) without heating or other reducing agents,

and loaded to an Invitrogen NuPAGE 12% gel (Catalog No.: NP0342BOX). The gel was run at 200 V on ice for 30 min. For SDS-PAGE analysis of the unreconstituted samples, lyophilized protein powder suspended in 1× LDS loading buffer (Invitrogen, Catalog No.: NP0007) was heated at 100°C for 10 min and loaded to an Invitrogen NuPAGE 12% gel (Catalog No.: NP0342BOX).

NMR Resonance Assignment

All NMR data was recorded at 30°C (303 K) on Bruker spectrometers operating at ^{1}H frequency of 800 MHz, 750 MHz, or 600 MHz and equipped with cryogenic probes. NMR data were processed using NMRPipe (Delaglio et al., 1995), and spectra are analyzed using XEASY (Bartels et al., 1995) and CcpNmr (Vranken et al., 2005). Triple resonance experiments were collected at ^{1}H frequency of 600 MHz using a (^{15}N, ^{13}C, ∼85% ^{2}H)-labeled sample. Sequence-specific assignment of backbone H^{N}, ^{15}N, $^{13}C^{\alpha}$, and ^{13}C' resonances was accomplished using 3D TROSY-based HNCA, HN(CO)CA, HN(CA)CO and HNCO experiments (Salzmann et al., 1999). The aliphatic and aromatic resonances of the protein side chains were assigned using the 3D ^{15}N-edited NOESY-TROSY-HSQC (τ_{NOE} = 100 ms) and 3D ^{13}C-edited NOESY-HSQC (τ_{NOE} = 150 ms) spectra, recorded at ^{1}H frequency of 750 MHz using a (^{15}N, ^{13}C)-labeled protein sample in deuterated bicelles. For assigning inter-chain distance restraints, the J_{CH}-modulated NOE experiment (Fu et al., 2019) was performed to exclusively detect inter-chain NOEs between the ^{15}N-attached protons of one chain and the ^{13}C-attached protons of the neighboring chains, using a mixed sample containing 50% (^{15}N, ^{2}H)-labeled and 50% ^{13}C-labeled protein. In this experiment, two interleaved spectra were recorded with different times of J_{CH} evolution (J_{CH} = 0 ms and J_{CH} = 8 ms) before the NOE mixing. Subtraction of the two spectra allowed selection of the inter-chain NOE crosspeaks.

Structure Calculation

The structures were generated using the program XPLOR-NIH (Schwieters et al., 2003). First, the monomer structure was generated using the short-range NOE restraints and the backbone dihedral restraints derived from the backbone ^{15}N, ^{1}H, ^{13}Cα, and ^{13}C' chemical shifts [using the TALOS + program (Shen et al., 2009)]. The $^{13}C^{\alpha}$ secondary chemical shifts of TNFR1 TMH are shown in **Supplementary Figure S2B**, providing a secondary structure mapping of the TM fragment. Second, the monomer structure and inter-chain NOE restraints were used with the ExSSO program (Yang et al., 2017) to generate a unique solution of trimeric assembly. Finally, the initial trimer solution was fed to the XPLOR-NIH for iterative refinement against all NMR restraints, including the newly assigned self-consistent inter-chain NOEs from each iteration.

For each inter-chain restraint between two adjacent chains, three identical distance restraints were assigned respectively to all pairs of neighboring chains to satisfy the condition of C3 rotational symmetry. The XPLOR refinement used a simulated annealing (SA) protocol in which the temperature in the bath was cooled from 1000 to 200 K with steps of 20 K. The NOE restraints were enforced by flat-well harmonic potentials, with the force constant ramped from 2 to 30 kcal/mol $Å^{-2}$ during annealing. Backbone dihedral angle restraints were taken from the "GOOD" dihedral angles from TALOS+, all with a flat-well (± the corresponding uncertainties from TALOS+) harmonic potential with force constant ramped from 5 to 1000 kcal/mol rad^{-2}. A total of 100 structures were calculated and 15 lowest energy structures were selected as the final structural ensemble (**Supplementary Figure S3** and **Supplementary Table S1**).

DATA AVAILABILITY STATEMENT

The datasets presented in this study can be found in online repositories. The atomic structure coordinate and structural constraints have been deposited in the Protein Data Bank (PDB), accession number 7K7A. The chemical shift values have been deposited in the Biological Magnetic Resonance Data Bank (BMRB), accession number 30799.

AUTHOR CONTRIBUTIONS

LZ and JC conceived the study. LZ, QF, and LP prepared samples for NMR and biochemical studies. LZ, AP, and JC collected and analyzed the NMR data and/or determined the structures. JC and LZ wrote the manuscript. All authors contributed to the editing of the manuscript.

FUNDING

This work was supported by NIH grant AI150709 (to JC). The NMR data were collected at the MIT-Harvard CMR (supported by NIH grants P41 GM132079 and S10 OD023513).

ACKNOWLEDGMENTS

We thank Hao Wu for insightful discussion.

SUPPLEMENTARY MATERIAL

The Supplementary Material for this article can be found online at: https://www.frontiersin.org/articles/10.3389/fcell.2020.569684/full#supplementary-material

REFERENCES

Ashkenazi, A. (2008). Targeting the extrinsic apoptosis pathway in cancer. *Cytokine Growth Factor Rev.* 19, 325–331. doi: 10.1016/j.cytogfr.2008.04.001

Baker, S. J., and Reddy, E. P. (1998). Modulation of life and death by the TNF receptor superfamily. *Oncogene* 17, 3261–3270. doi: 10.1038/sj.onc.1202568

Banner, D. W., D'Arcy, A., Janes, W., Gentz, R., Schoenfeld, H. J., Broger, C., et al. (1993). Crystal structure of the soluble human 55 kd TNF receptor-human TNF beta complex: implications for TNF receptor activation. *Cell* 73, 431–445. doi: 10.1016/0092-8674(93)90132-a

Bartels, C., Xia, T. H., Billeter, M., Guntert, P., and Wuthrich, K. (1995). The program XEASY for computer-supported NMR spectral analysis of biological macromolecules. *J. Biomol. NMR* 6, 1–10. doi: 10.1007/BF00417486

Branschadel, M., Aird, A., Zappe, A., Tietz, C., Krippner-Heidenreich, A., and Scheurich, P. (2010). Dual function of cysteine rich domain (CRD) 1 of TNF receptor type 1: conformational stabilization of CRD2 and control of receptor responsiveness. *Cell Signal.* 22, 404–414. doi: 10.1016/j.cellsig.2009.10.011

Chan, F. K. (2000). The pre-ligand binding assembly domain: a potential target of inhibition of tumour necrosis factor receptor function. *Ann. Rheum. Dis.* 59(Suppl. 1), i50–i53.

Chaudhary, P. M., Eby, M., Jasmin, A., Bookwalter, A., Murray, J., and Hood, L. (1997). Death receptor 5, a new member of the TNFR family, and DR4 induce FADD-dependent apoptosis and activate the NF-kappaB pathway. *Immunity* 7, 821–830. doi: 10.1016/s1074-7613(00)80400-8

Cooper, D., Bansal-Pakala, P., and Croft, M. (2002). 4-1BB (CD137) controls the clonal expansion and survival of CD8 T cells in vivo but does not contribute to the development of cytotoxicity. *Eur. J. Immunol.* 32, 521–529. doi: 10.1002/1521-4141(200202)32:2<521::aid-immu521>3.0.co;2-x

Croft, M., Benedict, C. A., and Ware, C. F. (2013). Clinical targeting of the TNF and TNFR superfamilies. *Nat. Rev. Drug Discov.* 12, 147–168. doi: 10.1038/nrd3930

Delaglio, F., Grzesiek, S., Vuister, G. W., Zhu, G., Pfeifer, J., and Bax, A. (1995). NMRPipe: a multidimensional spectral processing system based on UNIX pipes. *J. Biomol. NMR* 6, 277–293. doi: 10.1007/BF00197809

Deng, G. M. (2007). Tumor necrosis factor receptor pre-ligand assembly domain is an important therapeutic target in inflammatory arthritis. *BioDrugs* 21, 23–29. doi: 10.2165/00063030-200721010-00004

Fu, Q., Fu, T. M., Cruz, A. C., Sengupta, P., Thomas, S. K., Wang, S., et al. (2016). Structural basis and functional role of intramembrane trimerization of the Fas/cd95 death receptor. *Mol. Cell* 61, 602–613. doi: 10.1016/j.molcel.2016.01.009

Fu, Q., Piai, A., Chen, W., Xia, K., and Chou, J. J. (2019). Structure determination protocol for transmembrane domain oligomers. *Nat. Protoc.* 14, 2483–2520. doi: 10.1038/s41596-019-0188-9

Fu, Q., Shaik, M. M., Cai, Y., Ghantous, F., Piai, A., Peng, H., et al. (2018). Structure of the membrane proximal external region of HIV-1 envelope glycoprotein. *Proc. Nat. Acad. Sci. U.S.A.* 115, E8892–E8899. doi: 10.1073/pnas.1807259115

Glover, K. J., Whiles, J. A., Wu, G., Yu, N., Deems, R., Struppe, J. O., et al. (2001). Structural evaluation of phospholipid bicelles for solution-state studies of membrane-associated biomolecules. *Biophys. J.* 81, 2163–2171. doi: 10.1016/s0006-3495(01)75864-x

Goh, E. T. H., Lin, Z., Ahn, B. Y., Lopes-Rodrigues, V., Dang, N. H., Salim, S., et al. (2018). A small molecule targeting the transmembrane domain of death receptor p75(ntr) induces melanoma cell death and reduces tumor growth. *Cell Chem. Biol.* 25, 1485–1494.e5. doi: 10.1016/j.chembiol.2018.09.007

Gronbaek, K., Straten, P. T., Ralfkiaer, E., Ahrenkiel, V., Andersen, M. K., Hansen, N. E., et al. (1998). Somatic Fas mutations in non-Hodgkin's lymphoma: association with extranodal disease and autoimmunity. *Blood* 92, 3018–3024. doi: 10.1182/blood.v92.9.3018.421k52_3018_3024

Hatzoglou, A., Roussel, J., Bourgeade, M. F., Rogier, E., Madry, C., Inoue, J., et al. (2000). TNF receptor family member BCMA (B cell maturation) associates with TNF receptor-associated factor (TRAF) 1, TRAF2, and TRAF3 and activates NF-kappa B, elk-1, c-Jun N-terminal kinase, and p38 mitogen-activated protein kinase. *J. Immunol.* 165, 1322–1330. doi: 10.4049/jimmunol.165.3.1322

Karathanasis, C., Medler, J., Fricke, F., Smith, S., Malkusch, S., Widera, D., et al. (2020). Single-molecule imaging reveals the oligomeric state of functional TNFalpha-induced plasma membrane TNFR1 clusters in cells. *Sci. Signal.* 13, eaax5647. doi: 10.1126/scisignal.aax5647

Larkin, M. A., Blackshields, G., Brown, N. P., Chenna, R., McGettigan, P. A., McWilliam, H., et al. (2007). Clustal W and Clustal X version 2.0. *Bioinformatics* 23, 2947–2948. doi: 10.1093/bioinformatics/btm404

Lee, S. H., Shin, M. S., Kim, H. S., Park, W. S., Kim, S. Y., Jang, J. J., et al. (2000). Somatic mutations of Fas (Apo-1/CD95) gene in cutaneous squamous cell carcinoma arising from a burn scar. *J Invest. Dermatol.* 114, 122–126. doi: 10.1046/j.1523-1747.2000.00819.x

MacKenzie, K. R., Prestegard, J. H., and Engelman, D. M. (1997). A transmembrane helix dimer: structure and implications. *Science* 276, 131–133. doi: 10.1126/science.276.5309.131

Naismith, J. H., Devine, T. Q., Kohno, T., and Sprang, S. R. (1996). Structures of the extracellular domain of the type I tumor necrosis factor receptor. *Structure* 4, 1251–1262. doi: 10.1016/s0969-2126(96)00134-7

Pan, L., Fu, T. M., Zhao, W., Zhao, L., Chen, W., Qiu, C., et al. (2019). Higher-order clustering of the transmembrane anchor of DR5 drives signaling. *Cell* 176, 1477.e–1489.e. doi: 10.1016/j.cell.2019.02.001

Rogers, P. R., Song, J., Gramaglia, I., Killeen, N., and Croft, M. (2001). OX40 promotes Bcl-xL and Bcl-2 expression and is essential for long-term survival of CD4 T cells. . *Immunity* 15, 445–455. doi: 10.1016/s1074-7613(01)00191-1

Salzmann, M., Wider, G., Pervushin, K., and Wuthrich, K. (1999). Improved sensitivity and coherence selection for [15N,1H]-TROSY elements in triple resonance experiments. *J. Biomol. NMR* 15, 181–184. doi: 10.1023/a:1008358030477

Sanders, C. R.II, and Schwonek, J. P. (1992). Characterization of magnetically orientable bilayers in mixtures of dihexanoylphosphatidylcholine and dimyristoylphosphatidylcholine by solid-state NMR. *Biochemistry* 31, 8898–8905. doi: 10.1021/bi00152a029

Schneider, P., Holler, N., Bodmer, J. L., Hahne, M., Frei, K., Fontana, A., et al. (1998). Conversion of membrane-bound Fas(CD95) ligand to its soluble form is associated with downregulation of its proapoptotic activity and loss of liver toxicity. *J. Exp. Med.* 187, 1205–1213. doi: 10.1084/jem.187.8.1205

Schwieters, C. D., Kuszewski, J. J., Tjandra, N., and Clore, G. M. (2003). The Xplor-NIH NMR molecular structure determination package. *J Magn. Reson.* 160, 65–73. doi: 10.1016/s1090-7807(02)00014-9

Scott, F. L., Stec, B., Pop, C., Dobaczewska, M. K., Lee, J. J., Monosov, E., et al. (2009). The Fas-FADD death domain complex structure unravels signalling by receptor clustering. *Nature* 457, 1019–1022. doi: 10.1038/nature07606

Shen, Y., Delaglio, F., Cornilescu, G., and Bax, A. (2009). TALOS+: a hybrid method for predicting protein backbone torsion angles from NMR chemical shifts. *J. Biomol. NMR* 44, 213–223. doi: 10.1007/s10858-009-9333-z

Sheridan, J. P., Marsters, S. A., Pitti, R. M., Gurney, A., Skubatch, M., Baldwin, D., et al. (1997). Control of TRAIL-induced apoptosis by a family of signaling and decoy receptors. *Science* 277, 818–821. doi: 10.1126/science.277.5327.818

Tanaka, M., Itai, T., Adachi, M., and Nagata, S. (1998). Downregulation of Fas ligand by shedding. *Nat. Med.* 4, 31–36. doi: 10.1038/nm0198-031

Trenker, R., Call, M. E., and Call, M. J. (2015). Crystal structure of the glycophorin a transmembrane dimer in lipidic cubic phase. *J. Am. Chem. Soc.* 137, 15676–15679. doi: 10.1021/jacs.5b11354

Valley, C. C., Lewis, A. K., Mudaliar, D. J., Perlmutter, J. D., Braun, A. R., Karim, C. B., et al. (2012). Tumor necrosis factor-related apoptosis-inducing ligand (TRAIL) induces death receptor 5 networks that are highly organized. *J. Biol. Chem.* 287, 21265–21278. doi: 10.1074/jbc.M111.306480

Vanamee, E. S., and Faustman, D. L. (2018). Structural principles of tumor necrosis factor superfamily signaling. *Sci. Signal.* 11:eaao4910. doi: 10.1126/scisignal.aao4910

Vranken, W. F., Boucher, W., Stevens, T. J., Fogh, R. H., Pajon, A., Llinas, M., et al. (2005). The CCPN data model for NMR spectroscopy: development of a software pipeline. *Proteins* 59, 687–696. doi: 10.1002/prot.20449

Wajant, H. (2002). The Fas signaling pathway: more than a paradigm. *Science* 296, 1635–1636. doi: 10.1126/science.1071553

Wajant, H., Pfizenmaier, K., and Scheurich, P. (2003). Tumor necrosis factor signaling. *Cell Death Differ.* 10, 45–65. doi: 10.1038/sj.cdd.4401189

Wang, L., Yang, J. K., Kabaleeswaran, V., Rice, A. J., Cruz, A. C., Park, A. Y., et al. (2010). The Fas-FADD death domain complex structure reveals the basis of DISC assembly and disease mutations. *Nat. Struct. Mol. Biol.* 17, 1324–1329. doi: 10.1038/nsmb.1920

Weinelt, N., Karathanasis, C., Smith, S., Medler, J., Malkusch, S., Fulda, S., et al. (2020). Quantitative single-molecule imaging of TNFR1 reveals zafirlukast as antagonist of TNFR1 clustering and TNFalpha-induced NF-kB signaling. *J. Leukoc. Biol.* doi: 10.1002/JLB.2AB0420-572RR

Yang, J., Piai, A., Shen, H. B., and Chou, J. J. (2017). An exhaustive search algorithm to aid NMR-based structure determination of rotationally symmetric transmembrane oligomers. *Sci. Rep.* 7:17373. doi: 10.1038/s41598-017-17639-w

Yin, X., Li, W., Ma, H., Zeng, W., Peng, C., Li, Y., et al. (2019). Crystal structure and activation mechanism of DR3 death domain. *FEBS J.* 286, 2593–2610. doi: 10.1111/febs.14834

Conflict of Interest: The authors declare that the research was conducted in the absence of any commercial or financial relationships that could be construed as a potential conflict of interest.

frontiers in Cell and Developmental Biology

ORIGINAL RESEARCH
published: 29 October 2020
doi: 10.3389/fcell.2020.577572

Atsttrin Promotes Cartilage Repair Primarily Through TNFR2-Akt Pathway

Jianlu Wei[1,2†], Kaidi Wang[1†], Aubryanna Hettinghouse[1] and Chuanju Liu[1,3]*

[1] Department of Orthopaedic Surgery, Qilu Hospital of Shandong University, Jinan, China, [2] Department of Orthopaedic Surgery, New York University Langone Medical Center, New York, NY, United States, [3] Department of Cell Biology, New York University Grossman School of Medicine, New York, NY, United States

Background: Cartilage defects account for substantial economic and humanistic burdens and pose a significant clinical problem. The efficacy of clinical approaches to cartilage repair is often inadequate, in part, owing to the restricted proliferative capacity of chondrocytes. Molecules have the capacity to promote the differentiation of multipotent mesenchymal stem cells into chondrocytes and may also gain the ability to repair the damaged cartilage.

Objective: This study aimed to investigate the role of Atsttrin (progranulin-derived engineered protein) in cartilage repair as well as the signaling pathway involved.

Methods: Primary and mesenchymal stem cell lines were used for the micromass culture. A murine cartilage defect model was used to determine the role of Atsttrin in cartilage repair *in vivo*. Real-time polymerase chain reaction and Western blot analysis were used to monitor the effect of Atsttrin on the transcriptional and protein levels, respectively, of key anabolic and catabolic signaling molecules.

Results: Atsttrin stimulated chondrogenesis *in vitro* and accelerated cartilage repair *in vivo*. In addition, Atsttrin-mediated cartilage repair occurred primarily through tumor necrosis factor receptor 2-initiated Akt signaling and downstream JunB transcription factor.

Conclusion: Atsttrin might serve as a promising therapeutic modality for cartilage regeneration.

Keywords: Atsttrin, chondrogenesis, cartilage repair, TNFR2, signaling

OPEN ACCESS

Edited by:
Marta Rizzi,
University of Freiburg Medical Center, Germany

Reviewed by:
Michael A. Kalwat,
University of Texas Southwestern Medical Center, United States
Lucienne A. Vonk,
CO.DON AG, Germany
Shiwu Dong,
Third Military Medical University, China

***Correspondence:**
Jianlu Wei
18560089157@163.com

† These authors have contributed equally to this work

Specialty section:
This article was submitted to Signaling, a section of the journal Frontiers in Cell and Developmental Biology

Received: *29 June 2020*
Accepted: *12 October 2020*
Published: *29 October 2020*

Citation:
Wei J, Wang K, Hettinghouse A and Liu C (2020) Atsttrin Promotes Cartilage Repair Primarily Through TNFR2-Akt Pathway. Front. Cell Dev. Biol. 8:577572. doi: 10.3389/fcell.2020.577572

INTRODUCTION

Articular cartilage diseases affect more than 273 million of adults across the world (Helmick et al., 2008; Lawrence et al., 2008; Krishnan and Grodzinsky, 2018). Damage to the articular cartilage can result in potentially crippling symptoms, such as swelling, pain and decreased mobility, and, if left untreated, osteoarthritis (OA). Suboptimal therapeutic outcomes may be largely attributable to the limited reparative competence of chondrocytes (Berthiaume et al., 2011). Current surgical treatments include joint replacement, osteotomies, microfracture, autologous chondrocyte implantation, and/or allografts and autografts (Detterline et al., 2005; Devitt et al., 2017). Even minor cartilage injuries may lead to persistent tissue damage and eventual OA. Improved corrective approaches for cartilage damage are critical to limiting humanistic and financial losses incurred following cartilage injury.

Progranulin (PGRN) is a growth factor–like molecule with multiple functions in diverse biological processes (Wei et al., 2016; Cui et al., 2019). A previous study reported that PGRN was expressed in human articular cartilage. The level of PGRN was significantly upregulated in diseased cartilage with osteoarthritis (OA) and rheumatoid arthritis (Zhao et al., 2015). Additionally, PGRN is important for chondrocyte proliferation and differentiation, which are functions recapitulated in animal models of cartilage defect (Feng et al., 2010; Kong et al., 2016). Recent studies reported that PGRN and its engineered derivative Atsttrin demonstrated a therapeutic effect in inflammatory and degenerative arthritis murine models through binding to tumor necrosis factor receptors (TNFRs) (Tang et al., 2011; Wei et al., 2017; Wei and Liu, 2018). Atsttrin, comprising half-units of granulins A, C, and F plus linkers P3, P4, and P5, lacks the oncogenic activity of PGRN. However, Atsttrin has a longer half-life (about 120 h) compared with PRGN (about 40 h) (Tang et al., 2011; Liu et al., 2014).

Considering the stimulatory role of PGRN in chondrogenesis and the protective effects of PGRN-derived Atsttrin in animal models of arthritis (Feng et al., 2010; Tang et al., 2011; Xia et al., 2015; Wei et al., 2017), it was hypothesized that Atsttrin might represent a novel potential treatment for cartilage regeneration. This study found that Atsttrin could promote chondrogenesis *in vitro* and accelerated cartilage repair in a mouse full-thickness cartilage defect model wherein the subchondral bone was penetrated to allow for an influx of marrow-derived mesenchymal stem cells (MSCs). Mechanistic studies demonstrated that Atsttrin-mediated cartilage repair occurred primarily through TNFR2 signaling.

MATERIALS AND METHODS

Media and Reagents

Dulbecco's modified Eagle Medium (DMEM) and fetal bovine serum were purchased from Gibco-BRL (Sydney, Australia). Specific antibodies against JunB (Cat. #sc-73) and glyceraldehyde-3-phosphate dehydrogenase (GAPDH, Cat. # sc-25778) were obtained from Santa Cruz Biotechnology, Inc. (TX, United States). Phosphatidylinositol 3-kinase (PI3K), Akt, and MAPK/ERK1/2 activation were assessed using PathScan Multiplex Western Cocktail I from Cell Signaling (Cat. #5301, MA, United States). Secondary horseradish peroxidase–conjugated antibody was purchased from Jackson Immunoresearch Inc. (Cat. # 711-035-152, PA, United States). The blots were developed using Western Lightning Plus-ECL from Perkin-Elmer (Cat. # NEL103001EA, MA, United States). Tris, glycine, sodium dodecyl sulfate (SDS), and other regents were obtained from Sigma (MO, United States) unless stated otherwise.

Effect and Mechanism of Atsttrin on Chondrogenesis

Bone marrow stem cells (BMSCs) were obtained from mice, and multipotential murine C3H10T1/2 cells were also used for this experiment. Chondrogenic differentiation medium, consisted of high-glucose (4.5 g/L) DMEM supplemented with ITS + (Collaborative Research, MA, United States), 0.1 μM dexamethasone, and 50 μg/mL ascorbate 2-phosphate with 100 ng/mL BMP2 or 1000 ng/mL Atsttrin, was used for differentiation. Micromass culture was used for the induction of chondrogenesis. In detail, 500,000 BMSCs at passage 2 were plated in the center of a culture plate, and the cells were incubated at 37°C with 5% CO_2 for 3 h. After cell aggregation, the chondrogenic medium was carefully added to the cells. BMSCs isolated from wild-type (WT), TNFR1-deficient (TNFR1–/–), and TNFR2-deficient (TNFR2–/–) mice underwent chondrogenic induction for 10 days prior to safranin O staining and Alcian blue staining to determine chondrocyte differentiation.

The aforementioned micromass culture of C3H10T1/2 cells was performed in the absence or presence of Atsttrin at a concentration of 1000 ng/mL to examine the effects of Akt-signaling blockade on Atsttrin-mediated chondrogenesis. After 5 days in culture, 0.01% DMSO (*v*/*v*) or 1 μM Wortmannin was added to the cultured cells and further incubated for 2 or 7 days prior to collection for real-time polymerase chain reaction (rtPCR) analysis. C3H10T1/2 cells were stably transfected with pSuper vector, pSuper-JunB expressing a small interfering RNA (siRNA) against JunB (Feng et al., 2010), pCMV-JunB expression plasmid or sequential knockdown and expression plasmids using *Lipofectamine 2000* in serum-free medium with 6-h incubation, following the manufacturer's protocols, to examine the importance of downstream JunB transcription factor activation in Atsttrin-mediated chondrogenesis. A fresh complete medium was added, and the transfected cells were cultured in micromass with or without 1000 ng/mL Atsttrin for 2 or 7 days for the induction of chondrogenesis prior to collection for rtPCR.

Real-Time PCR Assay

Micromass cultures of C3H10T1/2 cells and BMSCs were treated with commercially available recombinant BMP2 prior to RNA extraction. The cells were harvested from 3 wells of 12-well plates, and 1 μg of total RNA per sample was reverse-transcribed using the Promega ImProm-II Reverse Transcription System (WI, United States). Quantitative real-time PCR was performed using the following sequence-specific primers: 5′-TGGTGGAGCAGCAAGAGCAA-3′ and 5′-CAGTGGACAGTA GACGGAGGAAA-3′ for collagen type II alpha 1 (*Col2a1*); 5′-CC TGCTACTTCATCGACCCC-3′ and 5′-AGATGCTGTTGACTC GAACCT-3′ for Aggrecan (*Acan*); 5′-GAGGCCACGGAA CAGACTCA-3′ and 5′-CAGCGCCTTGAAGATACGATT-3′ for Sox9; and 5′-AGGTCGGTGTGAACGGATTTG-3′ and 5′-TGTAGACCATGTAGTTGAGGTCA-3′ for *Gapdh*. The reactions were carried out in an *Applied Biosystems 7300* Sequence Detection System (CA, United States). In detail, more than 40 cycles of 15 s at 95°C and 1 min at 60°C were used for the experiment. GAPDH was employed as an internal control. Each sample and gene were evaluated in triplicate.

Murine Osteochondral Defect Model

All animal studies were performed following the institutional guidelines, and all performances were approved by the

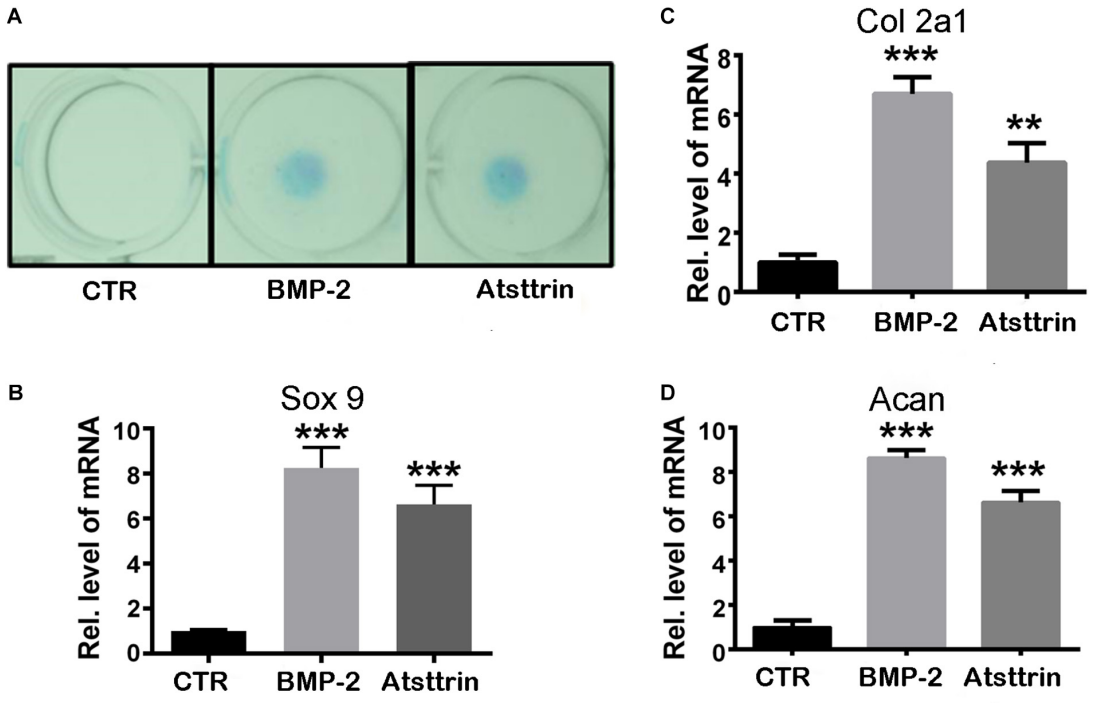

FIGURE 1 | Atsttrin promoted chondrogenesis in C3H10T1/2 cells. **(A)** C3H10T1/2 cells were incubated in the absence (CTR) or presence of 100 ng/mL BMP2 or 1000 ng/mL Atsttrin for 10 days, followed by Alcian blue staining. **(B–D)** C3H10T1/2 cells were stimulated with either 100 ng/mL BMP2 or 1000 ng/mL Atsttrin, and real-time PCR was performed to examine the expression of Sox9, collagen II (Col2a1), and aggrecan (Acan). Units were arbitrary; normalized values were calibrated against controls and set as 1. Experiments were conducted in triplicate. Three independent experiments were performed. ***$P < 0.001$, **$P < 0.01$.

Institutional Animal Care and Use Committee of New York University. The mice were group-housed within the rodent barrier facility at the Skirball Institute of Biomolecular Medicine with a standard assessment of food and water. The animal room had a specific-pathogen-free environment. The temperature and humidity were automatically controlled in accordance with a 12-h light/dark cycle. C57BL6/J background WT, TNFR1 knockout (TNFR1−/−), and TNFR2 knockout (TNFR2−/−) mice were acquired from Jackson Laboratory and maintained within the animal housing facility. The genotyping and housing of TNFR1−/−, TNFR2−/−, and WT littermate mice was performed as described previously (Tang et al., 2011). Eight-week-old male mice were used for this study.

The model was established and modified as previously described (Matsuoka et al., 2015). Briefly, the animals were subjected to general anesthesia. After that, the hind limbs were sterilized, and an ophthalmic ointment was applied to the eyes prior to positioning to a surgical microscope (SZX16; Olympus, Tokyo, Japan). A microsurgical scalpel was used for the anterior approach. The skin and the joint capsule were gently opened, and the patella was dislocated for exposing the trochlear groove. A unilateral, longitudinal full-thickness injury was generated along the articular surface of the trochlear groove using a constructed device comprising a 27G needle sheathed in a bisected 21G needle; the 21G needle was adjusted to expose 300 mm of the 27G needle beveled end. Subchondral bleeding was taken as indicative of the successful generation of the defect. The surgical site was irrigated with sterile saline, and a collagen sponge containing phosphate-buffered saline (PBS) ($n = 6$) or 6 μg Atsttrin ($n = 6$) was inserted into the defect site prior to stepwise suturing of the joint capsule and skin. The mice were postoperatively monitored for anesthetic recovery with thermal support. The contralateral limbs were subjected to a sham procedure wherein no defect was generated. The mice were sacrificed 6 weeks after the surgery.

Histological Analysis

The harvested knee joint tissues were fixed with 4% PFA for 2 days at room temperature. The tissues were then decalcified for 2 weeks in 10% EDTA (w/v) on a shaker at 4°C before dehydration, paraffin pre-processing, and embedding. Further, 5-μm serial sections were cut and stained with safranin O/fast green for the evaluation of cartilage repair. The degree of repair was evaluated by a blinded investigator using an International Cartilage Repair Score (ICRS) for cartilage repair (Mainil-Varlet et al., 2010).

Western Blot Analysis

The micromass cultures of BMSCs underwent starvation for 24 h to determine Atsttrin-mediated signaling in chondrogenesis. After that, the cells were stimulated with 1000 ng/mL Atsttrin over varied time courses, and the whole-cell lysates were collected for Western blot analysis. The cells were harvested and mixed

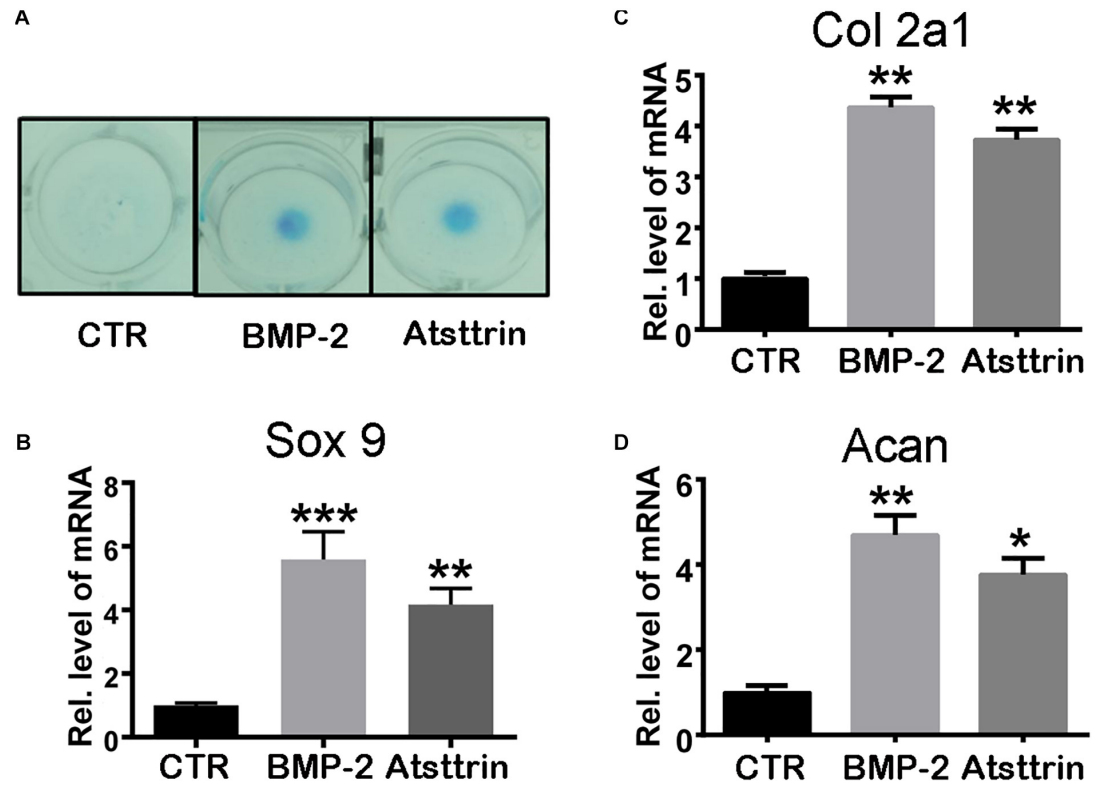

FIGURE 2 | Atsttrin promoted chondrogenesis in mouse primary bone marrow stem cells (BMSCs). **(A)** BMSCs were incubated in the absence (CTR) or presence of 100 ng/mL BMP2 or 1000 ng/mL Atsttrin for 10 days, followed by Alcian blue staining. **(B–D)** BMSCs were stimulated with either 100 ng/mL BMP2 or 1000 ng/mL Atsttrin, and real-time PCR was performed to examine the expressions of Sox9, collagen II (Col2a1), and aggrecan (Acan). Values were normalized to controls and set as 1. Experiments were conducted in triplicate. Three independent experiments were performed. ***$P < 0.001$, **$P < 0.01$, *$P < 0.05$.

with 5 × sample buffer (312.5 mM Tris-HCl, pH 6.8; 5% β-mercaptoethanol; 10% SDS; 0.5% bromphenol blue; and 50% glycerol). The samples were boiled at 95°C for 5 min, allowed to cool, and resolved on a 10% SDS-polyacrylamide gel followed by electro-transferring. After the blockage with 5% non-fat milk, the blots on the membrane were incubated overnight for 1 h with primary antibodies at the manufacturer-indicated assay-dependent dilution factor. BMSCs were starved for 24 h, followed by the stimulation with 1000 ng/mL Atsttrin over various time courses, to examine Atsttrin-mediated signaling in chrondrogenesis. The cells were collected, and the lysates were incubated with the PathScan Multiplex Western Cocktail I at 1:200 dilution. The cell lysates were incubated with a rabbit anti-JunB polyclonal antibody (1:1000 dilution) to determine the induction of JunB by Atsttrin. The blots were subjected to three 5-min washes with TBST prior to 1-h incubation with the horseradish peroxidase–conjugated anti-rabbit secondary antibody (1:2000 dilution), repeated washing, and signal development with Western Lightning Plus-ECL.

Statistical Analysis

The results were expressed as mean values ± standard error of the mean. Statistical significance was assessed using ANOVA and Student's *t* test with SPSS software (SPSS Inc, IL, United States). The data were checked for normality before analysis. A *P*-value < 0.05 indicated a statistically significant difference.

RESULTS

Atsttrin Stimulated Chondrogenesis *in vitro*

Given the stimulatory effect of PGRN on chondrogenesis, the present study first sought to investigate whether PGRN-derivative Atsttrin could similarly induce chondrogenesis. The chondrogenic potential of Atsttrin and BMP-2, a growth factor and well-known inducer of chondrogenic differentiation, were compared. A pluripotent stem cell line C3H10T1/2 capable of differentiation into chondrocytes was employed for these assays (Denker et al., 1999). The micromass cultured cells were incubated in the presence of 1000 ng/mL Atsttrin or 100 ng/mL BMP-2 for 10 days. As shown in **Figure 1A**, Alcian blue staining demonstrated chondrocyte differentiation in both the BMP-2- and Atsttrin-treated groups. Chondrogenesis was also examined at the transcriptional level by testing the expression of marker genes specific for chondrocytes. As shown in **Figures 1B–D**, BMP-2 and Atsttrin significantly induced the expression of Sox 9, collagen II, and aggrecan. BMSCs were maintained in

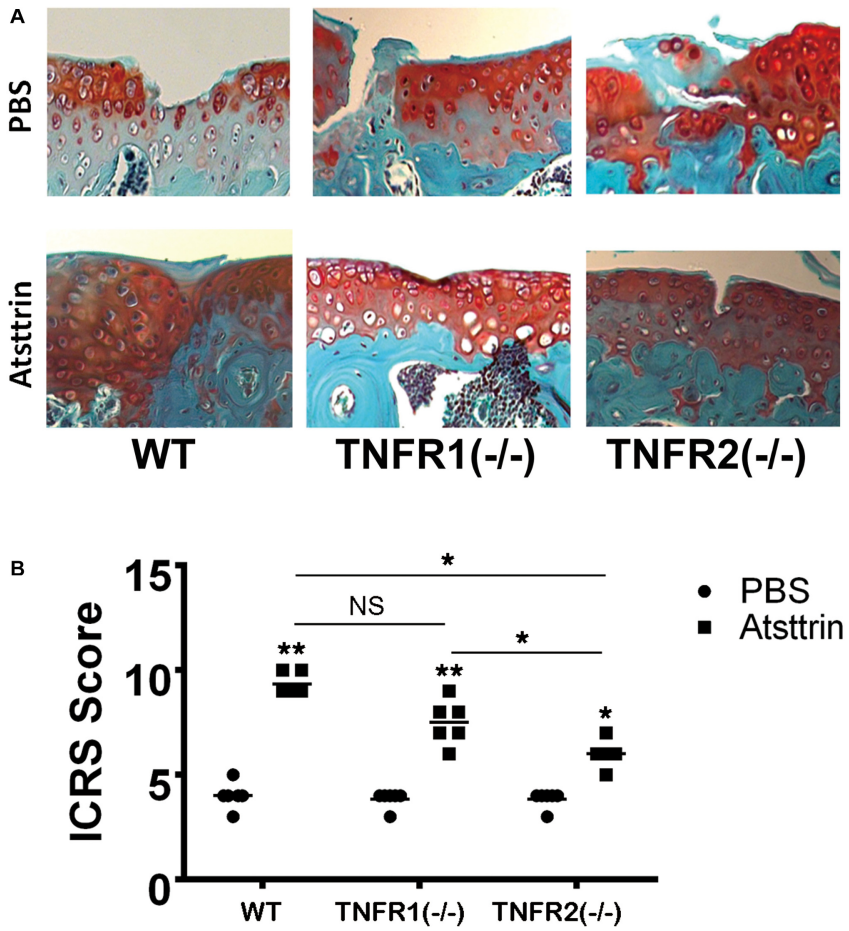

FIGURE 3 | Atsttrin accelerated cartilage repair through TNFRs. **(A)** Atsttrin promoted cartilage regeneration following surgically induced cartilage defect model relative to PBS (n = 6 per group), assayed using safranin O staining. **(B)** International Cartilage Repair Score (ICRS) based on the result of safranin O staining.

a micromass culture system as described earlier for 10 days. As shown in **Figure 2A**, Alcian blue staining validated the occurrence of Atsttrin-stimulated chondrogenesis in primary cells. Real-time PCR revealed significant upregulation of the expression of the chondrogenic marker genes, Sox9, collagen II, and aggrecan, in the treatment groups (**Figures 2B–D**). Collectively, these results indicated that Atsttrin could induce chondrocyte differentiation *in vitro*.

Atsttrin Promoted Cartilage Repair *in vivo* Primarily Through TNFR2

Considering a positive effect of Atsttrin on *in vitro* chondrogenesis, the study determined whether Atsttrin could accelerate cartilage regeneration *in vivo*. Atsttrin is composed of three TNFR-binding fragments (1/2F-1/2A-1/2C) of PGRN and exhibits selective TNFR-binding ability (Tang et al., 2011; Tian et al., 2014). Articular cartilage defects were established in the femoral trochlea of WT, TNFR1–/–, and TNFR2–/– mice, and a collagen sponge loaded with PBS or 6 μg Atsttrin was intra-operatively administered to investigate whether TNFR1 or TNFR2 or both receptors mediated the effect of Atsttrin on chondrogenesis and cartilage repair *in vivo*. The mice were sacrificed after 6 weeks for *ex vivo* evaluation. As indicated in **Figure 3** and **Supplementary Figure 1**, the scoring of Safranin O/Fast green staining indicated that Atsttrin could promote cartilage repair in WT, TNFR1–/–, and TNFR2–/– mice relative to their PBS-treated counterparts. Atsttrin-mediated cartilage repair showed no difference between TNFR1–/– mice and WT mice. However, Atsttrin-mediated cartilage repair was largely reduced in TNFR2–/– mice compared with WT mice. Additionally, Atsttrin-mediated cartilage repair was significantly reduced in TNFR2–/– mice compared with TNFR1–/– mice. These results indicated that Atsttrin-mediated cartilage repair depended mainly on the presence of TNFR2.

Atsttrin Promoted Cartilage Repair Through TNFR2-Akt Signaling

BMSCs were isolated from WT, TNFR1–/–, and TNFR2–/– mice and subjected to chondrogenic differentiation prior to treatment with Atsttrin to investigate the signaling pathways involved. The cells were collected for Western blot analysis of signaling pathway activation using an antibody cocktail. As illustrated in

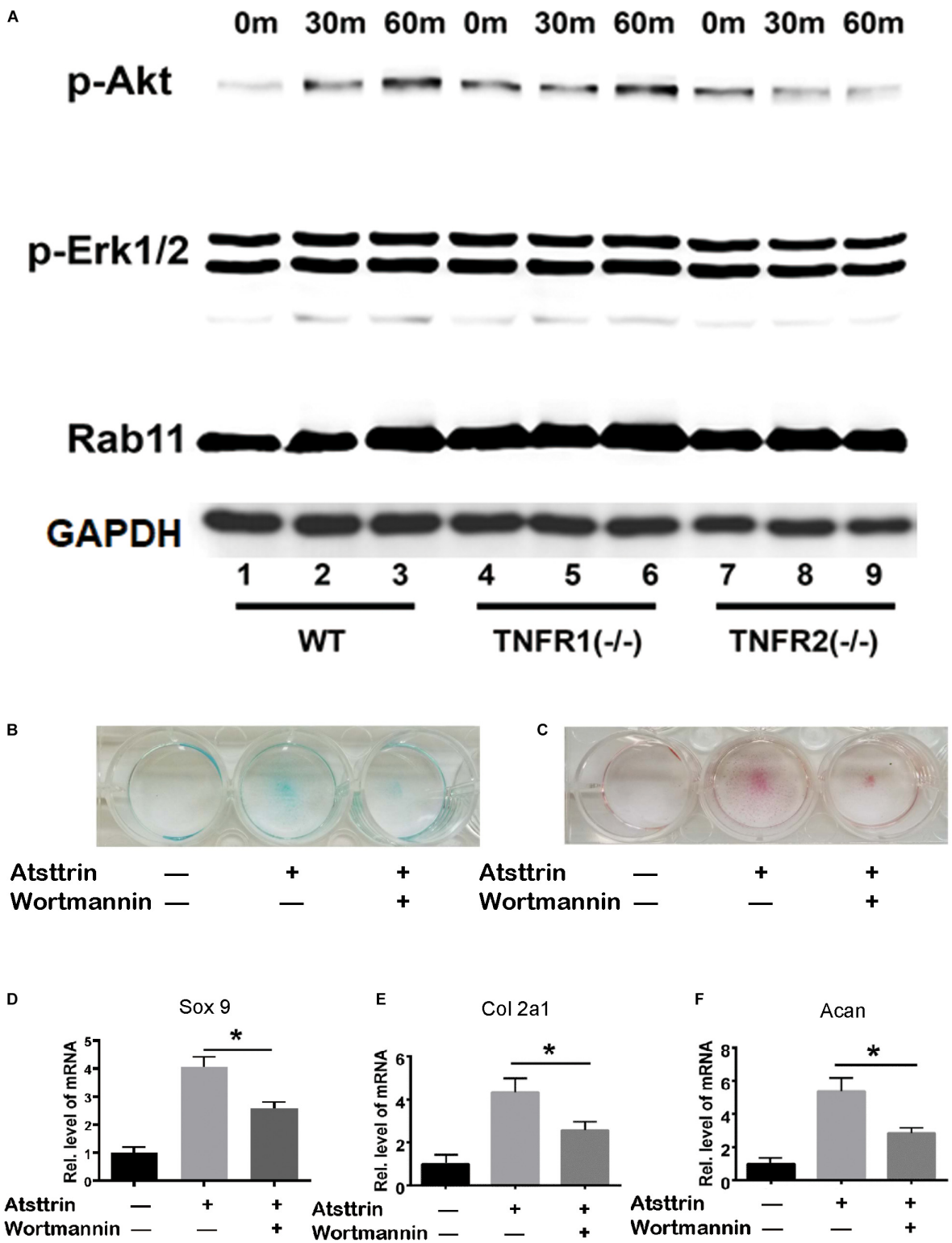

FIGURE 4 | Atsttrin-mediated chondrogenesis depended on TNFR2-Akt signaling. **(A)** Primary bone marrow stem cells were isolated from WT, TNFR1–/–, and TNFR2–/– mice, cultured in the presence of 1000 ng/mL Atsttrin, and collected at various time points, followed by Western blot analysis using PathScan Multiplex Western Cocktail I. **(B,C)** BMSCs were incubated in the absence (CTR) or presence of 1000 ng/mL Atsttrin with or without 1 μM Wortmannin for 10 days, followed by Alcian blue staining and safranin O staining. **(D–F)** BMSCs were incubated in the absence (CTR) or presence of 1000 ng/mL Atsttrin with or without 1 μM Wortmannin, and the expression of Sox9, collagen II (Col2a1), and aggrecan (Acan) was measured using real-time PCR. Values were normalized to controls, here given the value of 1. Three independent experiments were performed. *$P < 0.05$.

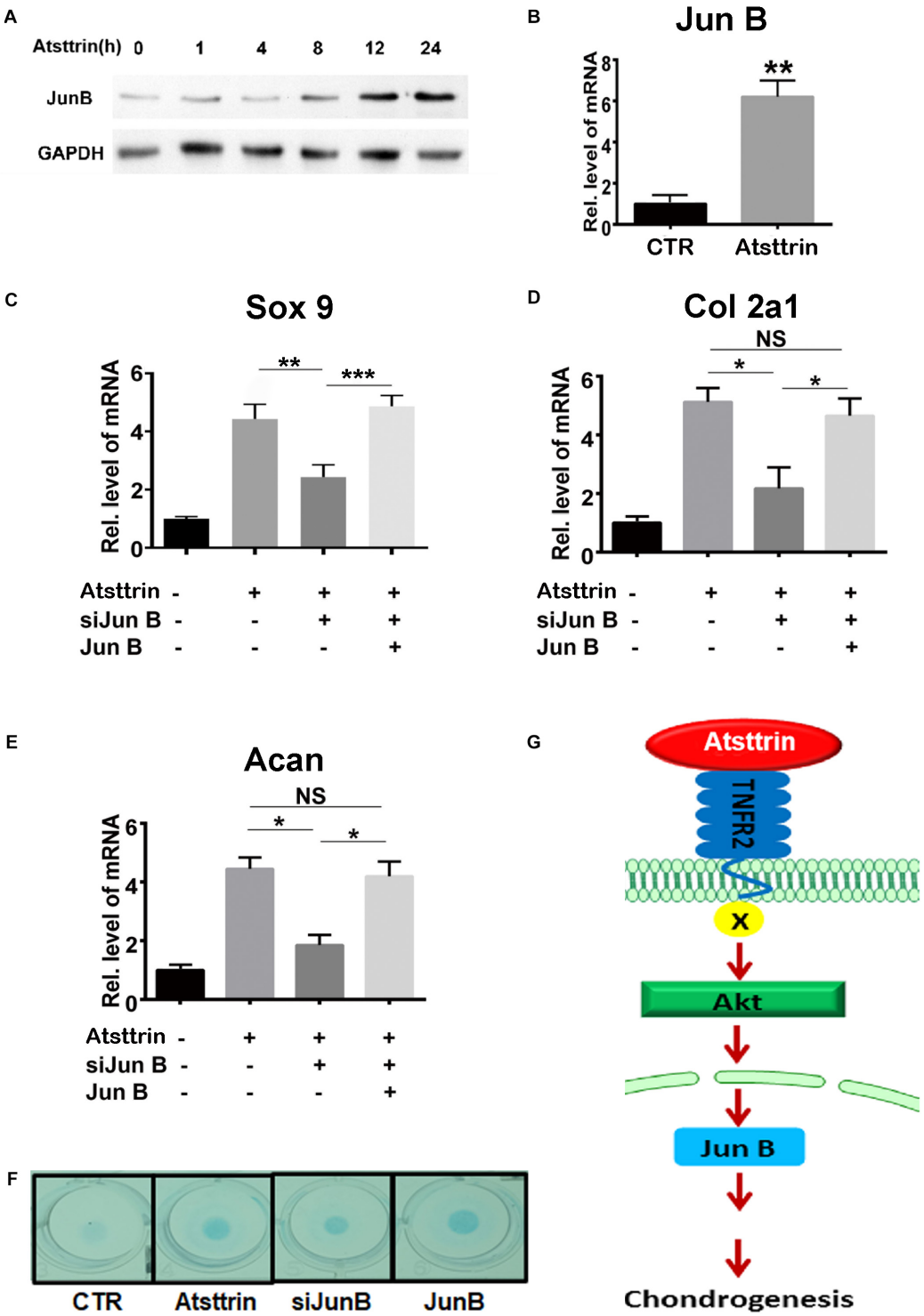

FIGURE 5 | Jun B was a downstream molecule of Atsttrin-mediated chondrogenesis. **(A)** Protein expression of Jun B in the presence of Atsttrin. C3H10T1/2 cells were micromass cultured with 1000 ng/mL Atsttrin for various time points, followed by Western blot analysis. **(B)** Transcriptional level of Jun B in C3H10T1/2 cells. C3H10T1/2 cells were micromass cultured in the absence or presence of 1000 ng/mL Atsttrin for 6 h, followed by real-time PCR. **(C–E)** Expression of Sox9, collagen II (Col2a1), and aggrecan (Acan) in C3H10T1/2 cells, which were micromass cultured in the absence or presence of 1000 ng/mL Atsttrin with or without transfection. C3H10T1/2 cells were transfected with pSuper JunB encoding an siRNA interfering with JunB expression, or a plasmid expressing JunB, or each plasmid in combination. Values were normalized to controls, here given the value of 1. Three independent experiments were performed. *$P < 0.05$. **(F)** C3H10T1/2 cells were incubated in the absence (CTR) or presence of 1000 ng/mL Atsttrin with transfected SiJunB or JunB for 10 days, followed by Alcian blue staining. **(G)** A proposed model for the role of Atsttrin in chondrogenesis.

Figure 4A, Atsttrin treatment did not activate Erk1/2 signaling in WT, TNFR1−/−, or TNFR2−/− BMSCs. Atsttrin activated Akt signaling in both WT and TNFR1−/− BMSCs, while activation was nearly abolished in TNFR2−/− chondrocytes.

BMSCs were incubated in the chondrogenic medium in the absence (CTR) or presence of 1000 ng/mL Atsttrin with or without PI3K/Akt-signaling inhibition using 1μM Wortmannin for 10 days, followed by Safranin O staining and Alcian blue staining. As indicated in **Figures 4B,C**, Atsttrin effectively promoted chondrogenesis in the absence of Wortmannin; however, the inclusion of Wortmannin remarkably reduced chondrocyte differentiation. Moreover, the transcriptional levels of Sox 9, aggrecan, and collagen II significantly increased in presence of Atsttrin and decreased in the presence of Wortmannin relative to the levels in control cells (**Figures 4D–F**). These results indicated that TNFR2/Akt signaling was integral to the chondrogenic effect of Atsttrin.

Jun B Was a Downstream Molecule of Atsttrin-Mediated Chondrogenesis

A previous study demonstrated that PGRN promoted chondrogenesis, at least in part, through the JunB transcription factor acting as a critical downstream mediator of chondrocyte differentiation (Feng et al., 2010). C3H10T1/2 cells were maintained in the micromass culture in the presence or absence of 1 μg/mL Atsttrin for various time points prior to protein or RNA collection for Western blot analysis and rtPCR, respectively, to address the potential existence of JunB as a shared downstream target of PGRN and Atsttrin. As shown in **Figure 5A**, the protein expression of JunB increased in Atsttrin-treated cells beginning at the 12-h treatment time point. As shown in **Figure 5B**, the transcriptional level of JunB also significantly increased following 6-h culture with Atsttrin. The study next determined whether silencing JunB could inhibit Atsttrin-mediated chondrogenesis by transfecting C3H10T1/2 cells with pSuper JunB encoding an siRNA (siJunB), or a plasmid overexpressing JunB, or each plasmid in combination. RNA was collected for PCR following the micromass culture in the absence or presence of Atsttrin. As indicated in **Figures 5C–E**, the transcriptional expression of Sox9, collagen II, and aggrecan significantly increased in the presence of Atsttrin. In contrast, siJunB remarkably reduced their expression. Additionally, the Atsttrin-mediated expression of Sox9, collagen II, and aggrecan were restored after JunB expression was restored. In addition, Alcian blue staining of micromasses of transfected cells with JunB overexpression and siRNA against JunB also demonstrated that JunB was required for Atsttrin-stimulated chondrogenesis (**Figure 5F**). Taken together, these results indicated that Atsttrin-mediated chondrogenesis, similar to previous observations of PGRN-stimulated chondrogenesis (Feng et al., 2010), depended on the activity of the JunB transcription factor.

DISCUSSION

The preset study examined the chondrogenic potential and underlying mechanism of PGRN-derivative Atsttrin. It was hypothesized that Atsttrin would promote chondrogenic differentiation and accelerate cartilage repair through a mechanism highly similar to that of its parent protein. Atsttrin, like PGRN, exhibited chondrogenesis-promoting capacity *in vitro* and improved cartilage repair *in vivo*. A model, wherein the generation of a full-thickness defect allowed for the entry of multipotent bone marrow − derived MSCs into the injury area, was used based on the same premise as clinically employed microfracture (Daher et al., 2009; Barry and Murphy, 2013). The stimulation of chondrogenic differentiation by Atsttrin occurred through TNFR1 and TNFR2 signaling, although TNFR2 seemed to be the major mediator of this effect as indicated by the comparative analysis of cartilage regeneration in WT, TNFR1−/−, or TNFR2−/− mice. The differentiating effects of PGRN and Atsttrin were each decisively arbitrated by JunB transcription factor activation, although the activation was achieved through different signaling pathways. Compared with the key role of Erk1/2 signaling in the chondrogenic effect of PGRN, Atsttrin relies solely on Akt signaling. The current results revealed some divergence with previous reports, as the slight activation of Erk1/2 signaling following Atsttrin treatment has been reported in chondrocytes previously [19]. However, the present results largely agree with previous findings. During the progression of arthritis, for example, Atsttrin similarly exhibited its cartilage-protective effect through both inhibiting TNFα/TNFR1-mediated inflammation and activating anabolic TNFR2 pathways [reviewed in (Wei et al., 2016)].

As parts of joints, the synovium and bone also play a non-negligible role in the development and progression of chondral defects. Atsttrin has also exhibited an anti-synovitis effect in both inflammatory and degenerative arthritis mouse models (Tang et al., 2011; Zhao et al., 2015; Wei and Liu, 2018). Recent studies also indicated that therapeutically targeting bone metabolism could mitigate osteoarthritis progression (Chu et al., 2019; Zheng et al., 2020). PGRN, as a downstream molecule of BMP-2, promoted bone formation under physiological and diabetic conditions (Zhao et al., 2013; Wei et al., 2019). A 3D-printed Atsttrin-incorporated alginate/hydroxyapatite scaffold was shown to effectively promote bone defect regeneration (Wang et al., 2015). These findings indicated that Atsttrin might also protect cartilage by reducing synovial inflammation and enhancing the strength of bone. The present study did not analyze bone or synovial tissues. Future studies should assess the potential of Atsttrin to simultaneously address the multidimensional aspects of joint injury and degeneration. Additionally, since Atsttrin was generated based on the binding capacity of PGRN-TNFRs, it was also expected that Atsttrin would lose its activities in TNFR1/2 double-deficient mice, which needs further investigation.

CONCLUSION

In conclusion, this study proposed a model for the role of Atsttrin in cartilage repair (**Figure 5G**). This model illustrated

that Atsttrin bound to TNFR2 and activated Akt signaling, followed by JunB activation, resulting in cartilage regeneration. Cumulatively, these findings not only provided new insights into the role of Atsttrin in cartilage homeostasis but also might lead to new therapeutic alternatives for cartilage damage as well as other related joint diseases.

DATA AVAILABILITY STATEMENT

The original contributions presented in the study are included in the article/**Supplementary Material**, further inquiries can be directed to the corresponding author.

ETHICS STATEMENT

The animal study was reviewed and approved by the Institutional Animal Care and Use Committee of New York University.

AUTHOR CONTRIBUTIONS

JW designed and acquired the data. KW analyzed and interpreted the data and performed the statistical analysis. AH and CL edited the manuscript. All authors drafted and reviewed the manuscript.

FUNDING

This study was supported partly by the National Natural Science Foundation of China (81900804) and the Natural Science Foundation of Shandong Province (ZR2019BH071).

SUPPLEMENTARY MATERIAL

The Supplementary Material for this article can be found online at: https://www.frontiersin.org/articles/10.3389/fcell.2020.577572/full#supplementary-material

REFERENCES

Barry, F., and Murphy, M. (2013). Mesenchymal stem cells in joint disease and repair. *Nat. Rev. Rheumatol.* 9, 584–594. doi: 10.1038/nrrheum.2013.109

Berthiaume, F., Maguire, T. J., and Yarmush, M. L. (2011). Tissue engineering and regenerative medicine: history, progress, and challenges. *Annu. Rev. Chem. Biomol. Eng.* 2, 403–430. doi: 10.1146/annurev-chembioeng-061010-114257

Chu, L., Liu, X., He, Z., Han, X., Yan, M., Qu, X., et al. (2019). Articular cartilage degradation and aberrant subchondral bone remodeling in patients with osteoarthritis and osteoporosis. *J. Bone Miner. Res.* 35, 505–515. doi: 10.1002/jbmr.3909

Cui, Y., Hettinghouse, A., and Liu, C. J. (2019). Progranulin: a conductor of receptors orchestra, a chaperone of lysosomal enzymes and a therapeutic target for multiple diseases. *Cytokine Growth. Factor. Rev.* 45, 53–64. doi: 10.1016/j.cytogfr.2019.01.002

Daher, R. J., Chahine, N. O., Greenberg, A. S., Sgaglione, N. A., and Grande, D. A. (2009). New methods to diagnose and treat cartilage degeneration. *Nat. Revi. Rheumatol.* 5, 599–607. doi: 10.1038/nrrheum.2009.204

Denker, A. E., Haas, A. R., Nicoll, S. B., and Tuan, R. S. (1999). Chondrogenic differentiation of murine C3H10T1/2 multipotential mesenchymal cells: I. Stimulation by bone morphogenetic protein-2 in high-density micromass cultures. *Differentiation* 64, 67–76. doi: 10.1046/j.1432-0436.1999.6420067.x

Detterline, A. J., Goldberg, S., Bach, B. R. Jr., and Cole, B. J. (2005). Treatment options for articular cartilage defects of the knee. *Orthopaed. Nurs.* 24, 361–368. doi: 10.1097/00006416-200509000-00012

Devitt, B. M., Bell, S. W., Webster, K. E., Feller, J. A., and Whitehead, T. S. (2017). Surgical treatments of cartilage defects of the knee: systematic review of randomised controlled trials. *Knee* 24, 508–517. doi: 10.1016/j.knee.2016.12.002

Feng, J. Q., Guo, F. J., Jiang, B. C., Zhang, Y., Frenkel, S., Wang, D. W., et al. (2010). Granulin epithelin precursor: a bone morphogenic protein 2-inducible growth factor that activates Erk1/2 signaling and JunB transcription factor in chondrogenesis. *FASEB J.* 24, 1879–1892. doi: 10.1096/fj.09-144659

Helmick, C. G., Felson, D. T., Lawrence, R. C., Gabriel, S., Hirsch, R., Kwoh, C. K., et al. (2008). Estimates of the prevalence of arthritis and other rheumatic conditions in the United States: part I. *Arthrit. Rheum.* 58, 15–25. doi: 10.1002/art.23177

Kong, L., Zhao, Y. P., Tian, Q. Y., Feng, J. Q., Kobayashi, T., Merregaert, J., et al. (2016). Extracellular matrix protein 1, a direct targeting molecule of parathyroid hormone-related peptide, negatively regulates chondrogenesis and endochondral ossification via associating with progranulin growth factor. *FASEB J.* 30, 2741–2754. doi: 10.1096/fj.201600261r

Krishnan, Y., and Grodzinsky, A. J. (2018). Cartilage diseases. *Matrix Biol.* 71–72, 51–69. doi: 10.1016/j.matbio.2018.05.005

Lawrence, R. C., Felson, D. T., Helmick, C. G., Arnold, L. M., Choi, H., Deyo, R. A., et al. (2008). Estimates of the prevalence of arthritis and other rheumatic conditions in the United States: part II. *Arthrit. Rheum.* 58, 26–35. doi: 10.1002/art.23176

Liu, C., Li, X. X., Gao, W., Liu, W., and Liu, D. S. (2014). Progranulin-derived Atsttrin directly binds to TNFRSF25 (DR3) and inhibits TNF-like ligand 1A (TL1A) activity. *PLoS One* 9:e92743. doi: 10.1371/journal.pone.0092743

Mainil-Varlet, P., Van Damme, B., Nesic, D., Knutsen, G., Kandel, R., and Roberts, S. (2010). A new histology scoring system for the assessment of the quality of human cartilage repair: ICRS II. *Am. J. Sports Med.* 38, 880–890. doi: 10.1177/0363546509359068

Matsuoka, M., Onodera, T., Sasazawa, F., Momma, D., Baba, R., Hontani, K., et al. (2015). An articular cartilage repair model in common C57Bl/6 mice. *Tissue Eng. Part C Methods* 21, 767–772. doi: 10.1089/ten.tec.2014.0440

Tang, W., Lu, Y., Tian, Q. Y., Zhang, Y., Guo, F. J., Liu, G. Y., et al. (2011). The growth factor progranulin binds to TNF receptors and is therapeutic against inflammatory arthritis in mice. *Science* 332, 478–484. doi: 10.1126/science.1199214

Tian, Q., Zhao, Y., Mundra, J. J., Gonzalez-Gugel, E., Jian, J., Uddin, S. M., et al. (2014). Three TNFR-binding domains of PGRN act independently in inhibition of TNF-alpha binding and activity. *Front. Biosci.* 19, 1176–1185.

Wang, Q., Xia, Q., Wu, Y., Zhang, X., Wen, F., Chen, X., et al. (2015). 3D-printed atsttrin-incorporated alginate/hydroxyapatite scaffold promotes bone defect regeneration with TNF/TNFR signaling involvement. *Adv. Healthc. Mater.* 4, 1701–1708. doi: 10.1002/adhm.201500211

Wei, J., Hettinghouse, A., and Liu, C. (2016). The role of progranulin in arthritis. *Ann. N. Y. Acad. Sci.* 1383, 5–20. doi: 10.1111/nyas.13191

Wei, J., Zhang, L., Ding, Y., Liu, R., Guo, Y., Hettinghouse, A., et al. (2019). Progranulin promotes diabetic fracture healing in mice with type 1 diabetes. *Ann. N. Y. Acad. Sci.* 1460, 43–56. doi: 10.1111/nyas.14208

Wei, J. L., Fu, W., Ding, Y. J., Hettinghouse, A., Lendhey, M., Schwarzkopf, R., et al. (2017). Progranulin derivative Atsttrin protects against early osteoarthritis in mouse and rat models. *Arthrit. Res. Ther.* 19:280. doi: 10.1186/s13075-017-1485-8

Wei, J. L., and Liu, C. J. (2018). Establishment of a modified collagen-induced arthritis mouse model to investigate the anti-inflammatory activity of progranulin in inflammatory arthritis. *Methods Mol. Biol.* 1806, 305–313. doi: 10.1007/978-1-4939-8559-3_20

Xia, Q., Zhu, S., Wu, Y., Wang, J., Cai, Y., Chen, P., et al. (2015). Intra-articular transplantation of atsttrin-transduced mesenchymal stem cells ameliorate osteoarthritis development. *Stem Cells Transl. Med.* 4, 523–531. doi: 10.5966/sctm.2014-0200

Zhao, Y. P., Liu, B., Tian, Q. Y., Wei, J. L., Richbourgh, B., and Liu, C. J. (2015). Progranulin protects against osteoarthritis through interacting with TNF-alpha

and beta-Catenin signalling. *Ann. Rheum. Dis.* 74, 2244–2253. doi: 10.1136/annrheumdis-2014-205779

Zhao, Y. P., Tian, Q. Y., Frenkel, S., and Liu, C. J. (2013). The promotion of bone healing by progranulin, a downstream molecule of BMP-2, through interacting with TNF/TNFR signaling. *Biomaterials* 34, 6412–6421. doi: 10.1016/j.biomaterials.2013.05.030

Zheng, W., Ding, B., Li, X., Liu, D., Yokota, H., and Zhang, P. (2020). Knee loading repairs osteoporotic osteoarthritis by relieving abnormal remodeling of subchondral bone via Wnt/beta-catenin signaling. *FASEB J.* 34, 3399–3412. doi: 10.1096/fj.201902117r

Conflict of Interest: The authors declare that the research was conducted in the absence of any commercial or financial relationships that could be construed as a potential conflict of interest.

frontiers in Cell and Developmental Biology

ORIGINAL RESEARCH
published: 06 November 2020
doi: 10.3389/fcell.2020.577662

BAFF 60-mer, and Differential BAFF 60-mer Dissociating Activities in Human Serum, Cord Blood and Cerebrospinal Fluid

*Mahya Eslami[1], Edgar Meinl[2], Hermann Eibel[3], Laure Willen[1], Olivier Donzé[4], Ottmar Distl[5], Holm Schneider[6], Daniel E. Speiser[7], Dimitrios Tsiantoulas[8], Özkan Yalkinoglu[9], Eileen Samy[10] and Pascal Schneider[1]**

[1] Department of Biochemistry, University of Lausanne, Epalinges, Switzerland, [2] Institute of Clinical Neuroimmunology, University Hospital of the Ludwig-Maximilians-Universität München, Munich, Germany, [3] Faculty of Medicine, Center for Chronic Immunodeficiency, Medical Center – University of Freiburg, Freiburg, Germany, [4] AdipoGen Life Sciences, Epalinges, Switzerland, [5] Institute for Animal Breeding and Genetics, University of Veterinary Medicine Hannover, Hannover, Germany, [6] Department of Pediatrics, Friedrich-Alexander University Erlangen-Nürnberg, Erlangen, Germany, [7] Department of Oncology, University of Lausanne, Lausanne, Switzerland, [8] Department of Laboratory Medicine, Medical University of Vienna, Vienna, Austria, [9] Clinical Pharmacology, Quantitative Pharmacology, Translational Medicine, Merck KGaA, Darmstadt, Germany, [10] Business of Merck KGaA, EMD Serono Research & Development Institute, Inc., Billerica, MA, United States

OPEN ACCESS

Edited by:
Olivier Micheau, Université de Bourgogne, France

Reviewed by:
William Stohl, University of Southern California, United States
Akshaya K. Meher, East Carolina University, United States

***Correspondence:**
Pascal Schneider
pascal.schneider@unil.ch

Specialty section:
This article was submitted to Signaling, a section of the journal Frontiers in Cell and Developmental Biology

Received: *29 June 2020*
Accepted: *15 October 2020*
Published: *06 November 2020*

Citation:
Eslami M, Meinl E, Eibel H, Willen L, Donzé O, Distl O, Schneider H, Speiser DE, Tsiantoulas D, Yalkinoglu Ö, Samy E and Schneider P (2020) BAFF 60-mer, and Differential BAFF 60-mer Dissociating Activities in Human Serum, Cord Blood and Cerebrospinal Fluid. Front. Cell Dev. Biol. 8:577662. doi: 10.3389/fcell.2020.577662

B cell activation factor of the TNF family (BAFF/BLyS), an essential B cell survival factor of which circulating levels are elevated in several autoimmune disorders, is targeted in the clinic for the treatment of systemic lupus erythematosus (SLE). The soluble form of BAFF can exist as 3-mer, or as 60-mer that results from the ordered assembly of twenty 3-mers and that can be obtained from naturally cleaved membrane-bound BAFF or made as a recombinant protein. However, which forms of soluble BAFF exist and act in humans is unclear. In this study, BAFF 3-mer and 60-mer in biological fluids were characterized for size, activity and response to specific stimulators or inhibitors of BAFF. Human cerebrospinal fluids (CSF) from patients with multiple sclerosis and adult human sera contained exclusively BAFF 3-mer in these assays, also when BAFF concentrations were moderately SLE or highly (BAFFR-deficient individual) increased. Human sera, but not CSF, contained a high molecular weight, saturable activity that dissociated preformed recombinant BAFF 60-mer into 3-mer. This activity was lower in cord blood. Cord blood displayed BAFF levels 10-fold higher than in adults and consistently contained a fair proportion of active high molecular weight BAFF able to dissociate into 3-mer but not endowed with all properties of recombinant BAFF 60-mer. If BAFF 60-mer is produced in humans, it is dissociated, or at least attenuated in the circulation.

Keywords: B-cell activating factor, cerebrospinal fluid, serum, cord blood, 60-mer, atacicept, belimumab

Abbreviations: BAFF, B cell activating factor of the TNF family; APRIL, A proliferation-inducing ligand; BAFFR, BAFF receptor; TACI, Transmembrane activator and CAML interactor; BCMA, B cell maturation antigen; SLE, systemic lupus erythematosus; CVID, common variable immunodeficiency; MS, multiple sclerosis; SEC, size exclusion chromatography; CSF, cerebrospinal fluid; FCS, fetal calf serum; BSA, bovine serum albumin.

INTRODUCTION

B cell activating factor (BAFF), a member of TNF family ligands, is a factor for the survival and development of B cells, as evidenced by the sharp reduction of peripheral B cells in BAFF-deficient mice (Schiemann et al., 2001; Craxton et al., 2005; Mackay and Schneider, 2009). Like other TNF family ligands, BAFF is a type II membrane-bound protein. It is expressed by cell types like macrophages, dendritic cells, neutrophils and monocytes, but also by stromal cells like astrocytes or carcinoma cells (Mackay et al., 2003; Krumbholz et al., 2005; Kato et al., 2006; Giordano et al., 2020). BAFF can be proteolytically processed by furin to release a soluble trimeric ligand, or can remain membrane-bound (Craxton et al., 2003; Bossen and Schneider, 2006). BAFF binds to three different receptors: BAFFR (BAFF receptor), TACI (transmembrane activator and CAML interactor) and BCMA (B cell maturation antigen), which are expressed on B lineage cells at different stages of their development (Bossen and Schneider, 2006). BAFF can form biologically active heteromers with A proliferation inducing ligand (APRIL), a related member of the TNF family (Hahne et al., 1998). Heteromers were first detected in the serum of patients with rheumatic diseases (Roschke et al., 2002). APRIL and BAFF-APRIL heteromers share with BAFF the two receptors TACI and BCMA (Schuepbach-Mallepell et al., 2015). BAFF activates non-canonical and/or canonical NF-κB pathways (Claudio et al., 2002; Hatada et al., 2003), which upregulate anti-apoptotic factors like Mcl-1 to improve B lymphocyte survival [reviewed in Mackay and Schneider (2009)]. Similar to the TNF system, in which soluble TNF is the prime activating ligand for TNFR1 while membrane-bound TNF more specifically stimulates TNFR2 (Grell et al., 1995), BAFF and APRIL receptors may respond differently to various forms of ligands. *In vitro* data indicate that, unlike BAFFR, TACI does not respond to the action of trimeric BAFF or APRIL, but requires higher order oligomers of these ligands to become activated efficiently (Bossen et al., 2008). These oligomers may mimic the action of membrane-bound ligands.

Circulating BAFF levels are elevated in patients with systemic lupus erythematosus (SLE; Zhang et al., 2001; McCarthy et al., 2013; Salazar-Camarena et al., 2016), multiple sclerosis (MS; Kannel et al., 2015; Steri et al., 2017), rheumatoid arthritis (Cheema et al., 2001), or IgA nephropathy (Xin et al., 2013; Li et al., 2014). A genetic variant of BAFF, enriched in Sardinia, results in elevated serum levels of BAFF and is associated with a risk for MS (Steri et al., 2017). Outside of Sardinia, serum levels of BAFF were found to be elevated in some (Kannel et al., 2015), but not all (Krumbholz et al., 2008) studies, but were consistently found to be elevated in response to IFN-β therapy (Krumbholz et al., 2008; Kannel et al., 2015) and rituximab (Pellkofer et al., 2008). Additionally, genetic alterations in BAFFR or TACI genes can lead to common variable immunodeficiency (CVID) which is characterized by hypogammaglobulinemia and recurrent respiratory or intestinal tract infections (Rosen et al., 1999; Warnatz et al., 2009). Individuals with BAFFR deficiency show defective B cell development and lower level of IgM and IgG. In contrast, circulating levels of BAFF are higher than in controls by one to two orders of magnitude (Warnatz et al., 2009; Kreuzaler et al., 2012). All receptors for BAFF and APRIL can be processed to soluble forms (Hoffmann et al., 2015; Laurent et al., 2015; Smulski et al., 2017). Soluble TACI and BCMA were present and shown to act as decoy receptors in SLE patients, with the result of blocking NF-κB signaling and subsequent B cell survival, at least *in vitro* (Hoffmann et al., 2015; Laurent et al., 2015). BAFF antagonists are investigated in the clinic to prevent activation of B cell-driven mechanisms that contribute to the pathology of autoimmune diseases. Belimumab (trade name Benlysta) is a human monoclonal antibody against human BAFF which has been approved for the treatment of lupus in 2011 (Hahn, 2013). Atacicept is a fully human recombinant protein in which the ligand-binding portion of the extracellular domain of TACI is fused to the Fc portion of a human IgG1 engineered not to bind Fc receptors and complement. Atacicept significantly decreased circulating B cells and antibodies in treated individuals and showed promising efficacy results in a phase IIb clinical trial on patients with active, autoantibody-positive SLE, under standard therapy (Merrill et al., 2018). Belimumab and atacicept both inhibit membrane-bound and soluble BAFF, but differ in their target specificity with regards to APRIL, BAFF-APRIL heteromers and BAFF 60-mer which are inhibited by atacicept but not by belimumab (Schuepbach-Mallepell et al., 2015; Kowalczyk-Quintas et al., 2018). BAFF 60-mer is an unusual form for a TNF family ligand in which twenty 3-mer are ordered in a pH-dependent capsid-like structure. It was discovered in 2002, when recombinant BAFF was crystallized alone or in complex with BAFFR or BCMA (Liu et al., 2002, 2003). Initial concerns that pH-dependent 60-mer formation might be an artifact of the poly-histidine tag used for purification (Zhukovsky et al., 2004) were wiped by the demonstration that untagged BAFF produced in yeast also formed 60-mer, with pH dependence being explained by the important role of a histidine residue (H218; Cachero et al., 2006). H218 is located in a unique loop of BAFF involved in BAFF-BAFF interactions and that serves two functions. The first is to allow weak and transient 3-mer to 3-mer interactions, that have no effect on receptor binding but are essential to induce productive signaling through BAFFR, probably by allowing interactions of BAFF-BAFFR complexes once BAFF has bound to receptors. This function characterized both *in vitro* and *in vivo* does not require 60-mer formation as it is not affected by mutation H218A, but is destroyed by the more "severe" E223K mutation in the flap (Vigolo et al., 2018). The second function is the formation and stabilization of BAFF 60-mer, in which each of the twenty BAFF 3-mer interacts with 3 neighbors via flap-flap interactions crucially involving His218 (Liu et al., 2002; Cachero et al., 2006; Vigolo et al., 2018). Cross-linking of BAFF with antibodies that do not interfere with receptor binding not only rescues the activity of "flap-dead" BAFF mutants, but also stimulates the activity of wild type BAFF (Kowalczyk-Quintas et al., 2016; Vigolo et al., 2018). Transition of BAFF 60-mer to BAFF 3-mer at pH $\leq$ 7 is believed to rely on protonation of His218. Atacicept can inhibit BAFF 60-mer, but belimumab cannot because its binding epitope in BAFF 60-mer is inaccessible for steric hindrance reasons (Shin et al., 2018; Vigolo et al., 2018). Given (a) the superior activity

of BAFF 60-mer over 3-mer (Liu et al., 2002, 2003), (b) its potential to stimulate receptors that BAFF 3-mer cannot (Bossen et al., 2008), (c) its differential susceptibility to clinical BAFF antagonists (Shin et al., 2018; Vigolo et al., 2018), and (d) the complete absence of data regarding its occurrence in humans, we characterized BAFF in human serum and other biological fluids making use of five criteria that are specific for BAFF 60-mer: its size, its high activity, its pH-sensitivity, its refractoriness to inhibition by belimumab and the inability to further activate its activity with cross-linking anti-BAFF antibodies. In this study, we distinguished three types of biological fluids: (i) human serum that had no or very little detectable endogenous BAFF 60-mer. On the contrary, a BAFF 60-mer inhibitory activity able to dissociate spiked recombinant 60-mer into 3-mer was present in adult human sera. Human lymph exudates behaved similarly. (ii) cerebrospinal fluid (CSF) that contained neither BAFF 60-mer nor BAFF 60-mer inhibitory activity and (iii) cord blood samples that contained low levels of inhibitory activity but all displayed a fair proportion of active, high molecular weight BAFF with the size of BAFF 60-mer. Similar to BAFF 60-mer, the specific activity of high molecular weight BAFF was higher than that of BAFF 3-mer. Also, like BAFF 60-mer, high molecular weight BAFF could dissociate into 3-mer. However, high molecular weight BAFF was recognized and inhibited by antibodies unable to bind undissociated recombinant BAFF 60-mer, suggesting either that high molecular weight BAFF is not a 60-mer, or that it is an easy-to-dissociate BAFF 60-mer. Regarding the BAFF 60-mer dissociating activity, it had a high molecular weight, was resistant to protease inhibitors and to heating at 56°C, did not bind to immobilized BAFF but was inactivated by boiling. We also describe that endogenous BAFF 3-mer does not re-associate as 60-mer, even under favorable conditions after affinity purification. Our data suggest two possible scenarios. In the first one, BAFF 60-mer does not exist *in vivo* and high molecular weight BAFF present in cord blood is part of an undefined complex. In the second one, BAFF 60-mer can form locally but is actively dissociated in adult human serum. It can persist in cord blood, but in a more labile form than recombinant BAFF 60-mer.

MATERIALS AND METHODS

Human and Animal Samples

Normal adult human serum samples and cord blood samples were as described (Podzus et al., 2017). Matched pairs of serum and plasma were collected under the approval of the Ethics Committee of the Medical University of Vienna, Austria (EK Nr: 1845/2015). Human SLE serum samples were from patients who were enrolled in the randomized, double-blind, APRIL-SLE trial, but before they received any treatment with atacicept (ClinicalTrials.gov Identifier NCT00624338). Serum sample from a BAFFR-deficient person, of a Bruton's tyrosine kinase (BTK)-deficient patient and a CVID patient were as previously described (Warnatz et al., 2009; Kreuzaler et al., 2012). CSF samples from MS patients were provided by the Institute of Clinical Neuroimmunology, Munich. This was approved by the Ethical Committee of the Medical Faculty of Ludwig-Maximilians-Universität München. Human lymphatic exudate samples were collected from three melanoma patients after sentinel lymph node surgery. Lymph was centrifuged and stored at −20°C until use (Broggi et al., 2019). For cows, sera were from purebred German Fleckvieh, Vorderwald, German Holstein cattle and from a Vorderwald by German Holstein crossbred. All animal work was conducted according to national and international guidelines for animal welfare. The Lower Saxony state veterinary office at the Niedersächsisches Landesamt für Verbraucherschutz und Lebensmittelsicherheit, Oldenburg, Germany, was the responsible Institutional Animal Care and Use Committee (IACUC) for this study. This specific study had been approved by the IACUC of Lower Saxony, the state veterinary office Niedersächsisches Landesamt für Verbraucherschutz und Lebensmittelsicherheit, Oldenburg, Germany (registration number 33.42502-05-04A247). Mouse sera were obtained by puncture of the facial vein of C57Bl6 mice according to Swiss Federal Veterinary Office guidelines, and under the authorization of the Office Vétérinaire Cantonal du Canton de Vaud (authorization 1370.7 to PS). Blood was incubated for 2 h at 37°C, spun at 13,000 rpm for 15 min at 4°C and supernatant was collected.

Proteins and Antibodies

Belimumab (registered trade name Benlysta) and etanercept (TNFR2-Fc, registered trade name Enbrel) were bought from the Pharmacy of Lausanne University Hospital (CHUV). Rat IgG2b anti-human BAFF monoclonal antibody 2.81 (Kreuzaler et al., 2012) was from Adipogen (#AG-20B-0018-C100). Mouse IgG anti-APRIL monoclonal antibody 104 was co-developed with and provided by Adipogen. Its characterization will be described in detail elsewhere. Mouse IgG1 anti-SHH 5E1 (Wang et al., 2000) was purified from hybridoma supernatants obtained from Developmental Studies Hybridoma Bank (University of Iowa, Department of Biology, Iowa City, IA, United States). Rat IgM anti-human BAFF monoclonal antibody Buffy2 was as described (Schneider et al., 1999). Atacicept was provided by Merck KGaA. Fc-BAFF and BCMA-Fc were stably transfected and produced in CHO cells and affinity-purified on Protein A-Sepharose as previously described (Schneider, 2000), or were from Adipogen [Fc-BAFF, AG-40B-0120 and BCMA(h):Fc(h), AG-40B-0080]. Fc-BAFF, atacicept, belimumab, mAb 104, and mAb 5E1 were coupled at 2 (Fc-BAFF, 104, 5E1) or 5 mg/ml (atacicept, belimumab, etanercept) to N-hydroxysuccinimide (NHS)-Sepharose beads (GE Healthcare #90-1004-00) according to manufacturer's instructions. An expression plasmid for Flag-BAFF was transiently transfected in 293T cells with the polyethyleneimide method (Tom et al., 2008). 7 days later, 400 ml of conditioned supernatants in serum-free OptiMEM medium were purified on a 1 ml column of atacicept-coupled Sepharose, eluted with 50 mM citrate-NaOH pH 2.7, neutralized with 1 M Tris–HCl pH 9, and buffer was exchanged for PBS by ultrafiltration in a centrifugal device with 30 kDa cut off (Amicon Ultra-4, Merck Millipore, #10210342). Flag BAFF forms exclusively 3-mer. It was not further purified by size exclusion chromatography (SEC). It was quantified by absorbance at 280 nm using an extinction coefficient of 16055 M^{-1} cm^{-1}

(absorbance at 1 mg/ml of 0.866). Naturally cleaved BAFF (wt, H218A or E223K) in about 15 ml of conditioned cell supernatants of transfected 293T cells was affinity purified on 12 µl of atacicept-coupled Sepharose beads and size fractionated by SEC in 20 mM Hepes, 130 mM NaCl, 10 µg/ml BSA, pH 8.2. Fractions corresponding to BAFF 60-mer (8–10 ml) and BAFF 3-mer (14–16 ml) were pooled, aliquoted and stored at −70°C until use. Naturally cleaved BAFF 60-mer and 3-mer were quantified by BAFF ELISA with a capture step at pH 5.5 (see section "ELISA"). 3-mer fractions of BAFF mutants H218A and E223K were quantified by Western blot using purified His-BAFF 60-mer as a standard and mAb Buffy2 to reveal. His-BAFF 60-mer expressed in Escherichia *coli* was from Adipogen (AG-40B-0112-C010). All plasmids used in this study are listed in **Supplementary Table 1**.

Cell Lines

HEK 293T cells were obtained from late Jürg Tschopp (University of Lausanne) and grown in DMEM 10% FCS. Jurkat JOM2 BAFFR:Fas-2308 cl21 and Jurkat BCMA:Fas-2309 clone 13 reporter cells were described previously and were grown in RPMI 10% FCS (Bossen et al., 2008; Nys et al., 2013; Schneider et al., 2014; Schuepbach-Mallepell et al., 2015). CHO-S cells were from Thermoscientific (A1155701). CHO-S-2825 clone G5 expressing Fc-BAFF was obtained by transfection of CHO-S cells by the polyethyleneimide method, selection by 3 passages in 500 µg/ml of G418 sulfate (Calbiochem, 345812) and cloning by limiting dilution. The clone with highest production as assessed by Western blot with horseradish peroxidase-coupled goat anti-human Fc antibodies was selected for production.

Cytotoxic Assay

The activity of endogenous or recombinant BAFF was measured using Jurkat BCMA:Fas-2309 clone 13 or Jurkat JOM2 BAFFR:Fas-2308 clone 21 reporter cells (Schneider et al., 2014). In flat-bottomed 96 well cell culture plates, samples were serially diluted as indicated into a final volume of 50 µl of RPMI, 10% FCS. Then, 50 µl of reporter cells (20'000–50'000/well) in the same medium were added and incubated overnight (∼16 h) at 37°C, 5% CO_2, after which time cell viability was monitored by addition of 20 µl of PMS/MTS (phenazine methosulphate at 45 µg/ml and 3-(4,5-dimethylthiazol-2-yl)-5-(3-carboxymethoxyphenyl)-2-(4-sulfophenyl)-2H-tetrazolium at 2 mg/ml in PBS) and measuring absorbance at 492 nm after 2–8 h (Nys et al., 2013; Schneider et al., 2014; Schuepbach-Mallepell et al., 2015). When tests were performed in the presence of modifiers of BAFF activity (atacicept, belimumab, or anti-BAFF 2.81), modifiers at 10-fold the desired final concentration in 10 µl of RPMI 10% FCS were added, followed by reporter cells in a volume of 40 µl instead of 50 µl. When tests were performed to measure the inhibitory activity of serum or other biological fluids on recombinant BAFF 60-mer, 2 µl of sera or fluid were added per well, unless stated otherwise. In some instances, serum was heated for 30 min at 56°C. In other instances, size exclusion chromatography fractions of normal human serum were heated for 5 min at 95°C, then spun for 15 min at 13,000 rpm in a tabletop centrifuge to remove precipitated proteins, and supernatant were used in the assay. Where indicated, one-fold concentrated protease inhibitor cocktail (Sigma, "cØmplete," 11697498001) was added to serum prior to the assay. Reporter cells were not affected by this concentration of protease inhibitors in the time frame of the assay. Optionally, antibiotics (Invitrogen, 15070–063) were added in samples or cells to have a final concentration of 50 U/ml streptomycin and 50 µg/ml penicillin, in particular when non-sterile samples were tested, such as size exclusion chromatography fractions. For the estimation of the percentage of high molecular weight BAFF at the activity level after size exclusion chromatography, EC_{50} expressed in µl of fraction was first determined for fractions 9, 14, and 15, then the following calculation was performed: % high molecular weight BAFF activity = [(1/EC_{50} of fraction 9)/(sum of (1/EC_{50}) of fractions 9, 14, and 15)] × 100.

BAFF ELISA

Endogenous or recombinant human BAFF was quantified using BAFF (human) ELISA kit from Adipogen (#AG-45B-0001-KI01) according to the manufacturer's protocol, using 2.5 µl or 10 µl of human sera as indicated, or 3 µl of serum from cord blood, or 100 µl of human CSF samples. For SEC fractions, adjusted volumes were used for the BAFF ELISA (**Supplementary Table 2**). The capture step was performed in ELISA buffer provided with the kit (pH 7.4). When indicated, for the detection of BAFF 60-mer, the capture step was performed for 3 h at room temperature in MES [2-(N-morpholino)ethanesulfonic acid] buffer pH 5.5. For this purpose, suitable amounts of 0.5 M MES pH 5 were added to samples prior to the capture step of the ELISA. This amount was determined for each type of buffer by controlling pH on a pH paper with a 0.5 pH unit scale. For the measurement of endogenous BAFF in 200 µl cord blood right after size exclusion chromatography, 150 µl of 1 ml fractions were immediately captured for 30 min at 4°C and pH 7.4 or pH 5.5. For the estimation of the percentage of high molecular weight BAFF at the protein level, the following calculation was performed: % high molecular weight BAFF protein = [signal in fraction 9/(sum of signals in fractions 9, 14, and 15)] × 100.

Size-Exclusion Chromatography

A dedicated Superdex S200 Increase HR 10/30 columns was used for the analysis of samples containing endogenous BAFF, and another for samples containing recombinant BAFF. This can explain small differences in the retention time of standards. Size-exclusion chromatography with 200 to 400 µl of samples was performed at a flow rate of 0.65 ml/min in 20 mM Hepes, 130 mM NaCl, pH 8.2. For diluted samples in the absence of a protein matrix, 10 µg/ml bovine serum albumin was added in the buffer. For samples with low endogenous BAFF levels requiring subsequent lyophilization, 10 mM Hepes, 30 mM NaCl, 10 µg/ml BSA, pH 8.2 was used. Fractions of 1 ml were collected. Lyophilized fractions were suspended into 100 or 200 µl of water to get 10-fold or 5-fold concentrated fractions, including salts and buffer. When indicated, pooled fractions were concentrated using 30 kDa cut off centrifugal concentration devices to a volume of about 300 µl prior to re-injection. Columns were calibrated with 100 µl of a mixture of protein standards, all at 1.4 mg/ml (except ferritin at 140 µg/ml): thyroglobulin (669 kDa), ferritin

(440 kDa), aldolase (158 kDa), ribonuclease A (13.7 kDa; all from GE Healthcare), bovine serum albumin (67 kDa), ovalbumin (43 kDa), carbonic anhydrase (29 kDa), and aprotinin (6.5 kDa; all from Sigma-Aldrich).

Immunoprecipitation

To purify or deplete endogenous or recombinant BAFF from human serum, CSF or other samples, samples were mixed with 20 μl of a 50% slurry in PBS of NHS-Sepharose beads coupled to the desired protein or antibody, and incubated overnight at 4°C on a rotating wheel. Beads were centrifuged for 5 min at 5,000 rpm (2,400 × *g*). The unbound fraction was collected, while beads were washed 3 times with 100 μl of PBS in mini columns (Schneider et al., 2014) and eluted with 30 μl of 50 mM citrate-NaOH pH 2.7. The eluate was neutralized with 10 μl of 1 M Tris–HCl pH 9.

Western Blot

Sodium dodecyl sulfate polyacrylamide gel electrophoresis (SDS-PAGE) of 12% acrylamide gels and Western blot on nitrocellulose membranes were performed according to standard protocols. His-BAFF-60mer at 50, 25, 12.5, and 6.25 ng per lane was used as a standard. Membrane were revealed with Buffy2 at 1 μg/ml, followed by horse radish peroxidase-coupled goat anti-rat IgM, μ chain specific (Jackson ImmunoResearch, 112-035-075) at 1/8000 and ECL. Concentrations of naturally cleaved BAFF H218A and E223K were estimated by comparing band intensities. The same Western blot procedure was used to reveal naturally cleaved BAFF in fractions of size exclusion chromatographies.

Statistics

Statistics were performed with Prism 8 (GraphPad Software). Normal distribution of data was assessed with D'Agostino Pearson normality test for $n \geq 8$, or assumed to be so for $n < 8$. Standard deviations were not assumed to be equal and comparisons of multiple groups was performed by Brown-Forsythe and Welch ANOVA test, followed by Dunnett T3 multiple comparison tests. For the comparison of 2 groups, *t*-test with Welch's correction was used. Differences were considered significant when $P < 0.05$. To determine the EC_{50} of titration curves, cell viability was first normalized, then fitted with the "Non-linear regression (curve fit)" followed by the "log(agonist) vs. normalized response-variable slope" functions of Prism 8 (GraphPad Software).

RESULTS

Elevated BAFF in BAFFR-Deficient Human Serum Is Exclusively in a Trimeric Form

Serum samples collected at different times from a BAFFR-deficient individual displayed BAFF levels by ELISA that were on average 500-fold higher than those of controls and 50-fold higher than those of SLE patients (**Figure 1A**). BAFF in BAFFR-deficient serum, but not normal serum, was detectable in a cell-based activity assay, in which target cells are Jurkat T cells expressing the chimeric receptor BCMA:Fas (**Figure 1B**). These cells divert BAFF (and APRIL) signals into death via the intracellular domain of the apoptosis-inducing receptor Fas. Endogenous BAFF and APRIL in normal human serum were under the detection limit (**Figure 1B**). As APRIL levels are not elevated in BAFFR-deficient serum (unpublished observation), APRIL likely did not contribute to signal in this experiment, as will be confirmed later with BAFF-specific reporter cells. The human BAFFR-deficient serum was thus used to investigate the ratio of activity associated with BAFF 3-mer and BAFF oligomers after a size-fractionation performed at pH 8.2, a pH that is favorable to BAFF 60-mer (Cachero et al., 2006). BAFF activity was recovered in late fractions (15–17). No activity was detected in early fractions (9 and 10) that would correspond to BAFF 60-mer (**Figures 1C,D**). To test the hypothesis that BAFF assembly into 60-mer at pH 8.2 might be a slow process, fractions 15–17 were pooled, concentrated and size-fractionated again at pH 8.2, but BAFF activity still eluted in late fractions (**Figure 1E**). The theoretical molecular weight of naturally processed BAFF is 51 kDa (3 × 17 kDa), and calibration markers indicated an apparent size of 46 kDa for endogenous BAFF activity (2.7-mer). Under identical conditions, a recombinant His-BAFF that was undoubtedly trimeric by electron microscopy and crystallization also eluted as an apparent 2.7-mer relative to molecular weight markers (Vigolo et al., 2018). Taken together, these results indicate that endogenous BAFF in BAFFR-deficient serum is present as 3-mer, and that the absence of 60-mer is not a consequence of a potentially inadequate pH of serum.

Human Serum Contains a High Molecular Weight Inhibitory Activity for BAFF 60-mer

We wondered whether BAFF 60-mer activity would have been detected if present in serum. Thus, the activity of recombinant His-BAFF 60-mer (Vigolo et al., 2018) spiked into normal human serum was measured, but this time on BAFFR:Fas reporter cells that are more sensitive to BAFF and, unlike BCMA:Fas reporter cells, cannot respond to APRIL. The activity of BAFF 60-mer was decreased by up to two orders of magnitude when it was spiked into normal human serum compared to 60-mer spiked into fetal calf serum (**Figure 2A**). This could have been due to the presence of shed soluble BAFFR, TACI, and/or BCMA, all of which have been described (Hoffmann et al., 2015; Laurent et al., 2015; Smulski et al., 2017), but pre-depletion of serum on beads coupled to recombinant Fc-BAFF, which could remove soluble TACI, BAFFR, and BCMA (**Supplementary Figure 1**), did not alter the inhibitory activity (**Figure 2A**). After serum concentration using an ultrafiltration device with 30 kDa cut off, and exchange of the serum matrix for PBS, all 60-mer inhibitory activity was recovered and enriched in the retained fraction, and none passed into the low molecular weight fraction (**Figure 2B**). In line with these results, the inhibitory activity recovered after size-exclusion chromatography was in the high-molecular weight fractions, and not in smaller molecular weight Ig- or albumin-containing fractions (**Figures 2C,D**). It was

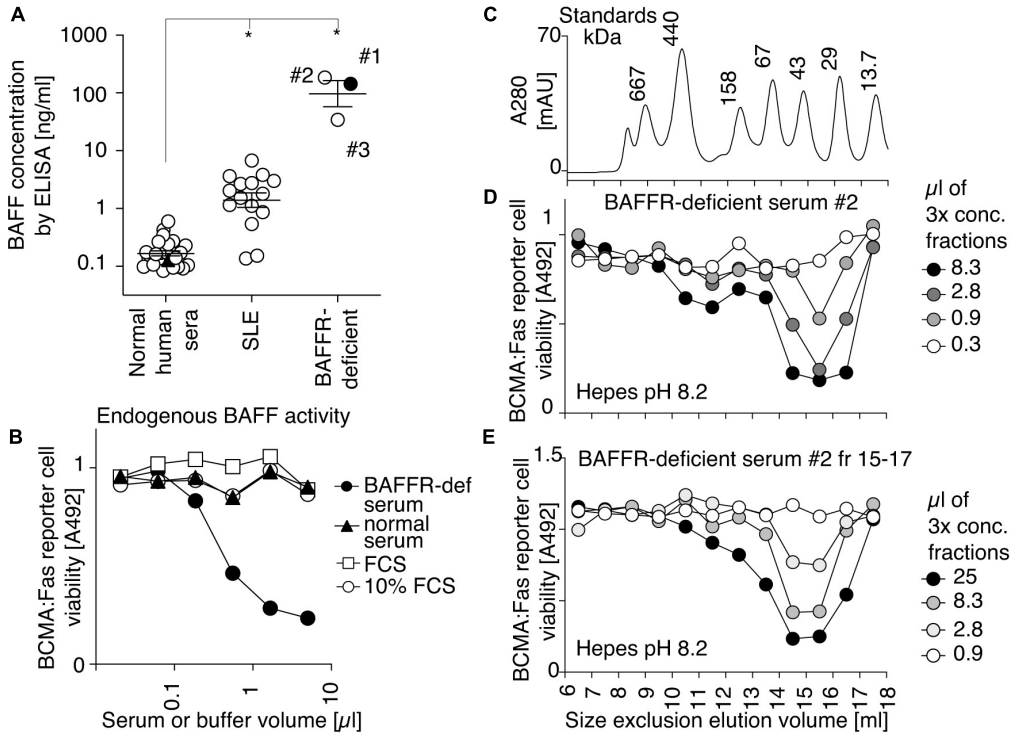

FIGURE 1 | Endogenous BAFF activity in serum of a BAFFR-deficient person has the size of a 3-mer. **(A)** Concentrations of endogenous BAFF measured by ELISA in 2.5 µl of normal human sera, in sera of SLE patients and in three independent serum samples of a BAFFR-deficient person. * indicates significant ($P < 0.001$) difference with the control group of normal human sera by one-way ANOVA with Bonferroni's multiple comparison test. One experiment out of three with comparable results is shown. **(B)** The activity of endogenous BAFF in the indicated volume of BAFFR-deficient and normal human serum, or in foetal calf serum (FCS), or in culture medium (10% FCS) was monitored with BCMA:Fas reporter cells. The final assay volume was 100 µl. Cell viability was measured with the PMS/MTS assay. This experiment was performed twice in this format, and three more times on similar reporter cells (BAFFR:Fas). **(C)** A mixture of molecular weight markers (top panel) was fractionated by SEC in Hepes buffer pH 8.2, and detected by on-line monitoring of absorbance at 280 nm. **(D)** a BAFFR-deficient human serum was fractionated by SEC in Hepes buffer pH 8.2. Fractions were concentrated 3-fold by ultrafiltration and BAFF activity in each fraction was monitored by its ability to kill BCMA:Fas reporter cells. The experiment was performed three times (plus once with a different readout). **(E)** Fractions 15–17 of the chromatography shown in panel **(D)** were pooled, concentrated by ultrafiltration, fractionated again by SEC, and analyzed for BAFF activity as shown in panel **(D)**. This experiment was performed once.

abolished by heating at 95°C (**Figure 2E**), but resisted heating at 56°C (**Supplementary Figure 2A**) and was unaffected by a cocktail of protease inhibitors (**Supplementary Figure 2B**). The inhibitory activity was consistently found in adult human sera and plasma (**Supplementary Figure 2C**), and in sera of adult cows (**Figure 2F**). It was present in varying amounts in sera obtained from human cord blood, but usually lower than in adult sera (**Figure 2G**). It was particularly low in two cord blood samples of pre-term babies born at gestational weeks 28 or 29 (**Figure 2H**). It was not present in fetal calf serum and adult mouse sera (**Figure 2I**).

A BAFF ELISA Recognizes BAFF 60-mer Only When BAFF Is Captured at pH 5.5

Purified recombinant Flag-BAFF was eluted by size-exclusion chromatography at a size of 67 kDa, slightly higher than its theoretical size of 56 kDa (3.6-mer). It was recognized in the BAFF ELISA at both pH 7.4 and pH 5.5 (**Figures 3A,B**). In contrast, His-BAFF 60-mer, and the 60-mer fraction of naturally processed full-length BAFF in supernatants of transfected 293T cells, were not recognized at pH 7.4 and only detected at pH 5.5 (**Figures 3C–E**). This probably indicates that a concealed epitope in BAFF 60-mer becomes available for capture upon acid-dissociation. Thus, the capture of BAFF at pH 5.5 is mandatory to detect BAFF 60-mer.

The BAFF 60-mer Inhibitory Activity of Human Serum Dissociates BAFF 60-mer Into 3-mer and Is Saturable

BAFF 60-mer spiked into Hepes buffer at pH 8.2 or in human serum was size-fractionated by size-exclusion chromatography and detected in fractions by ELISA at pH 5.5 and by its activity on BAFFR:Fas reporter cells. In Hepes buffer, both protein and activity eluted in high molecular weight fractions, as expected for BAFF 60-mer (**Figures 4A,B**), but when spiked into serum, BAFF 60-mer protein was recovered at the size of BAFF 3-mer, while the leftover activity was still mainly 60-mer and partially 3-mer, suggesting that highly active 60-mer was almost entirely dissociated to less active 3-mer by exposure

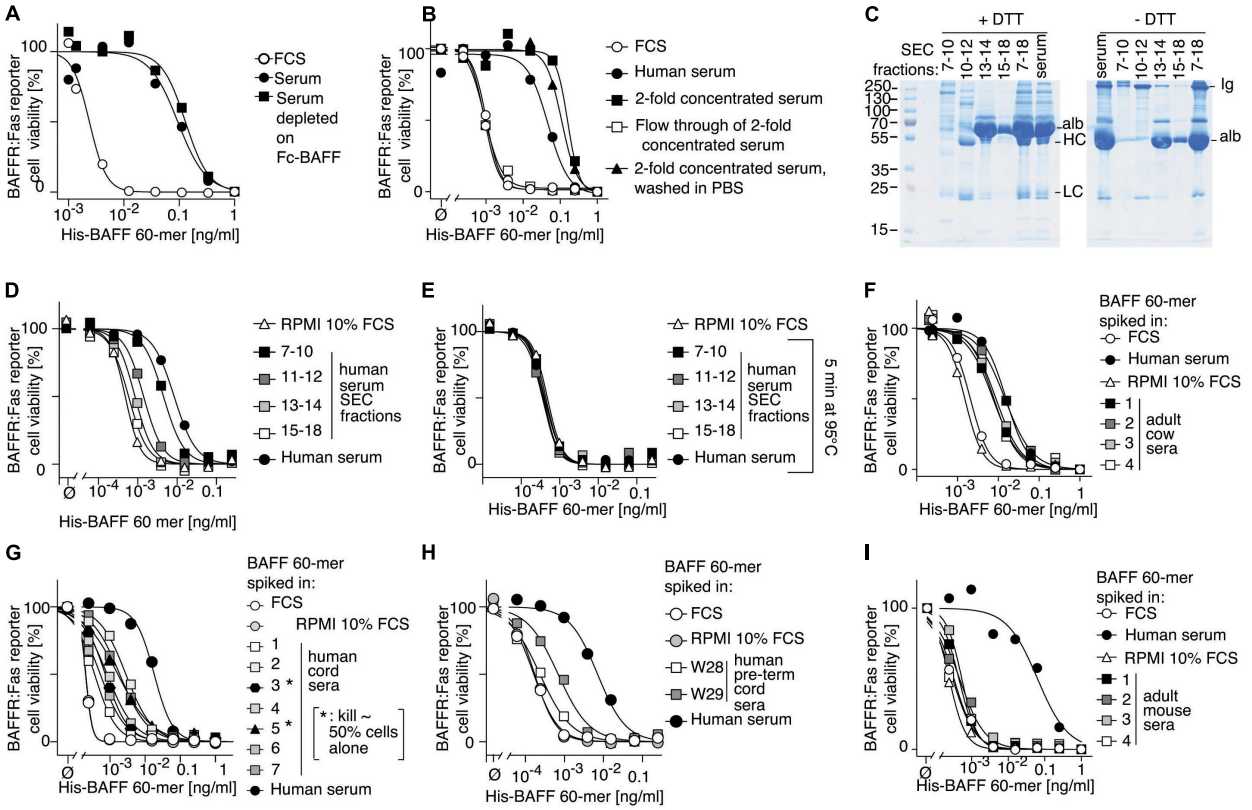

FIGURE 2 | Human serum contains a BAFF 60-mer inhibitory activity. **(A)** Recombinant His-BAFF 60-mer was titrated on BAFFR:Fas reporter cells in the presence of a constant amount of FCS (10%), or of normal human serum, or of normal human serum depleted on Fc-BAFF-coupled Sepharose beads. After an overnight incubation, cell viability was monitored. The experiment was performed three times. **(B)** Normal human serum was concentrated 2-fold by ultrafiltration, then washed with PBS by ultrafiltration. FCS, normal serum, 2-fold concentrated normal serum before and after wash with PBS, and the filtrated fraction of normal serum were tested on BAFFR:Fas reporter cells as described in panel **(A)**. The experiment was performed four times. **(C)** 400 μl of normal serum was size-fractionated by SEC. The indicated fractions were pooled, concentrated to 400 μl, and 1 μl was analyzed by SDS-PAGE and Coomassie blue staining under reducing (+DTT) or non-reducing conditions (-DTT). This experiment was performed twice. **(D)** Serum fractions as shown in panel **(C)** were analyzed for their BAFF 60-mer inhibitory activity as described in panel **(A)**. The experiment was performed four times. **(E)** Same as panel **(D)**, except that supernatants of fractions heated for 5 min at 95°C were analyzed. The result with medium only is the same as in panel **(D)**. **(F–I)** four adult cow sera **(F)**, 7 sera from human cord blood **(G)**, two sera from cord blood of pre-term babies at gestational weeks 28 and 29 **(H)** and 4 adult mouse sera **(I)** were analyzed with the indicated controls as described in panel **(A)**. In panel **(G)**, 3* and 5* indicate that cord sera 3 and 5 contained an intrinsic BAFF activity that killed about 50% of reporter cells in the absence of BAFF 60-mer. Experiment **(E)** was performed once. Experiments **(F)**, **(G)**, and **(I)** were performed three times each, and experiment **(H)** was performed twice.

to human serum (**Figures 4C,D**). If serum inhibits BAFF 60-mer by dissociation, then non-dissociable BAFF oligomers such as hexameric Fc-BAFF should be unaffected by serum. Indeed, human serum inhibited BAFF 60-mer in a concentration-dependent manner (**Figure 5A**), but did not affect the activity of Fc-BAFF (**Figure 5B**). To demonstrate whether the BAFF 60-mer inhibitory activity was saturable, increasing concentrations of BAFF 60-mer were spiked into a fixed volume of human serum, and then size fractionated. BAFF was then detected by ELISA at pH 5.5 in adequately diluted fractions, and the percentage of total BAFF in each fraction was calculated. BAFF 60-mer spiked into buffer at pH 8.2 eluted as 60-mer (**Figure 5C**). When 60-mer was spiked at 100 ng/ml in human serum, almost all of it dissociated to BAFF 3-mer. At 7 μg/ml, only about half dissociated into 3-mer, whereas at 500 μg/ml, almost all of it remained 60-mer (**Figure 5D**). We take these results as a strong indication that although the BAFF 60-mer-dissociating activity in human serum is limited and saturable, it is very high (EC_{50} of about 7 μg/ml) compared to usual circulating BAFF levels.

Recombinant BAFF 60-mer Activity Resists Affinity Purification but Is Irreversibly Attenuated in Normal Human Serum

To test whether attenuation of BAFF 60-mer activity in human serum is a reversible process, the activity of BAFF 60-mer spiked into different matrices was analyzed before and after affinity purification procedures on immobilized TACI-Fc (atacicept) or belimumab. BAFF 60-mer bound efficiently to atacicept but not to belimumab. About 10% of atacicept-bound BAFF 60-mer activity was recovered after acid elution, neutralization, and buffer exchange to Hepes pH 8.2 (**Supplementary Figure 3**). However, when BAFF 60-mer was spiked into human serum,

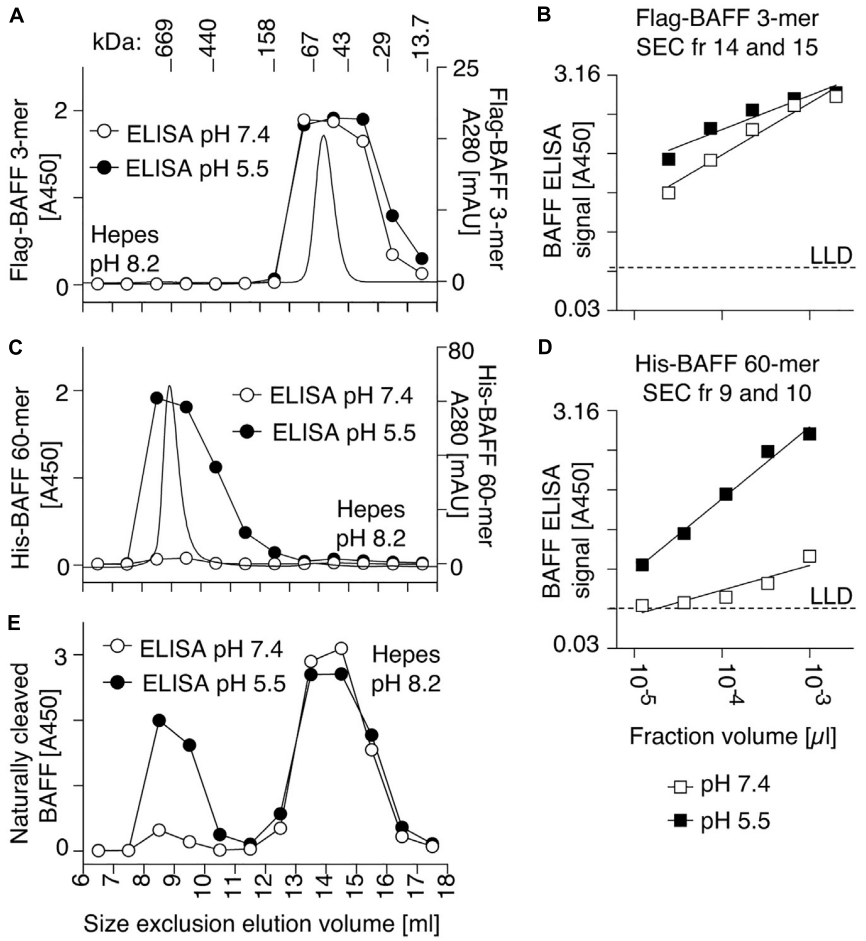

FIGURE 3 | A human BAFF ELISA detects BAFF 60-mer at pH 5.5 but not at pH 7.4. **(A)** 50 μg of Flag BAFF 3-mer was fractionated by SEC at pH 8.2 and detected by on-line UV monitoring (thin line). Fractions were tested by BAFF ELISA with the capture step performed at pH 7.4 (white circles) or pH 5.5 (black circles). **(B)** Titration of Flag-BAFF 3-mer from SEC fractions 14 + 15 measured by BAFF ELISA with capture at pH 7.4 (white squares) or pH 5.5 (black squares). LLD: lowest limit of detection. **(C,D)** Same as panels **(A,B)**, but with 100 μg of His-BAFF 60-mer and His-BAFF 60-mer from SEC fractions 9 + 10. Experiments of panels **(A–D)** were performed once in this format, but pH sensitive detection of BAFF 60-mer was confirmed in 3 more experiments in different formats. **(E)** Same as panels **(A)**, but with naturally cleaved BAFF in concentrated supernatants of 293T cells transfected with full length human BAFF, and with 10 μg/ml BSA in buffer. The experiment was performed twice.

very little activity was recovered after affinity purification on atacicept and buffer exchange to Hepes pH 8.2, suggesting that serum inhibition of BAFF 60-mer is irreversible and cannot be reversed by removing serum and reverting back to 60-mer-friendly conditions (**Supplementary Figure 3**).

Human Cerebrospinal Fluid Contains BAFF but no BAFF 60-mer Inhibitory Activity

Owing to its inhibitory activity, human serum might not be the right place to detect BAFF 60-mer. Human lymph exudate also inhibited BAFF 60-mer activity (**Figure 6A**), although we cannot exclude that this could be due to contaminating serum. In contrast, CSF of three patients with MS did not inhibit BAFF 60-mer activity, while their corresponding sera did (**Figures 6B,C**). The absence of BAFF-inhibitory activity was confirmed in four more CSF samples (**Figure 6D**) that all contained low but detectable levels of endogenous BAFF (**Figure 6E**). After concentration of pooled CSF samples, an atacicept inhibitable BAFF activity was indeed detectable using BAFFR:Fas reporter cells (**Figure 6F**), raising the possibility that BAFF 60-mer may exist in CSF.

BAFF in Human Cerebrospinal Fluid Forms 3-mer

Pooled CSF samples were concentrated, fractionated by size exclusion chromatography at pH 8.2 and assayed for BAFF content by ELISA at pH 5.5 and on BAFFR:Fas reporter cells. Both assays exclusively detected BAFF at the size of a 3-mer, while a positive control of BAFF 60-mer analyzed under the same conditions eluted with the expected high molecular weight (**Figures 7A–D**). We hypothesized that a portion of BAFF

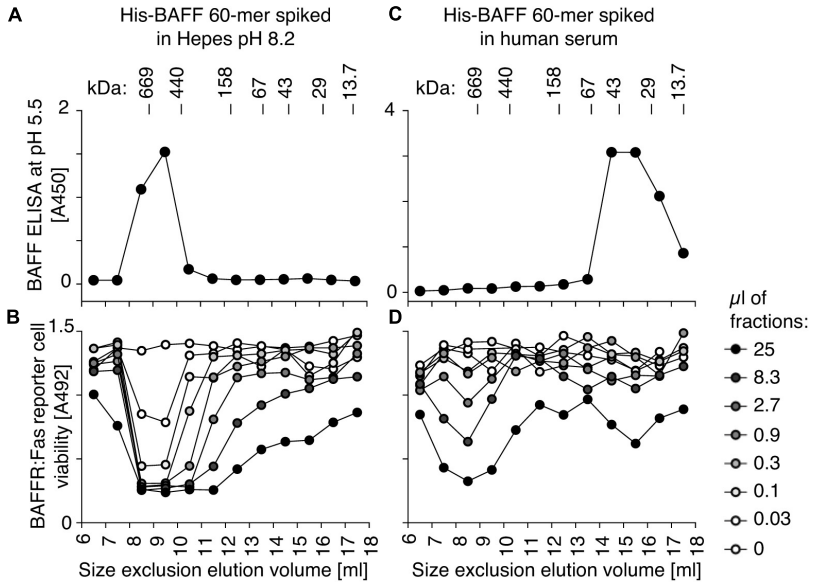

FIGURE 4 | Human serum dissociates His-BAFF 60-mer into less active 3-mer. **(A)** 40 ng of His-BAFF 60-mer in Hepes pH 8.2, 50 µg/ml BSA was size fractionated by SEC and the presence of BAFF in 70 µl of fractions was analyzed by BAFF ELISA with capture at pH 5.5. **(B)** The indicated volumes of the same factions as in panel **(A)** were analyzed for their activity on BAFFR:Fas reporter cells. **(C,D)** Same as panels **(A,B)**, except that the same amount of BAFF 60-mer was spiked into 400 µl of normal human serum at pH ∼8 prior to fractionation by SEC at pH 8.2. The experiments of panels **(A,C)** were performed 3 times, and those of panels **(B,D)** twice.

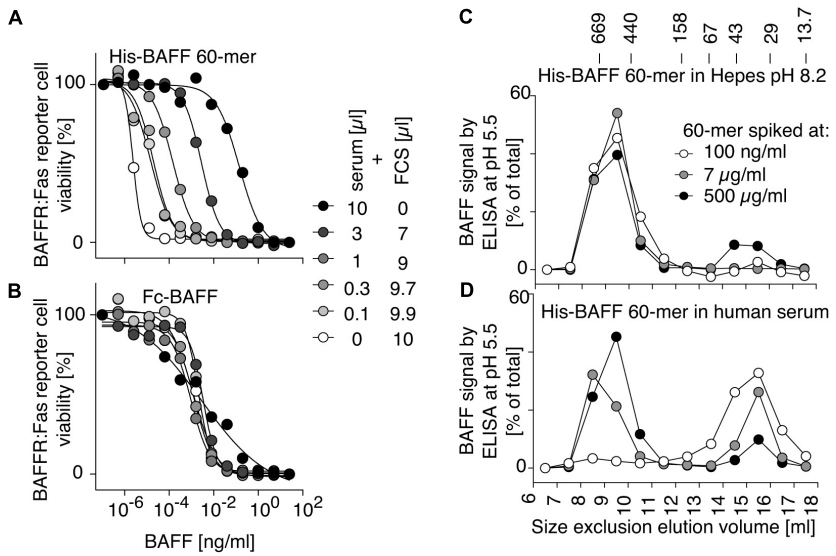

FIGURE 5 | BAFF 60-mer dissociation activity of human serum is saturable. **(A)** The inhibitory activity of normal human serum mixed with FCS at the indicated ratio on His-BAFF 60-mer was tested on BAFFR:Fas reporter cells. **(B)** Same as panel **(A)**, but using Fc-BAFF instead of His-BAFF 60-mer. The experiments of panels **(A,B)** were performed three times. **(C)** His-BAFF 60-mer spiked at 0.1 (white circles), 7 (gray circles), or 500 µg/ml (black circles) in 400 µl of Hepes buffer at pH 8.2 was size-fractionated by SEC at pH 8.2 and analyzed in adequately diluted fractions by BAFF ELISA with capture at pH 5.5. Data is normalized to the total signal in fractions 7 to 18 for each individual run. **(D)** Same as panel **(C)**, except that His-BAFF 60-mer was spiked into 400 µl of normal human serum. The experiment of panels **(C,D)** was performed twice.

in CSF could be engaged into BAFF-APRIL heteromers that would inhibit 60-mer formation, but after passage of CSF on an immobilized anti-APRIL antibody able to deplete BAFF-APRIL heteromers, BAFF was still present as 3-mer in CSF (**Figures 7E,F**). When endogenous BAFF present in CSF or in a BAFF-high serum sample (from a patient with common variable immunodeficiency) was affinity-purified on atacicept prior to size-fractionation at pH 8.2, only BAFF 3-mer was detected,

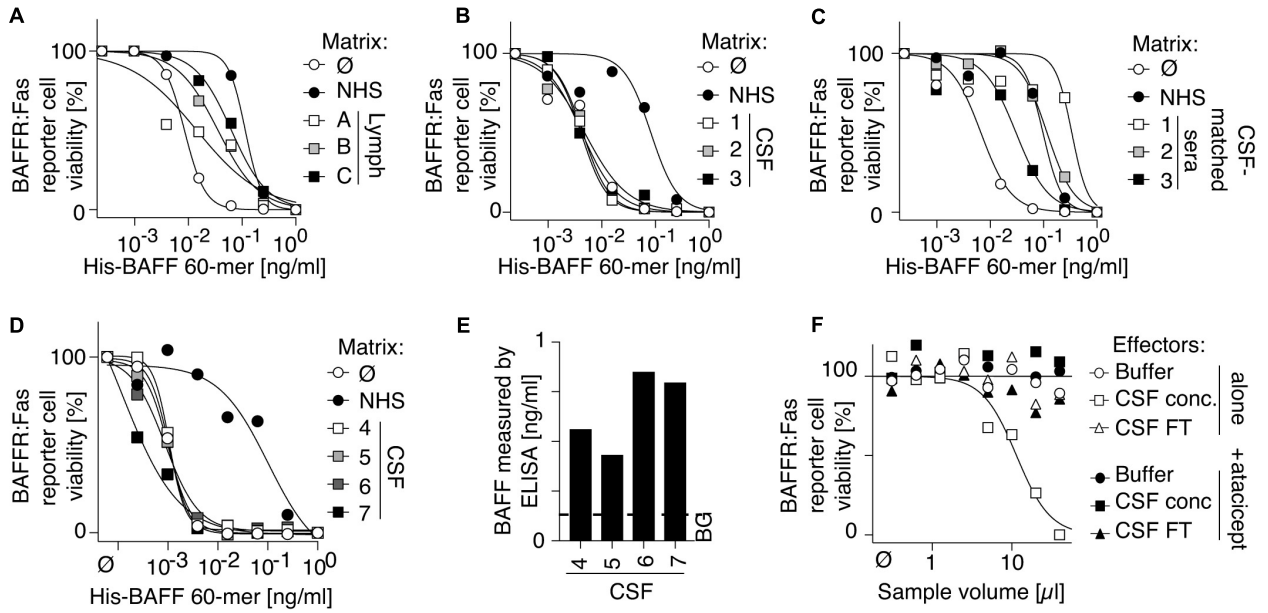

FIGURE 6 | Human cerebrospinal fluid contains BAFF protein and activity, but no BAFF 60-mer inhibitory activity. **(A–D)** Three human samples of lymph exudate **(A)**, 3 human CSF samples of multiple sclerosis patients **(B)**, 3 human sera of patients corresponding to CSF samples of panel **(B,C)** and 4 additional CSF samples from multiple sclerosis patients **(D)** were tested for their inhibitory activity on His-BAFF 60-mer using BAFFR:Fas reporter cells. Experiments in panels **(A–C)** were performed 3 times and that of panel **(D)** once. **(E)** BAFF levels measured by BAFF ELISA with capture at pH 7.4 in the 4 CSF samples of panel **(D)**. This experiment was performed once in this format. Detection of BAFF by ELISA in CSF sample was performed 4 times in different formats in these or other CSF samples. **(F)** A pool of CSF samples from panels **(D,E)** was concentrated 8-fold by ultrafiltration with cut off at 30 kDa. BAFF activity of concentrated CSF (CSF conc), of the filtered fraction of CSF (CSF FT) and of buffer was monitored on BAFFR:Fas reporter cells in the presence or absence of atacicept at 100 ng/ml. The experiment was performed once in this format. Detection of BAFF activity in these or other CSF samples was performed five times in different formats (including in **Figure 7**).

indicating the BAFF in CSF and in CVID serum is not only 3-mer, but also unable to associate as 60-mer under favorable conditions (**Figures 7G,H**).

A High Molecular Weight Form of BAFF in Cord Blood

Because fetal calf serum contains less BAFF 60-mer dissociating activity than adult cow serum, we tested whether human cord blood that also contains low dissociating activity may contain BAFF 60-mer. BAFF in fractions of the size exclusion chromatography was monitored by activity using BAFFR:Fas reporter cells, and by ELISA. As BAFFR:Fas reporter cells are highly sensitive to BAFF oligomers (Vigolo et al., 2018), but less so to BAFF 3-mer, they cannot detect low levels of endogenous BAFF 3-mer. Activity assays were therefore systematically performed in the presence of the cross-linking anti-human BAFF mAb 2.81, that we found was able to enhance the activity of BAFF 3-mer (see later). Also, the BAFF ELISA was systematically performed at pH 5.5 in order to detect both 3-mers and 60-mers. This also allows to compare total BAFF protein to activity. Finally, because the chromatography system was also used by our laboratory to purify recombinant BAFF 60-mer or TACI-Fc, the entire system was thoroughly cleaned until no trace of BAFF activity, or BAFF inhibitory activity was detected (**Figure 8A**). BAFF in normal adult sera was detected as 3-mer, with only traces of higher molecular weight BAFF, and we confirmed that this was also the case for CVID and BAFFR-deficient sera (**Figures 8B–F**). However, all cord blood sera, including one of a pre-term child at gestational week 29 contained fair proportions of high molecular weight BAFF in addition to 3-mers: up to 13% by ELISA and up to 40% in the activity test (**Figures 8G–N**). A single child serum was analyzed. It resembled adult serum more than cord serum (**Figure 8O**). An adult serum from a patient without B cells (BTK deficiency) contained 3-mer only, suggesting that differences observed for high molecular weight BAFF between cord blood and adults was not B cell-related (**Figure 8P**). In cord sera, despite the presence of the activating antibody, high molecular weight BAFF consistently displayed a higher specific activity compared to BAFF 3-mer, which is one of the characteristics of BAFF 60-mer. We excluded that formation of high molecular weight BAFF would be induced only in Hepes pH8.2, because it was also observed when the column was equilibrated in 25% fetal calf serum instead of Hepes buffer pH 8.2 (**Figure 8Q**). A direct measure in twelve cord blood samples revealed BAFF levels that were on average13-fold higher than in healthy adult sera (**Figure 8R**).

High Molecular Weight BAFF in Cord Blood Can Dissociate Into 3-mers

Size exclusion chromatography fractions of one of the cord blood samples were monitored for BAFF activity with or without activating antibody. As expected, the activity of BAFF 3-mer

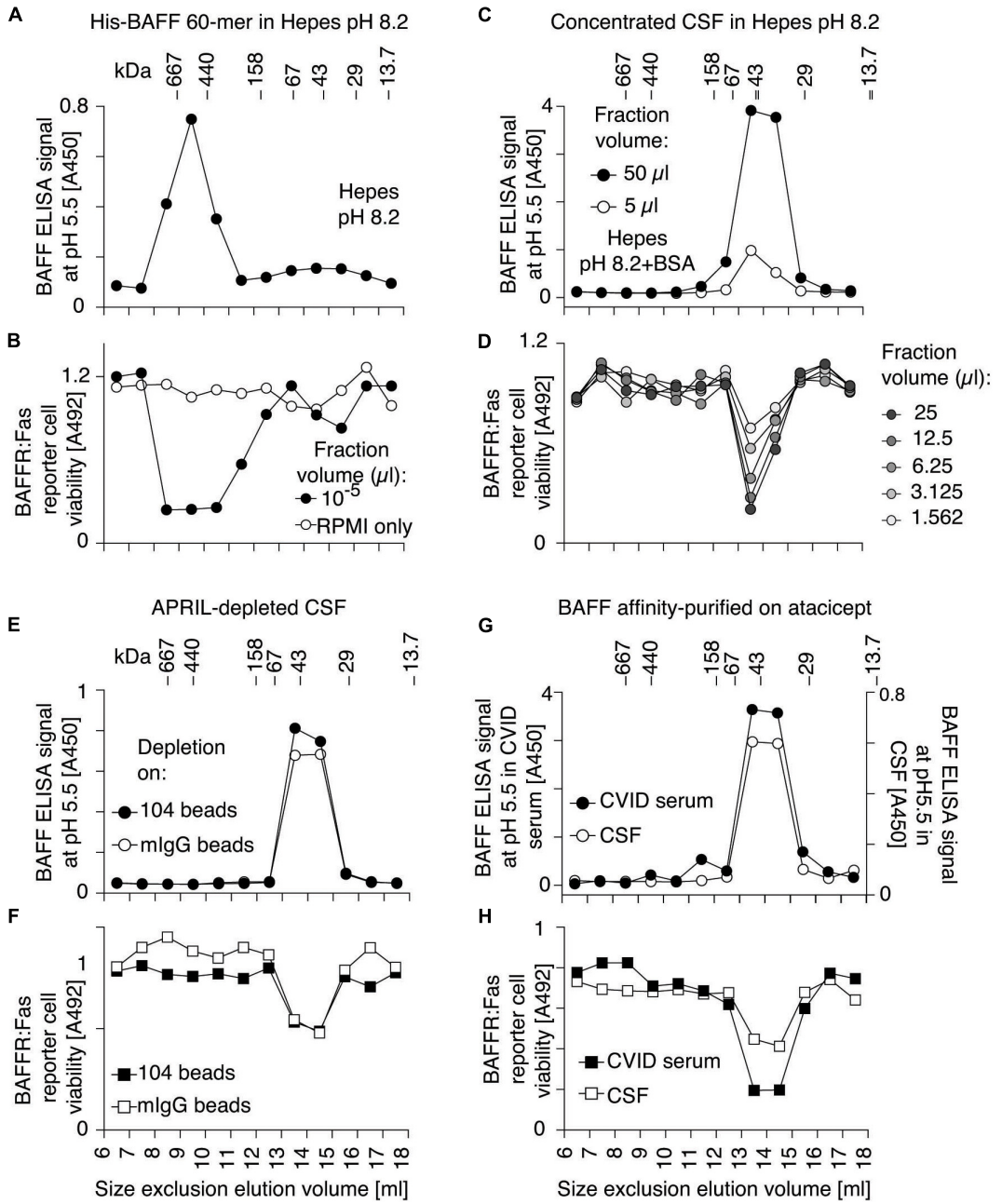

FIGURE 7 | BAFF protein and activity in human CSF has the size of a 3-mer, even after depletion of BAFF-APRIL heteromers or after affinity-purification. **(A)** His-BAFF 60-mer in Hepes buffer at pH 8.2 was fractionated by SEC at pH 8.2 in a buffer with 140 mM NaCl and no BSA. Small aliquots diluted in the same buffer with 30 mM NaCl were lyophilized, dissolved in a tenth of the volume and measured by BAFF ELISA with capture at pH 5.5. The experiment was performed once in this format, and three times in different formats. **(B)** Fractions of panel **(A)** were analyzed for BAFF activity on BAFFR:Fas reporter cells. This experiment was performed twice. **(C)** Same as panel **(A)**, except that 200 µl of an 8-fold concentrated pool of CSF from patients with multiple sclerosis (4–7 in **Figures 6D,E**) was analyzed instead of His-BAFF 60-mer, and that Hepes buffer contained 30 mM NaCl only, and that fractions were lyophilized and dissolved in a fifth of the initial volume prior to analysis. **(D)** Fractions of panel **(C)** were analyzed for BAFF activity on BAFFR:Fas reporter cells. Experiments of panels **(C,D)** were performed once in this format, and three times in different formats (panels **E–H**). **(E)** CSF depleted on mAb 104, which removes APRIL and BAFF-APRIL heteromers, was size-fractionated at pH 8.2 in the presence of Hepes buffer containing 30 mM NaCl and 10 µg/ml BSA. After lyophilization of fractions and suspension in a tenth of the original volume, BAFF was detected by ELISA with capture at pH 5.5 (black circles). Mock-depleted CSF was also analyzed (white circles). **(F)** Fractions of panel **(E)** were analyzed for BAFF activity on BAFFR:Fas reporter cells. **(G)** BAFF affinity-purified on atacicept from patients with multiple sclerosis (4–7 in **Figures 6D,E**; white circles), or serum from a CVID patient (black circles) were size fractionated by SEC at pH 8.2. BAFF in fractions was detected by ELISA with capture at pH 5.5. Note that the *Y*-axis scale is different for both samples. **(H)** Fractions of panel **(G)** were tested for BAFF activity on BAFFR:Fas reporter cells. A 4-fold higher fraction volume was used to measure BAFF activity in CSF compared to CVID. Experiments of panels **(E,G)** were performed once. Measures in panel **(F)** were performed twice, from the same fractions. Measures in panels **(F,H)** were performed at 3 different dilutions, one of which is shown.

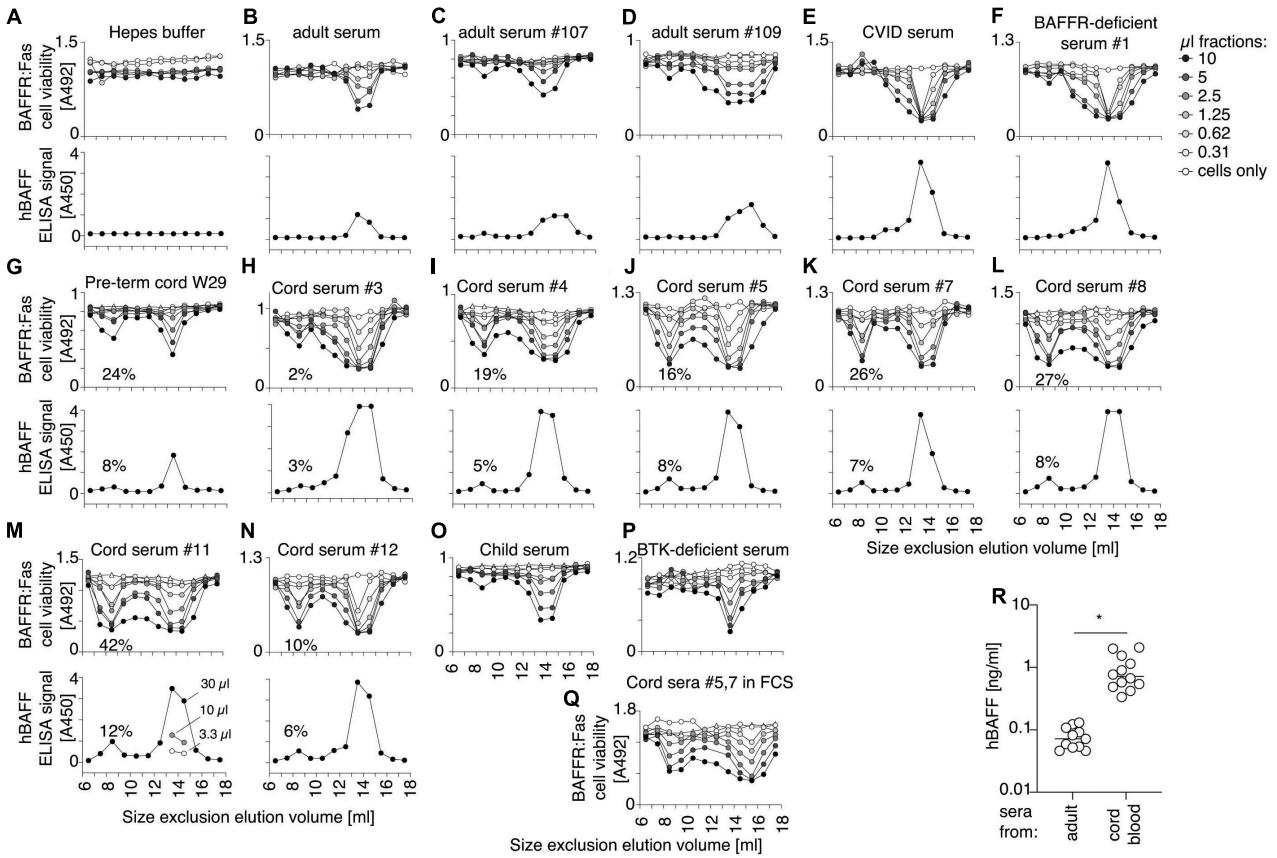

FIGURE 8 | Consistent detection of a high molecular weight form of BAFF in cord blood. Human sera were fractionated by SEC in Hepes pH 8.2, 30 mM NaCl, 10 μg/ml BSA. Fractions were lyophilized, redissolved in one tenth of the volume, and used to monitor BAFF activity on BAFFR:Fas reporter cells in the presence of the activating anti-BAFF antibody 2.81. Fractions were also measured for BAFF content by ELISA with a capture step at pH 5.5. **(A)** Negative control with buffer only. **(B–D)** Normal human adult sera. **(E)** Serum from a CVID patient. **(F)** Serum from a BAFFR-deficient individual. **(G)** Serum from cord blood of a pre-term baby at gestational week 29. **(H–N)** Cord blood sera. Note that serum in panel **(H)** was analyzed before in-depth cleaning of the chromatography system and may contain traces of TACI-Fc. Peak 3-mer fractions in panel **(M)** were measured at 3 different dilutions, showing a linear relationship between signal and dilution. **(O)** Serum from a 7 year-old child. **(P)** Serum from a BTK-deficient patient. **(Q)** Pooled cord blood sera #5 and #7 size fractionated in a column equilibrated in 25% fetal calf serum instead of Hepes buffer pH8.2 **(R)** Concentrations of BAFF were measured by ELISA at pH 7.4 in 10 μl of normal human sera (n = 11) and in 3 μl of sera of cord blood (n = 12), using Flag-BAFF as a standard. Groups were compared by t-test with Welch's correction. $^*p < 0.05$.

was enhanced with the activating antibody, but high molecular weight BAFF was activated too (**Figure 9A**), suggesting it might have dissociated into 3-mers. When the high molecular weight BAFF fraction was fractionated again, about 60% had dissociated into 3-mers while the remaining was still big (**Figure 9B**). On the contrary, the trimeric fraction did not detectably re-associate into multimers (**Figure 9C**). Naturally processed full-length recombinant BAFF yielded BAFF 3-mer and 60-mer in roughly similar quantities, as detected by Western blot (**Figure 9D**). Unexpectedly, the activity of the 60-mer on reporter cells was similar to that of BAFF 3-mer in terms of signal and of response to ligand (**Figure 9D**), which could be attributed at least in part to an equilibrium between 60-mer and 3-mer after size separation. Re-fractionation of BAFF 60-mer indeed yielded again 3-mer and 60-mer in equivalent amounts (**Figure 9E**), while the 3-mer remained essentially 3-mer, with moderate amounts of 60-mer detected by the activity test, but not by Western blot (**Figure 9F**). Taken together, these results show that high molecular weight BAFF in cord blood can dissociate into 3-mers similarly to naturally cleaved BAFF 60-mer.

Epitopes Concealed in Recombinant BAFF 60-mer Are Accessible in High Molecular Weight BAFF From Cord Blood

B cell activating factor 60-mer forms a defined, organized structure, with receptor-binding site always exposed at the surface, while other surfaces are always pointing inside of the 60-mer, or are buried in 3-mer to 3-mer interactions (Liu et al., 2002, 2003). Thus, antibodies against BAFF 3-mers do not necessarily recognize BAFF 60-mer. Belimumab is a well characterized example of an antibody that cannot recognize BAFF 60-mer (Shin et al., 2018; Vigolo et al., 2018). Our results also suggest that the capture antibody of the BAFF ELISA does not recognize BAFF 60-mer at pH 7.4, unless BAFF is first (presumably) dissociated into 3-mer at pH 5.5 (**Figures 3C,D**). We tested

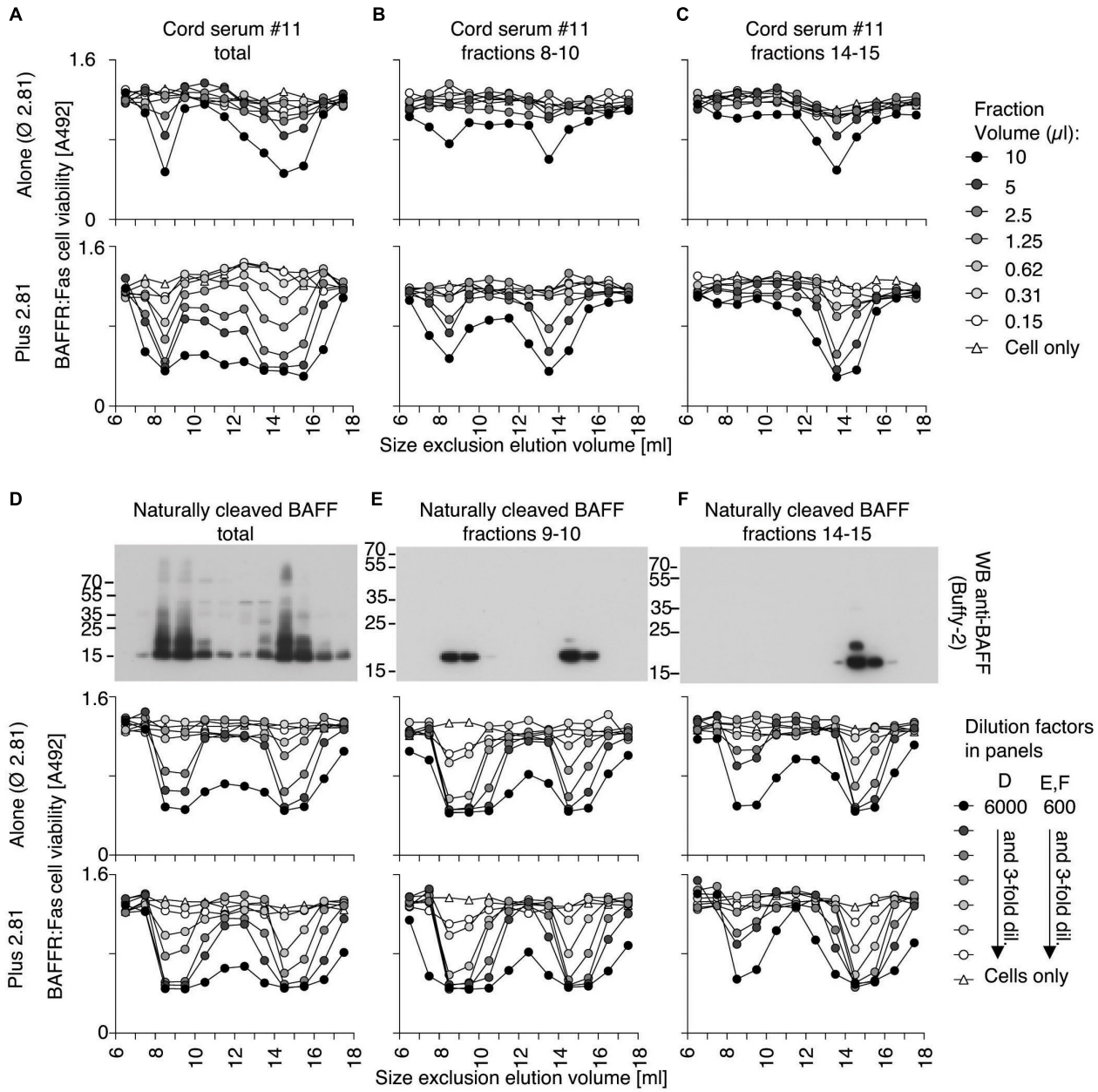

FIGURE 9 | High molecular weight cord blood BAFF and naturally cleaved BAFF 60-mer similarly dissociate into 3-mer. **(A)** Cord serum was analyzed as described in **Figure 8**, but in the absence (top panel) or presence (bottom panel) of activating anti-BAFF 2.81 antibody. **(B)** Fractions 8–10 of panel **(A)** were concentrated and re-fractionated by SEC. Lyophilized fractions were analyzed on BAFFR:Fas reporter cells without or with activating anti-BAFF 2.81 antibody. **(C)** Same as panel **(B)**, but with fractions 14–17 from panel **(A)**. **(D)** Conditioned supernatants of 293T cells transiently transfected with full-length human BAFF were size-fractionated by SEC in PBS pH 7.4. Fractions were analyzed by anti-BAFF (Buffy-2) western blot (top panel), or by activity on BAFFR:Fas reporter cells without (middle panel) or with 2.81 (bottom panel). **(E)** Fractions 9–10 of panel **(D)** were concentrated by affinity-purification on atacicept and analyzed again by SEC in Hepes at pH 8.2, Western blot and activity tests. **(F)** Same as panel **(E)**, but with affinity-purified fractions 14–17 of panel **(D)**. Note that affinity-purification steps render results of panels **(E,F)** not directly comparable with those of panels **(B,C)**.

whether high molecular weight BAFF in cord sera would escape recognition by antibodies specific for BAFF 3-mer. Thus, a serum of cord blood was analyzed in parallel with a standard of naturally cleaved BAFF 60-mer added in the same matrix. For this purpose, cord-blood was first depleted from endogenous BAFF with immobilized TACI-Fc, then supplemented with a close-to-endogenous concentration of recombinant 60-mer purified from naturally cleaved BAFF. These samples were size-fractionated by SEC. Fractions were immediately added to ELISA plates at 4°C so that the capture step was completed in less than an

hour post-elution. High molecular weight BAFF and BAFF 3-mer in cord blood were detected in the BAFF ELISA at both pH, suggesting it does not contain BAFF 60-mer (**Figure 10A**). Recombinant 60-mer spiked into the same matrix eluted as 60-mer and 3-mer. As expected, 60-mer was detected at pH 5.5, but poorly at pH 7.4, while the 3-mer was detected at both pH (**Figure 10B**). This suggests that high molecular weight BAFF in cord blood is different from naturally cleaved, recombinant BAFF 60-mer. Further controls indicated that BAFF 3-mer in purified naturally cleaved BAFF 60-mer was already present before spiking the depleted serum. Indeed, the ELISA recognized this standard at pH 5.5, as expected, but also to a fair extent at pH 7.4, while the more stable His-BAFF 60-mer was recognized at pH 5.5, but not or only weakly at pH 7.4 (**Figures 10C,D**).

We next tested whether high molecular weight BAFF in cord blood would be resistant to belimumab, as would be expected for BAFF 60-mer, using BAFFR:Fas reporter cells. The development and the characteristics of this assay are described in detail in the **Supplementary Material** (**Supplementary Figures 4–7**). Briefly, BAFF-containing samples were titrated on reporter cells, in a medium at pH 8.2 to favor 60-mers, in four different conditions: (i) without modifiers, (ii) with anti-BAFF antibody 2.81 that activates BAFF 3-mer by cross-linking but has no effect on BAFF 60-mer, (iii) with atacicept that inhibits all forms of BAFF, and (iv) with belimumab that inhibits BAFF 3-mer, but minimally affects BAFF 60-mer. This test permits the detection of recombinant His-BAFF 60-mer in the pg/ml range, even in the presence of an excess of Flag-BAFF 3-mer (**Supplementary Figure 5**). Thus, Flag-BAFF that exclusively forms 3-mer (Schneider et al., 1999), is activated about 10-fold by 2.81, but inhibited by belimumab and atacicept (**Figure 11A**). Similar results were observed for the 3-mer fraction of naturally cleaved WT BAFF, or of naturally cleaved BAFF with the H218A mutation that prevents 60-mer formation (Vigolo et al., 2018; **Figures 11B,C**). With the more "severe" mutation E223K that abolishes signaling ability, but not receptor binding (Vigolo et al., 2018), naturally cleaved BAFF was fully dependent on the cross-linking action of 2.81 (**Figure 10D**). In contrast, recombinant His-BAFF 60-mer was active on its own, was not further activated by 2.81, was fully resistant to inhibition by belimumab, but sensitive to inhibition by atacicept (**Figure 11E**). Similar results were obtained with the 60-mer fraction of naturally cleaved WT BAFF, except that the activity was overall lower, and that it was weakly inhibited by belimumab, as anticipated if a fair proportion of less active 3-mer would be inhibited in this preparation (**Figures 11F,G**). Cord blood samples consistently behaved as standards of BAFF 3-mer in this assay, and there was no difference between inhibitions by belimumab or atacicept (**Figures 11H–L**). Given the proportion of high molecular weight BAFF observed after SEC (**Figure 8**), if this high molecular weight BAFF would have had the activity of His-BAFF 60-mer, it should have been detected in this assay. We conclude that under conditions of this assay, high molecular weight BAFF in cord blood is recognized and inhibited by belimumab. In only one cord sample did we detect a BAFF activity that was resistant to belimumab and in good agreement with the percentage detected by ELISA post SEC (**Supplementary Figure 7**). The result could not be repeated because of insufficient amounts of sample. Taken together, these results indicate that the high molecular weight BAFF in cord blood is recognized by two antibodies that cannot bind recombinant BAFF 60-mer.

DISCUSSION

The ability of BAFF to form 60-mer is a likely evolutionary conserved feature, since the length and critical residues of the flap region are conserved across species (Bossen et al., 2008). Although the presence of mouse BAFF 60-mer in BAFF transgenic and TACI-ko mice (Bossen et al., 2008) and human BAFF 60-mer in conditioned medium of U937 cells (Cachero et al., 2006) were reported, there is still no evidence showing the existence of BAFF 60-mer in human. BAFF 60-mer is different from BAFF 3-mer, not only in terms of size and activity, but also with regards to recognition by different antibodies. We took advantage of some of these differences to develop test systems which are able to discriminate between the activities of BAFF 3-mers and 60-mers. We also adapted

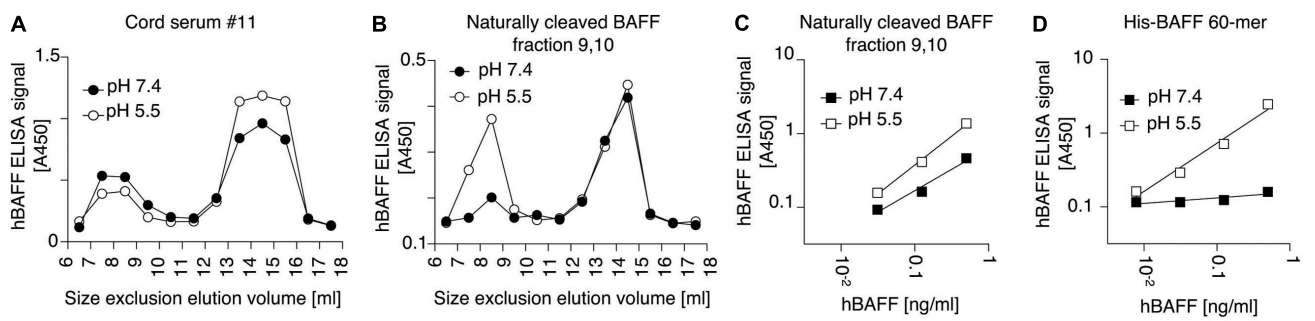

FIGURE 10 | High molecular weight cord blood BAFF is detected by BAFF ELISA also at pH 7.4. **(A)** A cord serum sample was size-fractionated by SEC. Fractions were immediately analyzed by BAFF ELISA with a short capture time (30 min at 4°C instead of 3 h at room temperature). **(B)** Same as panel **(A)**, except that the same cord serum sample was first depleted from endogenous BAFF and spiked with 5 ng/ml of recombinant, naturally cleaved BAFF 60-mer. **(C)** Naturally cleaved recombinant BAFF 60-mer used in panel **(A)** (but not spiked in serum) was measured in the BAFF ELISA with capture steps at pH 5.5 or pH 7.4. **(D)** Same as panel **(C)**, but with recombinant His-BAFF 60-mer.

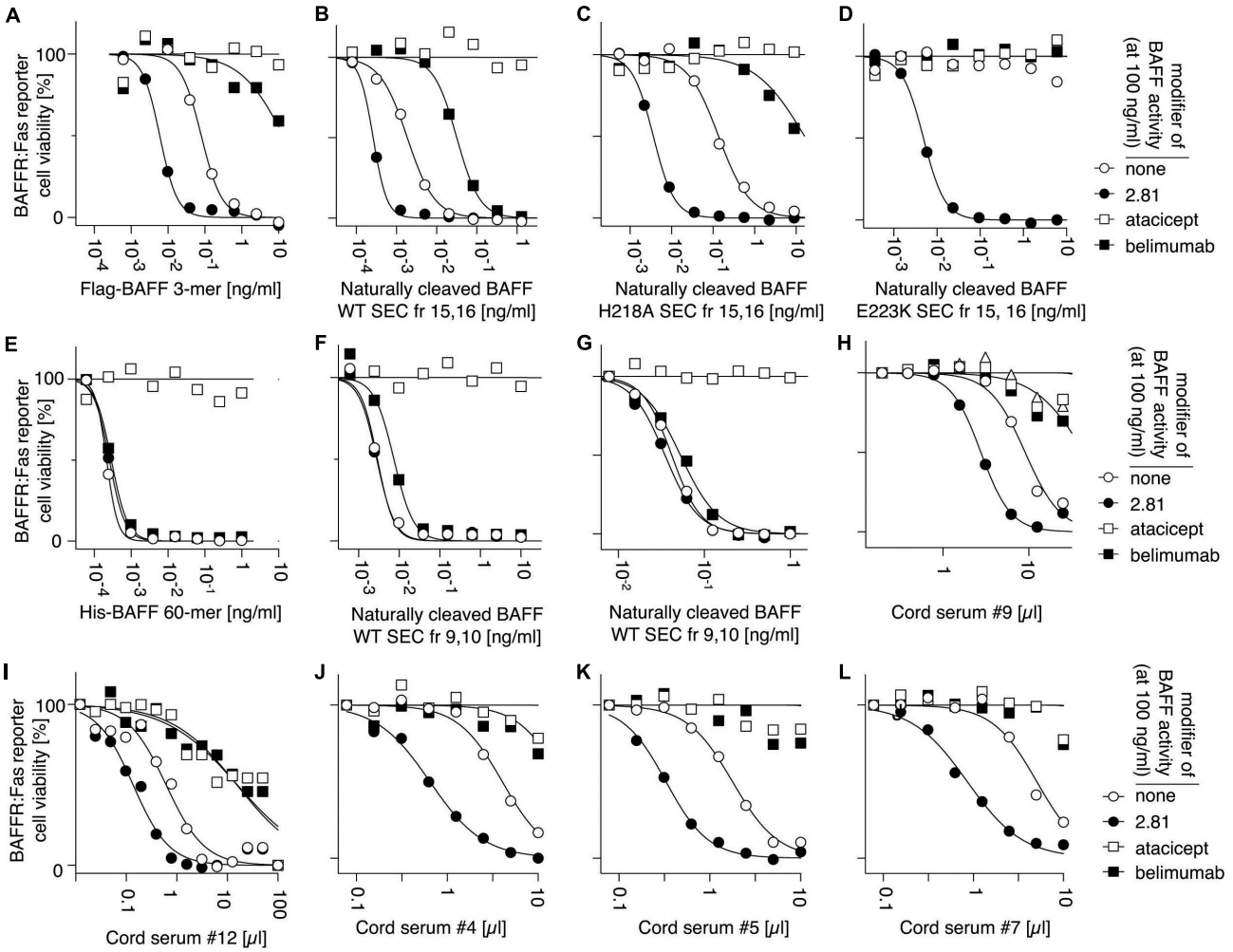

FIGURE 11 | BAFF in cord blood is inhibited by belimumab, as measured in a cell-based assay that distinguishes BAFF 60-mer from BAFF 3-mer. Activities of different forms of recombinant BAFF were monitored on BAFFR:Fas reporter cells in the presence of the following modifiers: (none, white circles), an activating anti-BAFF monoclonal antibody (2.81, black circles), a TACI-Fc decoy receptor (atacicept, white squares) or a blocking anti-BAFF monoclonal antibody (belimumab, black squares). **(A)** Flag-BAFF 3-mer. **(B)** Small molecular weight form (SEC fractions 15 + 16, 3-mer) of naturally processed WT BAFF in supernatants of transfected 293T cells. **(C)** Small molecular weight form (SEC fractions 15 + 16, 3-mer) of naturally processed BAFF with mutation H218A in the flap that prevents 60-mer formation but not signaling through BAFFR. **(D)** Small molecular weight form (SEC fractions 15 + 16, 3-mer) of naturally processed BAFF with mutation E223K in the flap region that prevents formation of 60-mer and signaling through BAFFR. **(E)** His-BAFF 60-mer. **(F)** High molecular weight form (SEC fractions 9 + 10, 60-mer) of naturally processed WT BAFF in supernatants of transfected 293T cells. **(G)** Same as panel **(F)**, but from another experiment. **(H–L)** Cord serum samples. Experiments in panels **(A–E)** and **(F + G)** were performed five, three, two, two, five, and six times, respectively. Experiments in panels **(H–L)** were performed once. Data for panels **(A–F)**, **(G–H)**, **(I)**, and **(J–L)** were collected in independent experiments.

an ELISA to enable recognition of both 3-mer and 60-mer, and not only 3-mer as is the case with the standard protocol. A potentially criticisable aspect of the present study is the use of the surrogate Fas signaling pathway in reporter cells, but the sensitivity of this assay is high, with an EC50 of 0.05 pg/ml, or 0.005 pg/100 µl (**Supplementary Figure 5A**). The molecular mass of BAFF 60-mer being 1,100 kDa, this is equivalent to about 3,000 molecules of 60-mer per well, i.e., less than one 60-mer per reporter cell. Despite the sensitivity of this assay, BAFF 60-mer remained undetected in adult human sera, even in those of a patient with CVID and of a patient with BAFFR-deficiency, in which circulating BAFF levels are up to 500 times higher than in normal human serum. Moreover, we found that serum is not a favorable environment for BAFF 60-mer as it considerably, but not totally, decreases its activity. BAFF 60-mer is known as a pH-sensitive structure which dissociates into less active trimers at acidic pH (Liu et al., 2002; Cachero et al., 2006). However, the 60-mer inhibitory activity was not due to the pH, salt concentration or other physical properties of human serum, as serum after ultrafiltration contained no inhibitory activity. This observation raised the question if BAFF 60-mers might be inhibited by soluble extracellular domains of BAFFR, TACI, and/or BCMA, all of which can be shed from the transmembrane forms of the

receptor (Smulski and Eibel, 2018). However, this hypothesis seems to be very unlikely. First, because this inhibitory activity could not be depleted on immobilized Fc-BAFF; second, because the inhibitory activity has a high molecular weight incompatible with that of soluble receptors, third, because it is inconceivable how soluble receptors should specifically target BAFF 60-mer and not Fc-BAFF, and fourth, because atacicept, which is a soluble dimeric form of TACI, binds to BAFF 60-mer without dissociating it (Bossen et al., 2008). We found that the high molecular weight, BAFF 60-mer dissociating activity could not bind to Fc-BAFF, but we do not exclude the possibility that it could bind specifically to BAFF 60-mer, for example if it recognizes the flap-flap interface. When we realized that human serum efficiently dissociated recombinant BAFF 60-mer into 3-mer, we immediately thought that the residual activity was due to the newly formed, less active BAFF 3-mer. This was, however, not the case, as most of this residual activity had the size and properties of BAFF 60-mer (**Figure 4D** and **Supplementary Figure 4B**). Whether longer incubations in serum would have destroyed this residual 60-mer activity, or whether there is a fraction of serum-resistant recombinant BAFF 60-mer remains to be investigated.

As BAFF and APRIL can heteromerize (Roschke et al., 2002; Dillon et al., 2010; Schuepbach-Mallepell et al., 2015), and as APRIL is devoid of the flap region that in BAFF is required for 3-mer to 3-mer interactions and 60-mer formation, it is possible that low concentrations of BAFF-APRIL heteromers could prevent 60-mer formation, explaining why all endogenous BAFF in serum is detected as 3-mer. However, depletion of APRIL, homomers and heteromers, with an anti-APRIL antibody did not restore 60-mer formation. This alone is, however, insufficient to discard the hypothesis that BAFF-APRIL heteromers would interfere with 60-mer formation because we find that endogenous BAFF 3-mer and BAFF 3-mer dissociated from recombinant 60-mer cannot re-associate into 60-mer, even after APRIL has been removed. In this context, it still remains to be solved why BAFF 3-mers originating from dissociated 60-mers and why endogenous human BAFF cannot assemble into 60-mers even in serum- or CSF-free conditions. An appealing hypothesis is that the flap region (or other portions of BAFF that interact with the flap) is modified by proteolytic processing. This would explain specific loss of activity of BAFF 60-mer, but not other forms of BAFF. Disruption of one flap out of 60 is in principle sufficient to prevent 60-mer formation. However, the inhibitory activity was not decreased when serum was first treated with a mix of protease inhibitors (**Supplementary Figure 2B**). An alternative mechanism could be a conformational change in the flap region, such as the one observed in one of the BAFF monomers in the crystal structure of the APRIL-BAFF-BAFF heteromer (Schuepbach-Mallepell et al., 2015). The flap has a defined structure that is virtually identical in all other available crystal structures, including those where flap-flap interactions are prevented by the Fab fragment of belimumab (Shin et al., 2018; Vigolo et al., 2018). There is no doubt that the marked refolding of the long loop of the "canonical" flap into the beta-hairpin seen in the crystal structure of the heteromer would abrogate 60-mer formation.

To try and answer the main question of this study, namely the detection of BAFF 60-mer in human body fluids, we investigated different samples in search of one unable to dissociate recombinant 60-mer. The implication of BAFF in autoimmune diseases such as MS has been studied for years (Kannel et al., 2015). While the transcript levels of BAFF are clearly elevated in active MS lesions (Krumbholz et al., 2005), data about CSF levels of BAFF in MS are not consistent. Some studies found elevated BAFF (Ragheb et al., 2011; Wang et al., 2012; Quan et al., 2013) in MS, others did not (Krumbholz et al., 2005; Kowarik et al., 2012). The BAFF levels in the CSF are influenced not only by local production, but also by consumption, and soluble receptors. The CSF of MS patients contains a variable number of B cells (Stangel et al., 2013) and it is plausible that the CSF levels of BAFF are also determined by consumption of B cells as are the blood levels of BAFF (Kreuzaler et al., 2012). Further, in the CSF of MS patients, the soluble receptors sBCMA and sTACI are elevated and function as decoys (Hoffmann et al., 2015; Laurent et al., 2015).

Here we show that CSF from patients with MS are devoid of BAFF 60-mer dissociating activity. Despite this, endogenous BAFF in CSF was exclusively present as 3-mer, even after purification on atacicept and size-fractionation at basic pH in CSF-free conditions. About 80% of the proteins in the CSF are derived from blood, 19% from the meninges and only 1% from cells in the brain (Stangel et al., 2013). Since the CSF from patients without inflammation in the brain contains BAFF at a similar level as the CSF from MS patients (Krumbholz et al., 2005; Kowarik et al., 2012), we would assume that the majority of the BAFF in the CSF also in MS patients is derived from blood, an hypothesis that would fit with our observations that the CSF contains BAFF-3mer, and that serum permanently transforms BAFF 60-mer into BAFF 3-mer. In addition to CSF, we find that fetal calf serum do not contain dissociating activity, while adult cow sera does. A partially similar situation was observed in humans, with high levels of dissociating activity in adult plasma or serum, lower levels in the umbilical blood of neonates, and even lower levels in two cord blood samples from pre-term babies. In mice, we found no dissociating activity for BAFF 60-mer in adult serum. The mouse BAFF gene contains an additional 30 amino acids at the N-terminus of the soluble form that likely prevents efficient formation of 60-mer. We hypothesize that a destabilization activity would not be required in mouse serum if its goal is to prevent systemic action of BAFF 60-mer. It was previously determined that administration of BAFF 3-mer into BAFF-ko mice restored B cell populations, but not expression of CD23, while administration of BAFF 60-mer restored both, suggesting that BAFF 60-mer may fulfill specific roles (Bossen et al., 2011).

Previous studies reported BAFF levels that were two-fold higher in cord blood compared to maternal blood, although these levels were not maintained in one- or four-month-old babies, suggesting that BAFF could be produced by the placenta (Bienertova-Vasku et al., 2015; Lundell et al., 2015). Interestingly, BAFF was higher in cord blood of babies whose mothers were exposed to dairy farm environment, correlating with more rapid

B cell maturation later in childhood and decreased risk of developing allergies (Lundell et al., 2015). Here we find that (i) cord blood contains high levels of BAFF, greater than 10-fold more than in adults, (ii) cord blood usually contains lower levels of BAFF 60-mer dissociating activity, and (iii) cord blood consistently contains up to 10% of a high molecular weight form of BAFF with some, but not all properties of BAFF 60-mer. In particular, this high molecular weight BAFF had a size very similar to that of BAFF 60-mer, i.e., big but still included into the active range of the size exclusion column. It was more active than the fraction of BAFF 3-mer contained in the same sample and could dissociate into 3-mer. These properties would not be expected from a random protein aggregate. However, our data strongly indicate that this high molecular weight BAFF lacked two important features of recombinant BAFF 60-mer: its pH sensitivity in the BAFF ELISA test, and its resistance to inhibition by belimumab. Interestingly, both of these features rely on the inaccessibility of antibody epitopes in BAFF 60-mer, suggesting that they are already accessible, or become rapidly accessible to antibodies in high molecular weight BAFF of cord blood. We excluded the confounding effect of BAFF 60-mer dissociating activity in serum by experiments of depletion and spiking. In addition, specific depletion of APRIL and heteromers did not decrease levels of high molecular weight BAFF, excluding the hypothesis that it may contain BAFF APRIL heteromers (unpublished observations). If high molecular weight BAFF in cord blood is not comparable to recombinant BAFF 60-mer, then what is its molecular nature? In a first scenario, BAFF 60-mer would never form *in vivo*. High molecular weight BAFF would be a complex of undefined nature, such as BAFF 3-mer bound to auto-antibodies or to any other big-sized partner, which would, however, not prevent BAFF activity. This would raise questions of why non-neutralizing anti-BAFF auto-antibodies should be present in cord blood, and similar hard-to-answer questions. In a second scenario, BAFF 60-mer could be formed *in vivo*, most probably locally after its synthesis by BAFF-producing cells. BAFF 60-mer would not be meant to act systemically, and thus would be dissociated into less active 3-mer. This inactivation may proceed through less stable, easy-to-dissociate BAFF 60-mer intermediates. Perhaps one or just a few flaps would adopt a different conformation (Schuepbach-Mallepell et al., 2015) that would render internal epitopes accessible. Binding of just one antibody, or perhaps even a receptor, would quickly dissociate the complex. Two different forms of recombinant BAFF 60-mer, one made in bacteria (His-BAFF 60-mer) and one made from naturally cleaved full-length BAFF expressed in 293T cells, seem to have different stabilities as judged by the proportion of 3-mer released from these structures at pH 8.2 (e.g., **Figures 3C**, **4A**, vs. **Figures 3E**, **9D–F**). Thus, formation of even less stable forms might be considered. Our data so far do not allow distinguishing between these two models, and in view of the minute amounts of BAFF available in these samples, it might be technically challenging to do so. Perhaps more information about a putative function of BAFF 60-mer *in vivo* could come from genetic models in which BAFF 60-mer can or cannot form. Our data, however, demonstrate that clinical BAFF inhibitors will neutralize BAFF in the circulation: highly active forms of BAFF 60-mer are unlikely to be predominant in blood or in CSF, and even the high molecular weight form of BAFF detected in cord blood can be inhibited by both belimumab and atacicept.

In summary, with the help of sensitive tools developed for the characterization of BAFF 60-mer in biologic fluids, we demonstrated the exclusive presence of BAFF 3-mer in adult human serum and CSF samples, and detected a high molecular weight form of BAFF with some but not all properties of BAFF 60-mer in cord blood. In addition, an activity that dissociates BAFF 60-mer into trimers was identified, which is higher in adult serum than in cord blood. Advancing knowledge on the endogenous forms of BAFF is relevant in view of its elevated levels in various disorders (Cheema et al., 2001; Zhang et al., 2001; McCarthy et al., 2013; Xin et al., 2013; Li et al., 2014; Kannel et al., 2015; Salazar-Camarena et al., 2016; Steri et al., 2017) and the use of BAFF antagonists with different ligand specificities in the clinic or in clinical trials.

DATA AVAILABILITY STATEMENT

The raw data supporting the conclusions of this article will be made available by the authors, without undue reservation, and are available as a data set doi: 10.5281/zenodo.4141692.

ETHICS STATEMENT

The studies involving human participants were reviewed and approved by Ethics Committee of the Medical University of Vienna, Austria (EK Nr: 1845/2015). Human systemic lupus erythematosus serum samples were from patients who were enrolled in the randomized, double-blind, APRIL-SLE trial, but before they received any treatment with atacicept (ClinicalTrials.gov Identifier NCT00624338). Cerebrospinal fluid (CSF) samples from MS patients were provided by the Institute of Clinical Neuroimmunology, Munich. This was approved by the Ethical Committee of the Medical Faculty of Ludwig-Maximilians-Universität München. Work with mice was performed according to Swiss Federal Veterinary Office guidelines, and under the authorization of the Office Vétérinaire Cantonal du Canton de Vaud (authorization 1370.7 to PS). Cow sera: this specific study had been approved by the IACUC of Lower Saxony, the state veterinary office Niedersächsisches Landesamt für Verbraucherschutz und Lebensmittelsicherheit, Oldenburg, Germany (registration number 33.42502-05-04A247).

AUTHOR CONTRIBUTIONS

PS and ME designed experiments. ME, LW, and PS performed experiments. ME and PS wrote the manuscript. EM, HE, ODo, ODi, HS, DS, DT, ÖY, and ES provided essential reagents. All authors reviewed the results and approved the final version of the manuscript.

FUNDING

This work was supported by the Swiss National Science Foundation (grant 310030310030A_176256) to PS, the DFG (SFB TR128), and the GMSI award 2018 (Merck KGaA) to EM.

ACKNOWLEDGMENTS

We thank Henry Hess (Merck KGaA, Darmstadt, Germany) for the gift of atacicept, Hélène Maby-El-Hajjami (University of Lausanne, Switzerland) for samples of lymphatic exudate, and Tania Kümpfel (LMU Munich, Germany) for CSF samples.

SUPPLEMENTARY MATERIAL

The Supplementary Material for this article can be found online at: https://www.frontiersin.org/articles/10.3389/fcell.2020.577662/full#supplementary-material

REFERENCES

Bienertova-Vasku, J., Zlamal, F., Tomandl, J., Hodicka, Z., Novak, J., Splichal, Z., et al. (2015). The presence of B-cell activating factor (BAFF) in umbilical cord blood in both healthy and pre-eclamptic pregnancies and in human breast milk. *J. Reprod. Immunol.* 109, 89–93. doi: 10.1016/j.jri.2014.12.003

Bossen, C., and Schneider, P. (2006). BAFF. APRIL and their receptors: structure, function and signaling. *Semin. Immunol.* 18, 263–275. doi: 10.1016/j.smim.2006.04.006

Bossen, C., Cachero, T. G., Tardivel, A., Ingold, K., Willen, L., Dobles, M., et al. (2008). TACI, unlike BAFF-R, is solely activated by oligomeric BAFF and APRIL to support survival of activated B cells and plasmablasts. *Blood* 111, 1004–1012. doi: 10.1182/blood-2007-09-110874

Bossen, C., Tardivel, A., Willen, L., Fletcher, C. A., Perroud, M., Beermann, F., et al. (2011). Mutation of the BAFF furin cleavage site impairs B-cell homeostasis and antibody responses. *Eur. J. Immunol.* 41, 787–797. doi: 10.1002/eji.201040591

Broggi, M. A. S., Maillat, L., Clement, C. C., Bordry, N., Corthesy, P., Auger, A., et al. (2019). Tumor-associated factors are enriched in lymphatic exudate compared to plasma in metastatic melanoma patients. *J. Exp. Med.* 216, 1091–1107. doi: 10.1084/jem.20181618

Cachero, T. G., Schwartz, I. M., Qian, F., Day, E. S., Bossen, C., Ingold, K., et al. (2006). Formation of virus-like clusters is an intrinsic property of the tumor necrosis factor family member BAFF (B cell activating factor). *Biochemistry* 45, 2006–2013. doi: 10.1021/bi051685o

Cheema, G. S., Roschke, V., Hilbert, D. M., and Stohl, W. (2001). Elevated serum B lymphocyte stimulator levels in patients with systemic immune-based rheumatic diseases. *Arthritis Rheum.* 44, 1313–1319. doi: 10.1002/1529-0131(200106)44:6<1313::aid-art223>3.0.co;2-s

Claudio, E., Brown, K., Park, S., Wang, H., and Siebenlist, U. (2002). BAFF-induced NEMO-independent processing of NF-kappa B2 in maturing B cells. *Nat. Immunol.* 3, 958–965. doi: 10.1038/ni842

Craxton, A., Draves, K. E., Gruppi, A., and Clark, E. A. (2005). BAFF regulates B cell survival by downregulating the BH3-only family member Bim via the ERK pathway. *J. Exp. Med.* 202, 1363–1374. doi: 10.1084/jem.20051283

Craxton, A., Magaletti, D., Ryan, E. J., and Clark, E. A. (2003). Macrophage- and dendritic cell-dependent regulation of human B-cell proliferation requires the TNF family ligand BAFF. *Blood* 16:16.

Dillon, S. R., Harder, B., Lewis, K. B., Moore, M. D., Liu, H., Bukowski, T. R., et al. (2010). B-lymphocyte stimulator/a proliferation-inducing ligand heterotrimers are elevated in the sera of patients with autoimmune disease and are neutralized by atacicept and B-cell maturation antigen-immunoglobulin. *Arthritis Res Ther.* 12:R48.

Giordano, D., Kuley, R., Draves, K. E., Roe, K., Holder, U., Giltiay, N. V., et al. (2020). BAFF Produced by Neutrophils and Dendritic Cells Is Regulated Differently and Has Distinct Roles in Antibody Responses and Protective Immunity against West Nile Virus. *J. Immunol.* 204, 1508–1520. doi: 10.4049/jimmunol.1901120

Grell, M., Douni, E., Wajant, H., Lohden, M., Clauss, M., Maxeiner, B., et al. (1995). The transmembrane form of tumor necrosis factor is the prime activating ligand of the 80 kDa tumor necrosis factor receptor. *Cell* 83, 793–802. doi: 10.1016/0092-8674(95)90192-2

Hahn, B. H. (2013). Belimumab for systemic lupus erythematosus. *N. Engl. J. Med.* 368, 1528–1535.

Hahne, M., Kataoka, T., Schroter, M., Hofmann, K., Irmler, M., Bodmer, J. L., et al. (1998). APRIL, a new ligand of the tumor necrosis factor family, stimulates tumor growth. *J. Exp.Med.* 188, 1185–1190. doi: 10.1084/jem.188.6.1185

Hatada, E. N., Do, R. K., Orlofsky, A., Liou, H. C., Prystowsky, M., MacLennan, I. C., et al. (2003). NF-kappa B1 p50 is required for BLyS attenuation of apoptosis but dispensable for processing of NF-kappa B2 p100 to p52 in quiescent mature B cells. *J. Immunol.* 171, 761–768. doi: 10.4049/jimmunol.171.2.761

Hoffmann, F. S., Kuhn, P. H., Laurent, S. A., Hauck, S. M., Berer, K., Wendlinger, S. A., et al. (2015). The immunoregulator soluble TACI is released by ADAM10 and reflects B cell activation in autoimmunity. *J. Immunol.* 194, 542–552. doi: 10.4049/jimmunol.1402070

Kannel, K., Alnek, K., Vahter, L., Gross-Paju, K., Uibo, R., and Kisand, K. V. (2015). Changes in Blood B Cell-Activating Factor (BAFF) Levels in Multiple Sclerosis: A Sign of Treatment Outcome. *PLoS One* 10:e0143393. doi: 10.1371/journal.pone.0143393

Kato, A., Truong-Tran, A. Q., Scott, A. L., Matsumoto, K., and Schleimer, R. P. (2006). Airway epithelial cells produce B cell-activating factor of TNF family by an IFN-beta-dependent mechanism. *J. Immunol.* 177, 7164–7172. doi: 10.4049/jimmunol.177.10.7164

Kowalczyk-Quintas, C., Chevalley, D., Willen, L., Jandus, C., Vigolo, M., and Schneider, P. (2018). Inhibition of Membrane-Bound BAFF by the Anti-BAFF Antibody Belimumab. *Front. Immunol.* 9:2698. doi: 10.3389/fimmu.2018.02698

Kowalczyk-Quintas, C., Schuepbach-Mallepell, S., Vigolo, M., Willen, L., Tardivel, A., Smulski, C. R., et al. (2016). Antibodies That Block or Activate Mouse B Cell Activating Factor of the Tumor Necrosis Factor (TNF) Family (BAFF). *Respectively, Induce B Cell Depletion or B Cell Hyperplasia. J. Biol. Chem.* 291, 19826–19834. doi: 10.1074/jbc.m116.725929

Kowarik, M. C., Cepok, S., Sellner, J., Grummel, V., Weber, M. S., Korn, T., et al. (2012). CXCL13 is the major determinant for B cell recruitment to the CSF during neuroinflammation. *J. Neuroinflammat.* 9:93.

Kreuzaler, M., Rauch, M., Salzer, U., Birmelin, J., Rizzi, M., Grimbacher, B., et al. (2012). Soluble BAFF levels inversely correlate with peripheral B cell numbers and the expression of BAFF receptors. *J. Immunol.* 188, 497–503. doi: 10.4049/jimmunol.1102321

Krumbholz, M., Faber, H., Steinmeyer, F., Hoffmann, L. A., Kumpfel, T., Pellkofer, H., et al. (2008). Interferon-beta increases BAFF levels in multiple sclerosis: implications for B cell autoimmunity. *Brain* 131, 1455–1463. doi: 10.1093/brain/awn077

Krumbholz, M., Theil, D., Derfuss, T., Rosenwald, A., Schrader, F., Monoranu, C. M., et al. (2005). BAFF is produced by astrocytes and up-regulated in multiple sclerosis lesions and primary central nervous system lymphoma. *J. Exp. Med.* 201, 195–200. doi: 10.1084/jem.20041674

Laurent, S. A., Hoffmann, F. S., Kuhn, P. H., Cheng, Q., Chu, Y., Schmidt-Supprian, M., et al. (2015). gamma-Secretase directly sheds the survival receptor BCMA from plasma cells. *Nat. Commun.* 6:7333.

Li, W., Peng, X., Liu, Y., Liu, H., Liu, F., He, L., et al. (2014). TLR9 and BAFF: their expression in patients with IgA nephropathy. *Mol. Med. Rep.* 10, 1469–1474. doi: 10.3892/mmr.2014.2359

Liu, Y., Hong, X., Kappler, J., Jiang, L., Zhang, R., Xu, L., et al. (2003). Ligand-receptor binding revealed by the TNF family member TALL-1. *Nature* 423, 49–56. doi: 10.1038/nature01543

Liu, Y., Xu, L., Opalka, N., Kappler, J., Shu, H. B., and Zhang, G. (2002). Crystal structure of sTALL-1 reveals a virus-like assembly of TNF family ligands. *Cell* 108, 383–394. doi: 10.1016/s0092-8674(02)00631-1

Lundell, A. C., Hesselmar, B., Nordstrom, I., Adlerberth, I., Wold, A. E., and Rudin, A. (2015). Higher B-cell activating factor levels at birth are positively associated with maternal dairy farm exposure and negatively related to allergy development. *J. Aller. Clinic. Immunol.* 136:e1073.

Mackay, F., and Schneider, P. (2009). Cracking the BAFF code. *Nat. Rev. Immunol.* 9, 491–502. doi: 10.1038/nri2572

Mackay, F., Schneider, P., Rennert, P., and Browning, J. (2003). BAFF and APRIL: a tutorial on B cell survival. *Annu. Rev. Immunol.* 21, 231–264.

McCarthy, E. M., Lee, R. Z., Ni Gabhann, J., Smith, S., Cunnane, G., Doran, M. F., et al. (2013). Elevated B lymphocyte stimulator levels are associated with increased damage in an Irish systemic lupus erythematosus cohort. *Rheumatology* 52, 1279–1284. doi: 10.1093/rheumatology/ket120

Merrill, J. T., Wallace, D. J., Wax, S., Kao, A., Fraser, P. A., Chang, P., et al. (2018). Efficacy and Safety of Atacicept in Patients With Systemic Lupus Erythematosus: Results of a Twenty-Four-Week. *Multicenter, Randomized, Double-Blind, Placebo-Controlled, Parallel-Arm, Phase IIb Study. Arthritis Rheumatol.* 70, 266–276. doi: 10.1002/art.40360

Nys, J., Smulski, C. R., Tardivel, A., Willen, L., Kowalczyk, C., Donze, O., et al. (2013). No evidence that soluble TACI induces signalling via membrane-expressed BAFF and APRIL in myeloid cells. *PLoS One* 8:e61350. doi: 10.1371/journal.pone.0061350

Pellkofer, H. L., Armbruster, L., Krumbholz, M., Titulaer, M. J., Verschuuren, J. J., Schumm, F., et al. (2008). Lambert-eaton myasthenic syndrome differential reactivity of tumor versus non-tumor patients to subunits of the voltage-gated calcium channel. *J. Neuroimmunol.* 204, 136–139. doi: 10.1016/j.jneuroim.2008.08.002

Podzus, J., Kowalczyk-Quintas, C., Schuepbach-Mallepell, S., Willen, L., Staehlin, G., Vigolo, M., et al. (2017). Ectodysplasin A in Biological Fluids and Diagnosis of Ectodermal Dysplasia. *J. Dent. Res.* 96, 217–224. doi: 10.1177/0022034516673562

Quan, C., Yu, H., Qiao, J., Xiao, B., Zhao, G., Wu, Z., et al. (2013). Impaired regulatory function and enhanced intrathecal activation of B cells in neuromyelitis optica: distinct from multiple sclerosis. *Mult. Scler.* 19, 289–298. doi: 10.1177/1352458512454771

Ragheb, S., Li, Y., Simon, K., VanHaerents, S., Galimberti, D., De Riz, M., et al. (2011). Multiple sclerosis: BAFF and CXCL13 in cerebrospinal fluid. *Mult. Scler.* 17, 819–829. doi: 10.1177/1352458511398887

Roschke, V., Sosnovtseva, S., Ward, C. D., Hong, J. S., Smith, R., Albert, V., et al. (2002). BLyS and APRIL form biologically active heterotrimers that are expressed in patients with systemic immune-based rheumatic diseases. *J. Immunol.* 169, 4314–4321. doi: 10.4049/jimmunol.169.8.4314

Rosen, F. S., Eibl, M., Roifman, C., Fischer, A., Volanakis, J., Aiuti, F., et al. (1999). Primary immunodeficiency diseases. Report of an IUIS Scientific Committee. International Union of Immunological Societies. *Clin. Exp. Immunol.* 118(Suppl. 1), 1–28. doi: 10.1046/j.1365-2249.1999.00109.x

Salazar-Camarena, D. C., Ortiz-Lazareno, P. C., Cruz, A., Oregon-Romero, E., Machado-Contreras, J. R., Munoz-Valle, J. F., et al. (2016). Association of BAFF. APRIL serum levels, BAFF-R, TACI and BCMA expression on peripheral B-cell subsets with clinical manifestations in systemic lupus erythematosus. *Lupus* 25, 582–592. doi: 10.1177/0961203315608254

Schiemann, B., Gommerman, J. L., Vora, K., Cachero, T. G., Shulga-Morskaya, S., Dobles, M., et al. (2001). An essential role for BAFF in the normal development of B cells through a BCMA-independent pathway. *Science* 293, 2111–2114. doi: 10.1126/science.1061964

Schneider, P. (2000). Production of recombinant TRAIL and TRAIL receptor:Fc chimeric proteins. *Meth. Enzymol.* 322, 322–345.

Schneider, P., MacKay, F., Steiner, V., Hofmann, K., Bodmer, J. L., Holler, N., et al. (1999). BAFF, a novel ligand of the tumor necrosis factor family, stimulates B cell growth. *J. Exp. Med.* 189, 1747–1756. doi: 10.1084/jem.189.11.1747

Schneider, P., Willen, L., and Smulski, C. R. (2014). Tools and techniques to study ligand-receptor interactions and receptor activation by TNF superfamily members. *Methods Enzymol.* 545, 103–125. doi: 10.1016/b978-0-12-801430-1.00005-6

Schuepbach-Mallepell, S., Das, D., Willen, L., Vigolo, M., Tardivel, A., Lebon, L., et al. (2015). Stoichiometry of heteromeric BAFF and APRIL cytokines dictates their receptor-binding and signaling propoerties. *J. Biol. Chem.* 290, 16330–16342. doi: 10.1074/jbc.m115.661405

Shin, W., Lee, H. T., Lim, H., Lee, S. H., Son, J. Y., Lee, J. U., et al. (2018). BAFF-neutralizing interaction of belimumab related to its therapeutic efficacy for treating systemic lupus erythematosus. *Nat. Commun.* 9:1200.

Smulski, C. R., and Eibel, H. (2018). BAFF and BAFF-Receptor in B Cell Selection and Survival. *Front. Immunol.* 9:2285. doi: 10.3389/fimmu.2018.02285

Smulski, C. R., Kury, P., Seidel, L. M., Staiger, H. S., Edinger, A. K., Willen, L., et al. (2017). BAFF- and TACI-Dependent Processing of BAFFR by ADAM Proteases Regulates the Survival of B Cells. *Cell Rep.* 18, 2189–2202. doi: 10.1016/j.celrep.2017.02.005

Stangel, M., Fredrikson, S., Meinl, E., Petzold, A., Stuve, O., and Tumani, H. (2013). The utility of cerebrospinal fluid analysis in patients with multiple sclerosis. *Nat. Rev. Neurol.* 9, 267–276. doi: 10.1038/nrneurol.2013.41

Steri, M., Orru, V., Idda, M. L., Pitzalis, M., Pala, M., Zara, I., et al. (2017). Overexpression of the Cytokine BAFF and Autoimmunity Risk. *N. Engl. J. Med.* 376, 1615–1626.

Tom, R., Bisson, L., and Durocher, Y. (2008). Transfection of HEK293-EBNA1 Cells in Suspension with Linear PEI for Production of Recombinant Proteins. *CSH Protoc.* 2008:rot4977.

Vigolo, M., Chambers, M. G., Willen, L., Chevalley, D., Maskos, K., Lammens, A., et al. (2018). A loop region of BAFF controls B cell survival and regulates recognition by different inhibitors. *Nat. Commun.* 9:1199.

Wang, H., Wang, K., Zhong, X., Qiu, W., Dai, Y., Wu, A., et al. (2012). Cerebrospinal fluid BAFF and APRIL levels in neuromyelitis optica and multiple sclerosis patients during relapse. *J. Clin. Immunol.* 32, 1007–1011. doi: 10.1007/s10875-012-9709-9

Wang, L. C., Liu, Z. Y., Gambardella, L., Delacour, A., Shapiro, R., Yang, J., et al. (2000). Regular articles: conditional disruption of hedgehog signaling pathway defines its critical role in hair development and regeneration. *J. Invest. Dermatol.* 114, 901–908. doi: 10.1046/j.1523-1747.2000.00951.x

Warnatz, K., Salzer, U., Rizzi, M., Fischer, B., Gutenberger, S., Bohm, J., et al. (2009). B-cell activating factor receptor deficiency is associated with an adult-onset antibody deficiency syndrome in humans. *Proc. Natl. Acad. Sci. U S A.* 106, 13945–13950. doi: 10.1073/pnas.0903543106

Xin, G., Shi, W., Xu, L. X., Su, Y., Yan, L. J., and Li, K. S. (2013). Serum BAFF is elevated in patients with IgA nephropathy and associated with clinical and histopathological features. *J. Nephrol.* 26, 683–690. doi: 10.5301/jn.5000218

Zhang, J., Roschke, V., Baker, K. P., Wang, Z., Alarcon, G. S., Fessler, B. J., et al. (2001). Cutting edge: a role for B lymphocyte stimulator in systemic lupus erythematosus. *J. Immunol.* 166, 6–10. doi: 10.4049/jimmunol.166.1.6

Zhukovsky, E. A., Lee, J. O., Villegas, M., Chan, C., Chu, S., and Mroske, C. (2004). TNF ligands: is TALL-1 a trimer or a virus-like cluster? *Nature* 427, 413–414. doi: 10.1038/427413a

Conflict of Interest: PS receives research funds from Merck KGaA for related research, and has a licence agreement with Adipogen Life Sciences. ODo is employee of Adipogen Life Sciences. ÖY is employee of Merck KGaA. ES was employee of EMD Serono.

The remaining authors declare that the research was conducted in the absence of any commercial or financial relationships that could be construed as a potential conflict of interest.

frontiers in Cell and Developmental Biology

BRIEF RESEARCH REPORT
published: 21 January 2021
doi: 10.3389/fcell.2020.577278

Coarse Grained Molecular Dynamic Simulations for the Study of TNF Receptor Family Members' Transmembrane Organization

Mauricio P. Sica[1,2] *and Cristian R. Smulski*[2]*

[1] *Instituto de Energía y Desarrollo Sustentable, Centro Atómico Bariloche, Comisión Nacional de Energía Atómica (CNEA), San Carlos de Bariloche, Argentina,* [2] *Medical Physics Department, Centro Atómico Bariloche, Comisión Nacional de Energía Atómica (CNEA), Consejo Nacional de Investigaciones Científicas y Técnicas (CONICET), San Carlos de Bariloche, Argentina*

OPEN ACCESS

Edited by:
Juan Jose Sanz-Ezquerro, National Center for Biotechnology (CNB), Spain

Reviewed by:
Antonio De Nicola, Yamagata University, Japan
Marçal Vilar, Superior Council of Scientific Investigations (CSIC), Spain
Tsjerk A. Wassenaar, University of Groningen, Netherlands

***Correspondence:**
Cristian R. Smulski
cristian.smulski@gmail.com

Specialty section:
This article was submitted to Signaling, a section of the journal Frontiers in Cell and Developmental Biology

Received: *29 June 2020*
Accepted: *21 December 2020*
Published: *21 January 2021*

Citation:
Sica MP and Smulski CR (2021) Coarse Grained Molecular Dynamic Simulations for the Study of TNF Receptor Family Members' Transmembrane Organization. Front. Cell Dev. Biol. 8:577278. doi: 10.3389/fcell.2020.577278

The Tumor Necrosis Factor (TNF) and the TNF receptor (TNFR) superfamilies are composed of 19 ligands and 30 receptors, respectively. The oligomeric properties of ligands, both membrane bound and soluble, has been studied most. However, less is known about the oligomeric properties of TNFRs. Earlier reports identified the extracellular, membrane-distal, cysteine-rich domain as a pre-ligand assembly domain which stabilizes receptor dimers and/or trimers in the absence of ligand. Nevertheless, recent reports based on structural nuclear magnetic resonance (NMR) highlight the intrinsic role of the transmembrane domains to form dimers (p75NTR), trimers (Fas), or dimers of trimers (DR5). Thus, understanding the structural basis of transmembrane oligomerization may shed light on the mechanism for signal transduction and the impact of disease-associated mutations in this region. To this end, here we used an *in silico* coarse grained molecular dynamics approach with Martini force field to study TNFR transmembrane homotypic interactions. We have first validated this approach studying the three TNFR described by NMR (p75NTR, Fas, and DR5). We have simulated membrane patches composed of 36 helices of the same receptor equidistantly distributed in order to get unbiassed information on spontaneous proteins assemblies. Good agreement was found in the specific residues involved in homotypic interactions and we were able to observe dimers, trimers, and higher-order oligomers corresponding to those reported in NMR experiments. We have, applied this approach to study the assembly of disease-related mutations being able to assess their impact on oligomerization stability. In conclusion, our results showed the usefulness of coarse grained simulations with Martini force field to study in an unbiased manner higher order transmembrane oligomerization.

Keywords: TNFRSF, tumor necrosis factor receptor superfamily, coarse grained, p75NTR, DR5, Fas (CD95), transmembrane helix assembly

INTRODUCTION

Several reports have shown the importance of pre-ligand assembly of different TNF receptor (TNFR) family members for proper ligand responses (Chan et al., 2000; Siegel et al., 2000; Clancy et al., 2005; Smulski et al., 2013, 2017; Pieper et al., 2014). This ligand-independent association of TNF receptors was initially suggested by the crystal structure of unliganded TNFR1 (Naismith et al., 1995). In that report the authors observed a parallel dimer in which the membrane distal cysteine-rich domain 1 mediated the main interaction interface. This region was not involved in ligand binding and thus seemed to play an exclusive role in pre-ligand assembly. Afterwards, two reports published back to back showed the importance of this region for proper ligand responses for TNFR1 and Fas (Chan et al., 2000; Siegel et al., 2000) and coined the term PLAD for pre-ligand assembly domain. Other reports confirmed these observations and extended it to other TNFR family members (Clancy et al., 2005; Smulski et al., 2013; Pieper et al., 2014). However, whether these associations persist following ligand binding or dissociate to give rise to different ligand-bound structures remains elusive. Moreover, how these oligomeric units (ligand free or ligand bound) impact on the intracellular organization and signal transduction ability, is completely unknown.

The link between extracellular events and intracellular signal transduction is clearly located in the transmembrane region. Thus, getting new insight into the oligomeric properties and the stoichiometry of associations on the transmembrane domains will allow a better understanding of ligand-independent associations, as well as ligand-induced transitions. Nuclear magnetic resonance (NMR) is the method of choice to study the structure and organization of transmembrane segments in a lipid environment. But protein solubility and non-native disulphide oligomerization mediated by free cysteines make this method very cumbersome to apply, especially with short peptides, which have to be mutated as in the cases of p75, Fas, and DR5. Alternatively, atomistic molecular dynamics simulations are suitable to study phenomena at sub-microsecond time-scale involving already formed oligomers of transmembrane segments. However, this approach is computationally infeasible to statistically sample processes at microsecond time-scales with membranes large enough to harbor dozens of individually separated transmembrane helices. Given these limitations, several methods were developed in order to reduce the computational burden of the simulations. Among them, coarse graining the system to a sub-residue level while keeping the relevant chemical properties of the beads, is able to establish a fine balance reaching the necessary sampling and statistical power with reasonable reduction in the detail of the system (Marrink et al., 2007). In addition it is also possible to identify different interfaces responsible for such interactions with sub-residue detail (Bradley and Radhakrishnan, 2013).

In this report we used coarse grained molecular dynamics simulations using the Martini force field to study the transmembrane domain of all available NMR structures of TNFR superfamily (SF) members: p75NTR wt and C257A (TNFRSF16), Fas (TNFRSF6), and DR5 (TNFRSF10B). Each one of these structures showed different association levels such as dimers (Nadezhdin et al., 2016), trimers (Fu et al., 2016), and dimer of trimers (Pan et al., 2019), respectively. Notably, this approach identified similar oligomeric units and similar residues involved in homotypic interactions for most of the simulated structures. This approach allowed to get unbiased information on higher order oligomers which are a key feature for signal transduction in the TNFR superfamily. Moreover, we have tested the impact of different disease related mutations on these associations as well as the differences between the NMR peptide sequences, where free cysteines were replaced by serine, vs. the wild type sequences. This method has proven to be reproducible and robust when compared to NMR data and set the bases for studying other TNFR family members, the impact of pathogenic mutations, different lipid compositions, and/or heteromeric associations.

METHODS

Coarse Grained Molecular Dynamic Simulations

Coarse-grained (CG) models were built to simulate the interactions of the transmembrane domains of DR5, Fas, and p75 embedded in a lipid bilayer environment solvated with explicit CG water. The CG peptides were constructed using the martinize.py tool (de Jong et al., 2013). The input structures for each helix were obtained from the oligomeric, all-atoms structures determined by NMR for DR5 (PDB: 6nhw), Fas (PDB: 2na7), and p75 (PDB: 2mic). Using pymol, the experimental structures were mutated when necessary to obtain the following input structures: p75 (dimer), Fas (wt), Fas (C178S), Fas (C178R), DR5 (wt), DR5 (A222Y), and DR5 (G217Y) (**Table 1**). It is worth noticing that Fas (C178S) corresponds to the peptide used in the NMR experiment (Fu et al., 2016).

The starting system consisted of a box of $25 \times 25 \times 10$ nm with 36 individual CG helices evenly spaced in the XY-plane with their axes oriented in the Z axis. The 36 helices were placed in a lipid bilayer on the XY-plane using the INSANE (INSert membrANE) tool, and randomly oriented around Z. The lipids were composed of DOPC and DLPC (7:3) equally distributed on both sides of the membrane. The coarse-grained chain L correlates with 12:0 (lauric) and 14:0 (miristic) saturated fatty acids, whereas chain O correlates with C16:1 (9c) (palmitoleic) and C18:1 (9c) (oleic) unsaturated fatty acids, allowing to build a model of a biological fluid membrane resembling the chain lengths used in NMR experiments. The system was completed with CG water beads and consisted of 36 peptides, 1,700 lipids, 26,000 waters, and 600 ions (150 mM concentration), totalling 48,000 particles. Simulations were carried out with the GROMACS package version 2016.5 (Abraham et al., 2015) using the Martini v2.1 forcefield (Marrink et al., 2007). After the initial steps of minimization and equilibration the systems were simulated with a 20 fs time step at 310 K and 1 bar using the velocity rescaling thermostat of Bussi et al. (2007) and the semi-isotropic Parrinello-Rahman barostat. Every system was simulated for at least 6 μs.

TABLE 1 | Description of the different transmembrane peptides and variants used in the present study, together with the simulation times reached for each peptide.

TNFR variant	Simulation time (μs)	Sequence
p75—NMR (2mic)	–	244-**M**TRGTTDNLIPVYCSILAAVVVGLVAYIAFKRWNS**S**KQNKQ-284
p75 dimer (SS)	6.7	248-TTDNLIPVYCSILAAVVVGLVAYIAFKRWNS**S**-279
p75 (SH)	6.5	248-TTDNLIPVYCSILAAVVVGLVAYIAFKRWNS**S**-279
p75—NMR (2mjo)	–	244-**M**TRGTTDNLIPVY**A**SILAAVVVGLVAYIAFKRWNS**S**KQNKQ-284
p75 (C257A)	8.6	248-TTDNLIPVY**A**SILAAVVVGLVAYIAFKRWNS**S**-279
Fas—NMR (2na7)	–	171-RSNLGWL**S**LLLLPIPLIVWVKRKEVQKT-198
Fas wt	7.3	171-RSNLGWLCLLLLPIPLIVWVKRKE-194
Fas-C178S	9.1	171-RSNLGWL**S**LLLLPIPLIVWVKRKE-194
Fas-C178R	7.3	171-RSNLGWL**R**LLLLPIPLIVWVKRKE-194
DR5—NMR (6nhw)	–	207-**M**P**G**SLSGIIIGVTVAAVVLIVAVFVCKSLLWKKVL-241
DR5 wt	8.6	207-SPCSLSGIIIGVTVAAVVLIVAVFVCKSLLWKKVL-241
DR5-A222Y	8.7	207-SPCSLSGIIIGVTVA**Y**VVLIVAVFVCKSLLWKKVL-241
DR5-G217Y	9.4	207-SPCSLSGIII**Y**VTVAAVVLIVAVFVCKSLLWKKVL-241

Bold letters indicate mutated residues.

Contact Maps

For each residue (i) of every helix (H) the number of contacts against all the other residues in the remaining helices, along the simulation time (T) was computed. A contact was defined when the BB atoms of two residues are located at XYZ-distance equal to or less than an arbitrary cut-off, as follows:

$$C_{ij}^{KL} = \begin{cases} 1, \text{ if } \left\| \mathrm{r}_i^K - \mathrm{r}_j^H \right\| \leq d_{\text{cutoff}} \\ 0, \text{ if } \left\| \mathrm{r}_i^K - \mathrm{r}_j^H \right\| > d_{\text{cutoff}} \end{cases}$$

where i and j are the residue number in the peptide sequence (i = {1,...,j,...,N}), and H and K are the helices analyzed (H = {1,...,K,...,36}). Thus, the number of contacts (NC) for every residue i against each residue j in the remaining (K) helices were computed as:

$$NC_{ij} = \sum_T \sum_j^{K \neq H} C_{ij}^{HK}$$

We always computed all 36 helices present in the membrane patch against each other. The NMR structures were analyzed considering each model of the PDB file (10 or 15) as a simulation-snapshot. Each individual model was converted to CG model prior to the analysis of contact residues and radial density. We applied two different cut-off distances: 0.5 and 0.8 nm based on the average distance of dimeric or trimeric associations observed in the three NMR structures used as reference in this study. DR5 dimers showed closer interaction interfaces when compared to trimeric assemblies and thus, it was necessary to use two cut-offs distances to fully characterize different assembly modes. Notably, shorter cut-offs distances (0.4 nm) fail to detect any interaction, whereas longer cut-offs distances (1 nm) loose specificity.

Radial Density

Radial density maps were built to observe the preferential contact side between helices in the XY-plane. First, the centroid (C) of every helix was computed between a defined central backbone (BB) atom (i) and one consecutive BB atom at each side in the sequence ($C_i = (r_{i-1}+r_i+r_{i+1})/3$), where r is the *XYZ*-coordinate of the atom (we tested the tool using two BB atoms at each side and observed no significant differences). Second, the unit bisection vector was computed between the central (i) and adjacent BB atoms (i±1), according to the method of Khan to identify the helix orientation (Kahn, 2001). Third, a reference frame was defined with the centroid of the reference helix as origin and its orientation vector as unit X-vector, and the position of the centroids of the remaining 35 helices were computed. This procedure was repeated for all 36 helices present in the membrane patch along the indicated simulation time every 100 ns until the end of the simulated period. The scatter plot of the accumulated XY-centroids positions was transformed to a density map with ggplot implemented in R. This procedure was repeated with every residue along the peptide.

Symmetry

Symmetry analysis was performed using the Analytical Analyzer of Symmetries software [Ananas (Popov and Grudinin, 2014; Pagès and Grudinin, 2018; Pagès et al., 2018)] using the selected snapshots from the CG simulations.

RESULTS

p75NTR (TNFRSF16)

Because p75NTR is a covalently linked dimer, we generated a membrane patch and placed 18 evenly distributed disulphide-bonded dimers (36 transmembrane segments) (sequences are shown in **Table 1**). We extended the coarse-grained (CG) molecular dynamic (MD) simulation to 6.7 μs and compared the output data with the reference NMR structural data (PDB: 2mic) by using the analytic tools described in Methods. We have observed that this and the following simulations converged before 3 μs. In addition, the area-per-lipid and membrane thickness also converged to the standard values of 0.73 nm^2 and 3.6 nm, respectively. We first evaluated the residues involved in helix-to-helix interactions between the 36 helices integrating all data points from the third μs of simulation until the end

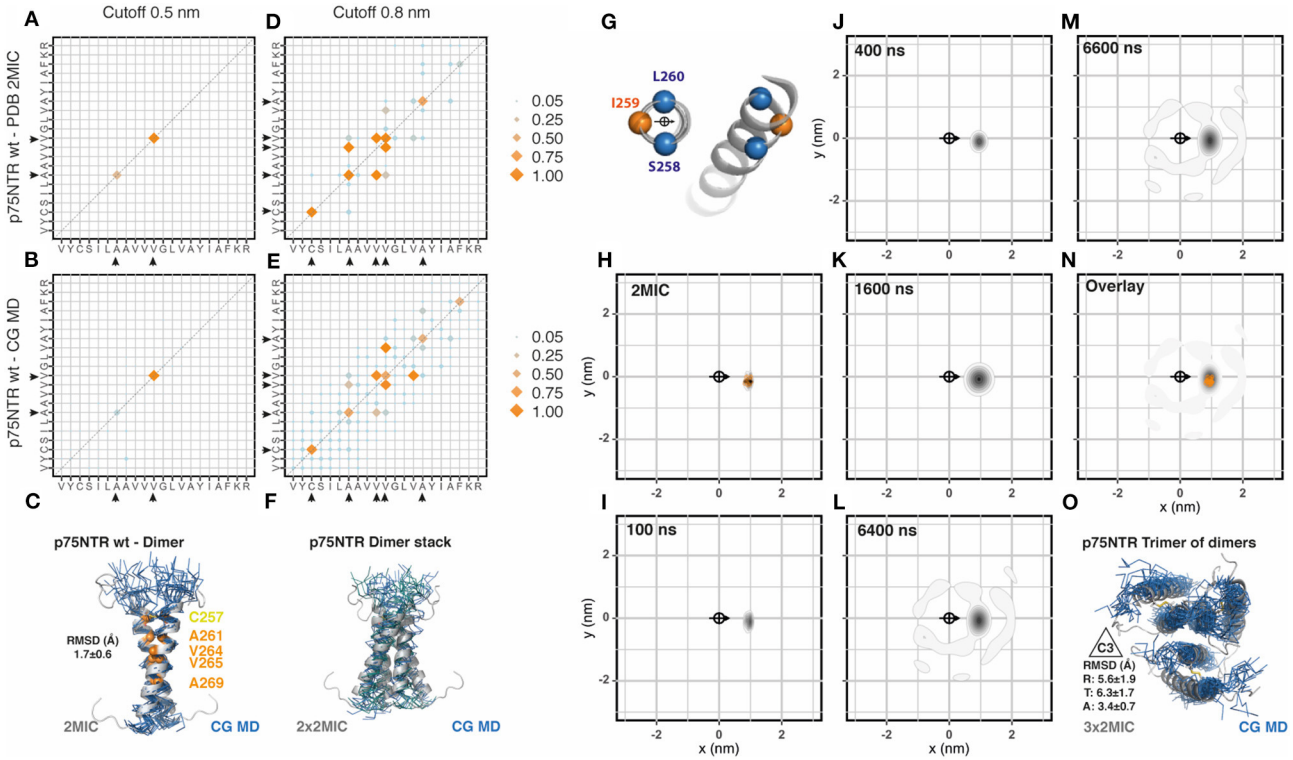

FIGURE 1 | p75NTR assembly. **(A)** Contact matrix of p75NTR wt NMR (PDB:2mic) at 0.5 nm cut-off distance. The amino acid sequence corresponds to residues V254 to R274. Black arrowheads indicate the residues involved in these interactions. Data corresponds to the averaged 10 NMR models. Scales correspond to the number of contacts normalized to the most frequent one [NC_{ij}/major(NC_{ij})]. **(B)** Same as **(A)**, for p75NTR coarse grained molecular dynamic (CG-MD) simulation. The analysis was performed on the full system (36x36) between 3 and 6 μs. **(C)** Alignment of the p75NTR NMR average model with a random p75NTR CG-MD dimer, together with the analysis of the averaged root mean square deviation (RMSD) of the alignment. **(D)** Same as **(A)**, but using a cut-off distance of 0.8 nm. **(E)** Same as **(B)**, but using a cut-off distance of 0.8 nm. **(F)** Example of stable interactions between dimers observed along the simulation, aligned to the reference structure 2 mic. **(G)** Residues chosen for the centroid and orientation vector used for radial distribution analysis. **(H)** Radial distribution analysis of p75NTR NMR structure 2mic, analyzed as coarse grained structure. The scale corresponds to the 2D-density function built from the scatter plot of *XY*-coordinates, as described in Methods. **(I–M)** Radial distribution analysis of different snapshots of p75NTR CG-MD at the indicated time points. **(N)** Overlay of the radial distribution of the reference structure (2mic, orange dots) and the CG-MD structures (gray density scale). **(O)** Example of a stable trimer of dimers found at early time points, assembled into the characteristic 3-fold symmetry axes C3, together with the averaged radial (R), tangential (T), and axial (A) RMSD.

of the simulated period. To this end, we generated a contact matrix of the residues closer than 0.5 nm for the NMR and the CG-MD simulated data (**Figures 1A,B**, respectively, and **Supplementary Figure 1**) which resulted in identical contact residues. These residues were located on the dimeric interface of the NMR structure at the crossing point (AxxxV). To further compare the similarity between the dimeric structure obtained by the two approaches, we aligned the NMR dimeric structures with the CG-MD structures backmapped to all atom structures as described in Wassenaar et al. (2014) and observed an average root mean square deviation (RMSD) value of 1.7 ± 0.6 Å (**Figure 1C**). Similar results were observed when analyzing the 0.8 nm cut-off but with a few additional contact points toward the C- and N-terminal regions for both NMR and CG simulations (**Figures 1D,E**). The residues observed in the 0.8 nm cut-off radius included the two residues observed in the 0.5 nm cut-off, indicating that both contact matrices are showing the same interaction interface. In addition to the main dimeric association, we observed several dimers stacks in a very conserved parallel arrangement (**Figure 1F**). In order to better characterize the dynamics of the spatial distribution of p75NTR dimers, we then analyzed the radial distribution around each one of the 36 helices present in the membrane patch against each other at different time points along the simulation period. The orientation was determined by the residues S258, I259, and L260 which were also used to determine the center of reference (**Figure 1G**). We performed this analysis on the 10 coarse-grained NMR (CG-NMR) models available in the 2mic PDB structure (**Figure 1H**) and, as expected, we observed only one position corresponding to the covalent dimer. When we applied this analysis to the CG-MD simulation, we observed a main spot corresponding to the covalent dimer at early time points (**Figures 1I–K**). Notably, higher order associations between dimers were observed at later time points (**Figures 1L,M**). The overlap of the radial distribution of the CG-NMR structure with the CG-MD simulation showed that the covalently linked dimers are exactly on the same relative position in the radial map (**Figure 1N**). Amongst the higher order associations formed during the CD-MD, we observed a

stable trimer of dimers with the characteristic 3-fold symmetry axes (C3) (**Figure 1O**). Using the C3 relative orientation as cutoff criteria we quantified four different disulphide linked dimers, with a mean association time of 325 ns, present at different time points. This observation is compatible with the trimeric organization observed in Fas and DR5, which is notably conserved across the structure of TNF superfamily ligands and signal adaptor molecules TRAFs. The evolution of the CG-MD simulation is shown in **Supplementary Movie 1**.

Experimental data showed that, under reducing conditions, p75NTR wt is in a monomer-dimer equilibrium with the C257 residue located on the dimeric interface (Nadezhdin et al., 2016). We therefore also simulated a reduced version of p75NTR wt and compared the results to another available NMR structure (2mjo) corresponding to the functionally inactive p75NTR C257A mutant, which shows a left handed dimer through the AxxxG motif located on the opposite face of the α-helix (**Supplementary Figure 1**). Both simulations showed a rather diffuse contact matrix when using a cut-off of 0.8 nm, which may suggest a diversity of configurations. These matrices do, however, include the contacts observed in the NMR structures. Notably, both CG-MD simulations showed many similarities between them regarding the radial distribution, which is in agreement with the lack of disulphide bonds between helices (**Supplementary Figure 1B**, bottom panels). Moreover, there were two visible spots (among others) in each simulation (reduced p75NTR and C257A) that overlapped partially with the corresponding dimers observed in the two NMR reference structures (**Supplementary Figure 1B**, bottom panels, orange and blue dots). Nevertheless, only the spots located close to the disulphide-linked-like region (**Supplementary Figure 1B**, bottom panels, orange dots) showed a main relative orientation of ∼180° for both non-dimeric structures (reduced p75NTR and C257A). Although these results do not match the NMR reference structure (2mjo), they could arise from differences between lipid phases since NMR experiments were made in detergent micelles and our simulation in phospholipid bilayers.

Fas (TNFRSF6)

Different from p75NTR, Fas NMR structure showed a trimeric assembly. We followed the procedure previously described and inserted 36 Fas transmembrane segments evenly distributed in the membrane patch. The Fas sequence used for the simulation corresponded to the Fas variant C178S used for the NMR structure (PDB: 2na7) as shown in **Table 1**. The analysis of the residues involved in helix-to-helix contacts using a cut-off distance of 0.5 nm showed very few contact residues, which is explained by the relative distance between the helices forming the trimeric assembly (**Figures 2A,B**, **Supplementary Figure 2**). Initially, mainly dimeric associations were observed. These dimers were placed in two main orientations compatible with a two-fold symmetry axis (∼25%) and with a 3-fold symmetry axis (C3, ∼19%) allowing the late inclusion of the third helix of the trimer. When aligned to the NMR structure, these dimers showed an average RMSD value of 3.4 ± 0.7 Å (**Figure 2C**). The analysis of the 0.8 nm cut-off distance showed very well-conserved residues. However, these residues seem to be rather flexible in the CG-MD, most probably due to the late formation of the complete trimeric unit or to the presence of alternative assembly modes using the same interfaces (**Figures 2D,E**). At later time points, it is possible to identify two trimeric assemblies which resemble the NMR structure (**Figure 2F**). Then, we analyzed the radial distribution around each one of the 36 helices present in the simulation against each other. The orientation was determined by the residues L181, L182, and P183 which were also used to determine the center of reference (**Figure 2G**). We performed this analysis for the CG-NMR structures computing the 15 different models available in the NMR structure file (PDB: 2na7) (**Figure 2H**). As expected, we observed two main positions corresponding to the trimeric assembly. When we applied this analysis to the CG-MD simulation we observed a main spot corresponding to the trimer-compatible dimer and two other, less strong signals at early time points (**Figures 2I–K**). At later time points, the second trimer-compatible spot starts to get defined (**Figures 2L,M**). The overlap of the radial distribution of the CG-NMR structure with the CG-MD simulation showed that the NMR trimer position corresponds to two out of the three spots observed in the CG-MD simulation. The third spot, located in the upper left side of the central helix corresponded to the asymmetric helix of the trimer when it is located at the center of the quadrant (**Figures 2N,O**). Using a clustering approach to isolate the main NMR-like cluster, we found an average of 26.2 ± 1.3 C2 dimers that were formed between 28 different transmembrane helices. The accumulated association time was 32.5 ± 1.3 μs and the most stable associations extended for over 5.4 μs. The combined analysis of trimeric assemblies on the two NMR-like clusters showed an average of 33.6 ± 1.2 C3 dimers that were formed between 34 different transmembrane helices. However, the accumulated association time was lower than C2 dimers (16.7 ± 1.1 μs), being the most stable association 3.8 μs. All together, these results suggested that Fas trimeric assembly during the CG-MD simulation might occur in at least three steps characterized by the initial assembly of a trimer-compatible dimer, the association of an asymmetric third helix (which produces the third spot on the top-left side of the central helix) and the re-placement of this third helix (**Figure 2O**). However, we could not find any inverse correlation between the amount of dimers and trimers along the simulated period. The evolution of the CG-MD simulation is shown in **Supplementary Movie 1**.

One drawback of NMR methodology is the presence of cysteine residues in the peptide sequence. The side chain of free cysteines is highly reactive and affects the solubility of the peptide so it is frequently replaced by serine. This was the case of Fas NMR reference structure (PDB: 2na7, C178S). We therefore generated and simulated the wt sequence of Fas as well as a pathogenic mutation C178R located at the same residue mutated in the NMR structure, which is associated with cutaneous squamous cell carcinoma (Lee et al., 2000). Similar to Fas C178S, Fas wt showed early time point stable dimers. However, these dimers were formed in a different position, which correspond to the asymmetric third helix observed in Fas C178S CG-MD (**Supplementary Figure 2**). The main NMR-like spot was severely reduced in these two structures (Fas wt and C178R) but in a different manner: while Fas wt showed an average of

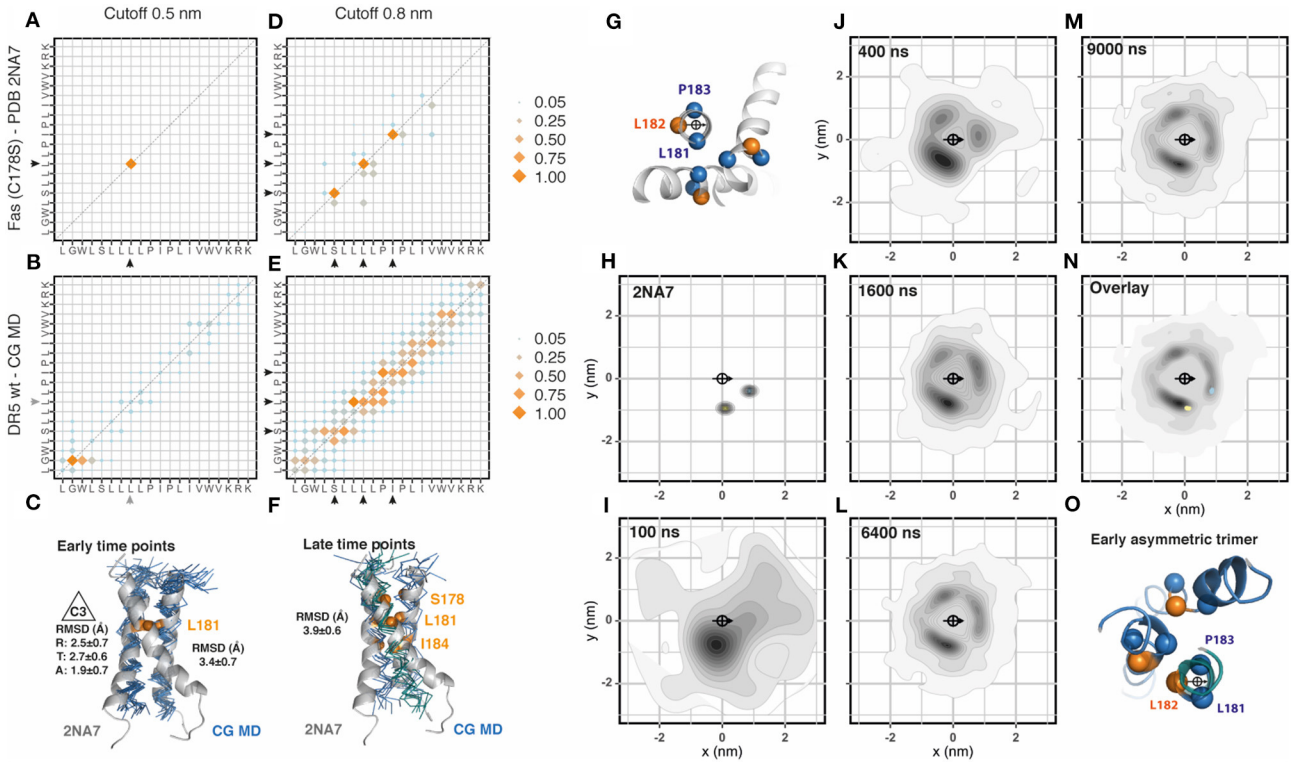

FIGURE 2 | Fas assembly. **(A)** Contact matrix of Fas C178S NMR (PDB:2na7) at 0.5 nm cut-off distance. The amino acid sequence corresponds to residues L174 to K193. Black arrowheads indicate the residues involved in these interactions. Data corresponds to the averaged 15 NMR models. Scales correspond to the number of contacts normalized to the most frequent one. **(B)** Same as **(A)**, for Fas C178S CG-MD simulations. Gray arrowheads indicate non-conserved interactions observed only in the simulation. The analysis was performed on the full system (36 × 36) between 3 and 6 μs. **(C)** Alignment of the Fas NMR average model with a Fas CG-MD dimer arranged in a 3-fold symmetry axes (C3). This structure is formed at early simulation times (0.5–1 μs). The averaged root mean square deviation (RMSD) of the alignment is indicated on the right and the averaged radial (R), tangential (T), and axial (A) RMSD is indicated on the left. **(D)** Same as **(A)**, but using a cut-off distance of 0.8 nm. **(E)** Same as **(B)**, but using a cut-off distance of 0.8 nm. **(F)**. Alignment of the Fas NMR average model with a Fas CG-MD trimer, together with the analysis of the averaged root mean square deviation (RMSD) of the alignment. This structure is formed at late time points (5–6 μs). **(G)** Residues chosen for the centroid and orientation vector used for radial distribution analysis. **(H)** Radial distribution analysis of the coarse grained Fas C178S NMR structure 2na7. The scale corresponds to the 2D-density function from the scatter plot, as described in Methods. **(I–M)** Radial distribution analysis of different snapshots of Fas C178S CG-MD at the indicated time points. **(N)** Overlay of the radial distribution of the reference structure (2na7, blue/yellow dots) and the CG-MD structures (gray density scale). **(O)** Example of an early trimer, where the third helix assembles in an asymmetric manner, generating the visible spot on top of the central helix.

27.6 ± 1.2 C2 pairs with an accumulated association time of 13.9 ± 0.7 μs, Fas C178R showed an average of 16.2 ± 0.9 C2 pairs with an accumulated association time of 7.0 ± 0.3 μs. These observations suggest that the main NMR-like spot is severely affected by these two mutations which are facing in that direction. Comparing Fas wt with Fas C178R we observed similar distribution patterns although the main spots of Fas C178R were rotated anti-clockwise when compared to Fas wt. Interestingly, we observed conserved numbers of C3 compatible dimers in Fas wt (35 ± 0.7) with an accumulated association time of 18.6 ± 1.1 μs, which is in clear contrast to Fas C178R that showed an average of 24.6 ± 1.2 C3 pairs with an accumulated association time of 9.1 ± 1.2 μs. We didn't observe any stable trimer formation in these two structures. Importantly, Fas wt contact matrix showed a rather organized assembly with three main contacts that differ from Fas C178R, indicating that the mutation alters the interaction interfaces thereby changing the geometry of the assembly (**Supplementary Figure 2**).

DR5 (TNFRSF10B)

The most recently published transmembrane NMR structure of a TNFRSF member corresponds to DR5 (Pan et al., 2019). In this structure (PDB: 6nhw) it is possible to observe a dimer of trimers, which is the most complex assembly described so far for the transmembrane region of a TNFRSF member. We followed the same procedure previously described and inserted 36 DR5 transmembrane segments evenly distributed in a membrane patch. The sequence corresponded to DR5 wt, which differs from the mutated version used for NMR (C209G) as shown in **Table 1**. The analysis of helix-to-helix residue contacts using a cut-off distance of 0.5 nm showed the same dimeric interface observed in NMR experiments (**Figures 3A,B**, **Supplementary Figure 3**). There were some minor differences in the pairing of the GxxxG motif known for mediating transmembrane helix dimerization but not trimerization (MacKenzie et al., 1997; Trenker et al., 2015). The reasons for these deviations may be multiple: i.e., a slight change in tilt can prevent the contact between two

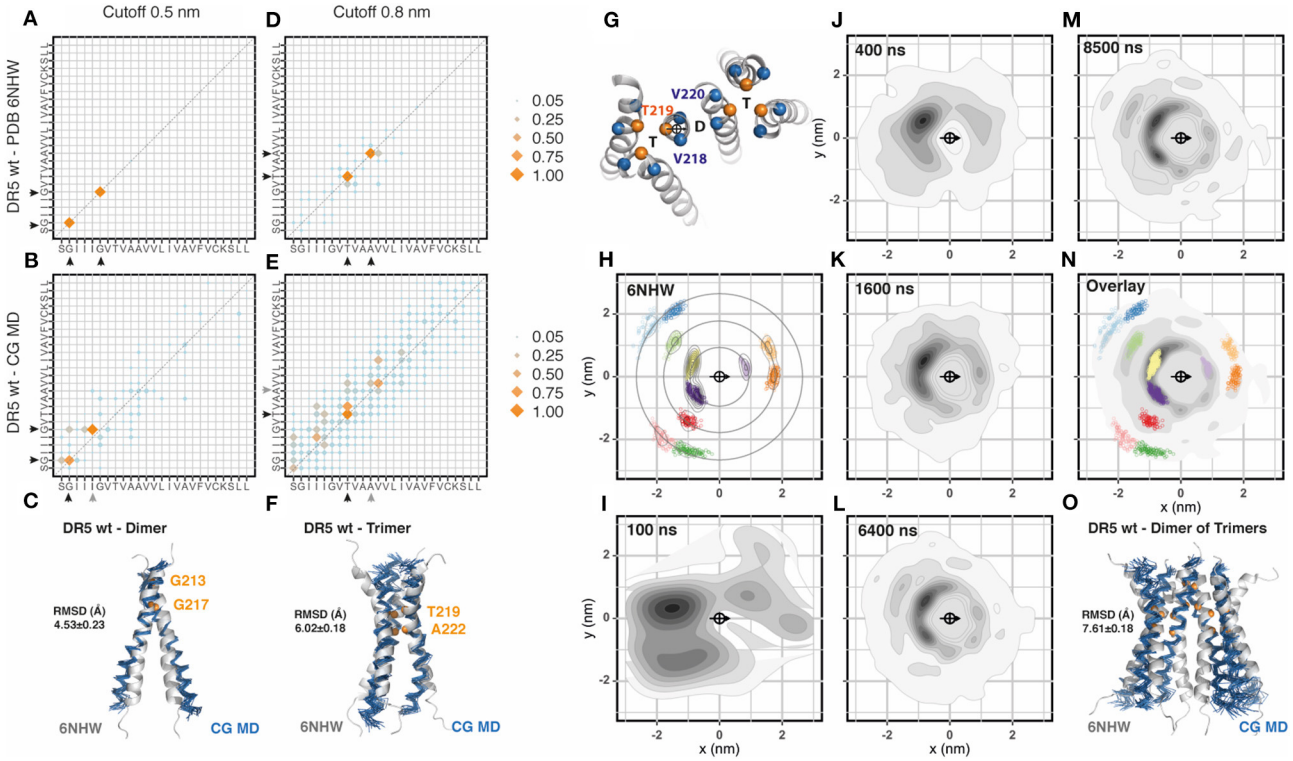

FIGURE 3 | DR5 assembly **(A)**. Contact matrix of DR5 NMR (PDB:6nhw) at 0.5 nm cut-off distance. The amino acid sequence corresponds to residues S212 to L236. Black arrowheads indicate the residues involved in these interactions (GxxxG motif). Data corresponds to the averaged 15 NMR models. Scale corresponds to the number of contacts normalized to the most frequent one. **(B)** Same as **(A)**, for DR5 coarse grained molecular dynamic (CG-MD) simulations. Black arrowheads indicate conserved interactions whereas gray arrowheads indicate non-conserved interactions. The analysis was performed on the full system (36 × 36) between 3 and 8 μs. **(C)** Alignment of DR5 NMR average dimer with a DR5 CG-MD dimer, together with the analysis of the averaged root mean square deviation (RMSD) of the alignment. **(D)** Same as **(A)**, but using a cut-off distance of 0.8 nm. **(E)** Same as **(B)**, but using a cut-off distance of 0.8 nm. **(F)** Alignment of DR5 NMR average model with a DR5 CG-MD trimer, together with the analysis of the averaged root mean square deviation (RMSD) of the alignment. **(G)** Residues chosen for the centroid and orientation vector used for radial distribution analysis. **(H)** Radial distribution analysis of coarse grained DR5 NMR structure 6nhw. Note that it is possible to identify dimers, trimers, and higher order assemblies in consecutive orbits. Scale corresponds to the 2D-density function from the scatter plot, as described in Methods. **(I–M)** Radial distribution analysis of different snapshots of DR5 CG-MD at the indicated time points. **(N)** Overlay of the radial distribution of the reference structure (6nhw, color dots) and the CG-MD structures (gray density scale). **(O)** Alignment of DR5 NMR average dimer of trimers with a DR5 CG-MD assembly, together with the analysis of the averaged root mean square deviation (RMSD) of the alignment.

glycine and slide this contact one position, especially if the glycine is flanked by two bulky residues as Ile and Leu. Next, we aligned the NMR dimer with the CG-MD structure and observed stable dimers that match the reference structure with an averaged RMSD of 4.53 ± 0.23 Å (**Figure 3C**). The analysis of the 0.8 nm cut-off distance showed very well-conserved residues with some minor differences toward the C-terminal region of the interaction interface (**Figures 3D,E**). Note that the residues observed at 0.5 and 0.8 nm cut-off were different and corresponded to the dimeric and trimeric assembly, respectively. The alignment of the NMR trimer to the CG-MD trimers showed an averaged RMSD of 6.02 ± 0.18 Å (**Figure 3F**). Then, we analyzed the radial distribution around each one of the 36 helices present in the simulation against each other. The orientation was determined by the residues V218, T219, and V220 which were also used to determine the center of reference (**Figure 3G**). We performed this analysis for the CG-NMR structure computing the 15 different models available in the NMR structure file (**Figure 3H**). As expected, we observed the full landscape of associations, namely dimers, trimers and dimers of trimers in consecutive orbits around the central helix. When we applied this analysis to the CG-MD simulation at early time points, we observed two main spots corresponding to one of the trimeric units and one clearly distinct spot corresponding to the dimer (**Figures 3I–K**). As the simulation proceeds, the second trimeric spot starts to get defined together with higher order oligomers present in consecutive orbits around the central helix (**Figures 3L,M**). The overlap of the radial distribution of the CG-NMR structure with the CG-MD simulation showed a striking similar distribution, even in regions far away from the central helix (**Figure 3N**). These results indicate that CG-MD simulation of DR5 transmembrane domain can identify the characteristic dimer of trimers observed in NMR studies (**Figure 3O**). However, there were a few unidentified spots around the central helix that could not be assigned to dimers or trimers. Using a clustering approach to isolate the

main spots on the first orbit (<1.5 nm) it was possible to analyse the distance and relative orientations of each cluster (**Supplementary Figures 4A,B**). We used two reference residues to study the dimeric (G217) and the trimeric (T219) assembly matching the contact matrix (**Supplementary Figures 4C,D**). Each cluster was isolated and analyzed in a comparative manner against the expected NMR distribution and against each other cluster for distance, radial location (alpha), and relative orientation (beta) (**Supplementary Figures 4C,D**). This analysis showed that the dimeric cluster although being less populated than others can be clearly identified by its proximity to the central helix and by its relative (beta) orientation, close to 180° (**Supplementary Figure 4C**). The trimeric assembly was clearly more populated but also showed distinct features that differentiate them from the neighbor spots. They showed a closer proximity to the central helix and a relative orientations closely matching the expected C3 relative orientation of 120 and 240° (beta) (**Supplementary Figure 4D**). The remaining spots showed complex mixed compositions in terms of relative orientations. We generated a Markov chain model with the trajectories along the radial clusters which showed that the unidentified spots travel toward the neighbor main spots with relatively high probability. Also, the probability of remaining in the same cluster is higher for the dimeric and trimeric spots (**Supplementary Figure 4E**). Using the clustering approach and the relative orientation criteria we observed an average of 17.8 ± 1 C2 dimers that were formed between 28 different transmembrane helices. These dimers showed an accumulated association time of 18.1 ± 0.9 μs (**Supplementary Figure 4C**). Additionally, there was an average of 11.3 ± 1 C3 trimers that were formed between 27 different transmembrane helices. These trimers showed an accumulated association time of 25.3 ± 1.8 μs (**Supplementary Figure 4D**). The evolution of the CG-MD simulation is shown in the **Supplementary Movie 1**.

Based on their NMR structure, Pan and colleagues (Pan et al., 2019) introduced two different mutations into the DR5 transmembrane sequence to disrupt dimeric (G217Y) or trimeric (A222Y) interactions. Therefore, we performed a CG-MD simulation for each one of these DR5 mutants and compared them to the wt sequence. Mutation G217Y, aimed at disrupting dimers, showed conserved trimeric spots but reduced dimeric spots in the radial distribution plots. The contact matrix confirmed the impact of the G217Y mutation on the dimerization face but also showed some differences in the trimerization face. As expected, the analysis of the dimerization rate showed reduced number of dimers with reduced association times. However, despite showing conserved NMR-like trimeric spots, the trimerization rate was also affected due to a wider distribution of the relative orientations (beta angles) of the helices when compared to wt DR5 simulation (**Supplementary Figure 4D**). Mutation A222Y, aimed at disrupting trimers, showed a clearly conserved dimeric spot while the two trimeric spots were fused into one strong signal in between the two wt positions (**Supplementary Figure 3**). The clustering analysis confirm this observation, showing a conserved dimeric assembly and a strongly impaired trimeric assembly (**Supplementary Figure 4**). Our results indicate that CG-MD simulation of DR5 transmembrane region recapitulates the main features described for the wt sequence like dimerization, trimerization, and the complex dimer of trimer assembly. Additionally, our results showed a broader impact of the specific mutations that were described to affect exclusively dimeric or trimeric associations.

DISCUSSION

Since the report of the first structure of the extracellular domain of the unliganded tumor necrosis factor receptor (Naismith et al., 1995), the TNF-related scientific community is interested in understanding the role of ligand independent receptor assembly in signal transduction. Naismith and colleagues showed that the soluble extracellular domain of TNFRSF1A was able to form homodimers in the absence of ligand and opened the discussion of whether these dimers restrain the receptor in an inactive ligand-free state or if they persist following ligand binding to extend an activating network (Naismith et al., 1996). Because TNF family ligands are trimeric molecules and signal adaptor molecules of the TNFR associated factors (TRAF) group are also trimeric proteins it seems possible that ligand independent dimers represented a "silent" receptor form. Several reports confirmed the occurrence of extracellular, ligand-independent associations, and its importance for proper ligand binding and signal transduction (Chan et al., 2000; Siegel et al., 2000; Clancy et al., 2005; Smulski et al., 2013; Pieper et al., 2014). However, such a model cannot be extended to small TNFR superfamily (TNFRSF) members which do not possess a pre-ligand assembly domain, and also it does not explain the impact of pathogenic mutations located in the transmembrane region of several TNFRSF members. Recent reports showed the active role of the transmembrane domains to stabilize homotypic interactions in different TNFRSF members, participating actively in signal transduction (Fu et al., 2016; Nadezhdin et al., 2016; Pan et al., 2019). These studies used the NMR technique to obtain structural information on the transmembrane domain organization. So far, 3 out of 30 TNFRSF members transmembrane regions have been studied by NMR and each one of them showed different association patterns: p75 assembles as a covalent dimer, Fas assembles as a trimer, and DR5 assembles as a dimer of trimers. Unfortunately, such differences between available structural data make it impossible to generalize any kind of conserved molecular determinants, pattern, or interaction motif. Moreover, NMR studies are complex and expensive and it is thus unlikely that sufficient data will be obtained on the remaining TNFRSF to conclude on the physiological function of their transmembrane associations or the impact of disease-associated mutations in the transmembrane region.

There are a few available methods to perform structural modeling of TM α-helical with the limitation that most of them are restricted to the simulation of dimers: PREDDIMER (Polyansky et al., 2014), CATM (Mueller et al., 2014), EFDOCK-TM (Wang and Barth, 2015), or TMDOCK (Lomize and Pogozheva, 2017). However, TNFRSF members seem to associate as higher order oligomers such as trimers, or dimers of trimers.

To be able to explore such complex level assemblies, we used CG-MD simulations which allowed us to explore oligomerization as a dynamic process occurring at the microsecond time scale, which would be impossible with atomistic simulations (Bradley and Radhakrishnan, 2013). Given the diversity of structures observed in these three NMR models, we could assess the potential and shortcomings of CG-MD simulations to study different transmembrane association modes in different TNFR superfamily members.

There are a few reports on the use of coarse-grained molecular dynamic simulations to study dimeric, trimeric or tetrameric assemblies. However, most of them just place in their membranes the exact number of helices that they want to study (Hall et al., 2014; Wassenaar et al., 2015; Han et al., 2016) (biased approach), or several copies with the aim of characterizing just one kind of association (i.e., dimers) (Periole et al., 2012). In order to allow the unbiassed formation of complex oligomeric arrays and increase the statistical sampling of our results, we introduced 36 evenly distributed and randomly oriented helices and let the system evolve for a time frame of at least 6 μs. The membranes were built with phospholipids of fatty acid length and head groups similar to the ones used in NMR experiments. To consolidate the unbiased approach, we analyzed all 36 helices against each other for close contact residues and relative positions of neighbor helices and compared the results to the corresponding structural data available.

Our data using p75NTR sequence (disulphide linked dimers) showed a striking similarity when compared to the PDB 2mic, both at the level of residues involved in helix to helix interactions and at the observed radial distribution. In addition, we could observe some higher order oligomers, dimers stacks and an intriguing trimer of dimers with a stable 3-fold symmetry axes (C3) along the simulation. These higher order complexes were less prominent than the covalently linked dimers and therefore, their detection was not evident in the radial distribution analysis. Whether these associations are of functional relevance need to be assessed under specific experimental conditions. Notably, the analysis of p75NTR C257A variant, despite being very similar to the reduced p75NTR wt form, did not match the NMR reference model (2mjo). However, NMR experiments with p75NTR used micelles of dodecyl phosphocholine detergent which might not mimic properly the lateral diffusion of plasmatic membranes as reported by a study on integrins that form dimers in detergents but oligomers in liposomes (Yu et al., 2015).

The analysis of Fas showed a few differences when compared to NMR data. Initially, mainly dimeric associations were observed placed in one of the expected NMR trimeric spots. These dimers were placed in a range of different orientations, being the main ones a two-fold (∼180°) and a 3-fold (∼120°) symmetry axis. Toward the latest time points of the simulation it was possible to observe slowly forming NMR-like trimers. These, behavior could arise from our simulation conditions. Longer simulation times or higher helix concentrations may be necessary to properly sample this system and approach reasonably to the equilibrium. It is noteworthy that Fu et al., proposed that the inactive receptor form corresponded to a dimer whereas the active form corresponded to the trimer and, thus, the NMR trimer may reflect the active receptor structure (Fu et al., 2016). Unfortunately, they did not provide any structural information on the dimeric assembly. Still, it is tempting to speculate that the inactive dimer may correspond to the incomplete trimer, which is formed in a C2 symmetry, ready to be reoriented in a C3 symetry and allow the inclusion of a third helix following ligand binding.

Because Fas NMR experiments were performed with Fas C178S, we simulated the wt sequence and a pathogenic mutation located in the same residue C178R (Lee et al., 2000). Intriguingly, Fas wt did not fully reproduce Fas C178S behavior but showed an alternative assembly mode forming mainly dimers. This seemingly discrepancy can be due to the impact of the mutation itself, to artifacts during the CG-MD simulations or could be a consequence of the lipid environment. Indeed, NMR studies were carried out in bicelles composed of homo-diacyl glycerophosphocholines with myristic fatty acid and hexanoic acid that might not reproduce the properties of a biological bilayer (Nadezhdin et al., 2016). Despite these differences, residue 178 is located toward the trimeric contact face and, although the Cys-to-Ser replacement implies only one atom, both residues have remarkable differences regarding their hydrophobicity, which may impact on wt-like associations.

The analysis of DR5 showed remarkable similarities when compared to the NMR structural data. This was the case for the contact residues involved in dimeric and trimeric interactions and also for the radial distribution. We could identify dimers, trimers and a dimer of trimers and the radial distribution showed conserved positions across several orbits beyond the central helix. However, the analysis of the mutation G271Y and A222Y showed not only altered dimeric and trimeric assembly, respectively, as it was described before (Pan et al., 2019), but also changes in the relative orientations of the remaining associations that were supposed to be unaffected. Despite the sequence of DR5 used for NMR studies was C209G, we used the wt sequence for CG-MD without observing major differences, most probably due to the fact that this residue was located in the extracellular interface and did not participate in any helix-helix interaction.

There are several types of *post-hoc* analysis that can be applied to the data depending on specific biological questions. In this study we systematically compared our observations to the corresponding NMR structures to validate the use of coarse-grained molecular dynamic simulations to study TNFR superfamily members. Among the several possible analyses, data can be filtered using geometrical criteria for dimers, trimers or more; or analyse the relative position of the spots around the central helix (alpha angle) vs. the relative orientation of the helices in each spot toward the central helix (beta angle); or several other analysis that may arise from specific questions that want to be explored in the system. In this manuscript we used a combination of these analysis as illustrated in **Supplementary Figure 4**.

Some reports have pointed out that Martini force field overestimates intermolecular interactions of peptides and proteins in membranes (Javanainen et al., 2017) and in solution (Stark et al., 2013). Thus, the system gets trapped in interactions that hardly dissociate and this reduces the power of sampling. However, in this study, Martini force field reproduced the vast

majority of association modes and oligomeric levels observed in all NMR reference structures. Moreover, once equilibrated, the helices are distributed in separated clusters and various association-dissociation events occur. Still, non-covalent dimers were more difficult to detect than trimers or higher order oligomers because of the presence of native and non-native interactions, which could indicate that CG-MD simulation may be not optimized for low affinity associations or that these interactions require longer exploration times. We expect that this method gains robustness with the new releases of the Martini force field. In addition, analyzing more NMR solved single span transmembrane proteins, will lead to a better understanding of the weaknesses and strengths of the method.

In summary, we have validated the use of CG with Martini force field to study the oligomerization of TNFRSF members by comparing our results to the available NMR structures, and we have extended this application to assess possible structural changes related to disease-associated mutations. Our study paves the way to analyse the transmembrane organization of different TNFRSF members and other single span transmembrane receptors in a dynamic mode along extended simulation times. The flexibility of the system allows to simulate and study the impact of lipid composition (high vs. low cholesterol and glycosphingolipids or asymmetric lipid compositions), post-translational modifications (such as palmitoylation) as well as heterotypic interaction with other integral membrane proteins.

DATA AVAILABILITY STATEMENT

The original contributions generated for the study are included in the article/**Supplementary Material**, further inquiries can be directed to the corresponding author/s.

AUTHOR CONTRIBUTIONS

All authors listed have made a substantial, direct and intellectual contribution to the work, and approved it for publication.

FUNDING

This work was supported by National research council (CONICET): MPS and CRS Salary. Fondo para la investigación Científica y Tecnológica (FONCYT) PICT-2018-01107: Research grant to CRS.

SUPPLEMENTARY MATERIAL

The Supplementary Material for this article can be found online at: https://www.frontiersin.org/articles/10.3389/fcell.2020.577278/full#supplementary-material

REFERENCES

Abraham, M. J., Murtola, T., Schulz, R., Páll, S., Smith, J. C., Hess, B., et al. (2015). GROMACS: high performance molecular simulations through multi-level parallelism from laptops to supercomputers. *SoftwareX* 1-2, 19–25. doi: 10.1016/j.softx.2015.06.001

Bradley, R., and Radhakrishnan, R. (2013). Coarse-grained models for protein-cell membrane interactions. *Polymers* 5, 890–936. doi: 10.3390/polym5030890

Bussi, G., Donadio, D., and Parrinello, M. (2007). Canonical sampling through velocity rescaling. *J. Chem. Phys.* 126:014101. doi: 10.1063/1.2408420

Chan, F. K., Chun, H. J., Zheng, L., Siegel, R. M., Bui, K. L., and Lenardo, M. J. (2000). A domain in TNF receptors that mediates ligand-independent receptor assembly and signaling. *Science* 288, 2351–2354. doi: 10.1126/science.288.5475.2351

Clancy, L., Mruk, K., Archer, K., Woelfel, M., Mongkolsapaya, J., Screaton, G., et al. (2005). Preligand assembly domain-mediated ligand-independent association between TRAIL receptor 4 (TR4) and TR2 regulates TRAIL-induced apoptosis. *Proc. Natl. Acad. Sci. U.S.A.* 102, 18099–18104. doi: 10.1073/pnas.0507329102

de Jong, D. H., Singh, G., Bennett, W. F. D., Arnarez, C., Wassenaar, T. A., Schäfer, L. V., et al. (2013). Improved parameters for the martini coarse-grained protein force field. *J. Chem. Theory Comput.* 9, 687–697. doi: 10.1021/ct300646g

Fu, Q., Fu, T.-M., Cruz, A. C., Sengupta, P., Thomas, S. K., Wang, S., et al. (2016). Structural basis and functional role of intramembrane trimerization of the Fas/CD95 death receptor. *Mol. Cell.* 61, 602–613. doi: 10.1016/j.molcel.2016.01.009

Hall, B. A., Halim, K. B. A., Buyan, A., Emmanouil, B., and Sansom, M. S. P. (2014). Sidekick for membrane simulations: automated ensemble molecular dynamics simulations of transmembrane helices. *J. Chem. Theory Comput.* 10, 2165–2175. doi: 10.1021/ct500003g

Han, J., Pluhackova, K., and Böckmann, R. A. (2016). Exploring the formation and the structure of synaptobrevin oligomers in a model membrane. *Biophys. J.* 110, 2004–2015. doi: 10.1016/j.bpj.2016.04.006

Javanainen, M., Martinez-Seara, H., and Vattulainen, I. (2017). Excessive aggregation of membrane proteins in the Martini model. *PLoS ONE* 12:e0187936. doi: 10.1371/journal.pone.0187936

Kahn, P. C. (2001). Defining the axis of a helix. *Comput. Chem.* 13, 185–189. doi: 10.1016/0097-8485(89)85005-3

Lee, S. H., Shin, M. S., Kim, H. S., Park, W. S., Kim, S. Y., Jang, J., et al. (2000). Somatic mutations of Fas (Apo-1/CD95) gene in cutaneous squamous cell carcinoma arising from a burn scar. *J. Invest. Dermatol.* 114, 122–126. doi: 10.1046/j.1523-1747.2000.00819.x

Lomize, A. L., and Pogozheva, I. D. (2017). TMDOCK: an energy-based method for modeling α-helical dimers in membranes. *J. Mol. Biol.* 429, 390–398. doi: 10.1016/j.jmb.2016.09.005

MacKenzie, K. R., Prestegard, J. H., and Engelman, D. M. (1997). A transmembrane helix dimer: structure and implications. *Science* 276, 131–133. doi: 10.1126/science.276.5309.131

Marrink, S. J., Risselada, H. J., Yefimov, S., Tieleman, D. P., and de Vries, A. H. (2007). The MARTINI force field: coarse grained model for biomolecular simulations. *J. Phys. Chem. B* 111, 7812–7824. doi: 10.1021/jp071097f

Mueller, B. K., Subramaniam, S., and Senes, A. (2014). A frequent, GxxxG-mediated, transmembrane association motif is optimized for the formation of interhelical Cα-H hydrogen bonds. *Proc. Natl. Acad. Sci. U.S.A.* 111, E888–E895. doi: 10.1073/pnas.1319944111

Nadezhdin, K. D., García-Carpio, I., Goncharuk, S. A., Mineev, K. S., Arseniev, A. S., and Vilar, M. (2016). Structural basis of p75 transmembrane domain dimerization. *J. Biol. Chem.* 291, 12346–12357. doi: 10.1074/jbc.M116.723585

Naismith, J. H., Devine, T. Q., Brandhuber, B. J., and Sprang, S. R. (1995). Crystallographic evidence for dimerization of unliganded tumor necrosis factor receptor. *J. Biol. Chem.* 270, 13303–13307. doi: 10.1074/jbc.270.22.13303

Naismith, J. H., Devine, T. Q., Kohno, T., and Sprang, S. R. (1996). Structures of the extracellular domain of the type I tumor necrosis factor receptor. *Structure* 4, 1251–1262. doi: 10.1016/S0969-2126(96)00134-7

Pagès, G., and Grudinin, S. (2018). Analytical symmetry detection in protein assemblies. II. dihedral and cubic symmetries. *J. Struct. Biol.* 203, 185–194. doi: 10.1016/j.jsb.2018.05.005

Pagès, G., Kinzina, E., and Grudinin, S. (2018). Analytical symmetry detection in protein assemblies. I. cyclic symmetries. *J. Struct. Biol.* 203, 142–148. doi: 10.1016/j.jsb.2018.04.004

Pan, L., Fu, T.-M., Zhao, W., Zhao, L., Chen, W., Qiu, C., et al. (2019). Higher-order clustering of the transmembrane anchor of DR5 drives signaling. *Cell* 176, 1477–1489. *E*14. doi: 10.1016/j.cell.2019.02.001

Periole, X., Knepp, A. M., Sakmar, T. P., Marrink, S. J., and Huber, T. (2012). Structural determinants of the supramolecular organization of G protein-coupled receptors in bilayers. *J. Am. Chem. Soc.* 134, 10959–10965. doi: 10.1021/ja303286e

Pieper, K., Rizzi, M., Speletas, M., Smulski, C. R., Sic, H., Kraus, H., et al. (2014). A common single nucleotide polymorphism impairs B-cell activating factor receptor's multimerization, contributing to common variable immunodeficiency. *J. Allergy Clin. Immunol.* 133, 1222–1225. doi: 10.1016/j.jaci.2013.11.021

Polyansky, A. A., Chugunov, A. O., Volynsky, P. E., Krylov, N. A., Nolde, D. E., and Efremov, R. G. (2014). PREDDIMER: a web server for prediction of transmembrane helical dimers. *Bioinformatics* 30, 889–890. doi: 10.1093/bioinformatics/btt645

Popov, P., and Grudinin, S. (2014). Rapid determination of RMSDs corresponding to macromolecular rigid body motions. *J. Comput. Chem.* 35, 950–956. doi: 10.1002/jcc.23569

Siegel, R. M., Frederiksen, J. K., Zacharias, D. A., Chan, F. K., Johnson, M., Lynch, D., et al. (2000). Fas preassociation required for apoptosis signaling and dominant inhibition by pathogenic mutations. *Science* 288, 2354–2357. doi: 10.1126/science.288.5475.2354

Smulski, C. R., Beyrath, J., Decossas, M., Chekkat, N., Wolff, P., Estieu-Gionnet, K., et al. (2013). Cysteine-rich domain 1 of CD40 mediates receptor self-assembly. *J. Biol. Chem.* 288, 10914–10922. doi: 10.1074/jbc.M112.427583

Smulski, C. R., Decossas, M., Chekkat, N., Beyrath, J., Willen, L., Guichard, G., et al. (2017). Hetero-oligomerization between the, TNF receptor superfamily members CD40, Fas and TRAILR2 modulate CD40 signalling. *Cell Death Dis.* 8, *e*2601–e2601. doi: 10.1038/cddis.2017.22

Stark, A. C., Andrews, C. T., and Elcock, A. H. (2013). Toward optimized potential functions for protein-protein interactions in aqueous solutions: osmotic second virial coefficient calculations using the MARTINI coarse-grained force field. *J. Chem. Theory Comput.* 9, 4176–4185. doi: 10.1021/ct400008p

Trenker, R., Call, M. E., and Call, M. J. (2015). Crystal structure of the glycophorin a transmembrane dimer in lipidic cubic phase. *J. Am. Chem. Soc.* 137, 15676–15679. doi: 10.1021/jacs.5b11354

Wang, Y., and Barth, P. (2015). Evolutionary-guided *de novo* structure prediction of self-associated transmembrane helical proteins with near-atomic accuracy. *Nat. Commun.* 6, 7196–7112. doi: 10.1038/ncomms8196

Wassenaar, T. A., Pluhackova, K., Böckmann, R. A., Marrink, S. J., and Tieleman, D. P. (2014). Going backward: a flexible geometric approach to reverse transformation from coarse grained to atomistic models. *J. Chem. Theory Comput.* 10, 676–690. doi: 10.1021/ct400617g

Wassenaar, T. A., Pluhackova, K., Moussatova, A., Sengupta, D., Marrink, S. J., Tieleman, D. P., et al. (2015). High-throughput simulations of dimer and trimer assembly of membrane proteins. the DAFT approach. *J. Chem. Theory Comput.* 11, 2278–2291. doi: 10.1021/ct5010092

Yu, L., Wang, W., Ling, S., Liu, S., Xiao, L., Xin, Y., et al. (2015). CW-EPR studies revealed different motional properties and oligomeric states of the integrin β1a transmembrane domain in detergent micelles or liposomes. *Sci. Rep.* 5, 7848–7811. doi: 10.1038/srep07848

Conflict of Interest: The authors declare that the research was conducted in the absence of any commercial or financial relationships that could be construed as a potential conflict of interest.

frontiers in Cell and Developmental Biology

REVIEW
published: 11 February 2021
doi: 10.3389/fcell.2020.615141

Receptor Oligomerization and Its Relevance for Signaling by Receptors of the Tumor Necrosis Factor Receptor Superfamily

*Kirstin Kucka and Harald Wajant**

Division of Molecular Internal Medicine, Department of Internal Medicine II, University Hospital Würzburg, Würzburg, Germany

With the exception of a few signaling incompetent decoy receptors, the receptors of the tumor necrosis factor receptor superfamily (TNFRSF) are signaling competent and engage in signaling pathways resulting in inflammation, proliferation, differentiation, and cell migration and also in cell death induction. TNFRSF receptors (TNFRs) become activated by ligands of the TNF superfamily (TNFSF). TNFSF ligands (TNFLs) occur as trimeric type II transmembrane proteins but often also as soluble ligand trimers released from the membrane-bound form by proteolysis. The signaling competent TNFRs are efficiently activated by the membrane-bound TNFLs. The latter recruit three TNFR molecules, but there is growing evidence that this is not sufficient to trigger all aspects of TNFR signaling; rather, the formed trimeric TNFL–TNFR complexes have to cluster secondarily in the cell-to-cell contact zone for full TNFR activation. With respect to their response to soluble ligand trimers, the signaling competent TNFRs can be subdivided into two groups. TNFRs of one group, designated as category I TNFRs, are robustly activated by soluble ligand trimers. The receptors of a second group (category II TNFRs), however, failed to become properly activated by soluble ligand trimers despite high affinity binding. The limited responsiveness of category II TNFRs to soluble TNFLs can be overcome by physical linkage of two or more soluble ligand trimers or, alternatively, by anchoring the soluble ligand molecules to the cell surface or extracellular matrix. This suggests that category II TNFRs have a limited ability to promote clustering of trimeric TNFL–TNFR complexes outside the context of cell–cell contacts. In this review, we will focus on three aspects on the relevance of receptor oligomerization for TNFR signaling: (i) the structural factors which promote clustering of free and liganded TNFRs, (ii) the signaling pathway specificity of the receptor oligomerization requirement, and (iii) the consequences for the design and development of TNFR agonists.

Keywords: TNF receptor (TNFR) family, TNF ligand superfamily, NFκB, cell death, receptor cluster

OPEN ACCESS

Edited by:
Marta Rizzi,
University of Freiburg Medical Center, Germany

Reviewed by:
Pascal Schneider,
University of Lausanne, Switzerland
Patrick Legembre,
University of Limoges, France

***Correspondence:**
Harald Wajant
harald.wajant@mail.uni-wuerzburg.de

Specialty section:
This article was submitted to Signaling, a section of the journal Frontiers in Cell and Developmental Biology

Received: *08 October 2020*
Accepted: *28 December 2020*
Published: *11 February 2021*

Citation:
Kucka K and Wajant H (2021) Receptor Oligomerization and Its Relevance for Signaling by Receptors of the Tumor Necrosis Factor Receptor Superfamily. Front. Cell Dev. Biol. 8:615141. doi: 10.3389/fcell.2020.615141

INTRODUCTION

The receptors of the tumor necrosis factor (TNF) receptor superfamily (TNFRSF) are of overwhelming importance in the regulation of the immune system but are also involved in the maintenance of tissue homeostasis and development. For example, the two receptors of TNF, TNF receptor-1 (TNFR1) and TNF receptor-2 (TNFR2), regulate the interaction of the various types of

immune cells and also the interplay of the latter with practically any type of non-hematopoietic cells; CD40 stimulates antigen-presenting cells; CD27, OX40, 41BB, and RANK costimulate T cells; BCMA, TACI, and BaffR regulate B-cell maturation; CD95 and the two death receptors of TRAIL contribute to tumor surveillance; Fn14 promotes tissue repair; and EDAR drives the development of skin appendages (Aggarwal et al., 2012). The TNFRSF receptors (TNFRs) are characterized by a cysteine-rich domain (CRD) which can be found in their ectodomain in one to six copies (Locksley et al., 2001). The CRDs are involved in ligand binding but can also promote receptor self-assembly. Besides the CRDs, there are no structural features which are present in all TNFRs. However, there are some structural and functional aspects which allow the definition of three functionally and structurally distinct subgroups of the TNFRSF. Most TNFRs contain one or more short binding motifs for proteins of the TNF receptor-associated factor (TRAF) family which link these TRAF-interacting TNFRs to intracellular signaling pathways enabling the activation of transcription factors of the NFκB family and various MAP kinase cascades (Xie, 2013; Park, 2018). A second subgroup of TNFRs, the death receptors, harbors a structurally conserved protein–protein interaction domain in the cytoplasmic part, the so-called death domain (DD) (Siegmund et al., 2017). The DD and the death receptors received their name due to the fact that some DD-containing TNFRs trigger cell death pathways by interaction with cytoplasmic DD-containing proteins. However, despite the name, DD-mediated interactions are also involved in the stimulation of non-cytotoxic signaling pathways by death receptors including TRAF-mediated engagement of NFκBs (Siegmund et al., 2017). Besides the signaling competent TNFRSF subgroups of the TRAF-binding and DD-containing TNFRs, there is a third signaling incompetent subgroup of decoy receptors which comprises soluble receptors, receptors anchored to the plasma membrane *via* a GPI moiety, and a receptor with a non-functional DD.

Besides a very few exceptions, for example p75NGFR, which is stimulated by proNGF, and DR6, which seems to be activated by an N-terminal fragment of the amyloid precursor protein (Lee et al., 2001; Nikolaev et al., 2009), the TNFRs become activated by ligands of the TNF superfamily (TNFSF; Locksley et al., 2001; Bodmer et al., 2002). The TNFSF ligands (TNFLs) form a structurally comparatively homogeneous protein family and are characterized by a C-terminal TNF homology domain (THD), which promotes the assembly into homotrimeric and in a few cases also into heterotrimeric molecules (Bodmer et al., 2002). In the trimeric state, the THD furthermore mediates then the interaction with the receptors of the TNFRSF. Typically, TNFLs are initially expressed as type II transmembrane (TM) proteins, in which the extracellular THD is connected to the TM domain and the intracellular domain by a "stalk" region (Bodmer et al., 2002). Most TNFLs also occur as soluble variants, which emerge from the membrane-bound molecules through proteolytic processing in the "stalk" region. Since the soluble TNFL variants still contain the THD, these molecules are also trimers and are typically still able to interact with high affinity with TNFRs. Noteworthy, the signaling competent TNFRs basically differ in their response to soluble ligand trimers (**Table 1**). TNFRs of one group, called as category I TNFRs, are robustly activated by soluble ligand trimers. Prominent representatives of the category I TNFRs are TNFR1 and LTβR. TNFRs of a second group, however, failed to comprehensively activate cell death signaling and/or classical NFκB signaling in response to soluble ligand trimers despite high affinity binding (Wajant, 2015). This second group of TNFRs, also named as category II TNFRs, comprises the majority of signaling competent TNFRs and includes many translational interesting TNFRs, such as 4-1BB, CD27, CD40, CD95, Fn14, OX40, TNFR2, and the two TRAIL death receptors (TRAILR1/DR4, TRAILR2/DR5). Intriguingly, some TNFLs interact with TNFRs of both categories. For example, TNF binds with high affinity to TNFR1 and TNFR2, but in contrast to TNFR1, which is efficiently activated by soluble and membrane TNF, TNFR2 becomes only potently stimulated by memTNF (Grell et al., 1995, 1998). Similarly, soluble Baff trimers efficiently interact with the TNFRs BaffR, BCMA, and TACI but only efficiently trigger BaffR signaling (Bossen et al., 2008). Thus, it seems that indeed TNFR-type intrinsic properties, and not the quality of the ligand, determine the responsiveness of TNFRs to TNFLs. Particularly, the inability of category II TNFRs to become fully activated by soluble TNFL trimers cannot be simply caused by the lack of specific sequence information present in the corresponding membrane-bound TNFL variants. This is evident from two fundamental observations/experiences in the field: First, for several category II TNFRs, it has been found that efficient receptor activation takes place when their soluble ligands are presented in plasma membrane-associated form, irrespective of how this is achieved. For example, soluble APRIL, which interacts *via* its THD with the TNFRs TACI and BCMA, contains N-terminally a heparan sulfate proteoglycan binding motif enabling soluble APRIL to bind to proteoglycans (Hendriks et al., 2005; Ingold et al., 2005), such as syndecan-1 (Joo et al., 2012) and syndecan-4 (Jarousse et al., 2011). More important, however, is that proteoglycan-bound APRIL is superior to soluble APRIL in the activation of B cells (Ingold et al., 2005; Kimberley et al., 2009; Joo et al., 2012). Similarly, it has been described that the extracellular matrix protein fibronectin and the keratan sulfate proteoglycan lumican bind soluble CD95L and enhance its ability to trigger apoptosis induction by the death receptor CD95 (Aoki et al., 2001; Vij et al., 2005). Likewise, trimeric soluble TNFL fusion proteins containing an anchor domain, which allows binding to a cell surface-exposed structure, acquire strong category II TNFR-stimulating potency when bound to their anchoring target. The anchoring-dependent mode of receptor activation has been demonstrated for several category II TNFRs (**Table 1**). Typically, scFv domains recognizing a cell surface-exposed tumor antigen or tumor stroma antigen are used as anchor domain, but the suitability of other types of protein domains has been demonstrated as well [for a review, see, e.g., (de Bruyn et al., 2013; Wajant et al., 2013; Wajant, 2019)]. Worth mentioning and of potential translational importance is the fact that the use of an appropriate anchor domain allows the generation of soluble TNFL fusion proteins which not only ensure full activation of category II TNFRs but also do this in a local fashion and/or link it with a second activity.

Second, soluble TNFL molecules convert to potent category II TNFR agonists upon physical linkage of two or more ligand trimers (**Table 1**). Oligomerization of soluble TNFLs by natural means has for example described for CD95L and Baff. Soluble CD95L present in the bronchoalveolar lavage fluid of patients suffering from acute lung injury turned out unexpectedly to be highly apoptotic (Herrero et al., 2011). It turned out that the soluble CD95L molecules of bronchoalveolar lavage fluid are aggregated due to oxidation. Moreover, the bronchoalveolar lavage fluid of acute lung injury patients promoted oligomerization of recombinant soluble CD95L *in vitro* resulting in an enhanced ability to trigger CD95-mediated cell death (Herrero et al., 2011). Soluble Baff occurs as other soluble TNFLs as a trimeric protein and also in the form of a 60-mer. The Baff 60-mer, however, displays approx. 100-fold higher capacity as trimeric soluble Baff to trigger TACI signaling (Bossen et al., 2008). Oligomerization of soluble TNFL trimers can be straightforwardly achieved with the help of genetically engineered recombinant TNFLs. Introduction of an N-terminal tag, e.g., a Flag tag, allows controlled oligomerization of soluble ligand trimers by treatment with an anti-tag antibody, and fusion with another multimerization domain, besides the THD, often

TABLE 1 | Activation of classical NFκB and cell death signaling by category I and category II TNFRs in response to soluble TNF ligands (sTNFLs).

TNFR	Category	TNFL	sTNFL variant/activity (EC_{50} trimer: EC_{50} hexa-, nonamer, etc.)		sTNFL variant/activity (EC_{50} no anchoring: EC_{50} PM anchoring)	
				References		References
BaffR	I	Baff	Flag-Baff/>100	Bossen et al., 2008		
			Baff 64-mer/>100			
DR3	I	TL1A	Flag-TNC-TL1A/1	Bittner et al., 2016		
GITR	I	GITRL	Flag-TNC-GITRL/5	Wyzgol et al., 2009; Richards et al., 2019	Sc40-GITRL/5	Wyzgol et al., 2009
			HERA-GITRL/10			
LTbR	I	$LTab_2$	Flag-scLTab$_{2/}$1	Lang et al., 2016		
		LIGHT	Flag-TNC-LIGHT/1	Lang et al., 2016		
TNFR1	I	TNF	Flag-TNF/1	Schneider et al., 1998		
		LTa	Flag-TNC-LTa/1	Lang et al., 2016		
41BB	II	41BBL	Flag-TNC-41BBL/>100	Wyzgol et al., 2009	Sc40-41BBL	Wyzgol et al., 2009
BCMA	II	APRIL	Flag-APRIL/>20	Bossen et al., 2008		
CD27	II	CD27L	Flag-TNC-CD27L/>100	Wyzgol et al., 2009		
CD40	II	CD40L	Flag-CD40L/20	Holler et al., 2003; Wyzgol et al., 2009	Sc40-CD40L/20	Wyzgol et al., 2009; Brunekreeft et al., 2014
			Flag-CD40L/>>100		scFv:EpCAM-CD40L/20	
CD95	II	CD95L	Flag-CD95L/>1,000	Schneider et al., 1998; Holler et al., 2003	Sc40-CD95L/>>100	Samel et al., 2003
			Fc-CD95L/>1,000			
			ACRP-CD95L > 1,000			
EDAR	II	EDA-A1	Flag-EDA-A1/>>100	Swee et al., 2009		
Fn14	II	TWEAK	Flag-TWEAK/>1,000	Roos et al., 2010	Sc40-TWEAK/>>100	Roos et al., 2010
			Fc-TWEAK/>>100			
OX40	II	OX40L	Flag-OX40L/>100	Muller et al., 2008	Sc40-OX40L/>100	Muller et al., 2008
			Fc-OX40L/>20			
TACI	II	APRIL	Flag-APRIL/>100	Bossen et al., 2008		
		Baff	Flag-Baff/>100	Bossen et al., 2008		
			Baff 64-mer/>100			
TNFR2	II	TNF	Flag-TNF/100	Schneider et al., 1998; Prada et al., 2020		
			TNC-scTNF(143N/145R)/>1,000			
TRAILR1	II	TRAIL	Flag-TNC-TRAILmutR1/100	Trebing et al., 2014a	scFv:CD70-TNC-TRAILmutR1/100	Trebing et al., 2014a
TRAILR2	II	TRAIL	Flag-TRAIL/>1,000	Schneider et al., 1998; Wajant, 2019	AD-TRAILs > 100	Wajant, 2019
			Oligomeric TRAILs/>100			

Please note that this is a non-exhaustive table listing representative reports.

results in the formation of molecules with defined stoichiometry containing, e.g., 6, 9, or 12 TNFL protomers. TNFL fusion proteins, for example, harboring N-terminally the dimerizing Fc domain of human IgG1 typically form hexameric molecules containing two parallel orientated trimeric "TNFL" subdomains (e.g., Holler et al., 2003; Muller et al., 2008; Wyzgol et al., 2009). Over the years, all ligands of the TNFSF have been expressed as soluble Flag-tagged trimers or hexameric Fc-fusion proteins and have been analyzed with respect to their TNFR-stimulating activities by various groups (**Table 1**). These studies clearly showed that the THD without any other specific sequence information encoded in membrane-bound TNFL molecules is fully sufficient to ensure TNFR binding and TNFR activation, of course in some case only upon oligomerization. Indeed, the absence or demonstration of strongly differing activation of a TNFR by trimeric and aggregated soluble TNFL variants provides the essential experimental evidence for identifying and defining category I and category II TNFRs. It is also worth mentioning that the oligomerization of soluble TNFLs, as far as examined, does not increase their affinity for TNFRs (Fick et al., 2012; Lang et al., 2012). The improved responsiveness of category II TNFRs to aggregated soluble TNFL variants can therefore not simply be attributed to increased receptor occupancy. This is particularly clear from the example of CD95L, since in this case it has even been shown that the soluble ligand variant acts as an inhibitor of its TM counterpart at least in the context of apoptosis induction (Suda et al., 1997).

TNFR ASSEMBLY IN THE ABSENCE OF LIGAND

In unstimulated cells, TNFRs are present as monomeric and dimeric or trimeric molecules (**Table 2**). Dimerization of TNFRs can occur covalently through the formation of cysteine bridges or by non-covalent interactions between specialized parts in the TNFRs not involved in ligand binding. For example, immunoprecipitation experiments with anti-CD27 antibodies revealed a major homodimeric molecule species in T cells (van Lier et al., 1987; Bigler et al., 1988), and immunoprecipitation of p75NTR revealed a mixture of monomeric and cysteine-bridged dimeric receptor species (Vilar et al., 2009). A minor fraction of disulfide-bonded homodimers has also been reported for CD40 in unstimulated B cells (Reyes-Moreno et al., 2004). Noteworthy,

TABLE 2 | Ligand-free assembly of TNFRs.

TNFR	Assembly state	Domain involved	Method	References
CD27	Dimer	Disulfide linked	SDS-PAGE of IPs	van Lier et al., 1987; Bigler et al., 1988
P75NGFR	Dimer	Disulfide linked	SDS-PAGE of IPs	Vilar et al., 2009
CD40	Fraction of dimers	Disulfide linked	Western blot	Reyes-Moreno et al., 2004
41BB	Fraction of dimers	Disulfide linked	SEC	Bitra et al., 2018
CD95	Dimer	AA 1–49 (CRD1)	SEC	Papoff et al., 1999; Siegel et al., 2000
	Dimers + trimers	AA 1–42 (CRD1)	Cross-linking	
			FRET	
TACI	At least trimers		SDS-PAGE of IPs	Garibyan et al., 2007
			Cross-linking	
			FRET	
TNFR1	Trimers	AA 1–54 (CRD1)	Cross-linking	Chan et al., 2000
			FRET	
TNFR2	Trimers	AA 1–54 (CRD1)	Cross-linking	Chan et al., 2000
			FRET	
CD40	Dimer	AA 20–62 (CRD1)	FRET	Chan et al., 2000; Smulski et al., 2013, 2017
			Cross-linking	
TRAILR1			FRET	Chan et al., 2000; Neumann et al., 2012, 2014
TRAILR2		AA 26–41 (CRD1)	Co-IP	Clancy et al., 2005; Neumann et al., 2012, 2014
			FRET	
TRAILR4		AA 27–42 (CRD1)	Co-IP	Clancy et al., 2005; Neumann et al., 2012, 2014
			FRET	
RANK		AA 534–539	Co-IP	Kanazawa and Kudo, 2005
CD30			Co-IP	Horie et al., 2002
Fn14	Minor dimer fraction	Cytoplasmic domain	Cross-linking	Brown et al., 2013

FRET, fluorescence resonance energy transfer; Co-IP, co-immunoprecipitation; SEC, size exclusion chromatography.

CD40 activation enhances covalent CD40 dimerization by promoting the formation of a cysteine bridge *via* C238 located in the cytoplasmic domain of the molecule (Reyes-Moreno et al., 2007). The expression of the 4-1BB ectodomain, furthermore, resulted in a mixture of monomers and C121-linked dimers (Bitra et al., 2018). Noteworthy, it has been furthermore reported that 4-1BB colocalizes with OX40 in activated T cells and also forms immunoprecipitable complexes with this TNFR, presumably again with the help of cysteine bridges (Ma et al., 2005).

Most TNFRs, however, seem to auto-associate with non-covalent mechanisms. Most important and best investigated in this context is certainly the preligand binding assembly domain (PLAD). This domain was initially functionally defined in CD95 and roughly comprises the first N-terminal CRD1, which is not involved in CD95L binding but present in several dominant-negative acting CD95 splice variants (Papoff et al., 1996, 1999). Cross-linking experiments, fluorescence resonance energy transfer (FRET) studies, and binding studies with a CD95 deletion mutation only comprising aa 1–49 of the mature receptor, indeed, revealed that the N-terminal part of CD95 promotes self-assembly of the molecule (Papoff et al., 1999; Siegel et al., 2000). In particular, it has been found that heterozygous mutations in CD95 causing the autoimmune lymphoproliferative syndrome (ALPS) interfere with CD95L binding in a dominant-negative fashion, too (Siegel et al., 2000). The dominant-negative effect of CD95L binding-defective mutants and splice variants is difficult to explain if one assumes that CD95L binds to CD95 monomers but becomes straightforwardly understandable if one takes into consideration that CD95L might also bind to pre-assembled dimeric or trimeric receptor species. The dominant-negative effect of CD95L binding-deficient CD95 variants is possibly also of relevance in tumor development as it has been observed that MMP-7 cleaves off a part of the CD95 PLAD resulting in reduced apoptosis sensitivity of tumor cells (Strand et al., 2004). Similarly, it has been demonstrated that the common variable immunodeficiency (CVID)-causing C104R TACI mutant prevents ligand binding but leaves PLAD/CRD1-mediated self-assembly intact (Garibyan et al., 2007). Self-assembly involving the N-terminal CRD1 or parts thereof has also been reported for TNFR1, TNFR2, CD40, TRAILR1, TRAILR2, and TRAILR4 (Chan et al., 2000; Clancy et al., 2005; Smulski et al., 2013; Neumann et al., 2014). Ligand binding-defective TNFR mutants with an intact PLAD may elicit their dominant-negative effect by two mechanisms: first, by decreasing the fraction of dimerized wt TNFR molecules, which often have superior ligand affinity compared with their monomeric counterparts and which therefore might act as the primary ligand binding receptor species; and second, by forming inactive heterocomplexes with liganded cell expressed wt receptor molecules. In view of this mode of action, soluble PLAD-containing protein variants should act as inhibitors of their parental TNFRs. Indeed, dimeric fusion proteins of the PLAD of TNFR1 with glutathione S-transferase or the Fc domain of human IgG1 have been successfully used in preclinical *in vivo* models to treat TNF/TNFR1-driven diseases, such as collagen- and CpG DNA-induced arthritis, skin lesion development in lupus-prone mice, spontaneous autoimmune diabetes, and myelin oligodendrocyte glycoprotein (MOG)-induced encephalomyelitis (Deng et al., 2005, 2010; Wang et al., 2011). However, with a monovalent soluble CRD1/PLAD construct of CD40, a significant agonism has been observed *in vitro* (Smulski et al., 2013). Thus, the quality of the effects of recombinant PLAD constructs could therefore be dependent on the receptor type considered, the valency of the construct, and/or other not yet investigated factors (e.g., receptor density).

An obvious question concerns the strength and specificity of the PLAD–PLAD interaction, but these issues have been only limitedly studied so far. The fact that concentrations in the micromolar range are required for dimerized TNFR1–PLAD constructs to elicit their inhibitory effect on TNF-induced TNFR1 signaling *in vitro* (Deng et al., 2005) suggests that the PLAD–PLAD affinity is rather low. Indeed, cell-free binding assays with immobilized TNFR1 and TNFR2 ectodomains and the monomeric PLAD of TNFR1 revealed half maximal binding of the soluble TNFR1–PLAD to TNFR1 with 9 μM and to TNFR2 with approx. 2 μM (Cao et al., 2011). Likewise, surface plasmon resonance (SPR) analysis revealed a K_D of 0.6 μM for the binding of the CD40 CRD1/PLAD to the ectodomain of CD40 (Smulski et al., 2013). SPR studies analyzing the interaction between the soluble ectodomains of TRAILR1, TRAILR2, TRAILR3, and TRAILR4, furthermore, revealed affinities between 1 and 10 μM for homotypic and heterotypic interactions (Lee et al., 2005). Low PLAD–PLAD affinities in the micromolar range match well with the fact that soluble TNFR molecules mainly occur as monomers and have thus to be fused with oligomerizing domains, e.g., the Fc domain, to obtain decoy receptors with high apparent affinity (avidity) for their corresponding ligands.

The lack of strong differences in the affinity of the TNFR1–PLAD for TNFR1 and TNFR2 reported in the abovementioned study by Cao et al. (2011) as well as the heterotypic interactions observed for the ectodomains of the various TRAIL receptors suggests that there can be some promiscuity in PLAD–PLAD interactions. Indeed, there is evidence from FRET and co-immunoprecipitation experiments that TRAILR2 and CD95, but not TRAILR1, TACI, BCMA, or BaffR, interact *via* their extracellular domain with CD40 in a competitive manner and so reduce homotypic CD40 dimerization (Smulski et al., 2017). In accordance with these findings, there was attenuated CD40L-induced signaling in cells with increased expression of TRAILR2 and CD95 (Smulski et al., 2017). The lack of discrimination between TNFR1 and TNFR2 in the study with the TNFR1–PLAD is nevertheless quite unexpected. In FRET experiments with intact cells, there was no evidence for an interaction of TNFR1 and TNFR2 (Chan et al., 2000), and in previous co-immunoprecipitation studies, there was no evidence for binding between TNFR1 and TNFR2 as well (Moosmayer et al., 1994; Pinckard et al., 1997). The reasons underlying this contradiction remain to be clarified but could mean that additional factors besides PLAD–PLAD interaction contribute to the specificity of TNFR interactions in the absence of ligand.

In view of the weak affinity of PLAD–PLAD interactions, at first glance, the question arises whether a significant fraction of the TNFR molecules of a cell occurs in dimeric or trimeric

form to become relevant for ligand binding. There are two factors to consider here: first, the volume which is available to TNFRs inserted into the plasma membrane. This volume is very low, so that high TNFR concentrations can be reached. For example, if one considers an idealized cell with a radius of 10 μm and a plasma membrane surface of 1,560 μm^2 which expresses 10,000 TNFR molecules with an ectodomain length of 0.1 μm, this results in an effective TNFR concentration of approximately 1.3 μM (**Figure 1**). Second is the stability of the TNFL–TNFR interaction, which is significantly higher than that of the PLAD–PLAD interaction. The ligand affinity of dimeric TNFRs, and even that of monomeric TNFRs (Lang et al., 2016), is significantly higher than the affinity of the PLAD–PLAD interaction. The ligand-bound TNFR dimers/trimers are therefore withdrawn from the equilibrium between free monomeric and free dimeric or trimeric TNFR species, so that, according to Le Chatelier's principle, there is net new formation of ligand-free dimeric and trimeric TNFR species, which in turn can be again removed from the equilibrium by ligand binding. Ultimately, over time, this mechanism enables the majority of TNFR molecules to recruit in their dimeric/trimeric form TNFL molecules, even if only a small fraction of the receptors are in the dimeric/trimeric state at a given point in time (**Figure 1**). In accordance with these considerations, it has been measured by quantitative single-molecule super-resolution microscopy in cells with physiological TNFR1 expression levels that in non-stimulated cells 66% of the TNFR1 molecules are present as monomers and 34% as dimers (Karathanasis et al., 2020). After TNF stimulation, evaluation of the TNF-bound TNFR1 pool revealed in the cited study 13% monomers, a trimeric fraction of 64%, and a significant fraction of TNFR1 molecules even appeared as oligomers (23%). Photoactivated localization microscopy studies with photoactivatable CD95 furthermore showed an incorporation of approx. 50% of the receptor molecules in clusters with two, three, or even more receptors (Fu Q. et al., 2016). However, these values were determined in cells with transient overexpression of CD95 in which the supraphysiological high-expression levels of CD95 lead to unnatural, ligand-independent CD95 activation. It can therefore be assumed that by far fewer CD95 molecules are organized in clusters at physiologically occurring expression levels.

Non-covalent TNFR dimerization/trimerization is not only mediated by the PLAD and might also be promoted by other less well-understood mechanisms. So, it has been described for RANK that self-assembly is dependent on a domain/motif which is located in the TM domain proximal part of its cytoplasmic domain (Kanazawa and Kudo, 2005). Similarly, there is evidence from BS3 cross-linking experiments that Fn14 weakly self-associates *via* its C-terminal tail (Brown et al., 2013). Co-immunoprecipitation experiments also argued for self-association by overexpressed CD30 involving the extra- but also the intracellular domain (Horie et al., 2002). There is furthermore strong evidence that at least some TNFRs can also interact *via* their TM domains. However, this type of interaction seems not to be involved in TNFR assembly in the absence of ligand and instead appears to be important in the context of ligand-induced formation of active TNFR signaling complexes. The corresponding literature will therefore be discussed in the next section.

In sum, although realized by different mechanisms, ligand-independent self-assembly has been demonstrated for most TNFRs. TNFR–TNFR interaction might be of dual relevance for the functioning of TNFRs. On the one side, it can improve the affinity for ligand binding by increasing avidity as discussed above in detail; but on the other side, it might also contribute to the regulation of formation of fully signaling competent TNFL–TNFR clusters as discussed in the following section.

TNFL-INDUCED TNFR COMPLEXES

The X-ray crystal structures of more than 15 TNFL–TNFR complexes have now been published. With the exception of the complex of the heterotrimeric TNFL $LTab_2$ with its receptor LTbR, which contains only two receptor molecules, all of these complexes show that a TNFL trimer interacts symmetrically

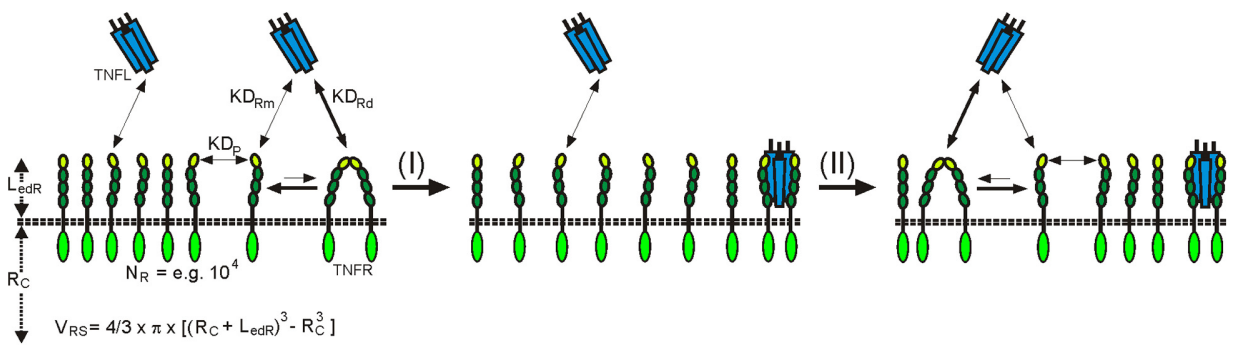

FIGURE 1 | Plasma membrane-associated expression results in high local TNFR concentrations in the TNFR-accessible shell (L_{edR}) around the cell resulting in dimer formation in the absence of ligand despite low auto-affinity (KD_P). Ligand trimers preferentially bind with higher affinity to dimeric (KD_{RD}) than to monomeric receptor (KD_{RM}) species. Liganded TNFR dimers are more stable than ligand-free TNFR dimers and are thus removed from the equilibrium with the monomers. Le Chatelier's principle promotes then the net formation of new ligand-free receptor dimers. R_C, radius of the cell; V_{RS}, volume of the receptor accessible shell.

with three receptor molecules (Wajant, 2015). It was therefore initially assumed that a TNFL trimer recruits three receptor molecules and induces the formation of a fully active trimeric receptor signaling complex. The simple finding that some TNFRs (category II TNFRs) bind soluble ligand trimers with high affinity, but, in contrast to membrane-bound TNFSF ligands, do not (or only weakly) stimulate signaling showed that this initial TNFR activation model is in many cases insufficient to reflect experimental reality. The fundamental observation, which was already broadly discussed in the *Introduction*, that category II TNFRs are efficiently activated by soluble TNFLs when they are presented in oligomerized or cell-associated form has led to a two-step model of TNFR activation (Wajant, 2015). According to this model, the secondary interaction of initially formed inactive (or less active) trimeric TNFL–TNFR complexes leads to the formation of oligomeric TNFR clusters, which, unlike the trimeric receptor complexes, are able to effectively activate intracellular signaling pathways (**Figure 2**). In accordance with this model, it has been observed that membrane-bound TNFL trimers, which are regularly highly active, induce the formation of supramolecular TNFL–TNFR clusters with high efficiency (e.g., Henkler et al., 2005). Factors that may explain the superior cluster-inducing potency of membrane-bound TNFLs are the reduced mobility of the membrane-associated ligands, the alignment of the ligand molecules caused by their membrane-associated state, and certainly also their high "local" concentration in the cell–cell contact. For example, when all TNFR molecules of a spherical cell with a radius of 10 μm, which expresses 10,000 receptors, are bound by the ligands of a neighboring memTNFL expressing cell in a 0.01-μm distance cell–cell contact, which comprises 0.1–10% of the cell surface, a local TNFR concentration of 10–1,000 μM is reached (**Figure 2**). At these high concentrations, even low TNFR auto-affinities, e.g., due to PLAD–PLAD interactions, are sufficient to ensure secondary clustering and, thus, receptor activation.

ASSEMBLY OF LIGANDED TNFRS

Nuclear magnetic resonance spectroscopy and biochemical studies with the TM domain of CD95 reconstituted in lipid bicells revealed the formation of stable trimers, and CD95 variants harboring mutations disrupting trimerization of the TM domain showed reduced apoptosis induction (Fu Q. et al., 2016). It is worth mentioning, however, that PLAD-mediated self-assembly of CD95 remained intact in these CD95 mutants (Fu Q. et al., 2016). This suggests that the TM domain-driven trimerization of CD95 is not crucial for the assembly of ligand-free receptors and only contributes to the formation of an active CD95L–CD95 signaling complex after ligand binding by not yet clarified mechanisms. The NMR structure of the TM domain of the CD95-related death receptor TRAILR2/DR5 reconstituted in lipid bicells showed surprisingly poor similarity to that of CD95. Admittedly, the TRAILR2 TM domain migrates in SDS-PAGE analysis like the CD95 TM domain as a trimer; in the lipid bicells, however, the TRAILR2 TM domain is packed as a hexamer which is formed by the interplay of a trimerizing and a dimerizing interface present in the TM domain (Pan et al., 2019). TRAILR2 TM domain mutants with a defective dimerization interface still form trimers which are similar in structure to the CD95 TM domain trimers (Pan et al., 2019). It is tempting to speculate, and in accordance with the structural data, that in the plasma membrane, without the space restraints given by the lipid bicells, the TRAILR2 TM domain forms a dimer–trimer network (Pan et al., 2019). TRAILR2 variants harboring mutations destroying either the dimerization or the trimerization interface of the TM domain interfere with apoptosis

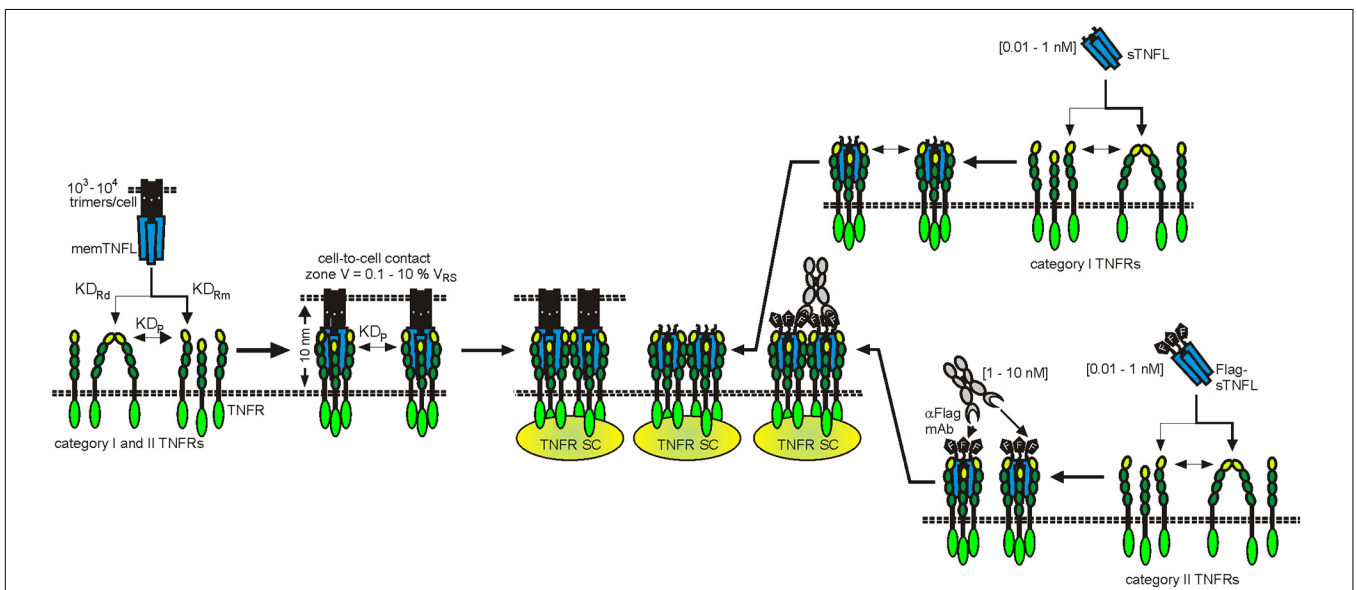

FIGURE 2 | Clustering of TNFRs by membrane-bound and soluble TNFLs. For details, see text.

induction and clustering of overexpressed receptor molecules but not with ligand-independent self-assembly (Pan et al., 2019). Most intriguingly, a genetically engineered TRAILR2 variant with a tobacco etch virus (TEV) protease cleaving side between the TM domain and the TRAILR2 ectodomain induces apoptosis in the absence of ligand upon cleavage with the TEV protease (Pan et al., 2019). This suggests that the unliganded TRAILR2 ectodomain prevents TM domain-driven clustering and activation of TRAILR2. Similar initial observations have been made with TNFR2 and OX40 variants with a TEV protease cleavable ectodomain (Pan et al., 2019).

APOPTOSIS INDUCTION AND ACTIVATION OF THE CLASSICAL NFκB PATHWAY BY SECONDARY CLUSTERING OF LIGANDED CATEGORY II TNFR TRIMERS

The necessity of secondary aggregation of trimeric TNFL–TNFR complexes for the activation of the classic NFκB signaling pathway and apoptosis induction can be straightforwardly explained from the current knowledge about the molecular mechanisms on how TRAF and DD adapter proteins act in these pathways. The TRAF2 adapter protein occurs as a homotrimeric molecule or as a heterotrimeric molecule in complex with TRAF1 (Xie, 2013). The TRAF1 and TRAF2 protomers share a C-terminal TRAF domain which comprises a coil–coil N-TRAF subdomain mediating trimerization followed by a C-terminal C-TRAF subdomain which contains a TNFR binding site (Xie, 2013; Park, 2018). Homotrimeric TRAF2 and TRAF1–TRAF2 heterotrimers interact with two of their three protomers (2xTRAF2 or TRAF1–TRAF2) in an asymmetric fashion with the baculoviral IAP repeat (BIR) 1 domain of a single monomer of the E3 ligase cIAP1 or the E3 ligase cIAP2 (Mace et al., 2010; Zheng et al., 2010). Monomeric cIAPs exist in an autoinhibited state that prevents the RING domain of the molecule from promoting dimerization. The activation of the E3 ligase activity of the cIAPs is based on the dimerization of the RING domain enabling the interaction with E2 proteins and subsequent K63 ubiquitination of signaling proteins involved in the stimulation of the classic NFκB signaling pathway through TNFRs (Dueber et al., 2011; Feltham et al., 2011; Varfolomeev et al., 2012). Most TRAF-binding TNFRs have one binding site for a protomer of TRAF1, TRAF2, TRAF3, or TRAF5; some TNFRs have in addition a TRAF6 binding site (**Table 3**). The three receptor molecules of a trimeric TNFL–TNFR complex thus interact with the C-TRAF domain of three protomers of a single TRAF2 homotrimer or a TRAF1/TRAF2 heterotrimer. Accordingly, a trimeric TNFL–TNFR complex only recruits a single and, therefore, inactive, cIAP1 (or cIAP2) molecule, which is not sufficient to efficiently stimulate the classical NFκB signaling pathway (**Figure 3**). In clusters of two or more trimeric TNFL–TNFR complexes, however, active cIAP1 or cIAP2 dimers can be formed due the close neighborhood of receptor-bound 3:1 TRAF–cIAP complexes so that the classical NFκB signaling pathway can be strongly activated (**Figure 3**).

For the initiation of the extrinsic apoptotic signaling pathway through some receptors of the death receptor subgroup of the TNFRSF, the dimerization of an inactive monomer is also necessary, namely that of the procaspase-8 molecule. In this case, too, structural data that were obtained for the DD of the death receptor CD95, the adapter molecule Fas associated

TABLE 3 | TRAF-binding sites in TRAF-interacting TNFRs.

TNFR	Method	TRAF1/2/3/5 site	References
41BB	Two hybrid system (THS)	E236–E249	Arch and Thompson, 1998
BaffR	Receptor mutants IP Crystal structure	P117–D122 + AA 160–183	Xu and Shu, 2002; Ni et al., 2004
BCMA	Receptor mutants IP	A 119–143	Hatzoglou et al., 2000; Granja et al., 2017
	Homology	A165–E168	
CD27	Receptor mutants IP	R238-250	Yamamoto et al., 1998
CD30	GST-receptor mutants IP	V575–G583 + P558–T565	Boucher et al., 1997; Lee et al., 1999
CD40	GST-receptor mutants IP THS	P230–V241	Lee et al., 1996; Lu et al., 2003
GITR	THS	E202–E213	Esparza and Arch, 2005
Fn14	THS	P113–E116	Brown et al., 2003
LTbR	Receptor mutants IP	P389–H402	Force et al., 2000
OX40	THS	T256–E261	Arch and Thompson, 1998
RANK	GST-receptor mutants IP	P607–Q611	Galibert et al., 1998; Kim et al., 1999
TACI	Homology	P270–E273	Granja et al., 2017
TNFR2	Crystal structure	Q420–E427	Park et al., 1999
TROY	Homology	T276–E279	Kojima et al., 2000
XEDAR	Receptor mutants IP	AA 249–254 + AA 273–281	Sinha et al., 2002

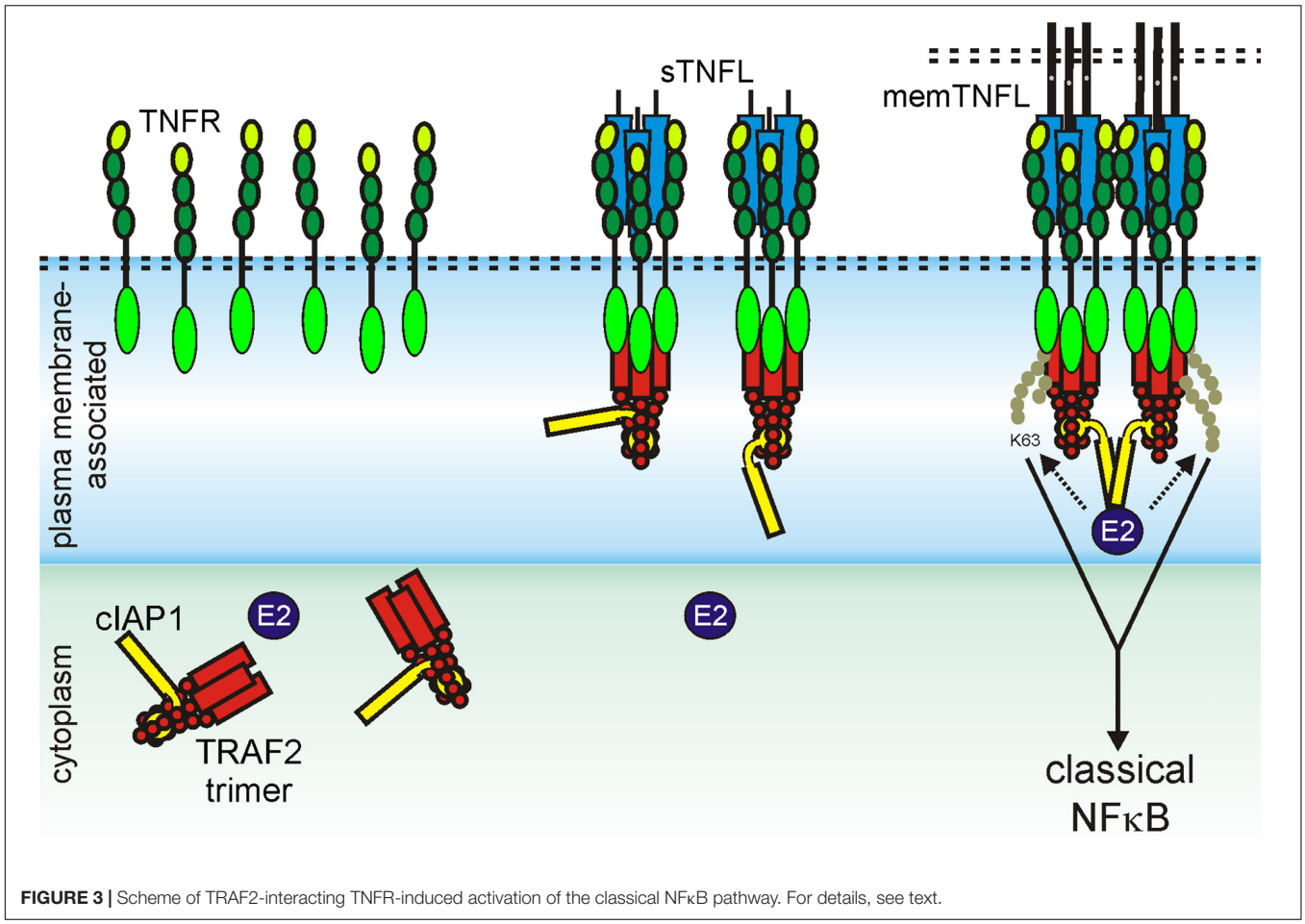

FIGURE 3 | Scheme of TRAF2-interacting TNFR-induced activation of the classical NFκB pathway. For details, see text.

death domain protein (FADD), the prodomain of caspase-8, and the complexes of these molecules suggest that at least two trimeric ligand–receptor complexes must come together in order to dimerize procaspase-8 to trigger activation of this enzyme and to engage the apoptotic signaling cascade (Carrington et al., 2006; Scott et al., 2009; Wang et al., 2010; Shen et al., 2015; Park, 2019). Indeed, it has been found that the prodomain of caspase-8 forms filaments which consist of three parallel helical prodomain strands (Fu T.M. et al., 2016). Furthermore, it has been observed that complexes of the CD95 DD and the adapter protein FADD serve as condensation nuclei for the formation of these filaments (Fu T.M. et al., 2016). Now, the adapter protein FADD, which consists of a DD and a death effector domain (DED), interacts with its DD with the DD of CD95 and with its DED with the caspase-8 prodomain. The latter, however, consists of two DEDs that interact in an asymmetrical manner with the single DD of two FADD molecules. Thus, to form the cap of a caspase-8 prodomain filament, six FADD molecules and therefore consequently six CD95-DDs are necessary (Fu T.M. et al., 2016). The formation of a CD95-FADD cap, which stimulates the assembly of procaspase-8 filaments, in which dimerization of two caspase-8 molecules can occur, can therefore explain the need of CD95 clustering required for robust CD95-induced apoptosis (**Figure 4**). The importance of the secondary interaction of two or more trimeric TNFL–TNFR for the efficient stimulation of the classical NFκB signaling pathway and extrinsic apoptosis obviously does not reflect any fundamental intrinsic receptor limitation. Rather, it is the special signaling pathway-specific way how the signaling proteins involved stimulate inactive enzymes that makes receptor clustering so important in these two examples. TNFRs of category II are not or hardly able to induce the classical NFκB signaling pathway or apoptosis after stimulation with physiological concentrations of soluble ligand trimers. Category I TNFRs, however, such as TNFR1, DR3, GITR, and LTβR, activate these signaling pathways maximally already at low concentrations of soluble ligand trimers. Moreover, further cross-linking of the soluble ligand molecules fails to further enhance their activity (Bittner et al., 2016; Lang et al., 2016). The obvious question for category I TNFRs is, therefore, why in the case of this receptor type the mere binding of soluble ligand trimers is sufficient to achieve maximum and extensive receptor activation. At least in the case of TNFR1 and BaffR, there is evidence that this is due to an increased intrinsic ability of the receptor molecules to self-aggregate. Studies evaluating the functional properties of chimeric receptors composed of the extracellular domain and TM domain of the category I TNFR TNFR1 and the intracellular domain of the category II TNFR CD95 showed strong recruitment

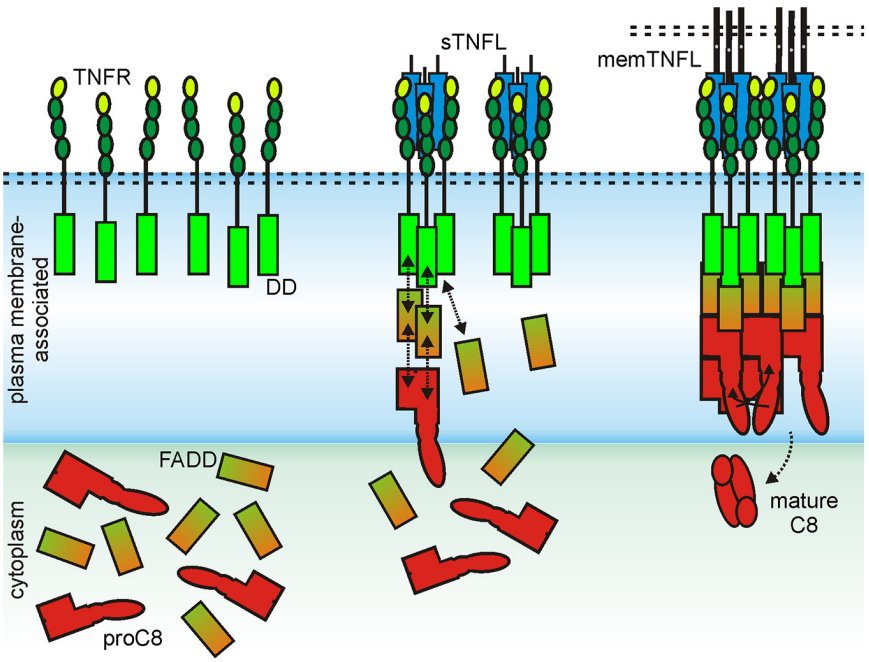

FIGURE 4 | Scheme of CD95-induced caspase-8 activation. For details, see text.

of FADD and caspase-8 and apoptosis induction by soluble TNF (Krippner-Heidenreich et al., 2002). However, a chimeric receptor composed of the extracellular and TM domain of the category II TNFR2 and the cytoplasmic CD95 domain needed cross-linking of sTNF for robust signaling (Krippner-Heidenreich et al., 2002). Similarly, chimeric receptors composed of the extracellular domain of the category I TNFR BaffR and the cytoplasmic domains of the category II TNFRs CD95 or TRAILR2 triggered efficient cell death in response to soluble Baff trimers in Jurkat and rhabdomyosarcoma cells (Schuepbach-Mallepell et al., 2015). Thus, transfer of the extracellular and the TM domain of a category I receptor was fully sufficient in this example to overcome the requirement for soluble ligand oligomerization to trigger category II TNFR signaling. Follow-up experiments with the TNFR1-CD95 and TNFR2-CD95 chimeras gave furthermore evidence that the stalk region separating the CRDs from the TM along with the TM crucially contributes to the need of category II TNFRs for cross-linking of soluble ligand trimers to become activated. Transfer of the stalk–TM region of TNFR2 to TNFR1-CD95 was sufficient to reconstitute the need for soluble ligand oligomerization to trigger CD95 signaling (Richter et al., 2012). Vice versa, insertion of the stalk–TM region of TNFR1 into TNFR2-CD95 was sufficient to convert this category II TNFR chimera into a category I receptor (Richter et al., 2012). TM replacement experiments with TNFR1-CD95 and the TMs of TRAILR1 and TRAILR2 furthermore suggest that the TM might affect clustering efficacy, too (Neumann et al., 2012). The simplest explanation of this observation is, of course, that the extracellular and TM domain of category I TNFR, such as TNFR1 and BaffR, has its own considerable intrinsic clustering ability. In view of the evidence discussed above that the extracellular region of category II TNFRs TNFR2 and TRAILR2 antagonizes clustering of liganded receptor trimers (Krippner-Heidenreich et al., 2002; Schuepbach-Mallepell et al., 2015), it is tempting to speculate that this TNFR type does not simply lack clustering ability but rather has evolved repulsive mechanisms to prevent PLAD-driven clustering of soluble ligand-bound TNFRs.

SIGNALING PATHWAY-SPECIFIC OLIGOMERIZATION REQUIREMENTS OF CATEGORY II TNFRS

As already discussed above, the fact that two or more trimeric TNFL–TNFR complexes have to aggregate in order to ensure robust activation of the classical NFκB signaling pathway or the extrinsic apoptotic signaling pathway is straightforwardly explained by the signaling pathway-specific requirements for the activation of enzymes (cIAPs, caspase-8), which are indirectly recruited to the TNFRs. The aggregation of liganded TNFRs therefore does not necessarily reflect a factor that is a general prerequisite for the activation of any TNFR-engaged intracellular signaling pathway. In fact, for the category II TNFRs Fn14 and CD95, activities have been described which are already maximally stimulated by soluble ligand trimers.

A systematic and comprehensive analysis with soluble TWEAK (sTWEAK) trimers; oligomeric and hexameric sTWEAK variants; an scFv-sTWEAK fusion protein, which is able to bind to a plasma membrane-presented antigen; and memTWEAK revealed that all sTWEAK variants trigger activation of the alternative NFκB pathway (NIK accumulation, p100 to p52 processing) with similar dose dependencies and

reach comparable pathway activity as upon stimulation with memTWEAK-expressing cells. Thus, neither physical connection of two or more sTWEAK trimers nor their anchoring to the plasma membrane resulted in a further enhancement of the ability of sTWEAK to stimulate this Fn14 response (Roos et al., 2010). In contrast, the various TWEAK variants split into two groups with respect to their ability to stimulate the classical NFκB pathway. Hexameric Fc-sTWEAK, oligomerized sTWEAK, and cell surface-anchored scFv-sTWEAK activated the classical NFκB pathway as efficiently as memTWEAK, while sTWEAK and free scFv-sTWEAK showed only at high concentrations a modest stimulatory effect (Roos et al., 2010). It turned out furthermore that irrespective of their oligomerization state and cell surface anchoring, all sTWEAK variants and memTWEAK induce the disappearance of TRAF2 from the cytoplasmic soluble compartment which explains the shared ability to activate the alternative NFκB pathway as follows. As already discussed above, a TRAF2 trimer associates with a single cellular inhibitor apoptosis 1 (cIAP1) or cIAP2 molecule. In the cytoplasm of unstimulated cells, the TRAF2–cIAP1/2 complexes interact with a complex of TRAF3 and the kinase NIK (Xie, 2013; Sun, 2017). The latter activates IKK1 which in turn triggers processing of the NFκB precursor protein p100 to p52 resulting in the nuclear translocation of p52-containing transcription factors and transcription of target genes of the alternative NFκB pathway (Xie, 2013; Sun, 2017). In the TRAF–cIAP–NIK complex, the cIAPs K48-ubiquitinate NIK trigger thereby the proteasomal degradation of NIK resulting eventually in the constitutive active suppression of the alternative NFκB pathway. The sole recruitment of a TRAF2 trimer and its single associated cIAP molecule to sTWEAK-liganded Fn14 without cIAP transactivation is thus already fully sufficient to interrupt the constitutively ongoing inhibition of the alternative NFκB pathway (**Figure 5**). It is obvious that clustering of the liganded TRAF2–cIAP-containing Fn14 complexes does not result in a further reduction of the cytoplasmic available pool of TRAF2–cIAP1 and TRAF2–cIAP2 complexes and, thus, does not enhance alternative NFκB signaling.

In accordance with the well-established finding that soluble CD95L binds CD95 but does not trigger CD95 clustering and apoptosis, it has been described that sCD95L acts as an inhibitor of memCD95L-induced apoptosis (Suda et al., 1997). However, sCD95L can stimulate Ca^{2+} signaling and migration of myeloid cells, T cells, and various tumor cells (Siegmund et al., 2017). There is evidence that this occurs by DD-dependent and DD-independent pathways which, in contrast to apoptosis induction, do not need FADD and caspase-8 (Tauzin et al., 2011; Poissonnier et al., 2016). The DD-independent mode of Ca^{2+} signaling and the stimulation of cell motility have been traced back to recruitment of PLCγ1 and the tyrosine kinase Yes to a calcium-inducing domain preceding the DD of CD95. The composition and stoichiometry of the sCD95L-induced cell migration-inducing CD95 signaling complex is quite different from the memCD95L-induced apoptotic signaling complex. In the case of TWEAK, it is obvious that the membrane-bound ligand also triggers the signaling events engaged by the soluble ligand. In the case of CD95L, this issue has not been clarified yet. Thus, it is unclear whether memCD95L simultaneously triggers the recruitment of the cell motility-inducing molecules along with FADD and caspase-8 or whether these signaling molecules are utilized by CD95 in an exclusive manner.

CELL INTRINSIC FACTORS CONTROL TNFR CLUSTERING AND ACTIVATION

Tumor necrosis factor receptor preassembly, ligand-induced receptor trimerization, and clustering of liganded receptor trimers occur in the complex environment of cellular membranes. It is therefore presumably not surprising that various cellular factors have been identified which regulate TNFR activation by direct or indirect modulation of the clustering process. For example, especially for the TRAIL death receptors and CD95, there is broad evidence that O- and N-glycosylation affect their death-inducing activity. O-glycosylation enhanced ligand-induced clustering of TRAILR1 and TRAILR2 (Wagner et al., 2007). Cancer cells frequently express membrane proteins with truncated *O*-glycans. In the case of the TRAIL death receptors, this results in reduced receptor clustering and, thus, in reduced sensitivity for apoptosis induction (Zhang B. et al., 2019; Jiang et al., 2020). For TRAILR1, it has been further shown that *N*-glycosylation promotes ligand-induced clustering, too (Dufour et al., 2017). Thus, glycosylation *per se* seems to act as a factor which contributes to the constitution of a "normal" interaction competence of TRAIL death receptors enabling efficient ligand-stimulated receptor clustering and formation of cell death-inducing receptor complexes. Noteworthy, glycosylation makes TRAIL death receptors also accessible for carbohydrate-binding proteins. Indeed, there is evidence that galectin-3 traps TRAIL death receptors in glycan nanoclusters and prevents the TRAIL-induced formation of apoptotic receptor complexes (Mazurek et al., 2012). CD95 is also N- and O-glycosylated (Seyrek et al., 2019). In the case of this death receptor, however, it has been reported that inhibition of glycosylation showed only a minor effect on receptor clustering and cell death induction (Shatnyeva et al., 2011) or that it even enhanced cell death induction (Charlier et al., 2010). In the latter study, whether this was again due to the interaction with galectin-3 or another carbohydrate-binding protein remained, however, unclear. There are also reports giving evidence that galectins also interact with the category II TNFRs CD40 and 41BB and the category I TNFR DR3 (Vaitaitis and Wagner, 2012; Madireddi et al., 2014, 2017). Galectin-9 has been found to interact with the CRD4 of 41BB in a carbohydrate-dependent manner without interfering with 41BBL binding. More importantly, the lack of galectin-9 resulted in reduced 41BB-mediated costimulation of $CD8^+$ T cells (Madireddi et al., 2014). Likewise, interaction of galectin-9 with DR3 has been demonstrated and correlated with reduced DR3-induced production of IL2 and IFNg in T cells in galectin-9 KO T cells (Madireddi et al., 2017). The functional consequences of the galectin-9–CD40 interaction have only been limitedly studied, but in this case, the interaction correlated with reduced CD40-dependent activity (Vaitaitis and Wagner, 2012). Another type of modification, which could

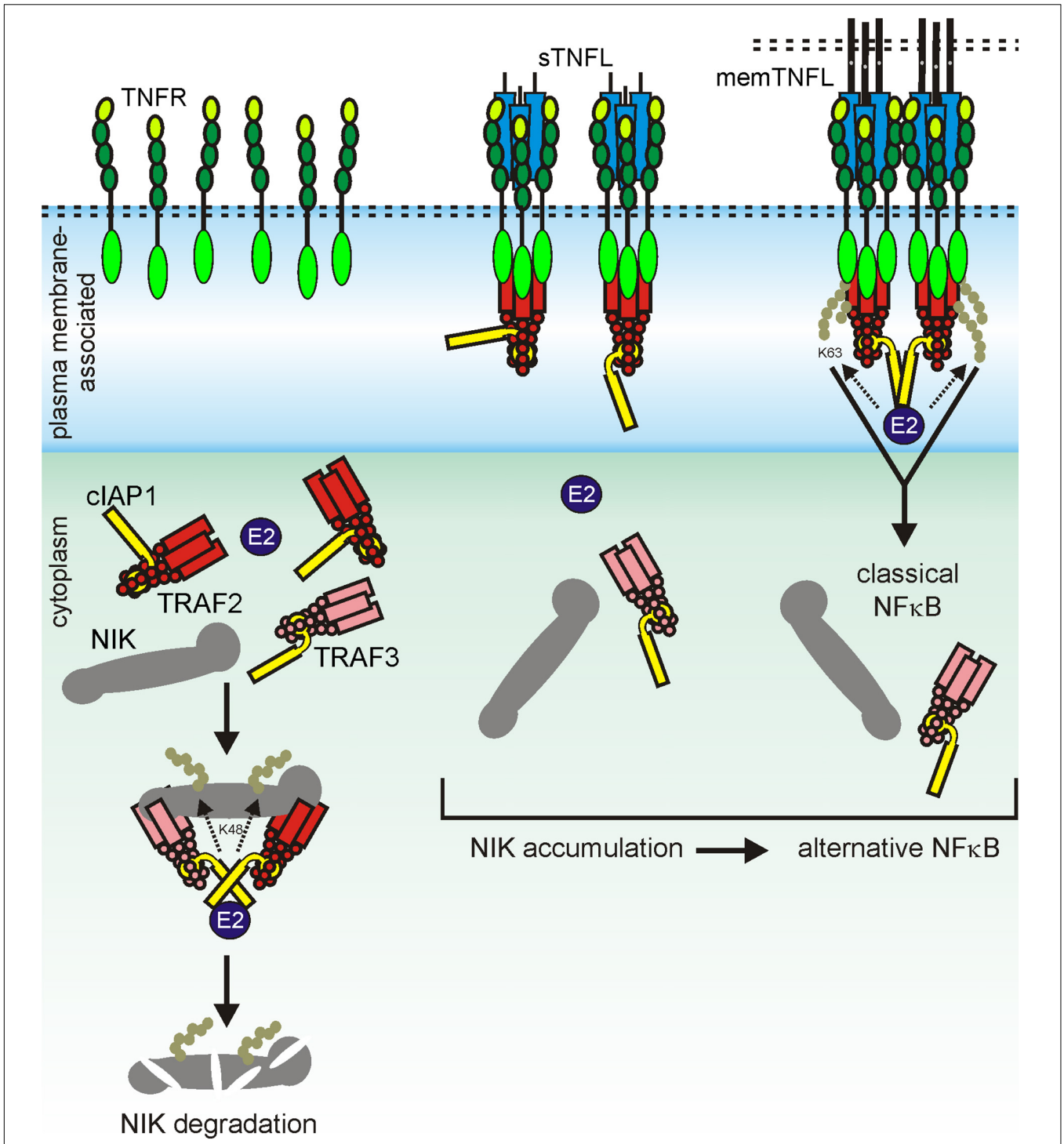

FIGURE 5 | Scheme of sTWEAK-induced activation of the alternative NFκB pathway. In non-stimulated cells, cytosolic TRAF2 and the cIAPs are engaged in NIK degradation, thus in suppression of the alternative NFκB pathway (left panel). Recruitment of TRAF2 and cIAPs to Fn14, irrespective whether triggered by soluble TWEAK or membrane TWEAK, results in reduced cytosolic TRAF2 and cIAP levels and thus reduced suppression of NIK degradation resulting in the activation of the alternative NFκB pathway by accumulated constitutively active NIK.

be implicated in the clustering of TNFRs, is palmitoylation. Intracellular palmitoylation near the TM domain of CD95 in L12.10.mFas cells has been reported to promote constitutive lipid raft association of CD95 and CD95L-induced association of CD95 with actin cytoskeleton-linked lipid rafts leading to the assembly of the caspase-8-activating CD95 receptor

signaling complex (Feig et al., 2007). It has been, however, not clarified yet how CD95 palmitoylation affects ligand binding and clustering of liganded CD95 complexes in detail. Investigation of this issue is also challenging in view of the observation that CD95 palmitoylation prevents lysosomal degradation of CD95 resulting in higher CD95 expression levels (Rossin et al., 2015). Palmitoylation has also been reported for the TNFRs TRAILR1, TNFR1, the low-affinity NGFR, and DR6 (Vesa et al., 2000; Klima et al., 2009; Rossin et al., 2009; Zingler et al., 2019). In the case of TRAILR1, palmitoylation has again been implicated in lipid raft association, whereas there was no evidence for such an effect in the case of DR6 (Klima et al., 2009; Rossin et al., 2015). The relevance of palmitoylation of TNFR1 and the low-affinity NGFR for ligand binding and receptor clustering has not been investigated yet (Vesa et al., 2000; Zingler et al., 2019). The effects of palmitoylation on the clustering and activation of TNFRs appear mainly to be mediated by controlling the association with lipid rafts. Indeed, the latter has been implicated in manifold studies in the activation of certain TNFRs but often with cell type-specific and/or agonist type-specific relevance. For this special aspect, one is therefore referred to corresponding reviews (e.g., Muppidi et al., 2004; Gajate and Mollinedo, 2015). In sum, although the relevance of receptor modifications and the "plasma membrane environment" for clustering and activation of TNFRs has been demonstrated in many studies for selected TNFRs, the importance for most receptors of the TNFR family has not been addressed so far and many aspects are still unclear. Indeed, even in the broadly investigated cases of CD95 and the TRAIL death receptors, it is largely unknown whether and if yes to which extent the effects of these factors are cell type-, pathway-, or agonist-specific.

TNF RECEPTOR ACTIVATION REQUIREMENTS: CONSEQUENCES FOR THE DESIGN AND DEVELOPMENT OF TNFR AGONISTS

Due to the relevance of TNFRs in immune regulation and maintenance of tissue homeostasis, both the inhibition of TNFRs and the activation of TNFRs can have beneficial therapeutic effects (Aggarwal et al., 2012). The inhibition of TNFRs is comparatively easy to achieve with the help of neutralizing anti-TNFL antibodies or by using decoy receptors, which contain the extracellular ligand binding domain of TNFRs. In fact, several such reagents have been approved for clinical use in various autoimmune diseases and, in particular, include various TNF blockers. In contrast, the therapeutic success of TNFR-activating reagents is so far rather modest. Although TNFR activation appears very attractive for cancer therapy and has indeed been evaluated in this respect in a plethora of preclinical and clinical trials since more than two decades, only recombinant TNF (Beromun) has been approved for clinical use, and this is only for the treatment of soft tissue sarcoma in isolated limb perfusion, a rather rare application. Noteworthy, a not yet approved Fc fusion protein of EDA1 has been successfully used for *in utero* therapy of X-linked hypohidrotic ectodermal dysplasia and restored sweating ability (Schneider et al., 2018). The disappointing clinical success of therapeutic reagents, particularly antibodies, acting by TNFR stimulation is at least partly related to the difficulties in the development of potent TNFR agonists which result from the special molecular mechanisms of TNFR activation described above.

Despite the approval of recombinant soluble TNF for the treatment of soft tissue sarcoma, the potential clinical use of recombinant soluble TNFLs is limited in several ways: First, due to their small size, soluble TNFLs are rapidly cleared from the circulation. For example, for soluble TNF, serum half-life of 6–7 min has been found in mice, and for soluble TRAIL, a serum half-life of 23–31 min has been reported in non-human primates (Beutler et al., 1985; Kelley et al., 2001). Second, category II TNFRs are not or only poorly activated by binding of soluble ligand trimers (see above). These two limitations can be overcome by genetic fusion of soluble TNFLs with heterologous protein domains improving serum retention and/or connecting two or more trimers or enabling cell surface anchoring. The development of soluble TNFL variants with good serum retention and high TNFR agonism was mainly advanced for TRAIL and immunostimulatory TNFLs, such as CD40L, etc. Accordingly, a large number of different TNFL fusion protein formats with considerable agonistic activity and often also good serum retention have been described to date. The various TNFL formats including their mode of action have been comprehensively reviewed recently (e.g., for TRAIL, see, de Bruyn et al., 2013; Wajant, 2019) and will therefore not be discussed here in detail. Several of these highly active soluble TNFL variants have been successfully evaluated in preclinical models for cancer treatment. However, TNFL fusion proteins are typically less efficiently produced as antibodies and often elicit antibody responses, and in general, there is less experience with the translational development and approval of such reagents. Agonistic antibodies are therefore still the means of choice when therapeutic TNFR activation is considered.

Already in the early 2000s, studies with FcγRIIb-deficient animal models showed that the *in vivo* agonism of CD95 antibodies is dependent on FcγR binding (Jodo et al., 2003; Xu et al., 2003). These observations were perceived as anecdotal reports and initially did not result in consideration in the development and *in vivo* functional analysis of anti-TNFRs. In the last decade, however, a growing list of studies exploiting FcγR-deficient animals and/or antibody variants with defective FcγR binding gives clear evidence for the idea that FcγR-dependent agonism is rather the rule than the exception for antibodies targeting 4-1BB, CD27, CD40, CD95, Fn14, OX40, TNFR2, TRAILR1, and TRAILR2 (Li and Ravetch, 2011, 2012, 2013; White et al., 2011, 2014; Wilson et al., 2011; Salzmann et al., 2013; Trebing et al., 2014b; Dahan et al., 2016; Medler et al., 2019; Zhang P. et al., 2019). To get a first impression to what extent FcγR-dependent agonism is a general phenomenon in the TNFRSF, we evaluated a panel of approx. 30 antibodies, targeting 11 different types of TNFRs, for their FcγR-dependent activity using the same methodology. This study came up with a clear and obvious correlation. Eight of eight antibodies specific

for category I TNFRs LTβR and TNFR1 elicit robust agonistic activity irrespective of FcγRIIB binding (Medler et al., 2019; patent WO2019129644). In contrast, all antibodies targeting category II TNFRs—4-1BB, CD27, CD40, CD95, Fn14, OX40, TNFR2, TRAILR1, and TRAILR2—turned out to be largely inactive but converted to strong agonist provided there was the possibility to bind to FcγRIIB (Medler et al., 2019; patent WO2019129644). Only one antibody which targeted GITR showed no agonism at all despite FcγR binding. Noteworthy, the maximum receptor activation reached with the FcγRIIB-anchored anti-TNFR antibodies was comparable to those elicited by transfectants expressing the TNFR-corresponding TM TNFL (Medler et al., 2019). Obviously, the type/category of a TNFR strongly impacts the relevance of FcγR binding for agonistic antibody activity. The fact that category II TNFRs are superiorly activated by FcγR-bound antibodies can be straightforwardly explained in view of the two-step model of TNFR activation described above and the superior ability of TM versus soluble ligands to promote TNFR clustering: When a soluble TNFL molecule, which is able to recruit three TNF receptors, is not sufficient to promote secondary clustering of category II TNFRs to activate the classical NFκB pathway and cell death signaling, it is plausible that the two TNFR molecules that can be bound by an anti-TNFR IgG fail as well to constitute an active signaling complex. In a similar fashion to TM TNFLs, however, FcγR-bound anti-TNFR antibodies are presented in an "immobilized" plasma membrane-attached manner. Consequently, secondary clustering of complexes between FcγR-bound anti-TNFRs on $FcγR^+$ anchor cells and TNFRs on $TNFR^+$ target cells is envisaged in the cell-to-cell contact zone due to the high local concentrations of the molecules involved (**Figure 6**). FcγR-bound anti-TNFRs seem to mimic the superior ability of TM TNFRs to promote secondary clustering of liganded TNFR complexes. This concept suggests that the sole FcγR binding rather than the concrete epitope recognized by category II anti-TNFR antibodies is decisive for their agonistic activity. Indeed, on the example of antibody panels recognizing different epitopes on the category II TNFRs TNFR2, Fn14, CD40, and OX40, it has been found that FcγR binding and not the antibody idiotype is the decisive factor for agonistic activity (Salzmann et al., 2013; Trebing et al., 2014b; Dahan et al., 2016; Yu et al., 2018; Medler et al., 2019; Zhang P. et al., 2019). Systematic studies with anti-TNFR2 and anti-Fn14 antibodies furthermore suggested that any antibody–FcγR interaction, irrespective of the antibody isotype and FcγR type involved, results in significant activation of category II TNFRs, whereas without FcγR binding, none of the IgG isotypes display robust agonism (Medler et al., 2019). Thus, the isotype of an IgG antibody seems to be only of importance for the agonistic activity of anti-TNFR antibodies as long as it determines the ability to bind to FcγRs (Medler et al., 2019). It has been furthermore reported that wild-type and signaling defective FcγR mutants are equally effective in conferring agonism to anti-TNFR antibodies (Li and Ravetch, 2013). In sum, it can be asserted that it is the sheer cell surface attachment, thus the mimicry of the mode of presentation of the THD in TM TNFLs, that constitutes the agonism of FcγR-bound antibodies, while FcγR-specific activities are largely irrelevant. However, although anti-category II TNFR antibodies display *in vitro* a quite similar agonistic activity upon FcγR binding, this does not necessarily imply that there are no major differences in their *in vivo* activity. Thus, although anti-category II TNFR antibodies generally act as agonists upon FcγR binding, their concrete net effect *in vivo* can be different, especially under conditions where FcγR expression is limited and where the "free" non-FcγR-anchored antibody fraction therefore gains relevance. For example, the "free" antibody fraction may block TNFR binding by endogenous ligand molecules and/or compete with the agonistic FcγR-anchored antibody fraction for TNFR binding. Such factors might explain the finding that panels of antibodies against CD40 and OX40 have been found to be uniformly agonistic *in vitro* upon FcγR binding but show different agonistic potentials *in vivo* (Yu et al., 2018; Zhang P. et al., 2019).

If the plasma membrane-attached mode of presentation is indeed the crucial factor conferring a high agonistic potential to otherwise poorly active anti-TNFR antibodies, one has to expect that the agonism-releasing antibody–FcγR interaction can be replaced by other interactions which link the antibody to the plasma membrane. This seems to be indeed the case. Plasma membrane binding-dependent agonism has, for example, been demonstrated by different groups for anti-TRAILR2

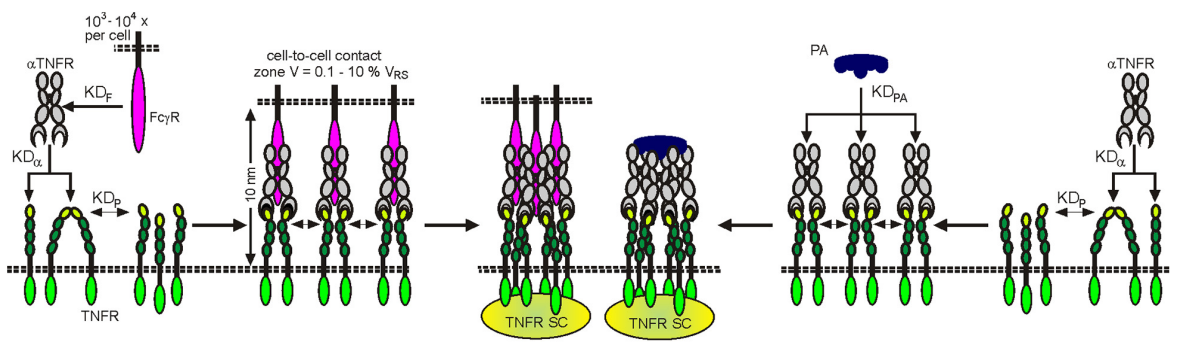

FIGURE 6 | Clustering and activation of TNFRs by antibodies (aTNFRs). Antibodies bind with medium to high affinity to FcγRs (KD_F) and also with affinity to TNFRs (KD_a). The FcγR-bound aTNFRs act then like memTNFLs. Protein A binds multiple aTNFR molecules with high affinity (KD_{PA}). The resulting complexes act then as oligomeric sTNFLs.

antibody fusion proteins with the ability to anchor to the plasma membrane with the help of a second antibody domain recognizing the cell surface antigens FAP, MCSP, and FolR1 (Brunker et al., 2016; He et al., 2016; Shivange et al., 2018). Similarly, a 50- to >1,000-fold plasma membrane anchoring-dependent increase in their TNFR-stimulating potential has also been reported for various antibody fusion proteins targeting the category II TNFRs 4-1BB, CD27, CD40, CD95, Fn14, and TNFR2 (Medler et al., 2019; Nelke et al., 2020).

There are also a few examples of antibodies against the category II TNFRs CD40 and DR5 in the literature showing FcγR-independent agonism (Guo et al., 2005; Motoki et al., 2005; White et al., 2015; Yu et al., 2018). It has been claimed that the fully antibody-intrinsic agonism is due to the particular epitope recognized by these antibodies. However, it has not been addressed whether these antibodies are special by inducing TNFR clustering despite being only bivalent or whether these antibodies instruct the formation of fully signaling competent TNFR dimers that would be hard to reconcile with the knowledge on the mechanisms of TNFR activation. Worth mentioning, in further parallelism to poorly active trimeric complexes formed between soluble TNFL trimers and category II TNFRs, complexes of two TNFRs and an antibody gain high activity, when close proximity of the TNFR dimers is enforced by cross-linking or oligomerization of the antibody, e.g., with anti-IgG antibodies or protein G or protein A (**Figure 6**; Wajant, 2015).

Against the background of the great translational potential of agonists of category II TNFRs, it should be mentioned that the FcγR binding which is required for these antibodies to unfold their agonism comes along with effects limiting their applicability. First, possibly only a subfraction of TNFRs might be reached, activated *in vivo* due to poor availability of FcγR-expressing cells and/or low cellular FcγR expression levels. Second, antibody binding can trigger FcγR-mediated effects which counteract the therapeutic effects which are actually aspired with by the anti-TNFR antibody treatment. Third, considerable antibody doses are typically required to overcome competition with serum IgGs for FcγR binding. Last but not least and not intrinsically related to the need for FcγR binding, there can be dose-limiting side effects caused by the systemic activation of the targeted TNFR type [e.g., CD40: cytokine release/storm (Piechutta and Berghoff, 2019); TRAIL death receptors: hepatotoxicity (Papadopoulos et al., 2015; Zuch de Zafra et al., 2016; Nihira et al., 2019)]. Complications and limitations arising from the FcγR dependency of the agonism of anti-category II TNFR antibodies, however, might be straightforwardly circumvented by the use of antibody fusion proteins with an anchoring domain enabling FcγR-independent plasma membrane attachment as described above.

AUTHOR CONTRIBUTIONS

Both authors listed have made a substantial, direct and intellectual contribution to the work, and approved it for publication.

FUNDING

This work was supported by a Deutsche Forschungsgemeinschaft (DFG, German Research Foundation) grant to HW (Projektnummer WA 1025/33-1) and has received funding from the European Union's Horizon 2020 Research and Innovation Programme under the Marie Skłodowska-Curie grant agreement No 813871.

REFERENCES

Aggarwal, B. B., Gupta, S. C., and Kim, J. H. (2012). Historical perspectives on tumor necrosis factor and its superfamily: 25 years later, a golden journey. *Blood* 119, 651–665. doi: 10.1182/blood-2011-04-325225

Aoki, K., Kurooka, M., Chen, J. J., Petryniak, J., Nabel, E. G., and Nabel, G. J. (2001). Extracellular matrix interacts with soluble CD95L: retention and enhancement of cytotoxicity. *Nat. Immunol.* 2, 333–337. doi: 10.1038/86336

Arch, R. H., and Thompson, C. B. (1998). 4-1BB and Ox40 are members of a tumor necrosis factor (TNF)-nerve growth factor receptor subfamily that bind TNF receptor-associated factors and activate nuclear factor kappaB. *Mol. Cell Biol.* 18, 558–565. doi: 10.1128/mcb.18.1.558

Beutler, B. A., Milsark, I. W., and Cerami, A. (1985). Cachectin/tumor necrosis factor: production, distribution, and metabolic fate in vivo. *J. Immunol.* 135, 3972–3977.

Bigler, R. D., Bushkin, Y., and Chiorazzi, N. (1988). S152 (CD27). A modulating disulfide-linked T cell activation antigen. *J. Immunol.* 141, 21–28.

Bitra, A., Doukov, T., Croft, M., and Zajonc, D. M. (2018). Crystal structures of the human 4-1BB receptor bound to its ligand 4-1BBL reveal covalent receptor dimerization as a potential signaling amplifier. *J. Biol. Chem.* 293, 9958–9969. doi: 10.1074/jbc.RA118.003176

Bittner, S., Knoll, G., Fullsack, S., Kurz, M., Wajant, H., and Ehrenschwender, M. (2016). Soluble TL1A is sufficient for activation of death receptor 3. *FEBS J.* 283, 323–336. doi: 10.1111/febs.13576

Bodmer, J. L., Schneider, P., and Tschopp, J. (2002). The molecular architecture of the TNF superfamily. *Trends Biochem. Sci.* 27, 19–26. doi: 10.1016/s0968-0004(01)01995-8

Bossen, C., Cachero, T. G., Tardivel, A., Ingold, K., Willen, L., Dobles, M., et al. (2008). TACI, unlike BAFF-R, is solely activated by oligomeric BAFF and APRIL to support survival of activated B cells and plasmablasts. *Blood* 111, 1004–1012. doi: 10.1182/blood-2007-09-110874

Boucher, L. M., Marengere, L. E., Lu, Y., Thukral, S., and Mak, T. W. (1997). Binding sites of cytoplasmic effectors TRAF1, 2, and 3 on CD30 and other members of the TNF receptor superfamily. *Biochem. Biophys. Res. Commun.* 233, 592–600. doi: 10.1006/bbrc.1997.6509

Brown, S. A., Cheng, E., Williams, M. S., and Winkles, J. A. (2013). TWEAK-independent Fn14 self-association and NF-kappaB activation is mediated by the C-terminal region of the Fn14 cytoplasmic domain. *PLoS One* 8:e65248. doi: 10.1371/journal.pone.0065248

Brown, S. A., Richards, C. M., Hanscom, H. N., Feng, S. L., and Winkles, J. A. (2003). The Fn14 cytoplasmic tail binds tumour-necrosis-factor-receptor-associated factors 1, 2, 3 and 5 and mediates nuclear factor-kappaB activation. *Biochem. J.* 371(Pt 2), 395–403. doi: 10.1042/BJ20021730

Brunekreeft, K. L., Strohm, C., Gooden, M. J., Rybczynska, A. A., Nijman, H. W., Grigoleit, G. U., et al. (2014). Targeted delivery of CD40L promotes restricted activation of antigen-presenting cells and induction of cancer cell death. *Mol. Cancer* 13:85. doi: 10.1186/1476-4598-13-85

Brunker, P., Wartha, K., Friess, T., Grau-Richards, S., Waldhauer, I., Koller, C. F., et al. (2016). RG7386, a novel tetravalent FAP-DR5 antibody, effectively triggers FAP-dependent, avidity-driven DR5 hyperclustering and tumor cell

apoptosis. *Mol. Cancer Ther.* 15, 946–957. doi: 10.1158/1535-7163.MCT-15-0647

Cao, J., Meng, F., Gao, X., Dong, H., and Yao, W. (2011). Expression and purification of a natural N-terminal pre-ligand assembly domain of tumor necrosis factor receptor 1 (TNFR1 PLAD) and preliminary activity determination. *Protein J.* 30, 281–289. doi: 10.1007/s10930-011-9330-4

Carrington, P. E., Sandu, C., Wei, Y., Hill, J. M., Morisawa, G., Huang, T., et al. (2006). The structure of FADD and its mode of interaction with procaspase-8. *Mol. Cell* 22, 599–610. doi: 10.1016/j.molcel.2006.04.018

Chan, F. K., Chun, H. J., Zheng, L., Siegel, R. M., Bui, K. L., and Lenardo, M. J. (2000). A domain in TNF receptors that mediates ligand-independent receptor assembly and signaling. *Science* 288, 2351–2354. doi: 10.1126/science.288.5475.2351

Charlier, E., Conde, C., Zhang, J., Deneubourg, L., Di Valentin, E., Rahmouni, S., et al. (2010). SHIP-1 inhibits CD95/APO-1/Fas-induced apoptosis in primary T lymphocytes and T leukemic cells by promoting CD95 glycosylation independently of its phosphatase activity. *Leukemia* 24, 821–832. doi: 10.1038/leu.2010.9

Clancy, L., Mruk, K., Archer, K., Woelfel, M., Mongkolsapaya, J., Screaton, G., et al. (2005). Preligand assembly domain-mediated ligand-independent association between TRAIL receptor 4 (TR4) and TR2 regulates TRAIL-induced apoptosis. *Proc. Natl. Acad. Sci. U.S.A.* 102, 18099–18104. doi: 10.1073/pnas.0507329102

Dahan, R., Barnhart, B. C., Li, F., Yamniuk, A. P., Korman, A. J., and Ravetch, J. V. (2016). Therapeutic activity of agonistic, human Anti-CD40 monoclonal antibodies requires selective FcgammaR engagement. *Cancer Cell* 29, 820–831. doi: 10.1016/j.ccell.2016.05.001

de Bruyn, M., Bremer, E., and Helfrich, W. (2013). Antibody-based fusion proteins to target death receptors in cancer. *Cancer Lett.* 332, 175–183. doi: 10.1016/j.canlet.2010.11.006

Deng, G. M., Liu, L., and Tsokos, G. C. (2010). Targeted tumor necrosis factor receptor I preligand assembly domain improves skin lesions in MRL/lpr mice. *Arthritis Rheum* 62, 2424–2431. doi: 10.1002/art.27534

Deng, G. M., Zheng, L., Chan, F. K., and Lenardo, M. (2005). Amelioration of inflammatory arthritis by targeting the pre-ligand assembly domain of tumor necrosis factor receptors. *Nat. Med.* 11, 1066–1072. doi: 10.1038/nm1304

Dueber, E. C., Schoeffler, A. J., Lingel, A., Elliott, J. M., Fedorova, A. V., Giannetti, A. M., et al. (2011). Antagonists induce a conformational change in cIAP1 that promotes autoubiquitination. *Science* 334, 376–380. doi: 10.1126/science.1207862

Dufour, F., Rattier, T., Shirley, S., Picarda, G., Constantinescu, A. A., Morle, A., et al. (2017). N-glycosylation of mouse TRAIL-R and human TRAIL-R1 enhances TRAIL-induced death. *Cell Death Differ.* 24, 500–510. doi: 10.1038/cdd.2016.150

Esparza, E. M., and Arch, R. H. (2005). Glucocorticoid-induced TNF receptor, a costimulatory receptor on naive and activated T cells, uses TNF receptor-associated factor 2 in a novel fashion as an inhibitor of NF-kappa B activation. *J. Immunol.* 174, 7875–7882. doi: 10.4049/jimmunol.174.12.7875

Feig, C., Tchikov, V., Schutze, S., and Peter, M. E. (2007). Palmitoylation of CD95 facilitates formation of SDS-stable receptor aggregates that initiate apoptosis signaling. *EMBO J.* 26, 221–231. doi: 10.1038/sj.emboj.7601460

Feltham, R., Bettjeman, B., Budhidarmo, R., Mace, P. D., Shirley, S., Condon, S. M., et al. (2011). Smac mimetics activate the E3 ligase activity of cIAP1 protein by promoting RING domain dimerization. *J. Biol. Chem.* 286, 17015–17028. doi: 10.1074/jbc.M111.222919

Fick, A., Lang, I., Schafer, V., Seher, A., Trebing, J., Weisenberger, D., et al. (2012). Studies of binding of tumor necrosis factor (TNF)-like weak inducer of apoptosis (TWEAK) to fibroblast growth factor inducible 14 (Fn14). *J. Biol. Chem.* 287, 484–495. doi: 10.1074/jbc.M111.287656

Force, W. R., Glass, A. A., Benedict, C. A., Cheung, T. C., Lama, J., and Ware, C. F. (2000). Discrete signaling regions in the lymphotoxin-beta receptor for tumor necrosis factor receptor-associated factor binding, subcellular localization, and activation of cell death and NF-kappaB pathways. *J. Biol. Chem.* 275, 11121–11129. doi: 10.1074/jbc.275.15.11121

Fu, Q., Fu, T. M., Cruz, A. C., Sengupta, P., Thomas, S. K., Wang, S., et al. (2016). Structural basis and functional role of intramembrane trimerization of the Fas/CD95 death receptor. *Mol. Cell* 61, 602–613. doi: 10.1016/j.molcel.2016.01.009

Fu, T. M., Li, Y., Lu, A., Li, Z., Vajjhala, P. R., Cruz, A. C., et al. (2016). Cryo-EM structure of Caspase-8 Tandem DED filament reveals assembly and regulation mechanisms of the death-inducing signaling complex. *Mol. Cell* 64, 236–250. doi: 10.1016/j.molcel.2016.09.009

Gajate, C., and Mollinedo, F. (2015). Lipid raft-mediated Fas/CD95 apoptotic signaling in leukemic cells and normal leukocytes and therapeutic implications. *J. Leukoc. Biol.* 98, 739–759. doi: 10.1189/jlb.2MR0215-055R

Galibert, L., Tometsko, M. E., Anderson, D. M., Cosman, D., and Dougall, W. C. (1998). The involvement of multiple tumor necrosis factor receptor (TNFR)-associated factors in the signaling mechanisms of receptor activator of NF-kappaB, a member of the TNFR superfamily. *J. Biol. Chem.* 273, 34120–34127. doi: 10.1074/jbc.273.51.34120

Garibyan, L., Lobito, A. A., Siegel, R. M., Call, M. E., Wucherpfennig, K. W., and Geha, R. S. (2007). Dominant-negative effect of the heterozygous C104R TACI mutation in common variable immunodeficiency (CVID). *J. Clin. Invest.* 117, 1550–1557. doi: 10.1172/JCI31023

Granja, A. G., Holland, J. W., Pignatelli, J., Secombes, C. J., and Tafalla, C. (2017). Characterization of BAFF and APRIL subfamily receptors in rainbow trout (Oncorhynchus mykiss). Potential role of the BAFF / APRIL axis in the pathogenesis of proliferative kidney disease. *PLoS One* 12:e0174249. doi: 10.1371/journal.pone.0174249

Grell, M., Douni, E., Wajant, H., Lohden, M., Clauss, M., Maxeiner, B., et al. (1995). The transmembrane form of tumor necrosis factor is the prime activating ligand of the 80 kDa tumor necrosis factor receptor. *Cell* 83, 793–802. doi: 10.1016/0092-8674(95)90192-2

Grell, M., Wajant, H., Zimmermann, G., and Scheurich, P. (1998). The type 1 receptor (CD120a) is the high-affinity receptor for soluble tumor necrosis factor. *Proc. Natl. Acad. Sci. U.S.A.* 95, 570–575. doi: 10.1073/pnas.95.2.570

Guo, Y., Chen, C., Zheng, Y., Zhang, J., Tao, X., Liu, S., et al. (2005). A novel anti-human DR5 monoclonal antibody with tumoricidal activity induces caspase-dependent and caspase-independent cell death. *J. Biol. Chem.* 280, 41940–41952. doi: 10.1074/jbc.M503621200

Hatzoglou, A., Roussel, J., Bourgeade, M. F., Rogier, E., Madry, C., Inoue, J., et al. (2000). TNF receptor family member BCMA (B cell maturation) associates with TNF receptor-associated factor (TRAF) 1, TRAF2, and TRAF3 and activates NF-kappa B, elk-1, c-Jun N-terminal kinase, and p38 mitogen-activated protein kinase. *J. Immunol.* 165, 1322–1330. doi: 10.4049/jimmunol.165.3.1322

He, Y., Hendriks, D., van Ginkel, R., Samplonius, D., Bremer, E., and Helfrich, W. (2016). Melanoma-directed activation of apoptosis using a bispecific antibody directed at MCSP and TRAIL Receptor-2/Death Receptor-5. *J. Invest. Dermatol.* 136, 541–544. doi: 10.1016/j.jid.2015.11.009

Hendriks, J., Planelles, L., de Jong-Odding, J., Hardenberg, G., Pals, S. T., Hahne, M., et al. (2005). Heparan sulfate proteoglycan binding promotes APRIL-induced tumor cell proliferation. *Cell Death Differ.* 12, 637–648. doi: 10.1038/sj.cdd.4401647

Henkler, F., Behrle, E., Dennehy, K. M., Wicovsky, A., Peters, N., Warnke, C., et al. (2005). The extracellular domains of FasL and Fas are sufficient for the formation of supramolecular FasL-Fas clusters of high stability. *J. Cell Biol.* 168, 1087–1098. doi: 10.1083/jcb.200501048

Herrero, R., Kajikawa, O., Matute-Bello, G., Wang, Y., Hagimoto, N., Mongovin, S., et al. (2011). The biological activity of FasL in human and mouse lungs is determined by the structure of its stalk region. *J. Clin. Invest.* 121, 1174–1190. doi: 10.1172/JCI43004

Holler, N., Tardivel, A., Kovacsovics-Bankowski, M., Hertig, S., Gaide, O., Martinon, F., et al. (2003). Two adjacent trimeric Fas ligands are required for Fas signaling and formation of a death-inducing signaling complex. *Mol. Cell Biol.* 23, 1428–1440. doi: 10.1128/mcb.23.4.1428-1440.2003

Horie, R., Watanabe, T., Morishita, Y., Ito, K., Ishida, T., Kanegae, Y., et al. (2002). Ligand-independent signaling by overexpressed CD30 drives NF-kappaB activation in Hodgkin-Reed-Sternberg cells. *Oncogene* 21, 2493–2503. doi: 10.1038/sj.onc.1205337

Ingold, K., Zumsteg, A., Tardivel, A., Huard, B., Steiner, Q. G., Cachero, T. G., et al. (2005). Identification of proteoglycans as the APRIL-specific binding partners. *J. Exp. Med.* 201, 1375–1383. doi: 10.1084/jem.20042309

Jarousse, N., Trujillo, D. L., Wilcox-Adelman, S., and Coscoy, L. (2011). Virally-induced upregulation of heparan sulfate on B cells via the action of type I IFN. *J. Immunol.* 187, 5540–5547. doi: 10.4049/jimmunol.1003495

Jiang, Y., Wen, T., Yan, R., Kim, S. R., Stowell, S. R., Wang, W., et al. (2020). O-glycans on death receptors in cells modulate their sensitivity to TRAIL-induced apoptosis through affecting on their stability and oligomerization. *FASEB J.* 34, 11786–11801. doi: 10.1096/fj.201900053RR

Jodo, S., Kung, J. T., Xiao, S., Chan, D. V., Kobayashi, S., Tateno, M., et al. (2003). Anti-CD95-induced lethality requires radioresistant Fcgamma RII+ cells. A novel mechanism for fulminant hepatic failure. *J. Biol. Chem.* 278, 7553–7557. doi: 10.1074/jbc.M211229200

Joo, H., Coquery, C., Xue, Y., Gayet, I., Dillon, S. R., Punaro, M., et al. (2012). Serum from patients with SLE instructs monocytes to promote IgG and IgA plasmablast differentiation. *J. Exp. Med.* 209, 1335–1348. doi: 10.1084/jem.20111644

Kanazawa, K., and Kudo, A. (2005). Self-assembled RANK induces osteoclastogenesis ligand-independently. *J. Bone Miner Res.* 20, 2053–2060. doi: 10.1359/JBMR.050706

Karathanasis, C., Medler, J., Fricke, F., Smith, S., Malkusch, S., Widera, D., et al. (2020). Single-molecule imaging reveals the oligomeric state of functional TNFalpha-induced plasma membrane TNFR1 clusters in cells. *Sci. Signal.* 13:eaax5647. doi: 10.1126/scisignal.aax5647

Kelley, S. K., Harris, L. A., Xie, D., Deforge, L., Totpal, K., Bussiere, J., et al. (2001). Preclinical studies to predict the disposition of Apo2L/tumor necrosis factor-related apoptosis-inducing ligand in humans: characterization of in vivo efficacy, pharmacokinetics, and safety. *J. Pharmacol. Exp. Ther.* 299, 31–38.

Kim, H. H., Lee, D. E., Shin, J. N., Lee, Y. S., Jeon, Y. M., Chung, C. H., et al. (1999). Receptor activator of NF-kappaB recruits multiple TRAF family adaptors and activates c-Jun N-terminal kinase. *FEBS Lett.* 443, 297–302. doi: 10.1016/s0014-5793(98)01731-1

Kimberley, F. C., van Bostelen, L., Cameron, K., Hardenberg, G., Marquart, J. A., Hahne, M., et al. (2009). The proteoglycan (heparan sulfate proteoglycan) binding domain of APRIL serves as a platform for ligand multimerization and cross-linking. *FASEB J.* 23, 1584–1595. doi: 10.1096/fj.08-124669

Klima, M., Zajedova, J., Doubravska, L., and Andera, L. (2009). Functional analysis of the posttranslational modifications of the death receptor 6. *Biochim. Biophys. Acta* 1793, 1579–1587. doi: 10.1016/j.bbamcr.2009.07.008

Kojima, T., Morikawa, Y., Copeland, N. G., Gilbert, D. J., Jenkins, N. A., Senba, E., et al. (2000). TROY, a newly identified member of the tumor necrosis factor receptor superfamily, exhibits a homology with Edar and is expressed in embryonic skin and hair follicles. *J. Biol. Chem.* 275, 20742–20747. doi: 10.1074/jbc.M002691200

Krippner-Heidenreich, A., Tubing, F., Bryde, S., Willi, S., Zimmermann, G., and Scheurich, P. (2002). Control of receptor-induced signaling complex formation by the kinetics of ligand/receptor interaction. *J. Biol. Chem.* 277, 44155–44163. doi: 10.1074/jbc.M207399200

Lang, I., Fick, A., Schafer, V., Giner, T., Siegmund, D., and Wajant, H. (2012). Signaling active CD95 receptor molecules trigger co-translocation of inactive CD95 molecules into lipid rafts. *J. Biol. Chem.* 287, 24026–24042. doi: 10.1074/jbc.M111.328211

Lang, I., Fullsack, S., Wyzgol, A., Fick, A., Trebing, J., Arana, J. A., et al. (2016). Binding studies of TNF receptor superfamily (TNFRSF) receptors on intact cells. *J. Biol. Chem.* 291, 5022–5037. doi: 10.1074/jbc.M115.683946

Lee, H. H., Dempsey, P. W., Parks, T. P., Zhu, X., Baltimore, D., and Cheng, G. (1999). Specificities of CD40 signaling: involvement of TRAF2 in CD40-induced NF-kappaB activation and intercellular adhesion molecule-1 up-regulation. *Proc. Natl. Acad. Sci. U.S.A.* 96, 1421–1426. doi: 10.1073/pnas.96.4.1421

Lee, H. W., Lee, S. H., Lee, H. W., Ryu, Y. W., Kwon, M. H., and Kim, Y. S. (2005). Homomeric and heteromeric interactions of the extracellular domains of death receptors and death decoy receptors. *Biochem. Biophys. Res. Commun.* 330, 1205–1212. doi: 10.1016/j.bbrc.2005.03.101

Lee, R., Kermani, P., Teng, K. K., and Hempstead, B. L. (2001). Regulation of cell survival by secreted proneurotrophins. *Science* 294, 1945–1948. doi: 10.1126/science.1065057

Lee, S. Y., Lee, S. Y., Kandala, G., Liou, M. L., Liou, H. C., and Choi, Y. (1996). CD30/TNF receptor-associated factor interaction: NF-kappa B activation and binding specificity. *Proc. Natl. Acad. Sci. U.S.A.* 93, 9699–9703. doi: 10.1073/pnas.93.18.9699

Li, F., and Ravetch, J. V. (2011). Inhibitory Fcgamma receptor engagement drives adjuvant and anti-tumor activities of agonistic CD40 antibodies. *Science* 333, 1030–1034. doi: 10.1126/science.1206954

Li, F., and Ravetch, J. V. (2012). Apoptotic and antitumor activity of death receptor antibodies require inhibitory Fcgamma receptor engagement. *Proc. Natl. Acad. Sci. U.S.A.* 109, 10966–10971. doi: 10.1073/pnas.1208698109

Li, F., and Ravetch, J. V. (2013). Antitumor activities of agonistic anti-TNFR antibodies require differential FcgammaRIIB coengagement in vivo. *Proc. Natl. Acad. Sci. U.S.A.* 110, 19501–19506. doi: 10.1073/pnas.1319502110

Locksley, R. M., Killeen, N., and Lenardo, M. J. (2001). The TNF and TNF receptor superfamilies: integrating mammalian biology. *Cell* 104, 487–501. doi: 10.1016/s0092-8674(01)00237-9

Lu, L. F., Cook, W. J., Lin, L. L., and Noelle, R. J. (2003). CD40 signaling through a newly identified tumor necrosis factor receptor-associated factor 2 (TRAF2) binding site. *J. Biol. Chem.* 278, 45414–45418. doi: 10.1074/jbc.M309601200

Ma, B. Y., Mikolajczak, S. A., Danesh, A., Hosiawa, K. A., Cameron, C. M., Takaori-Kondo, A., et al. (2005). The expression and the regulatory role of OX40 and 4-1BB heterodimer in activated human T cells. *Blood* 106, 2002–2010. doi: 10.1182/blood-2004-04-1622

Mace, P. D., Smits, C., Vaux, D. L., Silke, J., and Day, C. L. (2010). Asymmetric recruitment of cIAPs by TRAF2. *J. Mol. Biol.* 400, 8–15. doi: 10.1016/j.jmb.2010.04.055

Madireddi, S., Eun, S. Y., Lee, S. W., Nemcovicova, I., Mehta, A. K., Zajonc, D. M., et al. (2014). Galectin-9 controls the therapeutic activity of 4-1BB-targeting antibodies. *J. Exp. Med.* 211, 1433–1448. doi: 10.1084/jem.20132687

Madireddi, S., Eun, S. Y., Mehta, A. K., Birta, A., Zajonc, D. M., Niki, T., et al. (2017). Regulatory T Cell-mediated suppression of inflammation induced by DR3 signaling is dependent on galectin-9. *J. Immunol.* 199, 2721–2728. doi: 10.4049/jimmunol.1700575

Mazurek, N., Byrd, J. C., Sun, Y., Hafley, M., Ramirez, K., Burks, J., et al. (2012). Cell-surface galectin-3 confers resistance to TRAIL by impeding trafficking of death receptors in metastatic colon adenocarcinoma cells. *Cell Death Differ.* 19, 523–533. doi: 10.1038/cdd.2011.123

Medler, J., Nelke, J., Weisenberger, D., Steinfatt, T., Rothaug, M., Berr, S., et al. (2019). TNFRSF receptor-specific antibody fusion proteins with targeting controlled FcgammaR-independent agonistic activity. *Cell Death Dis.* 10:224. doi: 10.1038/s41419-019-1456-x

Moosmayer, D., Dinkel, A., Gerlach, E., Hessabi, B., Grell, M., Pfizenmaier, K., et al. (1994). Coexpression of the human TNF receptors TR60 and TR80 in insect cells: analysis of receptor complex formation. *Lymphokine Cytokine Res.* 13, 295–301.

Motoki, K., Mori, E., Matsumoto, A., Thomas, M., Tomura, T., Humphreys, R., et al. (2005). Enhanced apoptosis and tumor regression induced by a direct agonist antibody to tumor necrosis factor-related apoptosis-inducing ligand receptor 2. *Clin. Cancer Res.* 11, 3126–3135. doi: 10.1158/1078-0432.CCR-04-1867

Muller, N., Wyzgol, A., Munkel, S., Pfizenmaier, K., and Wajant, H. (2008). Activity of soluble OX40 ligand is enhanced by oligomerization and cell surface immobilization. *FEBS J.* 275, 2296–2304. doi: 10.1111/j.1742-4658.2008.06382.x

Muppidi, J. R., Tschopp, J., and Siegel, R. M. (2004). Life and death decisions: secondary complexes and lipid rafts in TNF receptor family signal transduction. *Immunity* 21, 461–465. doi: 10.1016/j.immuni.2004.10.001

Nelke, J., Medler, J., Weisenberger, D., Beilhack, A., and Wajant, H. (2020). CD40- and CD95-specific antibody single chain-Baff fusion proteins display BaffR-, TACI- and BCMA-restricted agonism. *MAbs* 12:1807721. doi: 10.1080/19420862.2020.1807721

Neumann, S., Bidon, T., Branschadel, M., Krippner-Heidenreich, A., Scheurich, P., and Doszczak, M. (2012). The transmembrane domains of TNF-related apoptosis-inducing ligand (TRAIL) receptors 1 and 2 co-regulate apoptotic signaling capacity. *PLoS One* 7:e42526. doi: 10.1371/journal.pone.0042526

Neumann, S., Hasenauer, J., Pollak, N., and Scheurich, P. (2014). Dominant negative effects of tumor necrosis factor (TNF)-related apoptosis-inducing ligand (TRAIL) receptor 4 on TRAIL receptor 1 signaling by formation of heteromeric complexes. *J. Biol. Chem.* 289, 16576–16587. doi: 10.1074/jbc.M114.559468

Ni, C. Z., Oganesyan, G., Welsh, K., Zhu, X., Reed, J. C., Satterthwait, A. C., et al. (2004). Key molecular contacts promote recognition of the BAFF receptor

by TNF receptor-associated factor 3: implications for intracellular signaling regulation. *J. Immunol.* 173, 7394–7400. doi: 10.4049/jimmunol.173.12.7394

Nihira, K., Nan-Ya, K. I., Kakuni, M., Ono, Y., Yoshikawa, Y., Ota, T., et al. (2019). Chimeric mice with humanized livers demonstrate human-specific hepatotoxicity caused by a therapeutic antibody against TRAIL-Receptor 2/Death Receptor 5. *Toxicol. Sci.* 167, 190–201. doi: 10.1093/toxsci/kfy228

Nikolaev, A., McLaughlin, T., O'Leary, D. D., and Tessier-Lavigne, M. (2009). APP binds DR6 to trigger axon pruning and neuron death via distinct caspases. *Nature* 457, 981–989. doi: 10.1038/nature07767

Pan, L., Fu, T. M., Zhao, W., Zhao, L., Chen, W., Qiu, C., et al. (2019). Higher-order clustering of the transmembrane anchor of DR5 Drives signaling. *Cell* 176, 1477.e14–1489.e14. doi: 10.1016/j.cell.2019.02.001

Papadopoulos, K. P., Isaacs, R., Bilic, S., Kentsch, K., Huet, H. A., Hofmann, M., et al. (2015). Unexpected hepatotoxicity in a phase I study of TAS266, a novel tetravalent agonistic Nanobody(R) targeting the DR5 receptor. *Cancer Chemother. Pharmacol.* 75, 887–895. doi: 10.1007/s00280-015-2712-0

Papoff, G., Cascino, I., Eramo, A., Starace, G., Lynch, D. H., and Ruberti, G. (1996). An N-terminal domain shared by Fas/Apo-1 (CD95) soluble variants prevents cell death in vitro. *J. Immunol.* 156, 4622–4630.

Papoff, G., Hausler, P., Eramo, A., Pagano, M. G., Di Leve, G., Signore, A., et al. (1999). Identification and characterization of a ligand-independent oligomerization domain in the extracellular region of the CD95 death receptor. *J. Biol. Chem.* 274, 38241–38250. doi: 10.1074/jbc.274.53.38241

Park, H. H. (2018). Structure of TRAF family: current understanding of receptor recognition. *Front. Immunol.* 9:1999. doi: 10.3389/fimmu.2018.01999

Park, H. H. (2019). Molecular basis of dimerization of initiator caspase was revealed by crystal structure of caspase-8 pro-domain. *Cell Death Differ.* 26, 1213–1220. doi: 10.1038/s41418-018-0200-x

Park, Y. C., Burkitt, V., Villa, A. R., Tong, L., and Wu, H. (1999). Structural basis for self-association and receptor recognition of human TRAF2. *Nature* 398, 533–538. doi: 10.1038/19110

Piechutta, M., and Berghoff, A. S. (2019). New emerging targets in cancer immunotherapy: the role of cluster of differentiation 40 (CD40/TNFR5). *ESMO Open* 4(Suppl. 3):e000510. doi: 10.1136/esmoopen-2019-000510

Pinckard, J. K., Sheehan, K. C., and Schreiber, R. D. (1997). Ligand-induced formation of p55 and p75 tumor necrosis factor receptor heterocomplexes on intact cells. *J. Biol. Chem.* 272, 10784–10789. doi: 10.1074/jbc.272.16.10784

Poissonnier, A., Sanseau, D., Le Gallo, M., Malleter, M., Levoin, N., Viel, R., et al. (2016). CD95-mediated calcium signaling promotes T Helper 17 trafficking to inflamed organs in lupus-prone mice. *Immunity* 45, 209–223. doi: 10.1016/j.immuni.2016.06.028

Prada, J. P., Wangorsch, G., Kucka, K., Lang, I., Dandekar, T., and Wajant, H. (2020). Asystems-biology model of the tumor necrosis factor (TNF) interactions with TNF receptor 1 and 2. *Bioinformatics* btaa844. doi: 10.1093/bioinformatics/btaa844 [Epub ahead of print].

Reyes-Moreno, C., Girouard, J., Lapointe, R., Darveau, A., and Mourad, W. (2004). CD40/CD40 homodimers are required for CD40-induced phosphatidylinositol 3-kinase-dependent expression of B7.2 by human B lymphocytes. *J. Biol. Chem.* 279, 7799–7806. doi: 10.1074/jbc.M313168200

Reyes-Moreno, C., Sharif-Askari, E., Girouard, J., Leveille, C., Jundi, M., Akoum, A., et al. (2007). Requirement of oxidation-dependent CD40 homodimers for CD154/CD40 bidirectional signaling. *J. Biol. Chem.* 282, 19473–19480. doi: 10.1074/jbc.M701076200

Richards, D. M., Marschall, V., Billian-Frey, K., Heinonen, K., Merz, C., Redondo Muller, M., et al. (2019). HERA-GITRL activates T cells and promotes anti-tumor efficacy independent of FcgammaR-binding functionality. *J. Immunother. Cancer* 7:191. doi: 10.1186/s40425-019-0671-4

Richter, C., Messerschmidt, S., Holeiter, G., Tepperink, J., Osswald, S., Zappe, A., et al. (2012). The tumor necrosis factor receptor stalk regions define responsiveness to soluble versus membrane-bound ligand. *Mol. Cell Biol.* 32, 2515–2529. doi: 10.1128/MCB.06458-11

Roos, C., Wicovsky, A., Muller, N., Salzmann, S., Rosenthal, T., Kalthoff, H., et al. (2010). Soluble and transmembrane TNF-like weak inducer of apoptosis differentially activate the classical and noncanonical NF-kappa B pathway. *J. Immunol.* 185, 1593–1605. doi: 10.4049/jimmunol.0903555

Rossin, A., Derouet, M., Abdel-Sater, F., and Hueber, A. O. (2009). Palmitoylation of the TRAIL receptor DR4 confers an efficient TRAIL-induced cell death signalling. *Biochem. J.* 419, 185–192. doi: 10.1042/BJ20081212 2 p following 92.,

Rossin, A., Durivault, J., Chakhtoura-Feghali, T., Lounnas, N., Gagnoux-Palacios, L., and Hueber, A. O. (2015). Fas palmitoylation by the palmitoyl acyltransferase DHHC7 regulates Fas stability. *Cell Death Differ.* 22, 643–653. doi: 10.1038/cdd.2014.153

Salzmann, S., Seher, A., Trebing, J., Weisenberger, D., Rosenthal, A., Siegmund, D., et al. (2013). Fibroblast growth factor inducible (Fn14)-specific antibodies concomitantly display signaling pathway-specific agonistic and antagonistic activity. *J. Biol. Chem.* 288, 13455–13466. doi: 10.1074/jbc.M112.435917

Samel, D., Muller, D., Gerspach, J., Assohou-Luty, C., Sass, G., Tiegs, G., et al. (2003). Generation of a FasL-based proapoptotic fusion protein devoid of systemic toxicity due to cell-surface antigen-restricted Activation. *J. Biol. Chem.* 278, 32077–32082. doi: 10.1074/jbc.M304866200

Schneider, H., Faschingbauer, F., Schuepbach-Mallepell, S., Korber, I., Wohlfart, S., Dick, A., et al. (2018). Prenatal correction of X-Linked hypohidrotic ectodermal dysplasia. *N. Engl. J. Med.* 378, 1604–1610. doi: 10.1056/NEJMoa1714322

Schneider, P., Holler, N., Bodmer, J. L., Hahne, M., Frei, K., Fontana, A., et al. (1998). Conversion of membrane-bound Fas(CD95) ligand to its soluble form is associated with downregulation of its proapoptotic activity and loss of liver toxicity. *J. Exp. Med.* 187, 1205–1213. doi: 10.1084/jem.187.8.1205

Schuepbach-Mallepell, S., Das, D., Willen, L., Vigolo, M., Tardivel, A., Lebon, L., et al. (2015). Stoichiometry of Heteromeric BAFF and APRIL cytokines dictates their receptor binding and signaling properties. *J. Biol. Chem.* 290, 16330–16342. doi: 10.1074/jbc.M115.661405

Scott, F. L., Stec, B., Pop, C., Dobaczewska, M. K., Lee, J. J., Monosov, E., et al. (2009). The Fas-FADD death domain complex structure unravels signalling by receptor clustering. *Nature* 457, 1019–1022. doi: 10.1038/nature07606

Seyrek, K., Richter, M., and Lavrik, I. N. (2019). Decoding the sweet regulation of apoptosis: the role of glycosylation and galectins in apoptotic signaling pathways. *Cell Death Differ.* 26, 981–993. doi: 10.1038/s41418-019-0317-6

Shatnyeva, O. M., Kubarenko, A. V., Weber, C. E., Pappa, A., Schwartz-Albiez, R., Weber, A. N., et al. (2011). Modulation of the CD95-induced apoptosis: the role of CD95 N-glycosylation. *PLoS One* 6:e19927. doi: 10.1371/journal.pone.0019927

Shen, C., Yue, H., Pei, J., Guo, X., Wang, T., and Quan, J. M. (2015). Crystal structure of the death effector domains of caspase-8. *Biochem. Biophys. Res. Commun.* 463, 297–302. doi: 10.1016/j.bbrc.2015.05.054

Shivange, G., Urbanek, K., Przanowski, P., Perry, J. S. A., Jones, J., Haggart, R., et al. (2018). A single-agent dual-specificity targeting of FOLR1 and DR5 as an effective strategy for ovarian cancer. *Cancer Cell* 34, 331.e11–345.e11. doi: 10.1016/j.ccell.2018.07.005

Siegel, R. M., Frederiksen, J. K., Zacharias, D. A., Chan, F. K., Johnson, M., Lynch, D., et al. (2000). . Fas preassociation required for apoptosis signaling and dominant inhibition by pathogenic mutations. *Science* 288, 2354–2357. doi: 10.1126/science.288.5475.2354

Siegmund, D., Lang, I., and Wajant, H. (2017). Cell death-independent activities of the death receptors CD95, TRAILR1, and TRAILR2. *FEBS J.* 284, 1131–1159. doi: 10.1111/febs.13968

Sinha, S. K., Zachariah, S., Quinones, H. I., Shindo, M., and Chaudhary, P. M. (2002). Role of TRAF3 and -6 in the activation of the NF-kappa B and JNK pathways by X-linked ectodermal dysplasia receptor. *J. Biol. Chem.* 277, 44953–44961. doi: 10.1074/jbc.M207923200

Smulski, C. R., Beyrath, J., Decossas, M., Chekkat, N., Wolff, P., Estieu-Gionnet, K., et al. (2013). Cysteine-rich domain 1 of CD40 mediates receptor self-assembly. *J. Biol. Chem.* 288, 10914–10922. doi: 10.1074/jbc.M112.427583

Smulski, C. R., Decossas, M., Chekkat, N., Beyrath, J., Willen, L., Guichard, G., et al. (2017). Hetero-oligomerization between the TNF receptor superfamily members CD40, Fas and TRAILR2 modulate CD40 signalling. *Cell Death Dis.* 8:e2601. doi: 10.1038/cddis.2017.22

Strand, S., Vollmer, P., van den Abeelen, L., Gottfried, D., Alla, V., Heid, H., et al. (2004). Cleavage of CD95 by matrix metalloproteinase-7 induces apoptosis resistance in tumour cells. *Oncogene* 23, 3732–3736. doi: 10.1038/sj.onc.1207387

Suda, T., Hashimoto, H., Tanaka, M., Ochi, T., and Nagata, S. (1997). Membrane Fas ligand kills human peripheral blood T lymphocytes, and soluble Fas ligand blocks the killing. *J. Exp. Med.* 186, 2045–2050. doi: 10.1084/jem.186.12.2045

Sun, S. C. (2017). The non-canonical NF-kappaB pathway in immunity and inflammation. *Nat. Rev. Immunol.* 17, 545–558. doi: 10.1038/nri.2017.52

Swee, L. K., Ingold-Salamin, K., Tardivel, A., Willen, L., Gaide, O., Favre, M., et al. (2009). Biological activity of ectodysplasin A is conditioned by its collagen and heparan sulfate proteoglycan-binding domains. *J. Biol. Chem.* 284, 27567–27576. doi: 10.1074/jbc.M109.042259

Tauzin, S., Chaigne-Delalande, B., Selva, E., Khadra, N., Daburon, S., Contin-Bordes, C., et al. (2011). The naturally processed CD95L elicits a c-yes/calcium/PI3K-driven cell migration pathway. *PLoS Biol.* 9:e1001090. doi: 10.1371/journal.pbio.1001090

Trebing, J., El-Mesery, M., Schafer, V., Weisenberger, D., Siegmund, D., Silence, K., et al. (2014a). CD70-restricted specific activation of TRAILR1 or TRAILR2 using scFv-targeted TRAIL mutants. *Cell Death Dis.* 5:e1035. doi: 10.1038/cddis.2013.555

Trebing, J., Lang, I., Chopra, M., Salzmann, S., Moshir, M., Silence, K., et al. (2014b). A novel llama antibody targeting Fn14 exhibits anti-metastatic activity in vivo. *MAbs* 6, 297–308. doi: 10.4161/mabs.26709

Vaitaitis, G. M., and Wagner, D. H. Jr. (2012). Galectin-9 controls CD40 signaling through a Tim-3 independent mechanism and redirects the cytokine profile of pathogenic T cells in autoimmunity. *PLoS One* 7:e38708. doi: 10.1371/journal.pone.0038708

van Lier, R. A., Borst, J., Vroom, T. M., Klein, H., Van Mourik, P., Zeijlemaker, W. P., et al. (1987). Tissue distribution and biochemical and functional properties of Tp55 (CD27), a novel T cell differentiation antigen. *J. Immunol.* 139, 1589–1596.

Varfolomeev, E., Goncharov, T., Maecker, H., Zobel, K., Komuves, L. G., Deshayes, K., et al. (2012). Cellular inhibitors of apoptosis are global regulators of NF-kappaB and MAPK activation by members of the TNF family of receptors. *Sci. Signal.* 5:ra22. doi: 10.1126/scisignal.2001878

Vesa, J., Kruttgen, A., Cosgaya, J. M., and Shooter, E. M. (2000). Palmitoylation of the p75 neurotrophin receptor has no effect on its interaction with TrkA or on TrkA-mediated down-regulation of cell adhesion molecules. *J. Neurosci. Res.* 62, 225–233. doi: 10.1002/1097-4547(20001015)62:2<225::AID-JNR7<3.0.CO;2-9

Vij, N., Roberts, L., Joyce, S., and Chakravarti, S. (2005). Lumican regulates corneal inflammatory responses by modulating Fas-Fas ligand signaling. *Invest. Ophthalmol. Vis. Sci.* 46, 88–95. doi: 10.1167/iovs.04-0833

Vilar, M., Charalampopoulos, I., Kenchappa, R. S., Simi, A., Karaca, E., Reversi, A., et al. (2009). Activation of the p75 neurotrophin receptor through conformational rearrangement of disulphide-linked receptor dimers. *Neuron* 62, 72–83. doi: 10.1016/j.neuron.2009.02.020

Wagner, K. W., Punnoose, E. A., Januario, T., Lawrence, D. A., Pitti, R. M., Lancaster, K., et al. (2007). Death-receptor O-glycosylation controls tumor-cell sensitivity to the proapoptotic ligand Apo2L/TRAIL. *Nat. Med.* 13, 1070–1077. doi: 10.1038/nm1627

Wajant, H. (2015). Principles of antibody-mediated TNF receptor activation. *Cell Death Differ.* 22, 1727–1741. doi: 10.1038/cdd.2015.109

Wajant, H. (2019). Molecular mode of action of TRAIL receptor agonists-common principles and their translational exploitation. *Cancers* 11, 954. doi: 10.3390/cancers11070954

Wajant, H., Gerspach, J., and Pfizenmaier, K. (2013). Engineering death receptor ligands for cancer therapy. *Cancer Lett.* 332, 163–174. doi: 10.1016/j.canlet.2010.12.019

Wang, L., Yang, J. K., Kabaleeswaran, V., Rice, A. J., Cruz, A. C., Park, A. Y., et al. (2010). The Fas-FADD death domain complex structure reveals the basis of DISC assembly and disease mutations. *Nat. Struct. Mol. Biol.* 17, 1324–1329. doi: 10.1038/nsmb.1920

Wang, Y. L., Chou, F. C., Chen, S. J., Lin, S. H., Chang, D. M., and Sytwu, H. K. (2011). Targeting pre-ligand assembly domain of TNFR1 ameliorates autoimmune diseases - an unrevealed role in downregulation of Th17 cells. *J. Autoimmun.* 37, 160–170. doi: 10.1016/j.jaut.2011.05.013

White, A. L., Chan, H. T., French, R. R., Willoughby, J., Mockridge, C. I., Roghanian, A., et al. (2015). Conformation of the human immunoglobulin G2 hinge imparts superagonistic properties to immunostimulatory anticancer antibodies. *Cancer Cell* 27, 138–148. doi: 10.1016/j.ccell.2014.11.001

White, A. L., Chan, H. T., Roghanian, A., French, R. R., Mockridge, C. I., Tutt, A. L., et al. (2011). Interaction with FcgammaRIIB is critical for the agonistic activity of anti-CD40 monoclonal antibody. *J. Immunol.* 187, 1754–1763. doi: 10.4049/jimmunol.1101135

White, A. L., Dou, L., Chan, H. T., Field, V. L., Mockridge, C. I., Moss, K., et al. (2014). Fcgamma receptor dependency of agonistic CD40 antibody in lymphoma therapy can be overcome through antibody multimerization. *J. Immunol.* 193, 1828–1835. doi: 10.4049/jimmunol.1303204

Wilson, N. S., Yang, B., Yang, A., Loeser, S., Marsters, S., Lawrence, D., et al. (2011). An Fcgamma receptor-dependent mechanism drives antibody-mediated target-receptor signaling in cancer cells. *Cancer Cell* 19, 101–113. doi: 10.1016/j.ccr.2010.11.012

Wyzgol, A., Muller, N., Fick, A., Munkel, S., Grigoleit, G. U., Pfizenmaier, K., et al. (2009). Trimer stabilization, oligomerization, and antibody-mediated cell surface immobilization improve the activity of soluble trimers of CD27L, CD40L, 41BBL, and glucocorticoid-induced TNF receptor ligand. *J. Immunol.* 183, 1851–1861. doi: 10.4049/jimmunol.0802597

Xie, P. (2013). TRAF molecules in cell signaling and in human diseases. *J. Mol. Signal.* 8:7. doi: 10.1186/1750-2187-8-7

Xu, L. G., and Shu, H. B. (2002). TNFR-associated factor-3 is associated with BAFF-R and negatively regulates BAFF-R-mediated NF-kappa B activation and IL-10 production. *J. Immunol.* 169, 6883–6889. doi: 10.4049/jimmunol.169.12.6883

Xu, Y., Szalai, A. J., Zhou, T., Zinn, K. R., Chaudhuri, T. R., Li, X., et al. (2003). Fc gamma Rs modulate cytotoxicity of anti-Fas antibodies: implications for agonistic antibody-based therapeutics. *J. Immunol.* 171, 562–568. doi: 10.4049/jimmunol.171.2.562

Yamamoto, H., Kishimoto, T., and Minamoto, S. (1998). NF-kappaB activation in CD27 signaling: involvement of TNF receptor-associated factors in its signaling and identification of functional region of CD27. *J. Immunol.* 161, 4753–4759.

Yu, X., Chan, H. T. C., Orr, C. M., Dadas, O., Booth, S. G., Dahal, L. N., et al. (2018). Complex interplay between epitope specificity and isotype dictates the biological activity of anti-human CD40 antibodies. *Cancer Cell* 33, 664.e4–675.e4. doi: 10.1016/j.ccell.2018.02.009

Zhang, B., van Roosmalen, I. A. M., Reis, C. R., Setroikromo, R., and Quax, W. J. (2019). Death receptor 5 is activated by fucosylation in colon cancer cells. *FEBS J.* 286, 555–571. doi: 10.1111/febs.14742

Zhang, P., Tu, G. H., Wei, J., Santiago, P., Larrabee, L. R., Liao-Chan, S., et al. (2019). Ligand-blocking and membrane-proximal domain targeting Anti-OX40 antibodies mediate potent T Cell-stimulatory and anti-tumor activity. *Cell Rep.* 27, 3117.e5–3123.e5. doi: 10.1016/j.celrep.2019.05.027

Zheng, C., Kabaleeswaran, V., Wang, Y., Cheng, G., and Wu, H. (2010). Crystal structures of the TRAF2: cIAP2 and the TRAF1: TRAF2: cIAP2 complexes: affinity, specificity, and regulation. *Mol. Cell* 38, 101–113. doi: 10.1016/j.molcel.2010.03.009

Zingler, P., Sarchen, V., Glatter, T., Caning, L., Saggau, C., Kathayat, R. S., et al. (2019). Palmitoylation is required for TNF-R1 signaling. *Cell Commun. Signal.* 17:90. doi: 10.1186/s12964-019-0405-8

Zuch de Zafra, C. L., Ashkenazi, A., Darbonne, W. C., Cheu, M., Totpal, K., Ortega, S., et al. (2016). Antitherapeutic antibody-mediated hepatotoxicity of recombinant human Apo2L/TRAIL in the cynomolgus monkey. *Cell Death Dis.* 7:e2338. doi: 10.1038/cddis.2016.241

Conflict of Interest: The authors declare that the research was conducted in the absence of any commercial or financial relationships that could be construed as a potential conflict of interest.

Advantages of publishing in Frontiers

OPEN ACCESS
Articles are free to read for greatest visibility and readership

FAST PUBLICATION
Around 90 days from submission to decision

HIGH QUALITY PEER-REVIEW
Rigorous, collaborative, and constructive peer-review

TRANSPARENT PEER-REVIEW
Editors and reviewers acknowledged by name on published articles

Frontiers
Avenue du Tribunal-Fédéral 34
1005 Lausanne | Switzerland

Visit us: www.frontiersin.org
Contact us: frontiersin.org/about/contact

REPRODUCIBILITY OF RESEARCH
Support open data and methods to enhance research reproducibility

DIGITAL PUBLISHING
Articles designed for optimal readership across devices

FOLLOW US
@frontiersin

IMPACT METRICS
Advanced article metrics track visibility across digital media

EXTENSIVE PROMOTION
Marketing and promotion of impactful research

LOOP RESEARCH NETWORK
Our network increases your article's readership